OSMIUM CARBONYL CLUSTERS CONTAINING GERMANIUM OR TIN

by

WENG KEE LEONG

B.A., M.A. (Cambridge, 1982 and 1986)

Dip.Ed., M.Sc. (Singapore, 1985 and 1992)

THESIS SUBMITTED IN PARTIAL FULFILLMENT OF

THE REQUIREMENTS FOR THE DEGREE OF

DOCTOR OF PHILOSOPHY

IN THE DEPARTMENT OF CHEMISTRY

©Weng Kee Leong, 1995

SIMON FRASER UNIVERSITY

September, 1995

Approval

Name: Weng Kee Leong

Degree: Doctor of Philosophy (Chemistry)

Title of Thesis: Osmium Carbonyl Clusters Containing Germanium or Tin

Examining Committee:

    Chairman: Dipankar Sen, Assistant Professor

Roland K. Pomeroy, Professor, Senior Supervisor

Andrew J. Bennet, Assistant Professor

Frederick W. B. Einstein, Professor

Colin H. W. Jones, Professor and Dean of Science

Kenton H. Whitmire, Professor, Rice University,
External Examiner

Date Approved: 8 Sep 1995

PARTIAL COPYRIGHT LICENSE

I hereby grant to Simon Fraser University the right to lend my thesis, project or extended essay (the title of which is shown below) to users of the Simon Fraser University Library, and to make partial or single copies only for such users or in response to a request from the library of any other university, or other educational institution, on its own behalf or for one of its users. I further agree that permission for multiple copying of this work for scholarly purposes may be granted by me or the Dean of Graduate Studies. It is understood that copying or publication of this work for financial gain shall not be allowed without my written permission.

Title of Thesis/Project/Extended Essay:

Osmium Carbonyl Clusters Containing

Germanium or Tin

Author:

(signature)

Weng Kee Leong

(name)

12 September 1995

(date)

Abstract

The synthesis, structural characterisation, and some aspects of the chemistry of clusters containing osmium and tin or germanium atoms have been investigated.

The photolysis of $[(OC)_4OsSnMe_2]_2$, **1(SnMe)**, in hexane gave $[Os_2(CO)_7(SnMe_2)_2]_2$, which has an almost planar arrangement of the metal atoms in 3- and 4-membered rings; pyrolysis of **1(SnMe)** at 130 °C gave, as the major product, the raft-like cluster $[(OC)_3OsSnMe_2]_3$; and reaction of **1(SnMe)** with Me_3NO gave as the only isolable product, $[Os_2(CO)_7O(SnMe_2)_2]_2$, which consists of a boat-like 6-membered ring of $Os_2Sn_2O_2$ and two Os_2SnO tetracycles.

The photolysis in hexane of $[(OC)_4OsGeMe_2]_2$, **1(GeMe)**, on the other hand, gave several clusters. One of these was $Os_3(CO)_{11}(GeMe_2)_2$, the Os_3Ge_2 skeleton of which is in the shape of a "bow-tie". Also isolated were the raft-like cluster $[(OC)_3OsGeMe_2]_3$, **5(Ge)**, and $Os_4(CO)_{12}(GeMe_2)_4$, **9**. NMR studies on **9** are consistent with the view that the peripheral $(OC)_4OsGeMe_2$ fragment rotates relative to the Os_3Ge_3 core. The pyrolysis of **1(GeMe)** at 100 °C gave, in addition to the above clusters, $Os_2(CO)_6(GeMe_2)_3$, which was shown to have a trigonal bipyramidal Os_2Ge_3 core reminiscent of that in $Fe_2(CO)_9$.

In the preparation of $[(OC)_4OsSnPh_2]_2$ by the reaction of Ph_2SnCl_2 with $[Os(CO)_4]^{2-}$, the cluster $[(OC)_4OsSnPh_2]_6$, **4**, was also formed. It was shown to have an unprecedented planar 12-membered ring with alternating Os and Sn atoms. Solution NMR studies indicated that there is rapid rotation of the $Os(CO)_4$ units in **4**. The formation of this cluster probably proceeds via the *trans* form of $Os(CO)_4(SnPh_2Cl)_2$ rather than the *cis* form. There was ^{13}C NMR evidence that other OsSn ring complexes were also formed in the reaction.

The cluster **1(SnMe)** is thermally robust, but substitution by C_2H_4 or $CH_2=CHCOOMe$ could be brought about by photolysis, albeit in low yields. The

substituted derivatives were, however, more readily available via $[Os_2(CO)_7(SnMe_2)_2]_2$, which reacted under mild conditions with PMe_3, $P(OMe)_3$ or $CH_2=CHCOOMe$ to give the clusters $Os_2(CO)_7(SnMe_2)_2L$ (L = PMe_3, $P(OMe)_3$ or $CH_2=CHCOOMe$). Likewise, the cluster **5(Ge)** was also found to be thermally robust, although it did react with PMe_3 at 120 °C to give the substituted derivatives $Os_3(CO)_{9-n}(GeMe_2)_3(PMe_3)_n$ (n = 1 - 3). In all the derivatives, both phosphine and alkene ligands are believed to occupy equatorial positions.

Dedication

To :   Doreen, Wendy, Cherie and Jermyn

Acknowledgements

I consider my 3 years here in SFU the best I have ever had, and it is in a very large measure the result of a great research environment that has been created for me by the many individuals that I have had the good fortune to work with. In particular, I like to thank the following individuals:

From the Land of Os,

        Dr. R. K. Pomeroy, the Wizard

        Dr. W. Wang (Weiberoo, a.k.a. Wonder Horse), "Cowardly" Lion

        Dr. J. L. Male (Mutley), the Scarecrow

In Reciprocal Space,

        Dr. F. W. B. Einstein, Captain of the ship

        Dr. R. J. Batchelor, Number One.

From the holy shrine of high-vacuum techniques, etc.,

        Dr. Dev Sharma, the Guru

And finally, the Glass Shop Boys - Les and Gerry.

Signed,

The Tin Man

vi

Table of Contents

Cluster Numbering Scheme

Number	Cluster
1(ER)	$[(OC)_4OsER_2]_2$ (E = Ge, Sn, Pb; R = Me, Bu^t, Ph)
2	$FeOs(CO)_8(EMe_2)_2$ (E = Ge, Sn)
3	$Ph_2Ge[Os(CO)_4H]_2$
4	$[(OC)_4OsSnPh_2]_6$
5(E)	$[(OC)_3OsEMe_2]_3$ (E = Ge, Sn)
6	$[Os_2(CO)_7(SnMe_2)_2]_2$
7	$[Os_2(CO)_7O(SnMe_2)_2]_2$
8	$Os_3(CO)_{11}(GeMe_2)_2$
9	$Os_4(CO)_{12}(GeMe_2)_4$
10	$Os_2(CO)_6(GeMe_2)_3$
11	$Os_2(CO)_7(SnMe_2)_2$(olefin)
	(olefin = $CH_2CHCOOMe$ (**a**); C_2H_4 (**b**))
12	$Os_2(CO)_7(SnMe_2)_2L$ (L = P(OMe)$_3$ (**a**), PMe$_3$ (**b**))
13	$Os_3(CO)_8(GeMe_2)_3(PMe_3)$
14	$Os_3(CO)_7(GeMe_2)_3(PMe_3)_2$
15	$Os_3(CO)_6(GeMe_2)_3(PMe_3)_3$

Conventions and Less Common Abbreviations

OsE   osmium-group 14 element.

E   to indicate generally the heavier group 14 elements, i.e., Si, Ge, Sn, and Pb.

$\nu(CO)$ carbonyl absorptions in the infrared.

hex   hexane

cyclohex cyclohexane

Molecular structures that are given in outline show only the metal skeleton and directly-bonded atoms of ligands of interest. Carbonyl ligands on osmium, and hydrocarbon substituents on group 14 elements, are represented by short lines indicating Os-CO and E-R bonds, respectively, as shown in the following example :
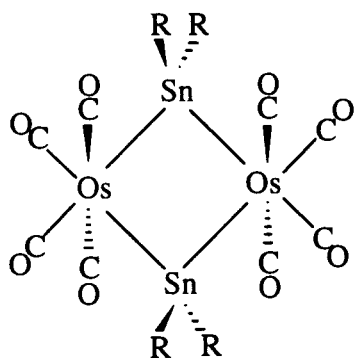
Full representation   Simplified representation
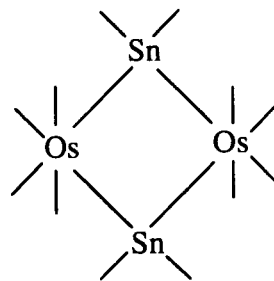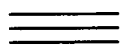
List of Tables

List of Figures

List of Schemes

Foreword

Like so many other research projects, the final outcome of my research for the PhD degree was somewhat removed from the original, short-term goal. That I have managed to stay more or less in the same broader perspective is in no small part due to both Professors Pomeroy and Einstein who have kept a constant and, most thankfully, painless reminder to "keep on track".

It is my good fortune to have had the opportunity to work on two different degree theses on similar chemistry. This second time round, I have become wiser with experience (or so I like to believe!). Yet it was **still** fraught with doubts and difficulties; most overcomed with various degrees of hardship and even luck, but others simply insurmountable - at least given my inability and under the circumstances. This has developed in me an urge to communicate some of the difficulties faced - not as a personal statement of triumph, but as a reassurance to my fellow students that should they face difficulties and uncertainties in their research (and they will!), they are far from being alone! Towards this end, I have deliberately organized my thesis in a quite unconventional way, and have also chosen to write in a rather informal and personal style.

In particular, I have attempted to place in Chapter II some of the thought processes that Professor Pomeroy and I went through during the course of my project. Of course, things were never as neat as it is recorded there, but I believe that it is quite a chronologically accurate account of the development of the project. My wish for this thesis, therefore, is that it will achieve a little of that communication mentioned in the second paragraph above, and that it will actually be less tedious reading than the usual.

Chapter I   Osmium-group 14 mixed-metal clusters : The status quo

A transition metal cluster may be defined as a molecular compound with three or more transition metal atoms, with at least some metal-metal bonding interactions connecting them [1]. An alternative definition has also been forwarded to include dinuclear compounds [2]; the first definition will be adhered to here. The surging interest in transition metal carbonyl clusters over the last 30 or so years has been due to two major reasons. The first is the analogy between ligands on clusters, and small molecules anchored on a metal surface, i.e., the idea that a metal cluster may serve as a molecular model for the surface of a heterogeneous metal catalyst [3]. Such analogies have since been shown to be of great utility to surface studies [4]. The second reason, a purely academic and very often an aesthetic one, is the sheer beauty and diversity in the structures adopted by the metal atom framework of cluster compounds.

Recent years have also witnessed the emergence of the concept of inorganometallic chemistry [5]. The concept is an attempt to redress the lack of recognition that the inorganic ligands in organometallic compounds have received in the past; they have often been relegated to the status of ancillary ligands, innocent bystanders as it were. Instead, they can and do have an important rôle to play in modifying the chemistry of the metal centre through their steric or electronic properties. Another related development has been that of mixed-metal clusters, in which two or more different types of metal atoms are found in the metal cluster framework. Interest in these clusters lies in their possible analogy to mixed-metal catalysts [6]. In these catalysts there is the potential of synergistic interactions among the different metals. For example, a WOs bimetallic cluster may bind a CO ligand so that the C atom is bound to the Os centre and the O atom to the W centre, as a result of the different affinities of the metals for the different light atoms.

This thesis attempts to look at a natural confluence of the two developments above, namely, that of mixed-metal clusters in which a main-group metal enters the metal cluster framework. The possible importance of the rôle the main-group element may play

in such clusters has been clearly stated by Whitmire [7]. In particular, we are interested in clusters where the transition metal is osmium and the main-group metals are the heavier group 14 elements, *viz.*, Si, Ge, Sn and Pb. A discussion of previously known compounds of this class can be found embedded in a number of reviews of a more general nature [8]. In this chapter, a review of the synthetic methodologies employed, the characterisation techniques used, and the diversity of structural types observed, will be made based on a comprehensive survey of the literature to the end of 1994 on osmium-heavier group 14 (henceforth abbreviated "OsE") clusters.

As has been pointed out by Fehlner, the distinction between a main-group metal acting as a ligand and as part of the metal cluster framework can be rather fuzzy [5a]. In keeping with his approach, therefore, no distinction has been made, and we have arbitrarily included only those compounds containing at least two osmium atoms (with at least some CO ligands on them) and at least one Si, Ge, Sn or Pb atom, with direct bonding interactions connecting them. Compounds of the type $Os(CO)_4(ER_3)_2$, (E = Si, Ge, Sn, Pb) are thus not included, nor are those of the type $[R_3E(\mu-X)Os(CO)_3]_2$ (X = halogen), in which the two OsE fragments have no bonding interactions except via the halogen bridges. Compounds which include other transition metals in addition to osmium are also excluded. We have also chosen to use the terms "chains", "rings" and "cages" as descriptions of the shapes of the metal framework, and not as descriptors of their bonding.

1.   Synthetic methodologies : The cookbook

As for metal clusters in general, most OsE clusters have been obtained serendipitously. Some element of rational synthesis is, however, present in the choice of starting materials, especially the osmium precursor. This is derived mainly from knowledge acquired in osmium carbonyl cluster chemistry itself. Hence, some activated form of the parent carbonyl cluster $Os_3(CO)_{12}$ is often employed to enable use of milder reaction conditions and introduce some specificity; $Os_3(CO)_{12}$ itself is rather unreactive, harsh conditions being usually required to bring about substitution of a carbonyl by some other

ligand [9]. The accessibility of milder conditions can be important when it involves Sn and Pb compounds, which are often thermally and photochemically unstable. The most oft-used of such activated clusters are the substitutionally-labile acetonitrile derivatives $Os_3(CO)_{11}(CH_3CN)$ and $Os_3(CO)_{10}(CH_3CN)_2$ [10], and the formally unsaturated, 46-electron cluster $Os_3(\mu\text{-}H)_2(CO)_{10}$ [11]. The synthetic methodologies may thus be classified according to the osmium precursor used and the type of reaction that they undergo.

 (a) <u>From the binary carbonyls of osmium</u>

 As mentioned above, the triosmium carbonyl cluster $Os_3(CO)_{12}$ requires rather drastic conditions for it to be activated towards reaction. The most common method is simply by heating it with a group 14 hydride, to temperatures above about 130 °C. Even with such high temperatures, long reaction times are often required. Photolysis has also been tried as a means of activation. Some reactions reported, which did give cluster products, are given in Table I.1.

Table I.1 : OsE cluster syntheses from $Os_3(CO)_{12}$.

Group 14 reactant	Conditions	Cluster product	Ref.
R_3SiH (R=Me,Et)	140 °C, hex or hv	$[R_3SiOs(CO)_4]_2$	12a
$Me_3SiSiMe_2H$	2 equiv., 160 °C, hex, 44 h	$[Me_3SiOs(CO)_3]_2(SiMe_2)_2$	13
$HSiRCl_2$ (R=Me,Cl)	135 °C, hex, 3 h, *in vacuo*	$H_3Os_3(CO)_9(SiRCl_2)_3$	14
$HSiRCl_2$ (R=Me,Cl)	140 °C, hex, 8 h, CO (80 atm)	$Os_3(CO)_{12}(SiRCl_2)_2$	15
$SnCl_4$	25 °C, benzene	$Os_3(CO)_{12}(Cl)(SnCl_3)$	16
Me_3GeH		$[Os(CO)_3]_2(GeMe_2)_3$	17
Me_3GeH	150 °C, hex, 260 h	$[Me_3GeOs(CO)_3(GeMe_2)]_2$	17
$(Tb)(Tip)SnY_4$ $(Y=S,Se)^*$	reflux, toluene, 10 h	$Os_3(CO)_8Y_2[YSn(Tb)(Tip)]$	18

*Tip = 2,4,6-tri-Pr^i-C$_6$H$_2$; Tb = 2,4,6-tri-CH(SiMe$_3$)$_2$-C$_6$H$_2$

As is evident from the tabulated data, the method has been limited mainly to the silicon compounds, presumably because of extensive decomposition at high temperatures as we move to the heavier group 14 congeners; Me_3SnH yields only the mononuclear compounds $HOs(CO)_4(SnMe_3)$ and $Os(CO)_4(SnMe_3)_2$ under both thermal and photochemical conditions [12a]. The course of the reaction of $Os_3(CO)_{12}$ with group 14 compounds can be influenced by the substituents on the group 14 centre as well as the reaction conditions. Thus the silicon compounds $HSiCl_3$ and $HSiMeCl_2$ give clusters, but $HSiMe_2Cl$ gives only mononuclear products [15]; thermolysis of $Os_3(CO)_{12}$ and $HSiCl_3$ (or $HSiMeCl_2$) *in vacuo* retains the triangular Os_3 framework to give $Os_3(\mu$-$H)_3(CO)_9(SiCl_3)_3$ while heating under a CO pressure gives the more open, chain structures $Os_3(CO)_{12}(SiCl_3)_2$.

A much milder set of reaction conditions can be employed if the lower nuclearity carbonyl, $Os(CO)_5$, is used, for example [19],

$$Os(CO)_5 + GeCl_4 \xrightarrow{60\ ^{\circ}C,\ hex,\ 16\ h} Os_2(CO)_8(Cl)((GeCl_3)$$
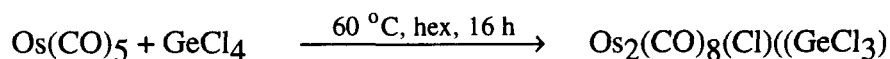
This probably reflects the ease of CO loss in $Os(CO)_5$, which is known to be thermally unstable towards decomposition to $Os_3(CO)_{12}$ [20].

A further noteworthy point in the above reactions is that the Si-H bond is cleaved preferentially over the Si-Cl bond, while the Ge-Cl and Sn-Cl bonds can be cleaved relatively easily; no doubt a reflection of the differing strengths of the E-Cl bonds.

The tetranuclear carbonyl $Os_4(CO)_{14}$ also reacts under mild conditions, undergoing addition reactions by opening up the metal framework from a tetrahedron to that of a butterfly [21]. Hence with the group 14 hydrides, reaction proceeds by an oxidative addition across the E-H bond, for example [22],

$$Os_4(CO)_{14} + R_3EH \xrightarrow{hex,\ 50\ ^{\circ}C} HOs_4(CO)_{14}(ER_3) \quad (E = Si,\ Ge,\ Sn;\ R = Me,\ Ph)$$

4
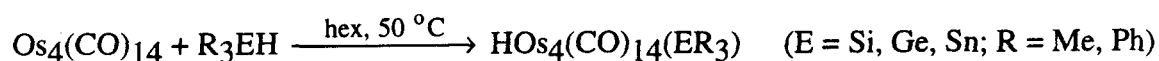
(b)   <u>Substitution reactions involving clusters with labile ligands</u>

Replacement of one or two carbonyls in $Os_3(CO)_{12}$ by a more labile ligand like acetonitrile or cyclooctene has proven to be among the most important routes into osmium cluster chemistry. To date, reactions leading to OsE clusters using this class of compounds have involved the acetonitrile derivatives $Os_3(CO)_{11}(CH_3CN)$ and $Os_3(CO)_{10}(CH_3CN)_2$, both of which can be readily prepared from $Os_3(CO)_{12}$ by Me_3NO activation in the presence of CH_3CN [10]. With group 14 hydrides, displacement of the acetonitrile ligand and insertion into the E-H bond proceeds in high yield and under mild conditions, for instance [23-27],

$$Os_3(CO)_{11}(CH_3CN) + R_3EH \xrightarrow{RT} Os_3(\mu\text{-}H)(CO)_{11}(ER_3)$$

$$(E = Si ; R_3 = (OMe)_3, (OEt)_3, Et_3, Ph_2H$$

$$\text{or } (o\text{-}BrC_6H_4CH_2)Me_{2-n}H_n \ (n=0\text{-}2)$$

$$E = Ge ; R_3 = Ph_3, Ph_2Me; \quad E = Sn ; R = Bu^n, Ph)$$

$$[Os_3(CO)_{10}(CH_3CN)]_2(\mu\text{-}dppe) + HSi(OR)_3 \xrightarrow{CH_3CN}$$

$$(R = Me, Et) \qquad\qquad [Os_3(\mu\text{-}H)(CO)_{10}\{Si(OR)_3\}]_2(\mu\text{-}dppe)$$
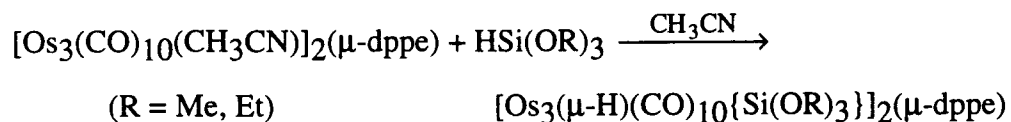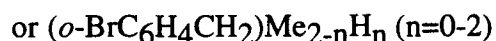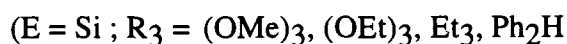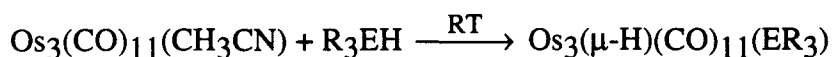
Displacement of the second acetonitrile ligand in $Os_3(CO)_{10}(CH_3CN)_2$, however, is not achieved with group 14 hydrides, as for example in [23-27],

$$Os_3(CO)_{10}(CH_3CN)_2 + R_3EH \xrightarrow{RT} Os_3(\mu\text{-}H)(CO)_{10}(CH_3CN)(ER_3)$$

$$(E = Si ; R_3 = (OMe)_3, (OEt)_3, Et_3 \ Ph_2H$$

$$\text{or } (o\text{-}BrC_6H_4CH_2)Me_{2-n}H_n \ (n = 0\text{-}2)$$

$$E = Ge, Sn ; R = Ph)$$
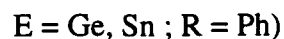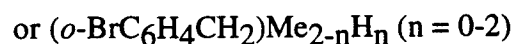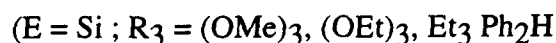
This second acetonitrile can, however, be displaced if the group 14 hydride has another good donor site, as in [28],

$$Os_3(CO)_{10}(CH_3CN)_2 + o\text{-}Ph_2PC_6H_4CH_2SiMeRH \longrightarrow$$

$$(R = Me, H) \qquad Os_3(\mu\text{-}H)(CO)_{10}(CH_3CN)(o\text{-}Ph_2PC_6H_4CH_2SiMeRH)$$

$$+ Os_3(\mu\text{-}H)(CO)_{10}(\mu_3\text{-}\eta^3\text{-}o\text{-}Ph_2PC_6H_4CH_2SiMeR)$$
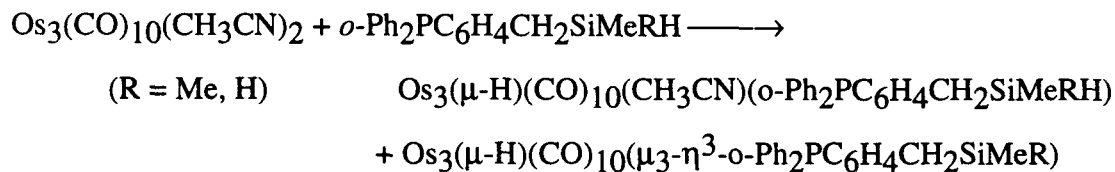
or if a stannylene is used, as in [29],

$$Os_3(CO)_{10}(CH_3CN)_2 + :SnR_2 \xrightarrow{\text{toluene, 1h}} Os_3(CO)_9(\mu\text{-}CO)(SnR_2)_2$$
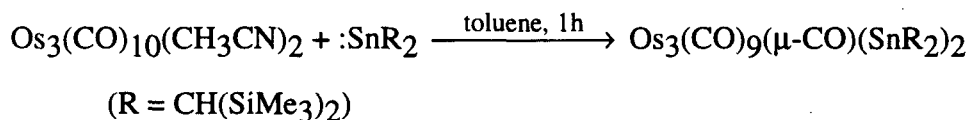
$$(R = CH(SiMe_3)_2)$$

The product in the last reaction is the only known example of an Os_3E_2 cluster; $Os_3(CO)_9(\mu\text{-}CO)(Sn[CH\{SiMe_3\}_2]_2)_2$ is isolobal to the raft-like cluster $Os_5(CO)_{18}$ [30].

Compounds of the type $Os_3(\mu\text{-}H)(CO)_{10}(CH_3CN)(ER_3)$ can be useful for the stepwise introduction of different ligand types or for changing the bonding mode of existing group 14 ligands, as in the following examples [24,26,31,32]:

$$Os_3(\mu\text{-}H)(CO)_{10}(CH_3CN)(GePh_3) + PPh_3 \longrightarrow Os_3(\mu\text{-}H)(CO)_{10}(PPh_3)(GePh_3)$$

$$Os_3(\mu\text{-}H)(CO)_{10}(CH_3CN)\{Si(OMe)_3\} + HC\equiv CR \xrightarrow{CH_2Cl_2,\ 34\ ^\circ C,\ 4.5\ h}$$

$$(R = Bu^t, p\text{-tolyl}) \qquad Os_3(CO)_{10}\{\mu\text{-}C(H)C(H)R\}\{Si(OMe)_3\}$$

$$Os_3(\mu\text{-}H)(CO)_{10}(CH_3CN)\{Si(OR)_3\} \xrightarrow{\text{heptane, reflux, } N_2 \text{ purge}}$$

$$(R = Me, Et) \qquad Os_3(\mu\text{-}H)(CO)_{10}\{\mu\text{-}\eta^2\text{-}Si(OR)_3\}$$

$$+ Os_3(\mu\text{-}H)(CO)_9\{\mu_3\text{-}\eta^3\text{-}Si(OR)_3\}$$
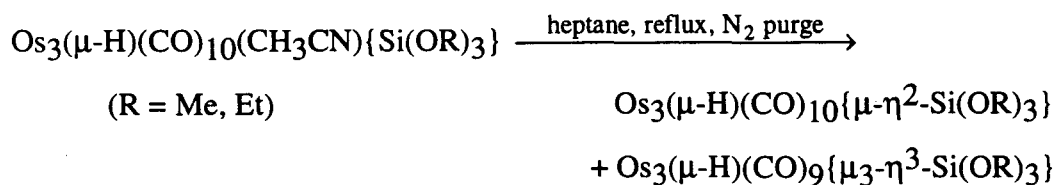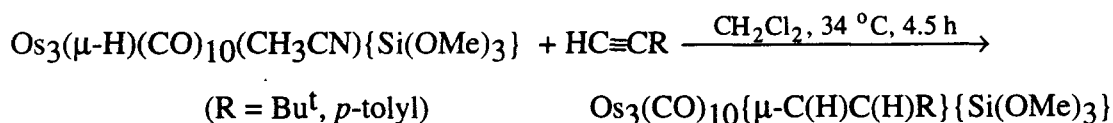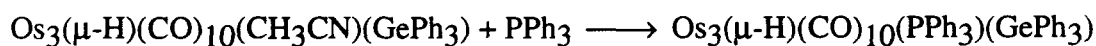
(c)   Addition reactions to clusters

Addition of a ligand to a cluster neccessarily involves a change in the bonding mode of the cluster in order to accommodate the incoming ligand. This can either be a change in the bonding within the metal framework, as is most often the case for the clusters $Os_3(\mu\text{-H})_2(CO)_{10}$ and $Os_4(CO)_{14}$, or a change in the bonding mode of one or more of the ligands already on the cluster. In the reaction of $Os_3(\mu\text{-H})_2(CO)_{10}$ with the group 14 hydrides (Table I.2), the reaction proceeds at a faster rate and under milder conditions on going from Si to Sn [33]. The initial product is usually $HOs_3(\mu\text{-H})_2(CO)_{10}(ER_3)$; further reaction can occur to give $Os_3(\mu\text{-H})_2(CO)_{10}(ER_3)_2$, and in the case of E = Si, a higher reaction temperature leads to decarbonylation of the initial product to yield the formally unsaturated cluster $Os_3(\mu\text{-H})_3(CO)_9(SiR_3)$.

Table I.2 : Addition reactions of $Os_3(\mu\text{-H})_2(CO)_{10}$ giving OsE clusters.

Reactants	Conditions	Cluster products (yield)	Ref.
Ph_3SiH	hex, 70 °C, 7h	$Os_3(\mu\text{-H})_3(CO)_9(SiPh_3)$ (58%)	34
$o\text{-}BrC_6H_4CH_2SiMe_2H$	hex, 60 °C, 17h	$Os_3(\mu\text{-H})_3(CO)_9(o\text{-}BrC_6H_4CH_2\text{-}SiMe_2)$	25
excess Ph_3SiH	hex, 70 °C, 24h	$Os_3(\mu\text{-H})_2(CO)_{10}(SiPh_3)_2$	34
excess $C_5H_4NSiMe_2H$	cyclohex, 72h	$Os_3(\mu\text{-H})_2(CO)_{10}(C_5H_4NSiMe_2)_2$	25
Ph_2SiH_2	hex, 4h	$HOs_3(\mu\text{-H})_2(CO)_{10}(SiPh_2H)$	35
$MeRR'SiH$ (R = Me,H; R' = $Ph_2P\text{-}o\text{-}C_6H_4CH_2\text{-}$, $Ph_2PCH_2\text{-}o\text{-}C_6H_4\text{-}$)		$Os_3(\mu\text{-H})_3(CO)_8(\mu_3\text{-}\eta^3\text{-}SiMeRR')$	28
Me_3SnH	hex, RT, 4d	$HOs_3(\mu\text{-H})_2(CO)_{10}(SnMe_3)$ (initial) $Os_3(\mu\text{-H})_2(CO)_{10}(SnMe_3)_2$ (94%)	35
:SnR_2 [R = $CH(SiMe_3)_2$]	hex, RT	$Os_3(\mu\text{-H})_2(CO)_{10}(SnR_2)$ (85%)	29, 36

Reaction with stannylenes can give unusual products [37] :

$$Os_3(\mu-H)_2(CO)_{10} + SnR_2 \xrightarrow{\text{hex, RT}} Os_3(\mu-H)(CO)_{10}(SnR)$$

$$(R = C(SiMe_3)_2C_5H_4N\text{-}2)$$
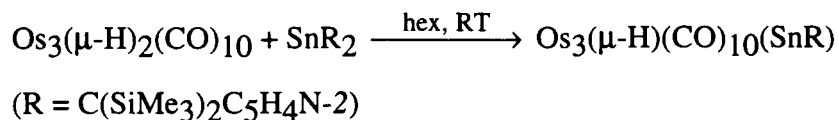
As already mentioned in Section (a) above, $Os_4(CO)_{14}$ can undergo ligand addition by opening up its metal framework. A similar type of reaction occurs between $Os_3(CO)_{11}(\mu-CH_2)$ and $SnCl_2$; in this instance, by the opening-up of the Os_3 triangle [38] :

$$Os_3(CO)_{11}(\mu-CH_2) + SnCl_2 \xrightarrow{22\ ^\circ C,\ THF,\ 30\text{-}45\text{mins}} Os_3(CO)_{11}(\mu-CH_2)(SnCl_2)$$

A change in the bonding mode of an existing ligand can also occur to accommodate the incoming ligand. For example, in the following reaction, the orthometallation of one of the phenyl rings of the original dppm ligand is apparently reversed to accommodate one of the two incoming stannylenes [39] :

$$Os_3(\mu-H)(CO)_8(o\text{-}Ph_2PCH_2P(Ph)C_6H_4) + SnR_2 \xrightarrow{\text{hex, reflux, 6h}}$$

$$(R = CH(SiMe_3)_2) \qquad\qquad Os_3(CO)_8(\mu\text{-dppm})(\mu\text{-}SnR_2)_2$$
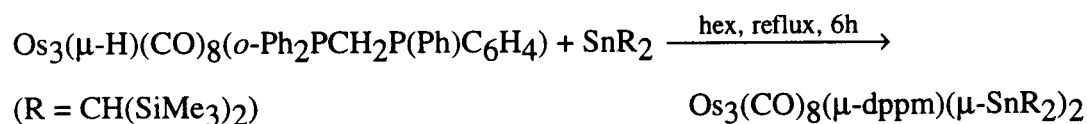
(d)   <u>Elimination reactions between osmium and group 14 precursors</u>

The elimination of a salt or a small molecule like H_2O has not been extensively exploited for the synthesis of OsE clusters. Some examples reported are [40-42]:

$$[Os_3(\mu-H)(CO)_{11}]^- + Ph_3SnCl \xrightarrow{Et_2O,\ 20\text{mins}} Os_3(\mu-H)(CO)_{11}(SnPh_3) \qquad \text{(minor)}$$

$$+ \text{unidentified} \qquad \text{(major)}$$

$$[Os(CO)_4]^{2-} + R_2SnCl_2 \longrightarrow [R_2SnOs(CO)_4]_2 \quad (R = Me; 40\% \text{ yield})$$
$$(R = Bu^n; 23\% \text{ yield})$$

$$H_2Os(CO)_4 + \textit{trans}-Os(CO)_4(Bu^n_2SnCl)_2 \xrightarrow{Et_3N} [Bu^n_2SnOs(CO)_4]_2$$
$$(12\%)$$

$$H_2Os(CO)_4 + Ph_2SnO \longrightarrow [Ph_2SnOs(CO)_4]_2 \quad (40\%)$$
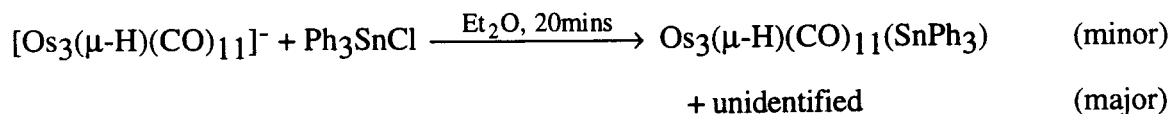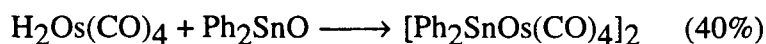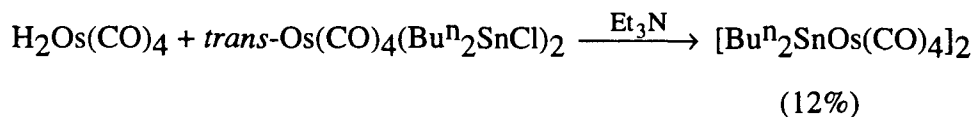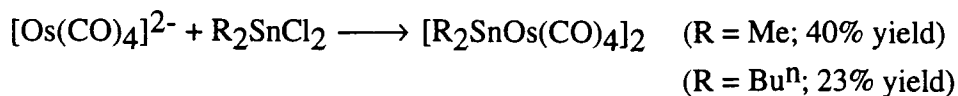
Considering the large driving force involved in salt elimination, the rather modest yields reported for some of the reactions are rather surprising and will be commented on in more detail later in this thesis.

A recent report has also suggested that HCl eliminations with the aid of a base can proceed in high yields and stereospecificity if the hydride ligand on the osmium is terminal [43] :

$$H_2Os_3(CO)_{12} + Ph_3SnCl \xrightarrow{Et_2NH} Os_3(CO)_{12}(SnPh_3)_2 \quad (\text{quantitative})$$
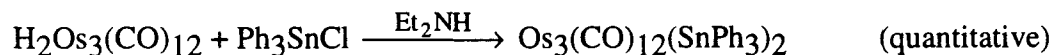
(e)   From OsE precursors

An obvious class of reaction to yield OsE clusters involves starting with a precursor that already has Os-E bonds. The following reactions of mononuclear precursors have been reported to give rise to OsE clusters [12,13,17]:

$$(Me_3Si)_2Os(CO)_4 \xrightarrow{heat} [(OC)_4OsSiMe_3]_2$$

$$R_3SiOs(CO)_4H \xrightarrow{heat} [(OC)_4OsSiR_3]_2 \ (R_3 = Me_3, MeCl_2, Cl_3)$$

$$(Me_3Ge)_2Os(CO)_4 \xrightarrow{160\,^{\circ}C,\ 20d} Os_2(CO)_6(GeMe_2)_3 + [(OC)_3OsGeMe_2]_3 \ (68\%)$$

$$(Me_3Si)_2Os(CO)_4 + Me_3SiSiMe_2H \xrightarrow{hex,\ \textit{hv},\ 120h} [Me_3SiOs(CO)_3]_2(\mu\text{-}SiMe_2)_2 \ (10\%)$$
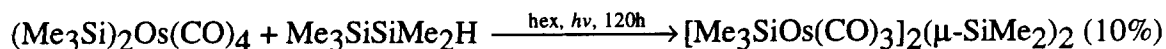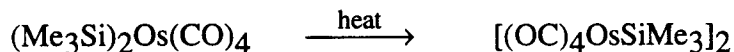
Such reactions give unpredictable products, often in low yields, and hence are usually not useful from a rational synthesis point of view. They are, however, often a good source of clusters with unusual structural features which are not accessible by other means.

The OsE precursors can also be other OsE clusters. The structural and chemical complexity of clusters ensure that a variety of interesting reaction pathways are open. Thus, we can have clusters undergoing rearrangement, for example [44],

$$Os_3(\mu\text{-}H)_2(CO)_{10}(SnR_2) \xrightarrow{\text{n-heptane, reflux}} Os_3(\mu\text{-}H)_2(CO)_9(RCOSnR)$$
$$(R = CH(SiMe_3)_2)$$

condensation, as in [32],

$$Os_3(\mu\text{-}H)(CO)_{11}\{Si(OEt)_3\} \xrightarrow{\text{97 °C, N}_2 \text{ purge}} Os_3(\mu\text{-}H)(CO)_9\{\mu_3\text{-}\eta^3\text{-}Si(OEt)_3\}$$
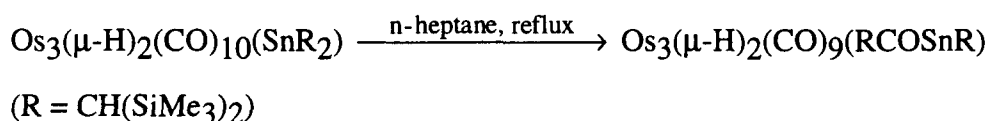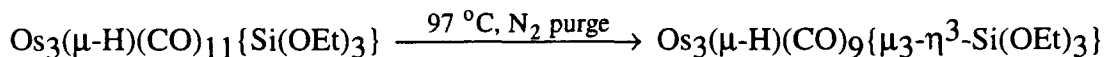
or further reaction, as shown below [44],

$$Os_3(\mu\text{-}H)_2(CO)_{10}(SnR_2) + MeO_2CC\equiv CCO_2Me \xrightarrow{\text{n-heptane, reflux}}$$
$$[R = CH(SiMe_3)_2] \qquad\qquad Os_3(CO)_9(MeO_2CCCH_2CO_2Me)(\mu\text{-}SnR_2)$$
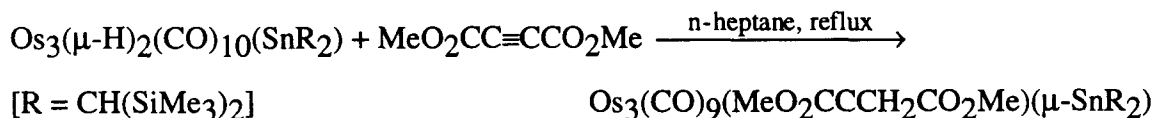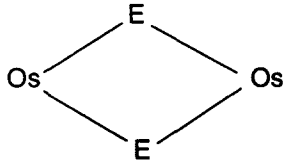
As can be gathered from the above, the study of OsE clusters is hampered by the lack of general, high-yield routes for their synthesis. Among the best routes available are those that lead to species containing an Os-ER$_3$ moiety, but these tend to have labile Os-E bonds. For instance, $Os_3(\mu\text{-}H)(CO)_{11}(EPh_3)$ (E = Ge, Sn) has been shown to react in wet methanol to give $Os_3(\mu\text{-}H)(CO)_{10}(\mu\text{-}OH)$ [26]. Clusters with more than one bond to the group 14 moiety may be more robust, but convenient and high-yield routes to such species are still lacking.

2. Characterisation : What have we got here ?

The 89 OsE clusters reported to date are given in Table I.3. The clusters are classified according to the connectivity of the OsE metal skeleton. No OsPb clusters have been reported. The structural complexity of cluster compounds has meant that X-ray crystallography is the single most important technique for their characterisation. Thus of the 89 clusters listed, 30 have been characterised by single crystal X-ray crystallography; the structures span almost the entire range of structural types observed to date. Interestingly, only one of the 30 is an OsGe cluster.
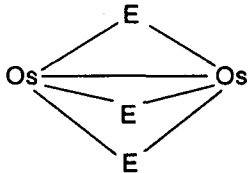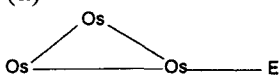
The pattern of IR stretches in the carbonyl, $v(CO)$, region (2250-1600 cm^{-1}) exhibited by a metal carbonyl complex depends on the number and arrangement of the CO ligands and can therefore serve as a tool for gauging if two clusters have the same number and arrangement of their CO's. For example, Table I.4 lists the $v(CO)$ of some clusters of general formula $Os_3(\mu-H)(CO)_{10}(L)(ER_3)$, in which L is a nitrogen or phosphorus donor ligand on an Os atom adjacent to that bonded to the group 14 moiety. For the clusters that have the same group 15 donor atom in L, the patterns are similar, while there is a difference in the pattern between complexes with N and P donors. This is because N donor ligands usually occupy axial sites whereas P donor ligands adopt equatorial positions. Changes in the number and dispositions of the carbonyl ligands are also clearly reflected in changes in the IR spectra in the carbonyl stretching region; thus changes in the pattern of the carbonyl stretches in the infrared on going from starting material to product may be used to monitor the course of reactions.

Table I.3.   Known OsE clusters by metal skeleton type.

Metal Skeleton Type	Compound*	Ref.
I. Chain		
(a) Os-Os-E	$Os_2(CO)_5(1\text{-}2,3\text{-}4\text{-}\eta{:}5\text{-}7\text{-}\eta\text{-}C_7H_7)(SiR_3)$ [R_3 = Me_3, Me_2Ph]	45
	$Os_2(CO)_5(1\text{-}2,3\text{-}4\text{-}\eta{:}5\text{-}7\text{-}\eta\text{-}C_7H_7)(GeMe_3)$	45
	$Os_2(CO)_8(Cl)(GeCl_3)$*	19
	$Os_2(CO)_8(X)(SnCl_3)$ [X = H, Cl, Br]	16b,c
	$Os_3(CO)_8Y_3Sn(2,4,6\text{-}C_6H_2Pr^i_3)(2,4,6\text{-}C_6H_2[CH\{SiMe_3\}_2]_3)$ [Y = S*, Se]	18
(b) E-Os-Os-E	$[(OC)_4OsSiR_3]_2$ [R = Me, Et, Cl; R_3 = MeCl_2]	12
(c) Os-Os-Os-E	$Os_3(CO)_{12}(Cl)(SnCl_3)$	16,46
	$Os_3(\mu\text{-}H)(CO)_7(PMe_2Ph)(\mu_3\text{-}S)(\mu_3\text{-}\eta^2\text{-}SCH_2)(SnMe_3)$*	47
(d) E-Os-Os-Os-E	$Os_3(CO)_{12}(SiRCl_2)$ [R = Me, Cl*]	15
	$Os_3(CO)_{12}(SnR_3)$ [R = Ph, Cl]	43
II. Rings and Cages (a)	$[(OC)_4OsSnR_2]_2$ [R = Me, Bu^n, Ph]	41,42
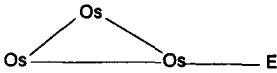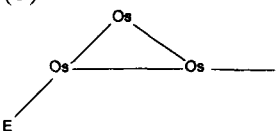
---

* Compounds that have been characterised by X-ray crystallography are marked by an asterisk (*).

Table I.3 continued.

Metal Skeleton Type	Compound[*]	Ref.
(b) E Os —— Os E E	$Os_2(CO)_6(GeMe_2)_3$	17
III. Deltahedra and Rafts (a) Os Os —— Os —— E	$Os_3(\mu\text{-}H)(CO)_9[\mu_3\text{-}\eta^3\text{-}Si(OR)_3]$ [R = Me, Et*] $Os_3(\mu\text{-}H)_3(CO)_9(SiR_3)$ $[R_3 = Ph_3*, (o\text{-}BrC_6H_4CH_2)Me_2]$ $Os_3(CO)_{10}[\mu\text{-}C(H)C(H)R][Si(OMe)_3]$ $[R = Bu^t {}^*, p\text{-}tolyl]$ $Os_3(\mu\text{-}H)(CO)_{10}[\mu\text{-}\eta^2\text{-}Si(OR)_3]$ [R = Me*, Et] $Os_3(\mu\text{-}H)(CO)_{10}(CH_3CN)[SiR_3]$ [R = OMe, OEt*, Et; $R_3 = Ph_2H$, $(o\text{-}BrC_6H_4CH_2)Me_{2\text{-}n}H_n$ (n = 0*, 1)] $Os_3(\mu\text{-}H)(CO)_{10}(CH_3CN)(GePh_3)$ $Os_3(\mu\text{-}H)(CO)_{10}(CH_3CN)(SnPh_3)$ $Os_3(\mu\text{-}H)(CO)_{10}(PPh_3)[SiMe_2(o\text{-}BrC_6H_4CH_2)*$ $Os_3(\mu\text{-}H)(CO)_{10}(PPh_3)(GePh_3)$	24,32 34,25 31 24 23-27, 31,32 26 26 25 26
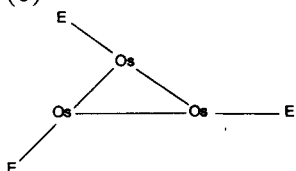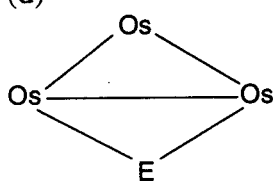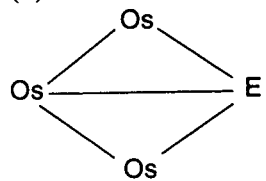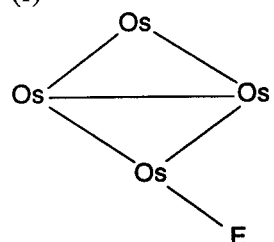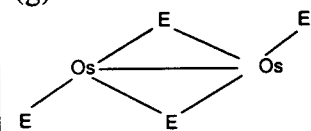
[*] Compounds that have been characterised by X-ray crystallography are marked by an asterisk (*).

Table I.3 continued.

Metal Skeleton Type	Compound*	Ref.
(a) continued. 	$Os_3(\mu\text{-H})(CO)_{10}(Me_2SiCH_2\text{-}o\text{-}C_6H_4PPh_2)$*	28
	$Os_3(\mu\text{-H})(CO)_{10}(Me_2Si\text{-}o\text{-}C_6H_4PPh_2)$*	28
	$Os_3(\mu\text{-H})(CO)_{10}(MeHSi\text{-}o\text{-}C_6H_4CH_2PPh_2)$*	28
	$Os_3(\mu\text{-H})(CO)_{10}(MeHSiCH_2\text{-}o\text{-}C_6H_4PPh_2)$	28
	$Os_3(\mu\text{-H})(CO)_{10}[dppm\text{-}P][Si(OR)_3]$ [R = Me, Et]	27
	$Os_3(\mu\text{-H})(CO)_{10}[dppe\text{-}P][Si(OR)_3]$ [R = Me, Et*]	27
	$Os_3(\mu\text{-H})_3(CO)_8(Me_2Si\text{-}o\text{-}C_6H_4CH_2PPh_2)$*	28
	$Os_3(\mu\text{-H})_3(CO)_8(MeHSiCH_2\text{-}o\text{-}C_6H_4PPh_2)$	28
	$HOs_3(\mu\text{-H})_2(CO)_{10}(SiPh_2H)$*	35
	$Os_3(\mu\text{-H})(CO)_{11}(SiR_3)$ [R = OMe, OEt, Et; R_3 = Ph_2H, $(o\text{-}BrC_6H_4CH_2)Me_{2-n}H_n$ (n = 0, 1, 2)]	23-25
	$Os_3(\mu\text{-H})(CO)_{11}(GeRPh_2)$ [R = Ph, Me]	26
	$HOs_3(CO)_{11}(SnR_3)$ [R = Ph, Bu^n]	26,40
	$Os_3(CO)_{11}[Si(OEt)_3]$ [NHEt_3]	23,24
	{$Os_3(CO)_9(dppe)$}(μ-	27
	dppe){$Os_3H(CO)_{10}[Si(OEt)_3]$}	27
	{$Os_3(\mu\text{-H})(CO)_{10}Si(OR)_3$}$_2$[$\mu$-dppe] [R = Me*, Et]	
(b) 	$Os_3(\mu\text{-H})_2(CO)_{10}(SiPh_3)_2$	34
	$Os_3(\mu\text{-H})_2(CO)_{10}(C_5H_4NSiMe_2)_2$*	25
	$Os_3(\mu\text{-H})_2(CO)_{10}(SnMe_3)_2$*	35
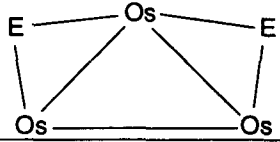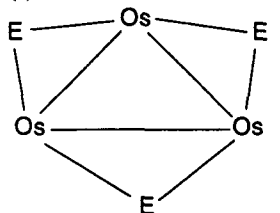
---

* Compounds that have been characterised by X-ray crystallography are marked by an asterisk (*).

Table I.3 continued.

Metal Skeleton Type	Compound*	Ref.
(c)	$Os_3(\mu\text{-H})_3(CO)_9(SiRCl_2)_3$ [R = Me*, Cl*]	14,15
(d)	$Os_3(CO)_8(MeO_2CCH_2CO_2Me)Sn[CH(SiMe_3)_2]_2$*	44
	$Os_3(\mu\text{-H})_2(CO)_9\text{-}$	44
	$[Sn(CH\{SiMe_3\}_2)(OCCH\{SiMe_3\}_2)]$*	36
	$Os_3(\mu\text{-H})_2(CO)_{10}Sn\{CH[SiMe_3]_2\}_2$*	37
	$Os_3(\mu\text{-H})(CO)_{10}Sn[C(SiMe_3)_2C_5H_4N\text{-}2]$*	
(e)	$Os_3(CO)_{11}(\mu\text{-CH}_2)(SnCl_2)$*	38
(f)	$Os_4(\mu\text{-H})(CO)_{14}(SiR_3)$	
	$\qquad$ [R$_3$ = Me$_3$, Me$_2$Ph, MePh$_2$, Ph$_3$, Ph$_2$H]	22
	$Os_4(\mu\text{-H})(CO)_{14}(GePh_3)$	22
	$Os_4(\mu\text{-H})(CO)_{14}(SnR_3)$ [R = Me*, Ph]	22
(g)	$[(OC)_3Os(\mu\text{-EMe}_2)EMe_3]_2$ (E = Si, Ge)	13,17

Table I.3 continued.

Metal Skeleton Type	Compound*	Ref.
(h) E——Os——E \ / \ / Os————Os	$Os_3(CO)_8[Sn\{CH(SiMe_3)_2\}_2]_2(\mu\text{-dppm})$* $Os_3(CO)_9(\mu\text{-CO})[Sn\{CH(SiMe_3)_2\}_2]_2$*	39 29
(i) E——Os——E \ / \ / Os————Os \ / E	$[(OC)_3OsEMe_2]_3$ [E = Si, Ge]	13,17

Once a representative of a structural type has been crystallographically characterised, other compounds of that class can therefore often be identified by a comparison of the ν(CO) patterns. Furthermore, this procedure can also be applied to compounds which have known Fe or Ru analogues. For example, the structures of the clusters in the classes (II), III(g) and III(i) of Table I.3 were based on the similarity in patterns of their ν(CO) to the Fe or Ru analogues [48]. This can be very useful as iron-group 14 chemistry has been more extensively explored; but the difference in iron and osmium chemistry is often reflected in the many differences in cluster types that are exhibited. Thus the cluster type III(i) is not known in iron chemistry, while the iron cluster $Sn[Fe(CO)_4]_4$ [49], which has the Sn atom bonded to four Fe atoms, has no known Ru or Os analogue.

---

* Compounds that have been characterised by X-ray crystallography are marked by an asterisk (*).

Table I.4.   Carbonyl absorptions for some $Os_3(\mu\text{-H})(CO)_{10}(L)(ER_3)$ clusters.

Cluster	$v(CO)$ in hydrocarbons, cm^{-1}	Ref.
$Os_3(\mu\text{-H})(CO)_{10}(CH_3CN)[Si(OMe)_3]$	2104m 2066vs 2042vs 2022vs 2009s 2001vs 1989vs 1977m	31
$Os_3(\mu\text{-H})(CO)_{10}(CH_3CN)[Si(OEt)_3]$	2103m 2065vs 2041vs 2021vs 2008s 2000vs 1988vs 1976m	32
$Os_3(\mu\text{-H})(CO)_{10}(CH_3CN)(SiEt_3)$	2098m 2060vs 2031s 2015s 1995s 1980m 1951w,sh*	23
$Os_3(\mu\text{-H})(CO)_{10}(CH_3CN)[SiPh_2H]$	2102m 2064s 2038s 2018s 2001s 1986ms*	23
$Os_3(\mu\text{-H})(CO)_{10}(CH_3CN)(GePh_3)$	2102m 2065s 2038s 2020s 2005s 1990m*	26
$Os_3(\mu\text{-H})(CO)_{10}(CH_3CN)(SnPh_3)$	2102m 2066s 2040s 2020s 2003s 1987m*	26
$Os_3(\mu\text{-H})(CO)_{10}(PPh_3)[SiMe_2(o\text{-}BrC_6H_4CH_2)]$	2104w 2060m 2038m 2019s 2000m 1985ms*	25
$Os_3(\mu\text{-H})(CO)_{10}(Me_2SiCH_2\text{-}o\text{-}C_6H_4PPh_2)$	2102m 2057ms 2037s 2017vs 2008m 1995m 1978m	28
$Os_3(\mu\text{-H})(CO)_{10}(Me_2Si\text{-}o\text{-}C_6H_4PPh_2)$	2103m 2059ms 2036s 2021vs 2006ms 1995s 1980m 1962w	28
$Os_3(\mu\text{-H})(CO)_{10}(MeHSiCH_2\text{-}o\text{-}C_6H_4PPh_2)$	2104w 2057m 2038m 2018vs 2008m 1996s 1980m	28
$Os_3(\mu\text{-H})(CO)_{10}(MeHSi\text{-}o\text{-}C_6H_4CH_2PPh_2)$	2104mw 2058m 2038ms 2021s 2007m 1996ms 1981m	28
$Os_3(\mu\text{-H})(CO)_{10}[dppm\text{-}P][Si(OMe)_3]$	2106w 2063m 2042s 2020vs 2009m,sh 2001s 1987w	27
$Os_3(\mu\text{-H})(CO)_{10}[dppm\text{-}P][Si(OEt)_3]$	2106w 2063m 2041s 2024s,sh 2020vs 2000s 1985m 1973w 1967w	27
$Os_3(\mu\text{-H})(CO)_{10}[dppe\text{-}P][Si(OMe)_3]$	2106w 2063m 2042s 2020vs 2010m,sh 2001s 1987w 1983w	27
$Os_3(\mu\text{-H})(CO)_{10}[dppm\text{-}P][Si(OEt)_3]$	2106mw 2063m 2041ms 2021vs 2010m,sh 2000ms 1986mw 1982w,sh 1973w	27
$\{Os_3(\mu\text{-H})(CO)_{10}Si(OMe)_3\}_2[\mu\text{-}dppe]$	2107mw 2063m 2041s 2021vs 2001m*	27
$\{Os_3(\mu\text{-H})(CO)_{10}Si(OEt)_3\}_2[\mu\text{-}dppe]$	2107m 2063ms 2050m,sh 2043s 2022vs 2003ms 1988m	27

*In dichloromethane.

17

Metal-hydrides are generally not located in X-ray crystallographic studies of cluster compounds. One useful tool for calculating metal hydrides positions in a crystallographically determined structure is Orpen's HYDEX program [50]. This program calculates potential energies, based on steric and bonding considerations, for possible hydride locations on a crystallographically determined structure. Despite the rather crude assumptions made, it has been shown to work very well [22,50,51].

The difficulty of directly locating metal-hydrides by X-ray crystallography has made ^{1}H NMR spectroscopy a most important tool for the study of metal hydride compounds. Assignment of the position and bonding mode of the hydride by NMR spectroscopy is, however, not always straightforward. It has been observed in osmium carbonyl chemistry that terminal hydrides are generally found at lower field than bridging hydrides; resonances for terminal hydrides occur at ca. -10 ppm. For the clusters in this review, resonances for a single hydride bridging an Os-Os edge have been reported in the range from ca. -12 to -20 ppm (Table I.5). The -9.2 ppm reported for $Os_3(\mu-H)_2(CO)_{10}Sn\{CH[SiMe_3]_2\}_2$ [36] is also consistent with a terminal OsH, barring no other reported data to suggest otherwise, although the -9.5 ppm signal for this cluster was unambiguously assigned to a hydride bridging an Os-Sn edge. Note that this also lies in the terminal OsH region; consistent with observations made on related SiH systems [52]. There is, however, an exception to these observations; the ^{1}H NMR resonances of complexes with the formally unsaturated $Os(\mu-H)_2Os$ linkage occur in the terminal region (in the -7 to -13 ppm range for the clusters listed in Table I.5). These linkages are now regarded as 3-centre-2-electron bonds [4a], although they may be treated as containing an Os=Os double bond for conventional electron-counting purposes.

Table I.5.   Chemical shifts of metal hydrides for some clusters.

Cluster	OsHOs	OsH$_2$Os	Ref.
HOs$_2$(CO)$_8$(SnCl$_3$)		-9.55[1]	16
Os$_3$(μ-H)(CO)$_7$(PMe$_2$Ph)(μ_3-S)(μ_3-η^2-SCH$_2$)(SnMe$_3$)	-16.30		47
Os$_3$(μ-H)(CO)$_9$[μ_3-η^3-Si(OEt)$_3$]	-13.38		24
Os$_3$(μ-H)$_3$(CO)$_9$(SiPh$_3$)	-12.29	-8.58,-12.42	34
Os$_3$(μ-H)$_3$(CO)$_9$[Si(o-BrC$_6$H$_4$CH$_2$)Me$_2$]	-12.60[2]	-8.24,-12.91	25
Os$_3$(μ-H)(CO)$_{10}$[μ-η^2-Si(OMe)$_3$]	-15.36		24
Os$_3$(μ-H)(CO)$_{10}$[μ-η^2-Si(OEt)$_3$]	-15.33		24
Os$_3$(μ-H)(CO)$_{10}$(CH$_3$CN)[Si(OMe)$_3$]	-16.56		23
Os$_3$(μ-H)(CO)$_{10}$(CH$_3$CN)[Si(OEt)$_3$]	-16.38		23
Os$_3$(μ-H)(CO)$_{10}$(CH$_3$CN)[SiEt$_3$]	-16.44		23
Os$_3$(μ-H)(CO)$_{10}$(CH$_3$CN)[SiPh$_2$H]	-16.09		23
Os$_3$(μ-H)(CO)$_{10}$(CH$_3$CN)[Si(o-BrC$_6$H$_4$CH$_2$)Me$_2$]	-16.23		25
Os$_3$(μ-H)(CO)$_{10}$(CH$_3$CN)[Si(o-BrC$_6$H$_4$CH$_2$)MeH]	-16.40		25
Os$_3$(μ-H)(CO)$_{10}$(CH$_3$CN)(GePh$_3$)	-16.1		26
Os$_3$(μ-H)(CO)$_{10}$(CH$_3$CN)(SnPh$_3$)	-16.4		26
Os$_3$(μ-H)(CO)$_{10}$(PPh$_3$)[SiMe$_2$(o-BrC$_6$H$_4$CH$_2$)]	-18.95		25
Os$_3$(μ-H)(CO)$_{10}$(Me$_2$SiCH$_2$-o-C$_6$H$_4$PPh$_2$)	-19.20		28
Os$_3$(μ-H)(CO)$_{10}$(Me$_2$Si-o-C$_6$H$_4$PPh$_2$)	-19.49		28
Os$_3$(μ-H)$_3$(CO)$_8$(Me$_2$Si-o-C$_6$H$_4$CH$_2$PPh$_2$)	-12.70	-7.90,-11.62	28
Os$_3$(μ-H)$_3$(CO)$_8$(MeHSi-o-C$_6$H$_4$CH$_2$PPh$_2$)	-12.63	-8.00,-11.86	28
HOs$_3$(μ-H)$_2$(CO)$_{10}$(SiPh$_2$H)	-17.35,-17.5	-9.4[1]	35

[1]Terminal OsH.

[2]Assignments based on cluster above; not given in original paper.

Table I.5 continued.

Cluster	OsHOs	Ref.
$Os_3(\mu\text{-H})(CO)_{10}(MeHSi\text{-}o\text{-}C_6H_4CH_2PPh_2)$	-19.72	28
$Os_3(\mu\text{-H})(CO)_{10}[dppm\text{-}P][Si(OMe)_3]$	-19.12	27
$Os_3(\mu\text{-H})(CO)_{10}[dppm\text{-}P][Si(OEt)_3]$	-19.01	27
$Os_3(\mu\text{-H})(CO)_{10}[dppe\text{-}P][Si(OMe)_3]$	-19.32	27
$Os_3(\mu\text{-H})(CO)_{10}[dppe\text{-}P][Si(OEt)_3]$	-19.22	27
$Os_3(\mu\text{-H})(CO)_{11}[Si(OMe)_3]$	-18.32	23
$Os_3(\mu\text{-H})(CO)_{11}[Si(OEt)_3]$	-18.32	23
$Os_3(\mu\text{-H})(CO)_{11}(SiEt_3)$	-18.76	23
$Os_3(\mu\text{-H})(CO)_{11}(SiPh_2H)$	-18.52	23
$Os_3(\mu\text{-H})(CO)_{11}[Si(o\text{-}BrC_6H_4CH_2)Me_2]$	-18.57	25
$Os_3(\mu\text{-H})(CO)_{11}[Si(o\text{-}BrC_6H_4CH_2)MeH]$	-18.76	25
$Os_3(\mu\text{-H})(CO)_{11}[Si(o\text{-}BrC_6H_4CH_2)H_2]$	-18.93	25
$Os_3(\mu\text{-H})(CO)_{11}(GePh_3)$	-18.4	26
$Os_3(\mu\text{-H})(CO)_{11}(GeMePh_2)$	-18.5	26
$Os_3(\mu\text{-H})(CO)_{11}(SnPh_3)$	-18.6	40
$Os_3(\mu\text{-H})(CO)_{11}(SnBu^n_3)$	-18.5	40
$\{Os_3(CO)_9(dppe)\}(\mu\text{-dppe})\{Os_3(\mu\text{-H})(CO)_{10}[Si(OEt)_3]\}$	-19.14	27
$\{Os_3(\mu\text{-H})(CO)_{10}Si(OMe)_3\}_2[\mu\text{-dppe}]$	-19.18	27
$\{Os_3(\mu\text{-H})(CO)_{10}Si(OEt)_3\}_2[\mu\text{-dppe}]$	-19.05	27
$Os_3(\mu\text{-H})_2(CO)_{10}(SiPh_3)_2$	-16.48,-16.70	34
$Os_3(\mu\text{-H})(CO)_{10}(C_5H_4NSiMe_2)_2$	-19.61	25
$Os_3(\mu\text{-H})(CO)_{10}(SnMe_3)_2$	-17.6,-18.4	35

Table I.5 continued.

Cluster	OsHOs	Ref.
$Os_3(\mu\text{-}H)_3(CO)_9(SiCl_3)_3$	-17.20	14
$Os_3(\mu\text{-}H)_3(CO)_9(SiMeCl_2)_3$	-16.59	14
$Os_3(\mu\text{-}H)_2(CO)_9[Sn(CH\{SiMe_3\}_2)(OCCH\{SiMe_3\}_2)]$	-16.14,-19.60	44
$Os_3(\mu\text{-}H)_2(CO)_{10}Sn\{CH[SiMe_3]_2\}_2$	-9.2,-9.5[3]	36
$Os_4(\mu\text{-}H)(CO)_{14}(SiMe_3)$	-13.70	22
$Os_4(\mu\text{-}H)(CO)_{14}(SnMe_3)$	-14.11	22
$Os_4(\mu\text{-}H)(CO)_{14}(SnPh_3)$	-13.69	22

[3]Bridges OsSn bond.

Coupling of hydride resonances to other nuclei of spin ½ can at times be useful in the location of metal hydrides. For example, in $HOs_4(CO)_{14}(SnMe_3)$, a $^2J_{SnH}$ coupling of 34.5 Hz indicated that the hydride was attached to the same Os atom as the $SnMe_3$ group [22]. Couplings to ^{29}Si and ^{187}Os have also been used to assign hydride resonances, and it has been suggested that single hydride bridges have $^1J_{OsH} < 40$ Hz, while the $Os(H)_2Os$ unit has $^1J_{OsH} \geq 40$ Hz [34].

^1H NMR spectroscopy can also be useful for monitoring the fate of hydrocarbon fragments; a useful feature in observing the changes around a group 14-hydrocarbon moiety in OsE clusters. The other NMR-active nuclei of spin ½ that can be expected to be useful in studying OsE clusters include ^{13}C (1.1%), ^{29}Si (4.5%), $^{117,119}Sn$ (total of 15%) and ^{207}Pb (22%) (percentages in parentheses are natural abundances). The incorporation of ^{13}C-labelled carbonyls into osmium carbonyls can be readily achieved, and is routinely carried out in this laboratory for both characterisation and studies of dynamic processes. Use of the group 14 nuclei in studies of OsE clusters have not been reported, although Wrackmeyer has recently shown that ^{119}Sn NMR can be a very powerful method for probing the bonding about tin in some FeSn clusters [53].

3.   Structural features : Aren't they pretty !

A survey of the 30 structures reported (Table I.6) shows that the length of an Os-Os bond not bridged by a hydride ligand ranges from 2.831(2) Å in $Os_3(\mu\text{-}H)_3(CO)_8(Me_2Si\text{-}o\text{-}C_6H_4CH_2PPh_2)$ [28] to 3.057(1) Å in $Os_3(SnCl_2)(CO)_{11}(\mu\text{-}CH_2)$ [38], a 0.24 Å difference; the shorter Os-Os bond length of 2.817(2) Å in $Os_3(\mu\text{-}H)(CO)_9[\mu_3\text{-}\eta^3\text{-}Si(OEt)_3]$ [24] may be argued to be due to the effect of the OSi bridge. The rather short Os-Os bond length of 2.745(1) Å in the cluster $Os_3(CO)_8(S)_2[SSn(2,4,6\text{-}C_6H_2Pr^i_3)(2,4,6\text{-}C_6H_2[CH\{SiMe_3\}_2]_3)]$ [18] is, from electron-counting considerations, almost certainly due to double bond character in the Os-Os bond . As has been observed elsewhere [54], the presence of a bridging hydride tends to lengthen the Os-Os distance, while a doubly hydride-bridged Os-Os edge tends to be contracted. The same lengthening effect of a bridging hydride probably applies to Os-E bonds as well, though there is only one example of a hydride-bridged Os-E bond, in the cluster $Os_3(\mu\text{-}H)_2(CO)_{10}Sn\{CH[SiMe_3]_2\}_2$ [36]. In drawing correlations like those above, however, it is important to keep in mind the large degree of distortion that metal-metal bonds can tolerate [1,55]. For example, in the clusters $Os_2(CO)_8(Cl)(GeCl_3)$ [19] and $Os_3SnCl_2(CO)_{11}(\mu\text{-}CH_2)$ [38], where more than one crystallographically independent molecules were found in the crystal structures, chemically equivalent bonds were found to differ by as much as 8σ's (where σ is the estimated standard deviations in the bond parameters); these are almost certainly due to crystal packing forces.

Table I.6.   Some bond parameters for the metal skeleton.

Cluster	Os–Os	OsHOs	Os(H)₂Os	Os–E	Ref.
Os$_2$(CO)$_8$(Cl)(GeCl$_3$)	2.931(1) 2.927(2) 2.916(2)			2.430(3) 2.425(3) 2.418(3)	19
Os$_3$(CO)$_{12}$(SiCl$_3$)$_2$	2.9120(9)			2.377(3)	15
Os$_3$(μ-H)(CO)$_9$[μ$_3$-η^3-Si(OEt)$_3$]	2.817(2) 2.848(2)	2.965(1)		2.32(1)	24
Os$_3$(μ-H)$_3$(CO)$_8$(Me$_2$Si-o-C$_6$H$_4$CH$_2$PPh$_2$)	2.831(2)	3.000(2)	2.705(2)	2.432(6)	28
Os$_3$(μ-H)$_2$(CO)$_{10}$(C$_5$H$_4$NSiMe$_2$)$_2$	2.909(4) 2.915(4)		2.997(4)[1]	2.431(4) 2.434(4)	25
H$_3$Os$_3$(CO)$_9$(SiMeCl$_2$)$_3$		3.125(2) 3.155(2)		2.400(6) 2.420(5)	14
Os$_3$(μ-H)$_3$(CO)$_9$(SiMeCl$_2$)$_3$		3.123(3) 3.132(3) 3.133(3)		2.367(13) 2.389(12) 2.394(14)	15
Os$_3$(μ-H)$_3$(CO)$_9$(SiPh$_3$)	2.8550(4)	3.0103(4)	2.7079(4)	2.429(2)	25
Os$_3$(CO)$_{10}$[μ-C(H)C(H)Bu^t][Si(OMe)$_3$]	Not available			2.427(4)	31

[1] Assignment of hydride position is dubious (see text).

Table I.6 continued.

Cluster	Os-Os	OsHOs	Os-E	Ref.
$Os_3(\mu\text{-H})(CO)_{10}[\mu\text{-}\eta^2\text{-Si(OMe)}_3]$	2.844(1) 2.9134(9)	2.947(1)	2.412(5)	24
$Os_3(\mu\text{-H})(CO)_{10}(CH_3CN)[Si(OEt)_3]$	2.888(2) 2.894(3)	3.008(2)	2.39(1)	32
$Os_3(\mu\text{-H})(CO)_{10}(CH_3CN)[Si(o\text{-}BrC_6H_4CH_2)Me_2]$	2.886(2) 2.892(1)	2.991(1)	2.452(5)	25
$Os_3(\mu\text{-H})(CO)_{10}(PPh_3)[SiMe_2(o\text{-}BrC_6H_4CH_2)]$	2.888(2) 2.921(1)	3.031(2)	2.463(9)	25
$Os_3(\mu\text{-H})(CO)_{10}(Me_2SiCH_2\text{-}o\text{-}C_6H_4PPh_2)$	2.884(1) 2.915(1)	3.024(1)	2.444(4)	28
$Os_3(\mu\text{-H})(CO)_{10}(Me_2Si\text{-}o\text{-}C_6H_4PPh_2)$	2.885(1) 2.898(1)	3.019(1)	2.453(5)	28
$Os_3(\mu\text{-H})(CO)_{10}(MeHSi\text{-}o\text{-}C_6H_4CH_2PPh_2)$	2.884(1) 2.907(1)	3.036(1)	2.425(7)	28
$Os_3(\mu\text{-H})(CO)_{10}[dppe\text{-}P][Si(OEt)_3]$	2.890(1) 2.924(1)	3.030(1)	2.400(4)	27
$HOs_3(\mu\text{-H})_2(CO)_{10}(SiPh_2H)$	2.9383(6)	3.0347(5) 3.0369(4)	2.455(2)	35

24

Table I.6 continued.

Cluster	Os-Os	OsHOs	Os-E	Ref
{Os3(μ-H)(CO)10Si(OMe)3}2[μ-dppe]	2.896(1) 2.903(1)	3.049(1)	2.404(6)	27
Os3(CO)8(S)2[SSn(2,4,6-C6H2Pr^{i}3)(2,4,6-C6H2[CH(SiMe3)2]3]	2.745(1)		2.662(2)	18
Os3[CH(SiMe3)2]3(CO)7(PMe2Ph)(μ3-S)(μ3-η^2-SCH2)(SnMe3)	2.942(1)	2.957(1)	2.653(1)	47
Os3(CO)8(MeO2CCH2CO2Me)Sn[CH(SiMe3)2]2	Not available		2.676(1) 2.816(1)	44
Os3(μ-H)2(CO)9[Sn{CH(SiMe3)2}2{OCCH(SiMe3)2}]	2.895(0)	3.010(0) 3.072(3)	2.658(0)	44
Os3(μ-H)2(CO)10Sn{CH[SiMe3]2}2	2.908(2) 2.936(3)	2.984(3)	2.645(3) 2.855(3)[2]	36
Os3(μ-H)(CO)10Sn[C(SiMe3)2C5H4N-2]	2.891(4) 2.899(4)	3.001(4)	2.641(4) 2.642(4)	37
Os3(μ-H)2(CO)10(SnMe3)2	2.896(3)	3.021(3) 3.070(2)	2.696(4) 2.726(5)	35
Os4(μ-H)(CO)14(SnMe3)	2.810(1) 2.851(1) 2.875(1) 3.050(1)	2.807(1)	2.697(2)	22

[2]Hydride bridged.

Table I.6 continued.

Cluster	Os–Os	Os–E	∠OsSnOs	Ref.
$Os_3(CO)_{11}(\mu\text{-}CH_2)(SnCl_2)$	2.989(1)	2.636(2)	63.6(1)	38
	2.985(2)	2.641(2)	63.2(1)	
	3.050(1)	2.868(2)	68.1(1)	
	3.057(1)	2.886(2)	68.2(1)	
		2.800(2)		
		2.811(2)		
$Os_3(CO)_8[Sn\{CH(SiMe_3)_2\}_2]_2(\mu\text{-dppm})$	2.854(2)	2.651(2)	62.1(1)	39
	2.909(2)	2.649(3)	66.8(1)	
	3.048(2)	2.866(3)		
		2.873(3)		
$Os_3(CO)_9(\mu\text{-CO})[Sn\{CH(SiMe_3)_2\}_2]_2$	2.893(0)	2.727(7)	65.8(2)	29
	2.967(0)	2.732(7)	65.8(2)	
	2.981(0)	2.736(6)		
		2.753(7)		

26

In going through the data presented in Table I.6, two interesting anomalies present themselves. The first is the rather long $Os(\mu$-$H)_2Os$ bond reported for $Os_3(\mu$-$H)_2(CO)_{10}(C_5H_4NSiMe_2)_2$ [25]. Electron counting rules out a double bond for that Os-Os edge, so that it is not a 3-centre-2-electron $Os(\mu$-$H)_2Os$ bond. If the location of the hydrides were correct, it would be the first example of a doubly hydride-bridged single Os-Os bond. The bond lengths found in $Os_4(\mu$-$H)(CO)_{14}(SnMe_3)$ are unusual in that NMR studies clearly showed that the hydride bridged the shortest Os-Os edge [22]. This finding serves as a reminder that placing a hydride solely on bond length arguments can be fallacious.

The lower and upper limits for Os-E bonds in the OsE clusters are :

Os-Si   2.32(1) - 2.463(9) Å

Os-Ge   2.418(3) - 2.430(3) Å (one structure only)

Os-Sn   2.636(2) - 2.886(2) Å

Given the small sample, these figures should be treated as indicative only, but it is quite clear that the Os-Si and Os-Ge bond lengths are quite similar while the Os-Sn bond lengths are significantly longer. This is in good agreement with the covalent radii of the Group 14 elements, viz., 1.17, 1.22 and 1.40 Å for Si, Ge and Sn respectively [56]. The range of Os-Sn bonds is especially large, and some of the shorter bond lengths observed, for example those in the clusters $Os_3(\mu$-$H)(CO)_{10}Sn[C(SiMe_3)_2C_5H_4N$-$2]$ and $Os_3(\mu$-$H)_2(CO)_9[Sn\{CH(SiMe_3)_2\}\{OCCH(SiMe_3)_2\}]$, have been rationalised in terms of stannyne character in the Sn fragments [37,44], i.e., that there is some Os=Sn double bond character present. The data gathered here, however, indicates that the lower limit of ~2.64 Å is quite general; this may indicate that the tin atom in those cases is truly participating in cluster-type bonding, i.e., that the bonding to tin is of a delocalised nature.

It is also clear that the heavier group 14 elements allow much more distortion from tetrahedral geometry, i.e., the associated ring strains are much smaller than in analogous

carbon compounds. This is reflected by the number of OsE clusters in which E is in a μ_2 bonding mode; OsSnOs angles as small as 62° have been observed [39].

Table I.3 also shows that the OsE clusters known to date span tri-, tetra-, penta-, and hexametallic systems; no higher nuclearity clusters had been reported before this work. If the clusters in Table I.3 were reclassified according to nuclearity, we find that trimetallic systems are characterised by chains only; no triangular units have been reported. This is in contrast to the triosmium clusters where the triangular arrangement of the osmium atoms abound. Arrangements for the other nuclearities are given below (Fig. I.1), and it will be noticed that a common arrangement is where there is a "terminal" ER_3 group protruding from a more compact metal core - these are compounds where the ER_3 groups behave very much like a substituent and hence are probably least cluster-like in both bonding and reactivity [5c]. This point will be developed further in the following chapter.

Fig. I.1. Metal atom arrangements found for nuclearity 4, 5 and 6 in OsE clusters.

4. References

[1] Johnson, B. F. G. In *Transition Metal Clusters*; Johnson, B. F. G., Ed.; J. Wiley: Chichester, 1980; Chapter 1.

[2] Cotton, F. A. *Quarterly Reviews* **1966**, *20*, 389.

[3] (a) Muetterties, E. L. *J. Organomet. Chem.* **1980**, *200*, 177. (b) Muetterties, E. L.; Rhoden, T. N.; Band, E.; Brucker, C. F.; Pretzer, W. R. *Chem. Rev.*, **1979**, *79*, 91.

[4] See for example (a) Crabtree, R. H. *The Organometallic Chemistry of the Transition Metals*, 2nd ed.; J. Wiley: New York, 1994; Chapter 13. (b) Kaesz, H. D.; Shriver, D. F. In *The Chemistry of Metal Cluster Complexes*; Shriver, D. F.; Kaesz, H. D.; Adams, R. D., Eds.; VCH: New York, 1990; Chapter 1. (c) Moskovits, M. In *Metal Clusters*; Moskovits, M., Ed.; J. Wiley: New York, 1986; Chapter 1; and references therein.

[5] (a) Fehlner, T. P. *Chemtracts-Inorganic Chemistry*, **1992**, *4*, 1.
(b) *Inorganometallic Chemistry*; Fehlner, T. P., Ed.; Plenum: New York, 1992.
(c) Fehlner, T. P. In *Encyclopedia of Inorganic Chemistry*; King, R. B., Ed.; J. Wiley: Chichester, 1994; pp 1543-1555.

[6] Farrugia, L. J. *Adv. Organomet. Chem.*, **1990**, *31*, 301.

[7] Whitmire, K. H. *J. Coord. Chem.*, **1988**, *17*, 95.

[8] (a) Ho, B. Y. K.; Zuckerman, J. J. *J. Organomet. Chem.*, **1973**, *49*, 1. (b) Zubieta, J. A.; Zuckerman, J. J. *Prog. Inorg. Chem.*, **1978**, *24*, 251.
(c) Glockling, F. In *Chemistry of Tin*, Harrison, P. G., Ed.; Blackie: Glasgow-London, 1989; Chapter 8. (d) Holt, M. S.; Wilson, W. L.; Nelson, J. H. *Chem. Rev.*, **1989**, *89*, 11. (e) Bonny, A. *Coord. Chem. Rev.*, **1978**, *25*, 229. (f) Molloy, K. C. *Adv. Organomet. Chem.*, **1991**, *33*, 171. (g) Compton, N. A.; Errington, R. J.; Norman, N. C. *Adv. Organomet. Chem.*, **1990**, *31*, 91.

[9] Deeming, A. J. *Adv. Organomet. Chem.*, **1986**, *26*, 1.

[10] Nicholls, J. N.; Vargas, M. D. *Inorg. Synth.*, **1990**, *28*, 232.

[11]   Kaesz, H. D. *Inorg. Synth.*, **1990**, *28*, 238.

[12]   (a) Knox, S. A. R.; Stone, F. G. A. *J. Chem. Soc. A*, **1970**, 3147. (b) Pomeroy, R. K. *J. Organomet. Chem.*, **1981**, *221*, 323.

[13]   Brookes, A; Knox, S. A. R.; Stone, F. G. A. *J. Chem. Soc. A*, **1971**, 3469.

[14]   van Buuren, G. A.; Willis, A. C.; Einstein, F. W. B.; Peterson, L. K.; Pomeroy, R. K.; Sutton, D. *Inorg. Chem.*, **1981**, *20*, 4361.

[15]   Willis, A. C.; van Buuren, G. N.; Pomeroy, R. K.; Einstein, F. W. B. *Inorg. Chem.*, **1983**, *22*, 1162.

[16]   (a) Firfiray, D. B.; Irving, A.; Moss, J. R. *J. Chem. Soc., Chem. Commun.*, **1990**, 377. (b) Moss, J. R.; Graham, W. A. G. *J. Organomet. Chem.*, **1969**, *18*, P24. (c) Moss, J. R.; Graham, W. A. G. *J. Chem. Soc., Dalton Trans.*, **1977**, 89.

[17]   (a) Stone, F. G. A.; Howard, J.; Knox, S. A. R.; Woodward, P. *J. Chem. Soc. D*, **1970**, 1477. (b) Knox, S. A. R.; Stone, F. G. A. *J. Chem. Soc. A*, **1971**, 2874.

[18]   Tokitoh, N.; Matsuhashi, Y.; Okazaki, R. *Organometallics*, **1993**, *12*, 2894.

[19]   Einstein, F. W. B.; Pomeroy, R. K.; Rushman, P.; Willis, A. C. *J. Chem. Soc., Chem. Commun.*, **1983**, 854.

[20]   Rushman, P.; van Buuren, G. N.; Shirilian, M.; Pomeroy, R. K. *Organometallics*, **1983**, *2*, 693.

[21]   Pomeroy, R. K. *J. Organomet. Chem.*, **1990**, *383*, 387.

[22]   Lu, C. Y.; Einstein, F. W. B.; Johnston, V. J.; Pomeroy, R. K. *Inorg. Chem.*, **1989**, *28*, 4212.

[23]   Johnson, B. F. G.; Lewis, J.; Monari, M. *J. Chem. Soc., Dalton Trans.*, **1990**, 3525.

[24]   Adams, R. D.; Cortopassi, J. E.; Pompeo, M. P. *Inorg. Chem.*, **1992**, *31*, 2563.

[25]   Ang, H. G.; Chang, B.; Kwik, W. L.; Sim, E. S. H. *J. Organomet. Chem.*, **1994**, *474*, 153.

[26]   Burgess, K.; Guerin, C.; Johnson, B. F. G.; Lewis, J. *J. Organomet. Chem.*, **1985**, *295*, C3.

[27]   Johnson, B. F. G.; Lewis, J.; Monari, M.; Braga, D.; Grepioni, F.; Gradella, C. *J. Chem. Soc., Dalton Trans.*, **1990**, 2863.

[28]   Ang, H. G.; Chang, B.; Kwik, W. L. *J. Chem. Soc., Dalton Trans.*, **1992**, 2161.

[29]   Cardin, C. J.; Cardin, D. J.; Lawless, G. A.; Power, J. M.; Power, M. B.; Hurthouse, M. B. *J. Organomet. Chem.*, **1987**, *325*, 203.

[30]   Wang, W.; Einstein, F. W. B.; Pomeroy, R. K. *J. Chem. Soc., Chem. Commun.*, **1992**, 1737.

[31]   Adams, R. D.; Cortopassi, J. E.; Pompeo, M. P. *Organometallics*, **1992**, *11*, 1.

[32]   Adams, R. D.; Cortopassi, J. E.; Pompeo, M. P. *Inorg. Chem.*, **1991**, *30*, 2960.

[33]   Ramadan, R. M.; Pomeroy, R. K., Simon Fraser University, unpublished results.

[34]   Willis, A. C.; Einstein, F. W. B.; Ramadan, R. M.; Pomeroy, R. K. *Organometallics*, **1983**, *2*, 935.

[35]   Einstein, F. W. B.; Pomeroy, R. K.; Willis, A. C. *J. Organomet. Chem.*, **1986**, *311*, 257.

[36]   Cardin, C. J.; Cardin, D. J.; Parge, H. E.; Power, J. M. *J. Chem. Soc., Chem. Commun.*, **1984**, 609.

[37]   Cardin, C. J.; Cardin, D. J.; Convery, M. A.; Devereux, M. M. *J. Chem. Soc., Chem. Commun.*, **1991**, 687.

[38]   Viswanathan, N.; Morrison, E. D.; Geoffroy, G. L.; Geib, S. J.; Rheingold, A. L. *Inorg. Chem.*, **1986**, *25*, 3100.

[39]   Bartlett, R. A.; Cardin, C. J.; Cardin, D. J.; Lawless, G. A.; Power, J. M.; Power, P. P. *J. Chem. Soc., Chem. Commun.*, **1988**, 312.

[40]   Johnson, B. F. G.; Lewis, J.; Whitton, A. J.; Bott, S. G. *J. Organomet. Chem.*, **1990**, *389*, 129.

[41]   George, R. D.; Knox, S. A. R.; Stone, F. G. A. *J. Chem. Soc., Dalton Trans.*, **1973**, 972.

[42]   Collman, J. P.; Murphy, D.W.; Fleischer, E.B.; Swift, D. *Inorg. Chem.*, **1974**, *13*, 1.

[43]   Lewis, J.; Moss, J. R. *Can. J. Chem.*, in press.

[44]   Cardin, C. J.; Cardin, D. J.; Power, J. M.; Hurthouse, M. B. *J. Am. Chem. Soc.*, **1985**, *107*, 505.

[45]   Knox, S. A. R.; Phillips, R. P.; Stone, F. G. A. *J. Chem. Soc., Dalton Trans.*, **1976**, 552.

[46]   Becalska, A.; Pomeroy, R. K.; Graham, W. A. G. *Can. J. Chem.*, **1989**, *67*, 1236.

[47]   Adams, R. D.; Katahira, D. A. *Organometallics*, **1982**, *1*, 460.

[48]   (a) King, R. B.; Stone, F. G. A. *J. Am. Chem. Soc.*, **1960**, *82*, 3833. (b) Brooks, E.; Elder, M.; Graham, W. A. G.; Hall, D. *J. Am. Chem. Soc.*, **1968**, *90*, 3587. (c) Watkins, S. F. *J. Chem. Soc. A*, **1969**, 1552. (d) Howard, J.; Woodward, P. *J. Chem. Soc. A*, **1971**, 3648 .

[49]   (a) Lindley, P. F.; Woodward, P. *J. Chem. Soc. A*, **1967**, 382. (b) Cotton, J. D.; Knox, S. A. R.; Paul, I.; Stone, F. G. A. *J. Chem. Soc. A*, **1967**, 264.

[50]   Orpen, A. G. *J. Chem. Soc., Dalton Trans.*, **1980**, 2509.

[51]   Wang, W. Ph.D. Thesis, Simon Fraser University, 1994.

[52]   Schubert, U. *Adv. Organomet. Chem.*, **1990**, *30*, 151.

[53]   Wrackmeyer, B.; Distler, B.; Herberhold, M. *Z. Naturforsch.*, B, **1992**, *47*, 1749.

[54]   Leong, W. K. M.Sc. Thesis, National University of Singapore, 1992.

[55]   Pomeroy, R. K. In *Comprehensive Organometallic Chemistry II*; M.I. Bruce, Ed.; 1995; Chapter 15, in press.

[56]   Cotton, F. A.; Wilkinson, G. *Advanced Inorganic Chemistry*, 5th ed.; J. Wiley: New York, 1988; p 266.

Chapter II   Rationale and Results : Going for OsE clusters.

There are examples in the chemistry of tetraosmium and -ruthenium clusters containing phosphorus in which the phosphorus atom, from the point of electron counting at least, should be regarded as part of the cluster framework. Figure II.1 illustrates the increasing ambiguity in the rôle of the phosphorus fragment as we move through from $Os_4(CO)_{14}(PR_3)$ to $Ru_4(CO)_{11}(PPh)_2$; the cluster geometries predicted on the basis of the phosphorus atom as a ligand, or as part of the cluster core, are given against each cluster. In the cluster $Os_4(CO)_{14}(PR_3)$, the phosphine is most certainly considered simply
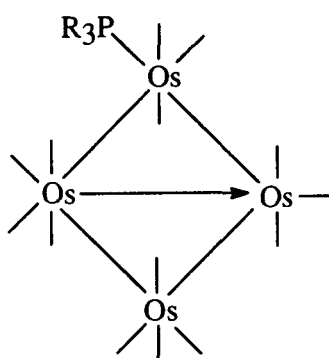
Obeys EAN/PSEPT rule
R_3P is ligand
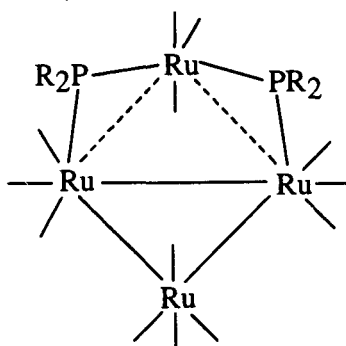
Ligand : 64 e = "square"
Cluster : 72 e, 10 CBP = *hypho* 9-vertex polyhedron
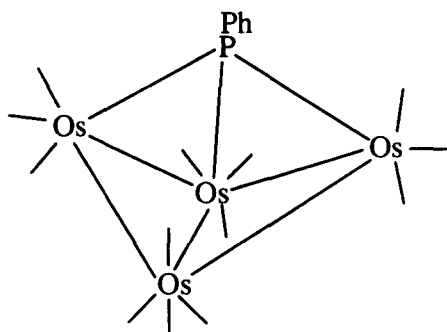
Ligand : 62 e = "butterfly"
Cluster : 64 e or 7 CBP = *nido* octahedron
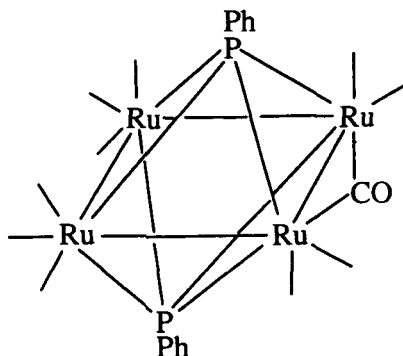
Ligand : 62 e = "butterfly"
Cluster : 66 e, 7 CBP = closo octahedron

Fig. II.1. Progression of the phosphorus fragment from ligand to cluster core [2].

34

as a ligand, while the face-capping phosphinidenes in the cluster $Ru_4(CO)_{11}(PPh)_2$ must be considered as part of the cluster core if the electron count were to satisfy polyhedral skeleton electron pair theory (PSEPT) [1].

There is thus precedence for main group atoms occupying and behaving, at least with respect to electron-count, as a cluster vertex. Such examples in osmium-group 14 clusters, or even group 8-group 14 for that matter, is almost non-existent; this is in large part due to the very sparse amount of data currently available. The question that comes to mind is how extensive such occurrences are and what are suitable criteria, if any, upon which the question of whether a main-group atom is participating in cluster bonding with transition-metals, is to be settled. Furthermore, the question also arises as to whether such clusters exhibit different chemistry from their parent element homonuclear clusters.

What follows in the rest of this chapter is an account of the course the research took, the thoughts that when into it, and the results that were obtained. Discussions of the chemical and structural aspects of the study are given in the two chapters following. One of the reasons for this choice of an unconventional presentation of the study has been given in the foreword. The other was that the results were so interlinked that there was, on the one hand, little merit in trying to divide them into chapters along the lines, for example, of different group 14 elements or substituents, and on the other, much to recommend a holistic consideration of the chemistry and structures. This latter point will become apparent in the discussion chapters.

1. Decarbonylation of $[(OC)_4OsSnMe_2]_2$: Towards an isolobal analogue of $Os_4(CO)_{15}$

The initial impetus for our work was along the lines outlined above, but with a rather narrower scope, namely, the attempted synthesis of an isolobal* analogue of the tetraosmium cluster $Os_4(CO)_{15}$ [3]. Interest in this cluster lies in its bonding which, in valence bond terms, can be described as possessing either a single donor-acceptor metal-metal bond (Fig. II.2a), or peripheral metal-metal bonds with bond orders of ½ and 1½ (Fig. II.2b).

(a)   (b)
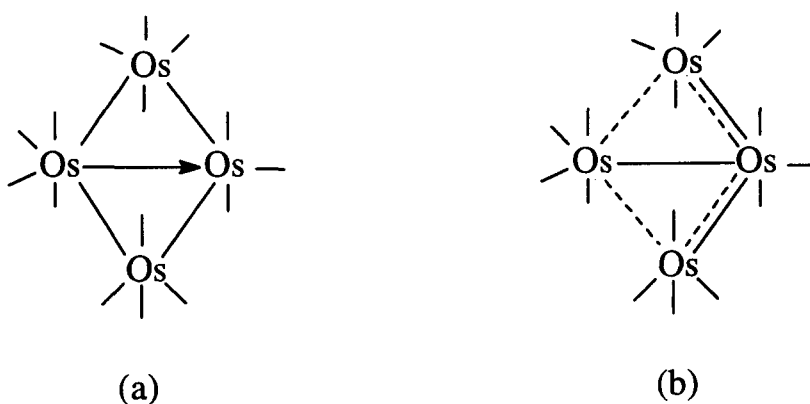
Fig. II.2.   Alternative bonding descriptions for $Os_4(CO)_{15}$.

Both bonding descriptions are interesting in their own right, and the idea suggested itself that it would be interesting to investigate the possibility of synthesizing an isolobal analogue in which the two "wing-tip" $Os(CO)_4$ units were replaced by ER_2 units (E = group 14 element). Such a synthesis may conceivably be achieved according to the reaction given in Scheme II.1, which also shows the isolobal relationship between the proposed starting cluster $[(OC)_4OsER_2]_2$ and another unusual tetraosmium cluster $Os_4(CO)_{16}$ [5]. Routes to $[(OC)_4OsER_2]_2$ had previously been reported for E = Sn and R = Me, Bu^n, Ph [6, 7].

---

* Two fragments are isolobal if they have the same number of frontier orbitals with similar extents in space, and energies, and they have the same occupancies and symmetry properties [4].

The first starting cluster studied was $[(OC)_4OsSnMe_2]_2$, **1(SnMe)**, which was prepared by the action of $[Os(CO)_4]^{2-}$ on Me_2SnCl_2 in THF as previously reported [6]. The yields we obtained were in the 40-60 % range and, as noted earlier, somewhat lower than expected for a salt elimination reaction. The compound was usually isolated as slightly yellow crystals after filtration through silica and crystallisation from hexane, although they satisfactorily passed analytical and spectroscopic examinations. Colourless samples may be obtained by chromatographic separation on silica, although such samples do yellow on prolonged exposure to light.
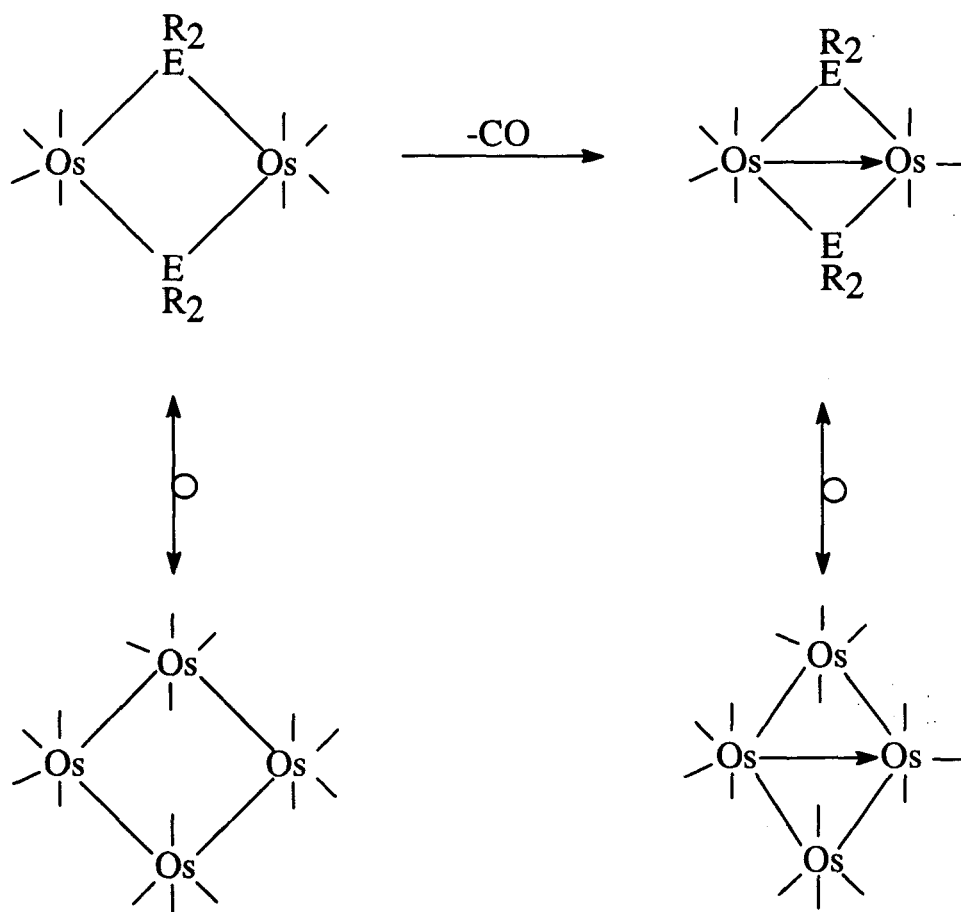
Scheme II.1. Proposed synthesis and isolobal relationships for "$Os_2(CO)_7(ER_2)_2$".

Our next step involved the decarbonylation of **1(SnMe)**. A number of methods exist for decarbonylation in transition metal carbonyl chemistry, and we attempted the three most commonly used methods, viz., photolysis, pyrolysis and chemical activation, with very different and surprising results.

It has been shown that photolysis of the iron analogues $[(OC)_4FeER_2]_2$ (E = Si, Ge, Sn) leads to the compounds $[(OC)_3FeER_2]_2(\mu$-CO), which have been viewed as isolobal analogues of $Fe_2(CO)_9$ in which two of the bridging COs have been replaced by bridging ER_2 groups [8]. Bridging carbonyls are, however, much less common in osmium chemistry, and we had hoped that that would disfavour formation of a compound with an analogous structure in the case of **1(SnMe)**, and hence allow attainment of the desired product.

Indeed, on the photolysis of **1(SnMe)** in hexane, a yellow powder precipitated. This powder has very low solubility in most of the common solvents; a characteristic of some of the $[(OC)_3FeER_2]_2(\mu$-CO) compounds obtained. Absence of a bridging carbonyl vibration in the IR spectrum of the yellow powder, together with a satisfactory elemental analysis, led us initially to believe that we had indeed achieved our goal of synthesizing $Os_2(CO)_7(SnMe_2)_2$. Its mass spectrum showed the heaviest cluster of peaks centered at m/z 874, in accord with that calculated for $Os_2(CO)_7(SnMe_2)_2$. It thus came as a great surprise when it turned out, on examination by X-ray crystallography, that the product was twice as large and has the metal skeleton shown in Fig. II.3!
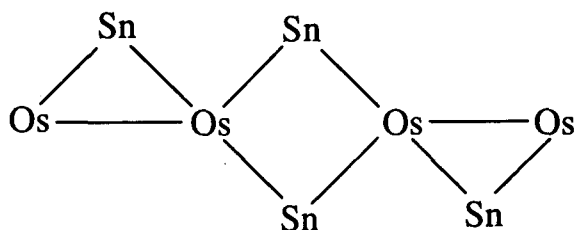
Fig. II.3.   Metal skeleton of $[Os_2(CO)_7(SnMe_2)_2]_2$, **6.**

The anomaly in the mass spectrum may be ascribed to the fact that the spectrometer has an upper limit of 1000 amu; but more importantly, it suggested that $[Os_2(CO)_7(SnMe_2)_2]_2$, **6**, may behave as a dimeric form of $Os_2(CO)_7(SnMe_2)_2$, i.e., that the Os-Sn bonds in its central 4-membered ring are weak. As we shall see later, this is borne out by both the X-ray structural study (Section IV.3) and its chemistry (Sections II.5 and III.3).

Pyrolysis is generally not a very selective decarbonylation method, usually giving rise to a large number of products: condensation to higher nulearity clusters often occurs. At times, however, careful pyrolysis can lead to stepwise decarbonylation, as in the stepwise transformation of $Os_5(CO)_{19}$ to $Os_5(CO)_{18}$ and finally $Os_5(CO)_{16}$ [9]. The cluster **1(SnMe)** proved to be thermally rather robust, showing signs of transformation only above about 120 °C. The major product was a more condensed cluster, $[(OC)_3OsSnMe_2]_3$, **5(Sn)**. Its identity was fairly easily established by comparison of its IR spectrum in the carbonyl stretching region with that of the known clusters $[(OC)_3RuSnMe_2]_3$ and $[(OC)_3OsGeMe_2]_3$ [10]. The structure of **5(Sn)** was also confirmed by X-ray crystallography; a view of the metal skeleton is shown in below (Fig. II.4).
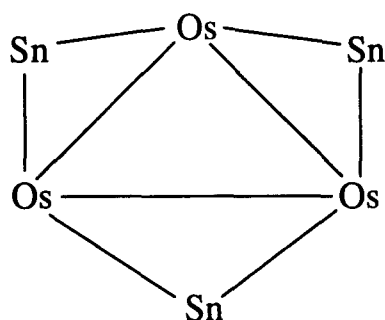
Fig. II.4.   Metal skeleton of $[(OC)_3OsSnMe_2]_3$, **5(Sn)**.

Chemical activation using Me_3NO has been proven to be a very powerful method for decarbonylation in osmium carbonyl clusters. The Me_3NO acts as an O-atom transfer

reagent to remove a CO ligand as CO_2. Unfortunately, this reagent proved unsuitable for **1(SnMe)**: Monitoring of the reaction by IR spectroscopy showed that the reaction was very complex, giving many intermediates and products throughout the course of the reaction. The only isolable product was obtained in very low yield through fractional crystallisation. This product was characterised by elemental analysis, IR and ^{1}H NMR spectroscopy, and its structure confirmed by X-ray crystallography; its metal skeleton is shown in Fig. II.5. This product was stable enough for chromatography on silica, though it could not be separated cleanly from the starting cluster.
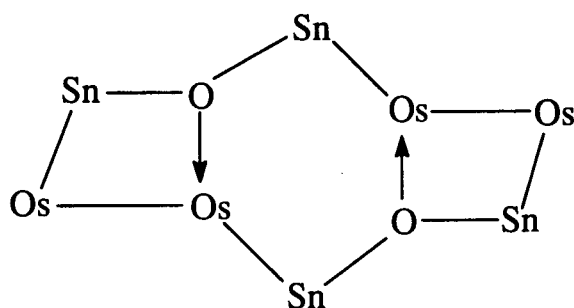
Fig. II.5.   Metal skeleton of $[Os_2(CO)_7O(SnMe_2)_2]_2$, **7**.

2. Germanium and lead analogues : Different reactivity ?

The diverse OsSn clusters obtained in the reactions above led naturally to the question as to whether analogous behaviour would be exhibited by the Si, Ge and Pb analogues. To begin with, the preparation of some of the starting clusters, viz., $[(OC)_4OsEMe_2]_2$ (E = Si, Ge, Pb), proved to be less than trivial. A number of attempts were made to prepare the Si analogue, including the reaction between $Na_2Os(CO)_4$ and Me_2SiCl_2 or $Os(CO)_4(SiMe_2Cl)_2$, and thermolyses and photolyses of $Os(CO)_5$ or $Os_3(CO)_{12}$ with Me_2SiH_2; all without success.

The Pb analogue, **1(PbMe)**, however, was prepared by salt elimination between $Na_2Os(CO)_4$ and Me_2PbCl_2, or by the pyrolysis of $Os(CO)_4(PbMe_3)_2$. It was obtained as dark-red, hexane-soluble, crystalline blocks which quickly decomposed to a brown, insoluble powder in the presence of light. UV irradiation of a hexane solution of **1(MePb)** precipitated a yellow-brown insoluble powder which has not been identified; the supernatant was colourless and an IR spectrum of it did not show any carbonyl-containing compound. An IR spectrum of the precipitate in nujol did not show the presence of any bridging carbonyls, nor did the pattern resemble that for $[Os_2(CO)_7(SnMe_2)_2]_2$. The rather low carbon content in its elemental analysis is consistent with loss of more than one CO per formula unit.

Preparation of the Ge analogue of **1(SnMe)** proved to be the most straightforward; the analogous salt elimination reaction between $Na_2Os(CO)_4$ and Me_2GeCl_2 gave the desired product in moderate yield. UV irradiation and pyrolysis of the cluster $[(OC)_4OsGeMe_2]_2$, **1(GeMe)**, however, proved to be quite different from the Sn analogue. UV irradiation of a hexane solution of $[(OC)_4OsGeMe_2]_2$ did not give a precipitate but resulted in the formation of a red solution. Chromatography of this (concentrated) solution gave two red bands on elution with hexane, both of which turned out to be mixtures. From the first band was isolated, after crystallisation, yellow-orange hexagonal prisms of the known cluster $[(OC)_3OsGeMe_2]_3$, **5(Ge)**, [10] and colourless

plates of a new cluster $Os_3(CO)_{11}(GeMe_2)_2$, **8**. The second band yielded another new cluster, $Os_4(CO)_{12}(GeMe_2)_4$, **9**, and at least one other unidentified product. Pyrolysis in hexane at 100 °C gave the same products, with **5(Ge)** as the major product, together with a very small yield of the known cluster $Os_2(CO)_6(GeMe_2)_3$, **10** [11]. The new clusters were characterised by IR and NMR spectroscopy, elemental analyses, and by X-ray crystallography. A view of their metal skeletons is shown in Figure II.6.

5(Ge)   **8**   **10**

(a)   **(b)**

9
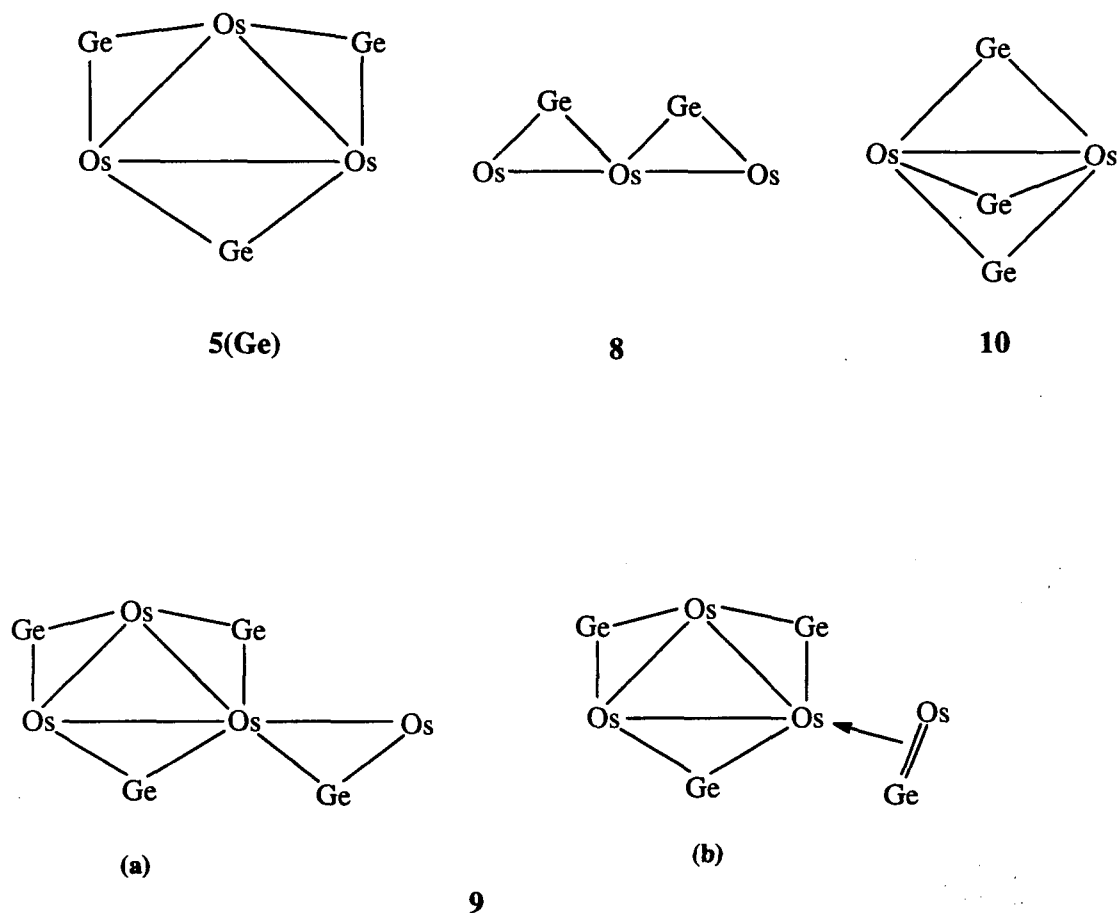
Fig. II.6.   Metal skeleton of clusters **5(Ge)**, **8**, **9** and **10**, including two

different bonding descriptions for **9**.

The cluster **9** can be viewed as a derivative of **5(Ge)** in which an equatorial carbonyl has been substituted with the germylene $Me_2Ge=Os(CO)_4$ (structure 9(b) in Fig. II.6). If this were so, then the germylene would be expected to rotate about its bond to the Os_3Ge_3 core, and the ^{1}H NMR signals due to the two $GeMe_2$ groups closer to the

germylene should become equivalent since the two groups are rendered equivalent by the rotation. Evidence for such an exchange was provided by a variable-temperature (VT) ^{1}H NMR study (Fig. II.7) and a ^{1}H NOESY experiment (Fig. II.8).

The VT ^{1}H NMR experiment showed that two of the CH$_3$ signals (the signals at 1.16 and 1.84 ppm) broadened as the temperature was raised, although coalescence was not achieved even at 353K; the spectra also showed development of new signals which may be attributed to either thermal decomposition or reaction with the solvent. Further indication that the broadening of the two peaks were due to exchange was provided by the observation of positive crosspeaks between them in the ambient temperature NOESY spectrum (Fig. II.8); exchange crosspeaks for small molecules are predicted to have the same phase as the diagonal peaks, while NOE crosspeaks should have the opposite phase [12]. As it turned out, this spectrum also showed a negative crosspeak betweeen the 1.16 and 1.26 ppm signals, indicating NOE and hence spatial proximity of the corresponding CH$_3$ groups. Consequently, all the ^{1}H signals could be assigned as shown in the inset of Figure II.8.

In the ^{13}C NMR spectra of osmium carbonyl clusters, it is generally observed that the resonances due to axial carbonyls occur downfield of the signals due to the equatorial carbonyls [13]. In the ^{13}C{^{1}H} spectrum of 9 (Fig. II.9), the relative intensities of the signals allowed partial assignment of the carbonyl signals to either equatorial or axial CO's and showed that the trend observed for osmium carbonyls breaks down for this cluster. For example, two resonances of intensity 1 (at δ 191.39 and 187.44), which must be due to equatorial carbonyls, are to lowest field whereas a resonance of intensity 2 (at δ 170.35), which must be due to an axial carbonyl, is at highest field. This reversal of trend is also observed in the cluster 5(Ge), so that assuming the reversal of trend is a general one for OsGe clusters, the three highest field signals (at δ 170.35, 178.77 and 180.31) may be assigned to the Os(CO)$_4$ unit.
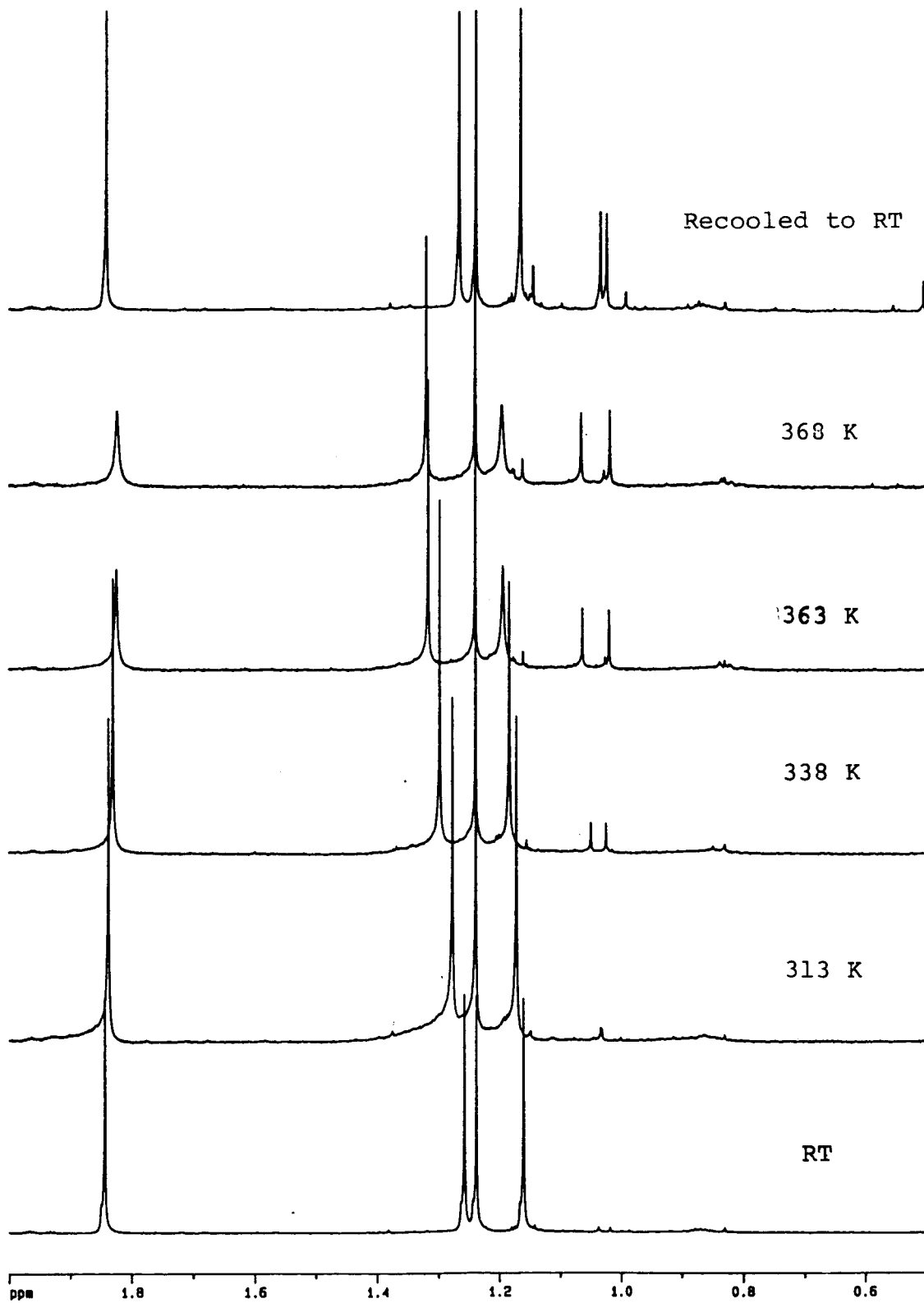
Fig. II.7.   VT ^{1}H NMR spectrum for cluster **9**.
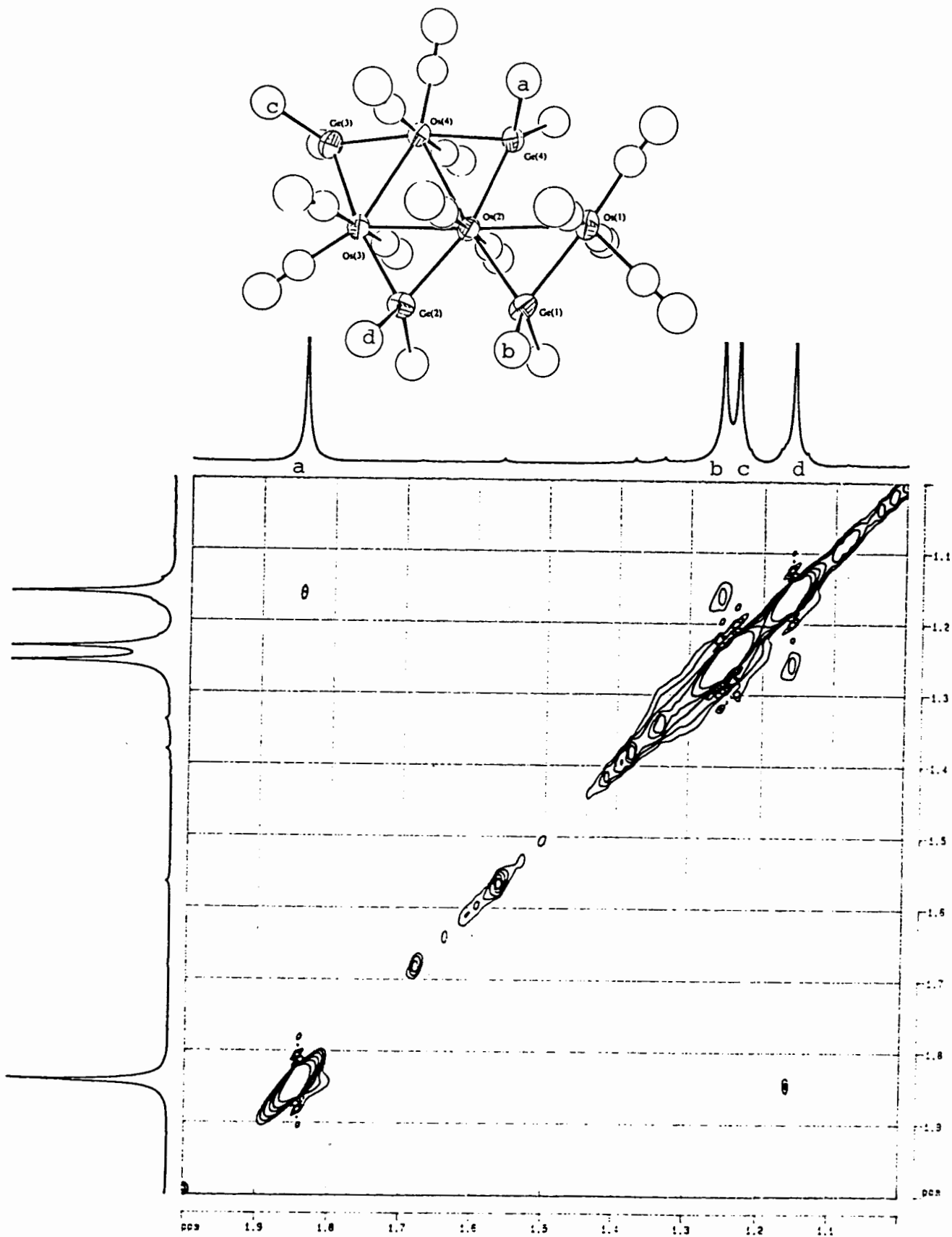
Fig. II.8.   NOESY spectrum and assignment (inset) for cluster **9**.
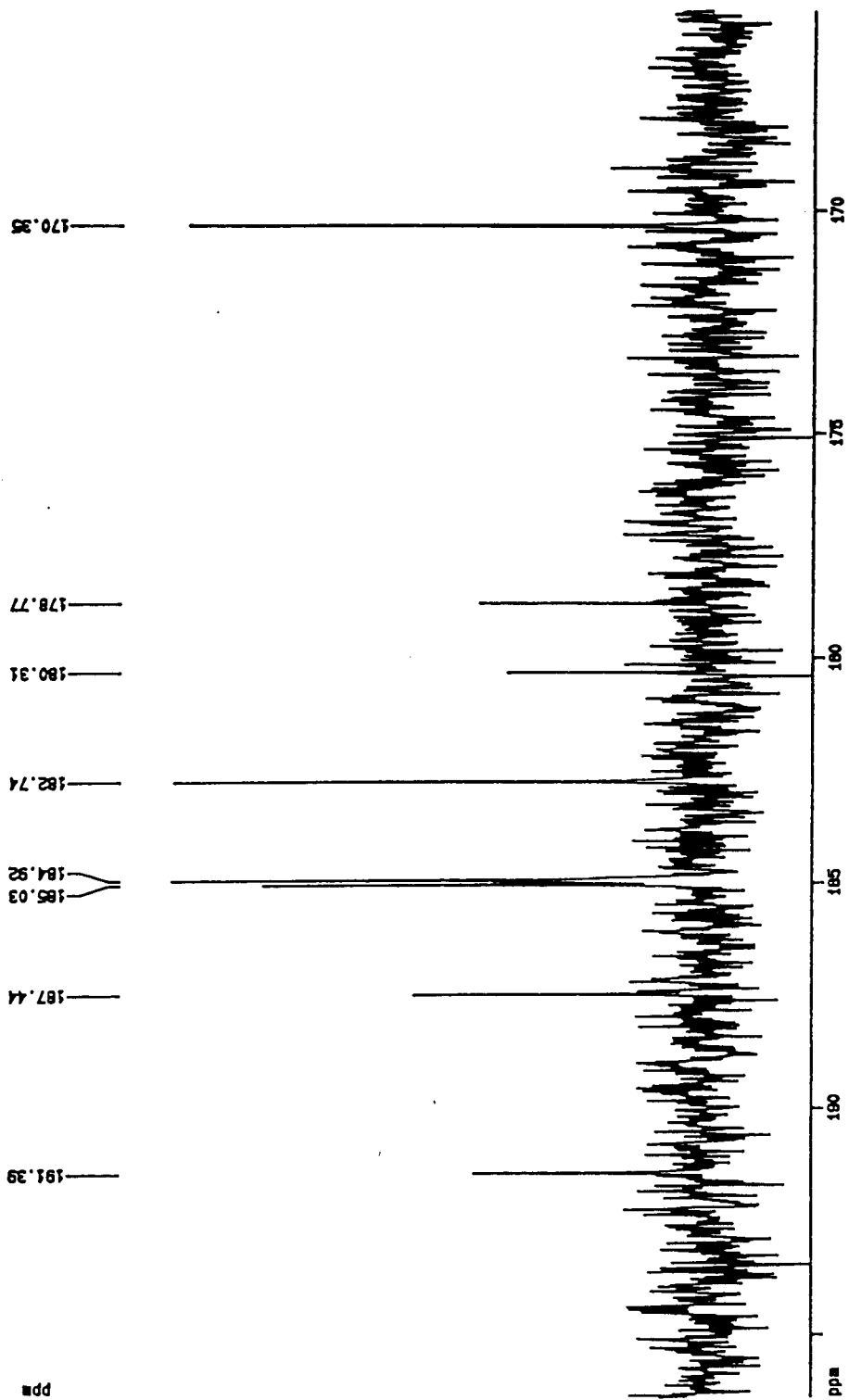
Fig. II.9.   13C{1H} NMR spectrum for cluster **9**.

46

3. Further variations : More surprises !

It quickly became obvious that the chemistry was turning out to be much more varied and was going in rather unexpected directions. In a final vain attempt at the original goal of achieving an isolobal analogue of $Os_4(CO)_{15}$, a number of closely-related reactions on related compounds were made. We again began with a tin analogue....

Our first thoughts were that increasing the bulk of the substituent on the Sn centre in **1(SnMe)** to, say, Bu^t or Ph, may prevent formation of the dimeric form of the target cluster, viz., $[Os_2(CO)_7(SnMe_2)_2]_2$. The Bu^t analogue, $[(OC)_4OsSnBu^t_2]_2$, **1(SnBu^t)**, was obtained in low yield, and investigation of this compound was side-tracked by the observation that other compounds were also formed in the synthesis. One of these was a colourless, crystalline substance which from X-ray crystallographic studies had the "incomplete" formulation "$(OC)_3HOs(SnBu^t_2)_2O$". The short supply of the material did not allow further investigation of its nature, although the absorption at 1925 cm^{-1} in the infrared spectrum of the compound was consistent with the presence of an OsH linkage.

The preparation of the Ph analogue also took a twist. Taking Collman's cue that the $[Os(CO)_4]^{2-}$ and R_2SnCl_2 route was a general one to $[(OC)_4OsSnR_2]_2$ clusters [7], we tried reacting Ph_2SnCl_2 with $[Os(CO)_4]^{2-}$. Besides the expected product $[(OC)_4OsSnPh_2]_2$, **1(SnPh)**, a pale yellow, crystalline compound was also obtained in moderate yield. This had an IR spectrum in the carbonyl region which suggested a *trans*-$Os(CO)_4(X)(Y)$ unit, with an uncommon splitting of the E mode [14]. This *trans*-$Os(CO)_4(X)(Y)$ formulation was also supported by the $^{13}C\{^1H\}$ NMR spectrum of it, which showed a singlet at 185.4 ppm, with satellites from $^{117,119}Sn$ coupling. The compound also gave C, H analyses that matched that required for **1(SnPh)**. We therefore suspected at this point that we were looking at a larger-ring version of **1(SnPh)**.

Despite numerous attempts, we could not grow a large enough crystal for a complete X-ray structural analysis on a conventional diffractometer; the problem was

compounded by the observation that the crystal decayed fairly rapidly under the X-ray beam, and calculations indicated that a full data set would require about 8 days of data collection. Still, sufficient data was collected (out to $\theta = 13^{\circ}$) to allow determination of the heavy-atom positions, and it was established that the compound probably had the formulation $[(OC)_4OsSnPh_2]_6$, **4**, with a 12-membered metallic ring! It was rather fortuitous that shortly after, the structure was confirmed (Fig. II.10) by a complete structural determination on a diffractometer equipped with a newly-developed charge-coupled device (CCD) detector, which allowed complete data collection overnight!

The establishment of the molecular structure allows a more conventional interpretation of the $v(CO)$ pattern in the infrared spectrum. The 3-band pattern is consistent with local C_{2v} symmetry at the $Os(CO)_4$ fragments if the rotation of the carbonyl ligands were slow on the IR timescale; a ^{13}C NMR spectrum of the cluster taken at -95 $^{\circ}$C did not show any significant broadening, so that this rotation must be fast on the NMR timescale. One of the A_1 modes is probably too weak in intensity to be observable, since four bands are predicted $(3A_1 + B_1$ for the conformation in which two of the carbonyls lie along the C_2 axis) for C_{2v} symmetry. This reduction in symmetry to C_{2v} may be ascribed either to a distortion in the Sn-Os-Sn vector away from linearity, or to the fact that the $Os(CO)_4$ fragment is part of a ring.

In an attempt at studying the fluxional properties of this ring compound by VT $^{13}C\{^1H\}$ NMR on a ^{13}CO-enriched sample, we found what appeared to be three singlets of very similar chemical shifts (Fig. II.11). The crude sample was chromatographed on both a silica and a Biobead column to purify it, but the $^{13}C\{^1H\}$ NMR spectrum in the 185 ppm region of the eluate was virtually unchanged. The Biobead column did, however, remove the smaller, tetracyclic **1(SnPh)**. It was found in a subsequent preparation that the $^{13}C\{^1H\}$ NMR spectrum of the dichloromethane extract from the reaction mixture contained the same three signals as well as those of **1(SnPh)** only. A pure sample of **4** was obtained by fractional crystallisation, and showed that the lowest-field signal corresponded
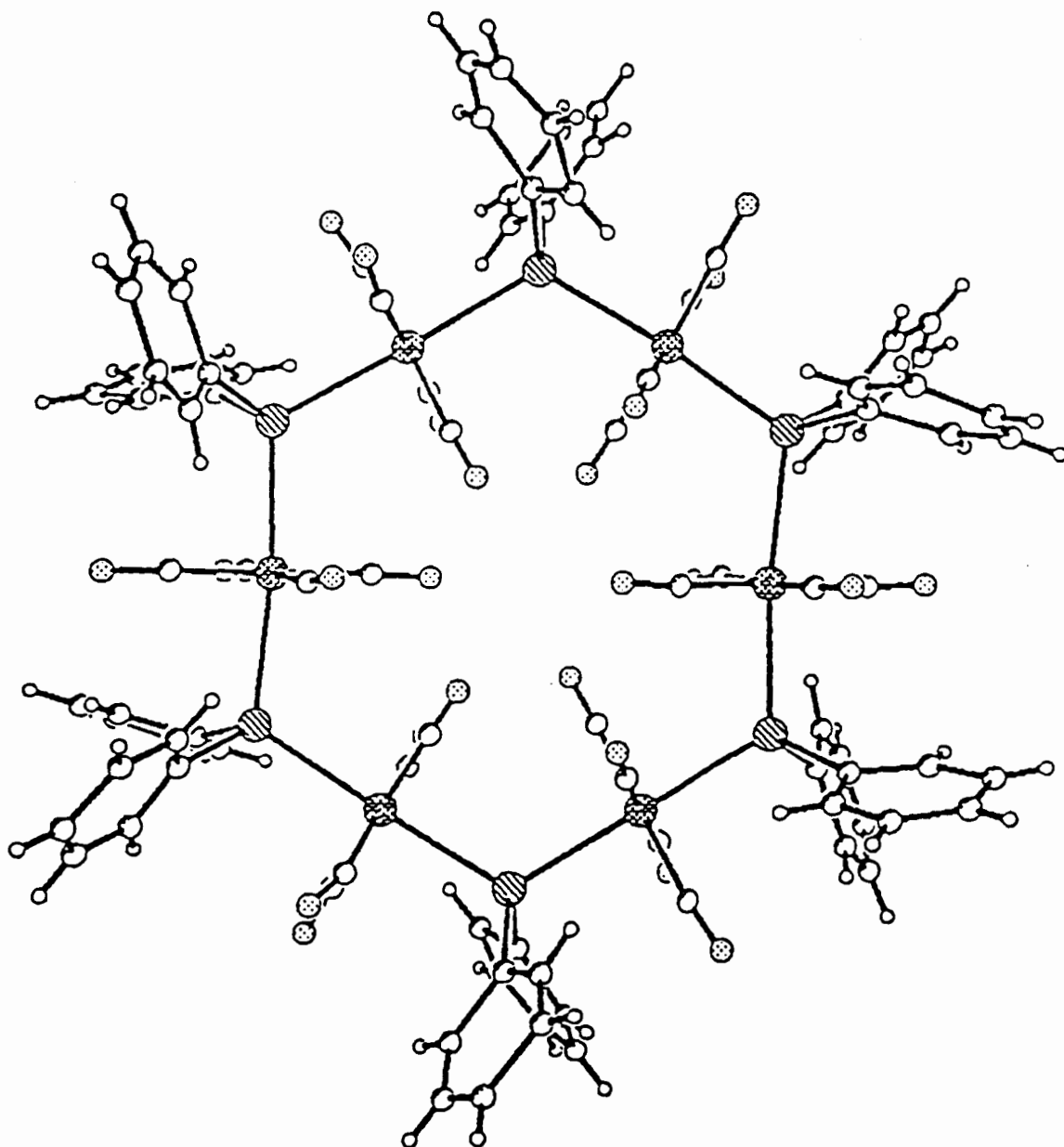
Fig. II.10.   X-ray structure of $[(OC)_4OsSnPh_2]_6$, 4.
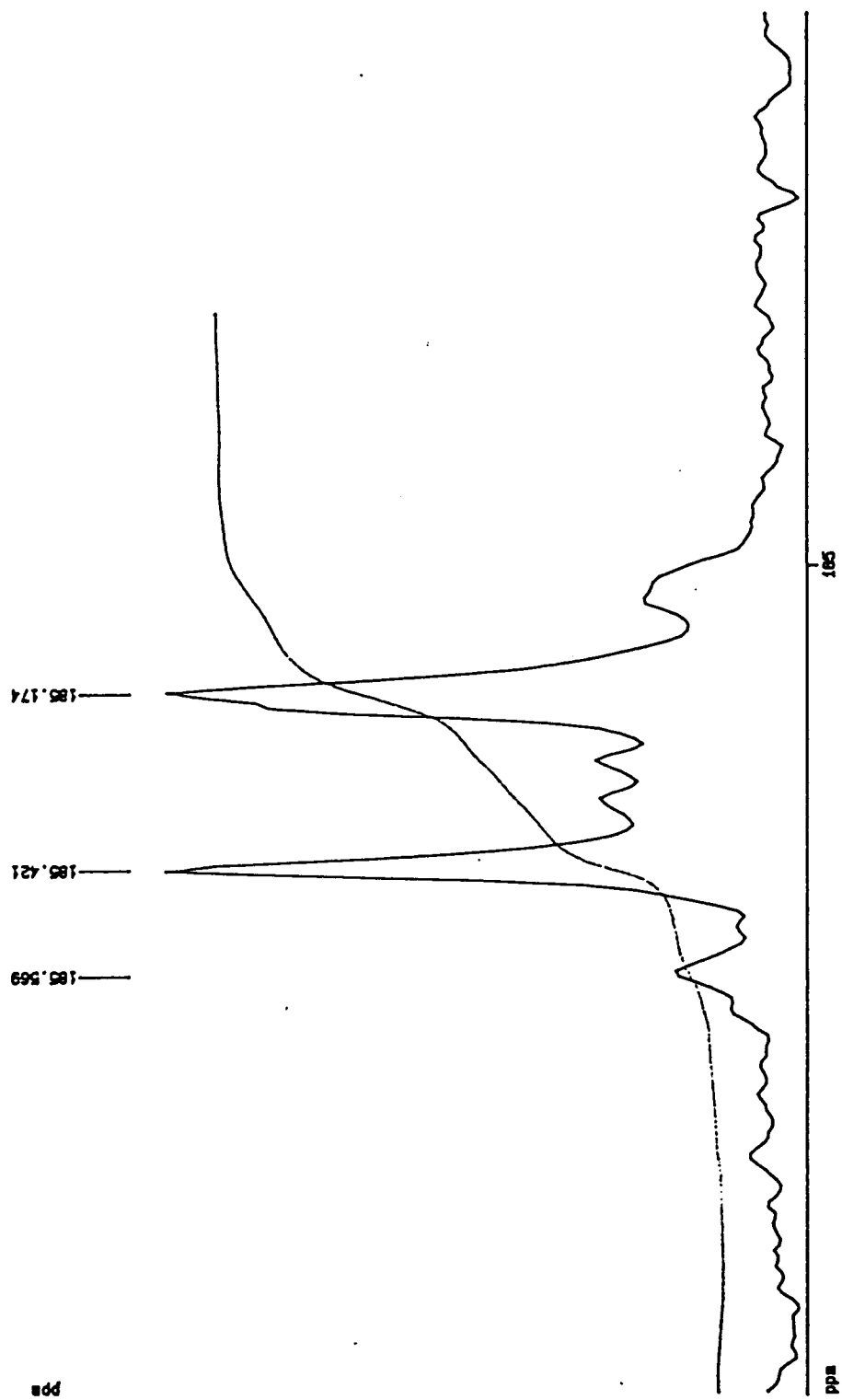
Fig. II.11. $^{13}C\{^1H\}$ NMR spectrum of ^{13}CO-enriched crude 4.

50

to **4**. The similarity in chemical shifts and ^{117,119}Sn-^{13}C coupling constants of the three signals suggested that the two additional signals probably belonged to two other oligomers that also have all-*trans* $Os(CO)_4$ units.

The next logical step was to attempt similar syntheses of the Ge and Pb analogues. The analogous Pb reaction led to a red solution after dichoromethane extraction; the product was however very light-sensitive as brief exposure to light led rapidly to precipitation of an insoluble red-brown powder. We did manage to obtain a small amount of orange crystals of the tetracycle $[(OC)_4OsPbPh_2]_2$, **1(PbPh)**, which was characterised by IR, ^{13}C NMR spectroscopy and elemental analyses. The corresponding reaction with Ph_2GeCl_2 gave the tetracycle$[(OC)_4OsGePh_2]_2$, **1(GePh)**, as the major product, together with another pale yellow compound which turned out to be an unusual trimetallic chain, $Ph_2Ge[Os(CO)_4H]_2$, **3**. The identity of both were established by spectroscopic and elemental analyses, and the latter also by an X-ray structural study.

Another class of variations sought was that of changing one of the Os centres to Fe; since the analogous $Fe_2(CO)_7(ER_2)_2$ clusters were already known, albeit with a bridging carbonyl, it was thought that introduction of the Fe centre may facilitate formation of the desired product. As it turned out, synthesizing the starting clusters $OsFe(CO)_8(EMe_2)_2$ (E = Ge, Sn) was not entirely straightforward either. The Sn compound was synthesised from the reaction of $Fe(CO)_4(SnMe_2Cl)_2$ with $[Os(CO)_4]^{2-}$, although the reaction also gave some $[(OC)_4OsSnMe_2]_2$, presumably by the reaction of the dianion with unreacted Me_2SnCl_2 present in the $Fe(CO)_4(SnMe_2Cl)_2$; the last two were not separated from one another by recrystallisation, and sublimation led to some decomposition, apparently to $[(OC)_4FeSnMe_2]_2$ (bands matching literature values for this species [15] were found in the IR of the light green sublimate). Separation of the compound $OsFe(CO)_8(SnMe_2)_2$, which was characterised spectroscopically and analytically, from $[(OC)_4OsSnMe_2]_2$ could be effected, though not very efficiently, by column chromatography on silica. Preliminary investigations on $OsFe(CO)_8(SnMe_2)_2$

suggested (surprisingly) that it was thermally more stable than $[(OC)_4OsSnMe_2]_2$, as prolonged heating at 120 ^oC of a mixture of the two compounds in hexane led to a decrease in the infrared absorptions of $[(OC)_4OsSnMe_2]_2$ with respect to that of $OsFe(CO)_8(SnMe_2)_2$.

The attempt at synthesizing the Ge analogue, viz., $OsFe(CO)_8(GeMe_2)_2$, was hampered by the fact that $Fe(CO)_4(GeMe_2Cl)_2$ could not be obtained free from decomposition products; it appears to be much more air- and heat-sensitive than the Sn analogue.

4. Derivatives of [(OC)$_4$OsSnMe$_2$]$_2$ and [(OC)$_3$OsGeMe$_2$]$_3$: Chemistry of OsE clusters

Investigations were also directed towards probing the chemistry of some of the OsE clusters, particularly their substitution chemistry. These studies were confined to three clusters, viz., [(OC)$_4$OsSnMe$_2$]$_2$, **1(SnMe)**, [Os$_2$(CO)$_7$(SnMe$_2$)$_2$]$_2$, **7**, and [(OC)$_3$OsGeMe$_2$]$_3$, **5(Ge)**, since convenient synthetic routes to them were available.

The cluster **1(SnMe)** was stable towards donor solvents like THF and pyridine, in contrast to the Fe analogue which has been reported to undergo Fe-Sn bond cleavage to form the base-stabilised stannylenes (OC)$_4$Fe=SnMe$_2$←L (where L = pyridine, THF) [15]. No evidence for such cleavage was found, even on gentle warming, for the cluster studied here. Under photolytic conditions, however, a blood-red solution was obtained in THF. We have not been able to identify the product(s), although an infrared spectrum of the THF solution showed carbonyl vibrations at 2109w, 2067m and 2008vs,br cm^{-1}, and its ^{13}C{^{1}H} NMR spectrum showed signals of 1:1 intensity at 153.53 and 184.05 ppm in the carbonyl region, as well as a signal at -10.54 ppm in the upfield region.

On photolysing a hexane solution of **1(SnMe)** with the olefins C$_2$H$_4$ or CH$_2$=CHCOOMe, substitution of carbonyls occurred to form Os$_2$(CO)$_7$(SnMe$_2$)$_2$L, **11** (where L = CH$_2$=CHCOOMe (**a**), C$_2$H$_4$ (**b**)). In both reactions, there was also formation of the cluster **7**. In the case of **11b**, the low yield of product only allowed an X-ray structural study and again, unfortunately, the crystal turned out to be badly disordered. There is the possibility that a disubstituted species, i.e., [(C$_2$H$_4$)(OC)$_3$OsSnMe$_2$]$_2$, was also present in the crystal; this is consistent with the observation that the IR spectrum in the carbonyl region of the crystals was more complicated than that for the methylacrylate analogue. The ^{1}H NMR spectrum also had major signals ascribable to **1(MeSn)** ($\delta_{Sn\underline{Me}}$ 1.007 ppm), the monosubstituted derivative **11b** ($\delta_{Sn\underline{Me}}$ 0.960 and 0.939 ppm), and the disubstituted derivative ($\delta_{Sn\underline{Me}}$ 0.993 ppm).

In the case of the methylacrylate derivative, the formulation of the product was based on IR, ^{1}H NMR and analytical evidence. The cluster was thermally unstable, decomposing slowly in solution (much more rapidly on gentle warming) to afford yellow crystalline deposits of **6** and free methylacrylate. The solution IR spectrum of **11a** showed a distinct resonance at 1726 cm^{-1} attributable to the ν(C=O) vibration of the carboxylate group. Four signals attributable to SnMe$_2$ groups were found in the ^{1}H NMR spectrum of **11a**; it also had an AMX pattern in the olefinic region, and a methyl signal, attributable to a coordinated methylacrylate. Their relative intensities were consistent with monosubstitution, in accord with elemental analyses. The olefin was assumed to occupy an equatorial site as in the C$_2$H$_4$ case; this is also consistent with the similarity in pattern of its ν(CO) to that of the PMe$_3$-substituted analogue described below. Although there is no data to indicate the relative orientation of the olefin with respect to the Sn centres, it may be argued on steric grounds that the carboxylate group most probably occupies the end of the olefin which is further away from the adjacent Sn centre (Fig. II.12).
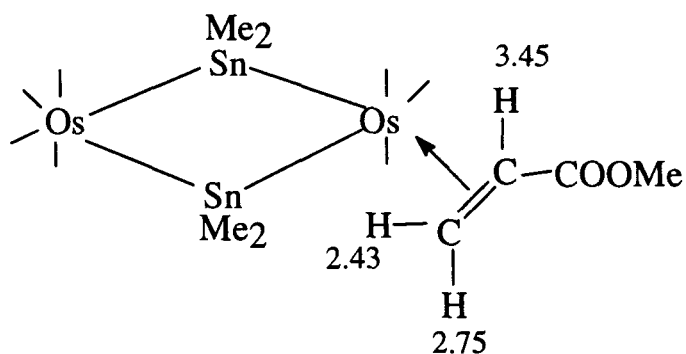
Fig. II.12. ^{1}H NMR assignments for the methylacrylate ligand in **11a**.

The cluster [Os$_2$(CO)$_7$(SnMe$_2$)$_2$]$_2$, **6**, was found to react with methylacrylate on heating in CH$_2$Cl$_2$, forming the same compound as that above, viz., **11a**. Compound **6** also reacted under similar conditions with CO to reform **1(SnMe)**, and with PMe$_3$ to form Os$_2$(CO)$_7$(SnMe$_2$)$_2$(PMe$_3$), **12b**. The latter compound was characterised by IR, NMR,

elemental analyses, and an X-ray structural study which showed that the phosphine occupied an equatorial site.

The more condensed cluster 5(Ge) has earlier been reported to be rather robust and unreactive; for example, it did not react with PPh$_3$ in refluxing hexane [11b]. Our own interest in it originated from the observation that 9 may be regarded as a derivative of 5(Ge). Our thoughts were that the latter may therefore be a suitable starting point to a high-yield synthesis of 9, and so the natural thing to do first was to investigate the substitution chemistry of 5(Ge). In the event, we found that the reaction of 5(Ge) with excess PMe$_3$ did proceed at higher temperatures; reaction was appreciable only at 100 $^{\circ}$C, and even then it was still fairly slow. Chromatographic separation of the resultant mixture afforded the mono-, di-, and tri-substituted products, viz., Os$_3$(CO)$_{9-n}$(GeMe$_2$)$_3$(PMe$_3$)$_n$ (n = 1-3; 12, 13 and 14, respectively). All three products were characterised by IR, ^{1}H NMR, and elemental analyses. The simple two-band pattern in the ν(CO) of Os$_3$(CO)$_6$(GeMe$_2$)$_3$(PMe$_3$)$_3$, 14, suggests high symmetry; the 2:3 intensity ratio signals observed in its ^{1}H NMR spectrum, which can be attributed to GeMe$_2$ and PMe$_3$ groups respectively, is consistent with the phosphines occupying equatorial positions. Similarly, the ^{1}H NMR spectra for the other two clusters are also consistent with phosphine substitution at the equatorial sites. This is in accord with the general observation that phosphorus donor ligands occupy the sterically less hindered equatorial positions in trinuclear carbonyl clusters of the group 8 metals [16].

5. References

[1]   (a) Wade, K. *Adv. Inorg. Radiochem.*, **1976**, *18*, 1. (b) Mingos, D. M. P. *Acc. Chem. Res.*, **1984**, *17*, 311. (c) McPartlin, M. *Polyhedron*, **1984**, *3*, 1279.

[2]   (a) Martin, L. R.; Einstein, F. W. B.; Pomeroy, R. K. *Organometallics*, **1988**, *7*, 294. (b) Hogarth, G.; Phillips, J. A.; van Gastel, F.; Taylor, N. J.; Marder, T. B.; Carty, A. J. *J. Chem. Soc., Chem. Commun.*, **1980**, 278. (c) Cherkas, A. A. *Inorg. Chem.*, **1993**, *32*, 1662. (d) Field, J. S.; Haines, R. J.; Smit, D. N. *J. Chem. Soc., Dalton Trans.*, **1988**, 1315.

[3]   Pomeroy, R. K. *J. Organomet. Chem.*, **1990**, *383*, 387.

[4]   Hoffman, R. *Angew. Chem. Int. Ed. Engl.*, **1982**, *21*, 711.

[5]   Johnston, V. J.; Einstein, F. W. B.; Pomeroy, R. K. *J. Am. Chem. Soc.*, **1987**, *109*, 8111.

[6]   George, R. D.; Knox, S. A. R.; Stone, F. G. A. *J. Chem. Soc., Dalton Trans.*, **1973**, 972.

[7]   Collman, J. P.; Murphy, D.W.; Fleischer, E.B.; Swift, D. *Inorg. Chem.*, **1974**, *13*, 1.

[8]   (a) Bonny, A.; MacKay, K. M. *J. Chem. Soc., Dalton Trans.*, **1978**, 722. (b) Kummer, D.; Furrer, J. *Z. Naturforsch.*, B, **1971**, *26*, 162. (c) Marks, T. J.; Grynkewich, G. W. *J. Organomet. Chem.*, **1975**, *91*, C9. (d) Marks, T. J.; Grynkewich, G. W.; *Inorg. Chem.*, **1976**, *15*, 1307. (e) Corriu, R. J. P.; Moreau, J. J. E. *J. Chem. Soc., Chem. Commun.*, **1980**, 278.

[9]   (a) Farrar, D. H.; Johnson, B. F. G.; Lewis, J.; Raithby, P. R.; Rosales, M. J. *J. Chem. Soc., Dalton Trans.*, **1982**, 2051. (b) Wang, W.; Einstein, F. W. B.; Pomeroy, R. K. *J. Chem. Soc., Chem. Commun.*, **1992**, 1737.

[10]   (a) Howard, J.; Knox, S. A. R.; Stone, F. G. A.; Woodward, P. *J. Chem. Soc., Chem. Commun.*, **1970**, 1477. (b) Howard, J.; Woodward, P. *J. Chem. Soc. A*, **1971**, 3648.

[11]   (a) Stone, F. G. A.; Howard, J.; Knox, S. A. R.; Woodward, P. *J. Chem. Soc. D*, **1970**, 1477. (b) Knox, S. A. R.; Stone, F. G. A. *J. Chem. Soc. A*, **1971**, 2874.

[12]   Williams, K. R.; King, R. W. *J. Chem. Educ.*, **1990**, *67*, A125.

[13]   Martin, L. R.; Einstein, F. W. B.; Pomeroy, R. K. *Inorg. Chem.*, **1988**, *27*, 2986 and references therein.

[14]   (a) Jetz, W.; Graham, W. A. G. *J. Am. Chem. Soc.*, **1967**, *89*, 2773. (b) Klahn, A. H.; Sutton, D. *Organometallics*, **1989**, *8*, 198.

[15]   Marks, T. J.; Newman, A. R. *J. Am. Chem. Soc.*, **1973**, *95*, 769.

[16]   (a) Leong, W. K. M.Sc. Thesis, National University of Singapore, 1992. (b) Ang, H. G.; Kwik, W. L.; Leong, W. K. *Bull. Sing. N. I. Chem.*, **1991**, *19*, 25. (c) Wang, W.; Batchelor, R. J.; Einstein, F. W. B.; Lu, C. Y., Pomeroy, R. K. *Organometallics,* **1993**, *12*, 3598 and references therein.

Chapter III Discussion of the chemistry : A potpourri of reactivity.

1. Reactions of $[Os(CO)_4]^{2-}$: Steric control?

The anion $[Os(CO)_4]^{2-}$ was first prepared as a solution in THF in 1970 by L'Eplattenier [1]. The solution was very air- and moisture-sensitive, reacting with trace amounts of moisture to form first the anion $[HOs(CO)_4]^-$, and subsequently the volatile hydride $H_2Os(CO)_4$. Its preparation as a solid was reported a little later, and it was originally described as a cream coloured, air-stable solid, and there were doubts about its precise formulation [2]. Other workers have since shown that the formulation was correct and that the compound was indeed very air- and moisture-sensitive [3]. Our own experience corroborates the reported sensitivities, for we have found that a sample on standing for a day in a vessel with an improperly greased stopcock led to its decomposition into a black solid. The dianion is conveniently prepared by the reduction of $Os_3(CO)_{12}$ with sodium in liquid ammonia, and has found extensive use in the synthesis of mononuclear osmium carbonyl derivatives.

The reaction of $[Os(CO)_4]^{2-}$ with Me_2SnCl_2 to form the tetracyclic cluster $[(OC)_4OsSnMe_2]_2$ was first reported by Stone and coworkers in 1973 [2]. The reaction was ascribed to be a general one by Collman and coworkers shortly after [4]. It was also shown that $[(OC)_4OsSnBu^n_2]_2$, which contained a tetracyclic Os_2Sn_2 metal core, resulted from the reaction of $H_2Os(CO)_4$ with $trans$-$Os(CO)_4(SnBu^n_2Cl)_2$, and it was proposed that isomerisation of an intermediate like $trans$-$(HOs(CO)_4SnBu^n_2)Os(CO)_4(SnBu^n_2Cl)$ to the cis isomer was responsible for the formation of this tetracyclic product.

The reaction of $[Os(CO)_4]^{2-}$ with Me_2ECl_2 (E = Ge, Sn, Pb) gave the tetracycles $[(OC)_4OsEMe_2]_2$, **1(EMe)**, in moderate yields (Equation 1); the Pb product was isolated as red blocks, while the others were colourless. A similar attempt to prepare the Si analogue was unsuccessful; the only isolable product was $H_2Os(CO)_4$. It is likely that a

small amount of the moisture-sensitive Me_2SiCl_2 had been hydrolysed by moisture in the air to form HCl, which attacked the $[Os(CO)_4]^{2-}$ to form $H_2Os(CO)_4$. In the reaction with $Bu^t_2SnCl_2$, it was found, by monitoring the reaction by IR spectroscopy, that other compounds beside the tetracycle were formed. Although no extensive attempts were made to isolate and characterise these other products, we did manage to obtain evidence that one of these had an $OsSn_2O$ ring.

$$[Os(CO)_4]^{2-} + Me_2ECl_2 \longrightarrow [(OC)_4OsEMe_2]_2 \qquad (1)$$

$$(E = Ge, Sn, Pb) \qquad\qquad\qquad \mathbf{1(EMe)}$$
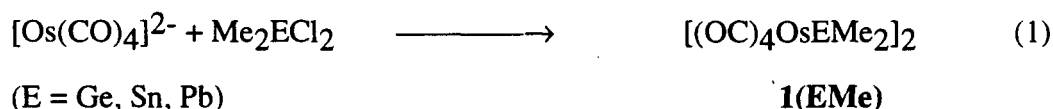
The analogous reactions with the phenyl analogues Ph_2ECl_2 (E = Ge, Sn, Pb) were more interesting. For the Ge analogue, the reaction gave, besides the tetracycle, a compound which we have characterised to contain an OsGeOs chain, viz., $Ph_2Ge[Os(CO)_4H]_2$, **3** (Equation 2).

$$[Os(CO)_4]^{2-} + Ph_2GeCl_2 \longrightarrow [(OC)_4OsGePh_2]_2 + Ph_2Ge[Os(CO)_4H]_2 \qquad (2)$$

$$\mathbf{1(GePh)} \qquad\qquad \mathbf{3}$$
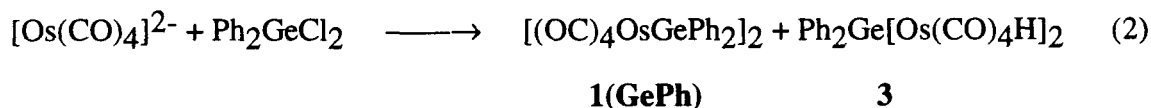
The product is again presumably the result of partial protonation of $[Os(CO)_4]^{2-}$ to $[HOs(CO)_4]^-$ by small amounts of HCl present in the Ph_2GeCl_2, which then reacts to form the product. If this hypothesis is correct, then a better route to **3** may be from $[HOs(CO)_4]^-$, the preparation of which is known [5].

The analogous Sn reaction gave a quite unexpected product, namely, $[(OC)_4OsSnPh_2]_6$, **4**, containing a 12-membered ring of metal atoms (Equation 3).

$$Os(CO)_4^{2-} + Ph_2SnCl_2 \longrightarrow [(OC)_4OsSnPh_2]_2 + [(OC)_4OsSnPh_2]_6 \qquad (3)$$

$$\mathbf{1(SnPh)} \qquad\qquad \mathbf{4}$$
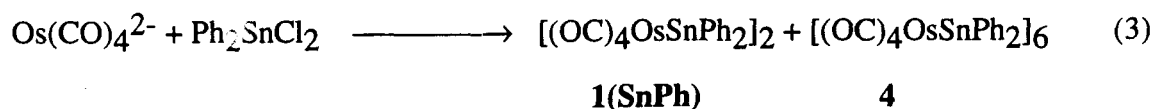
One of the many interesting features of this compound is that the Os centres are all in the *trans* $Os(CO)_4(X)_2$ configuration. It therefore seems likely that the intermediates involved in the formation of these centres must also have a *trans* configuration about the Os centre. We believe that the intermediate is most likely *trans*-$Os(CO)_4(SnPh_2Cl)_2$. Indeed, this latter compound was isolated from a reaction of $[Os(CO)_4]^{2-}$ with two equivalents of Ph_2SnCl_2; the *cis* isomer was hardly detectable. A similar result was obtained with $Bu^t_2SnCl_2$, though this showed a little (< 10%) of the *cis* isomer. In contrast, the analogous reaction with Me_2SnCl_2 gave a roughly equal proportion of *cis*- and *trans*-$Os(CO)_4(SnMe_2Cl)_2$. We also found that at room temperature, samples of the two isomers isomerize slowly to give a small amount of the other isomer; in fact, on warming a hexane solution of *cis*-$Os(CO)_4(SnMe_2Cl)_2$, rapid precipitation of the less soluble *trans*-$Os(CO)_4(SnMe_2Cl)_2$ was observed.

Given the above results, we believe that the formation of either the tetracycle or the 12-membered ring in the Sn reactions is dictated by the configuration of the intermediate $Os(CO)_4(SnR_2Cl)_2$ formed, and that this is in turn a reflection of the steric bulk on the Sn centre; Stone and coworkers have previously observed that the *cis/trans* ratio in $Ru(CO)_4(SnR_3)_2$ decreases with the increasing bulk of R (for a series where the R groups have similar electronic properties) [6]. Hence, the less bulky the groups on the Sn, the more favoured is the tetracycle. Furthermore, given the observation that the isomerization of $Os(CO)_4(SnMe_2Cl)_2$ is slow even at room temperature, isomerization of the $Os(CO)_4(SnR_2Cl)_2$ intermediates under the reaction conditions used (usually involving slowly warming from ca. -50 °C to room temperature) is an unlikely proposition. We are thus left with the conclusion that part of the reason for the unexpected low yields of the tetracycles **1** may be due to the formation of *trans*-$Os(CO)_4(SnR_2Cl)_2$, which would lead to a different kind of compound. In the case of **1(EMe)** (E = Ge, Sn) at least, we have not been able to find any evidence for an analogous 12-membered ring species. But we have noticed that a fair amount of light-yellow, insoluble material was invariably

formed in these reactions, and wonder if these may be even higher oligomers or polymers! Indeed, the 12% yield of the tetracycle reported for the reaction of $H_2Os(CO)_4$ with trans-$Os(CO)_4(SnBu^n_2Cl)_2$ [4] can most probably be attributed to the presence of small amounts of cis-$Os(CO)_4(SnBu^n_2Cl)_2$ (as is evident from the IR spectrum reported for the trans-$Os(CO)_4(SnBu^n_2Cl)_2$), and the rest of the reaction product is some higher oligomer.

The hope for a similar kind of higher oligomer from the analogous reaction with Ph_2PbCl_2 could not be realized because of the very light-sensitive nature of the product(s). So far, the evidence is that the major product is the tetracycle $[(OC)_4OsPbPh_2]_2$, **1(PbPh)**; this was the only isolated product, and an IR spectrum of the reaction mixture did not seem to indicate any other significant product. The different reaction paths taken by the compounds Ph_2ECl_2 (E = Ge, Sn, Pb) is worthy of a further comment: We have not found any evidence for an Sn or Pb analogue to **3**. Although this may be explained, at least in part, by the presence of HCl in samples of Ph_2GeCl_2 but not in the much less moisture-sensitive Sn and Pb analogues, it does not explain why an analogous compound to **3** was not obtained with Me_2GeCl_2. We believe that this may be due to a more ready reaction of the type shown in Equation 4.

$$Ph_2E[Os(CO)_4H]_2 + Ph_2ECl_2 \longrightarrow [(OC)_4OsEPh_2]_n + 2HCl \qquad (4)$$
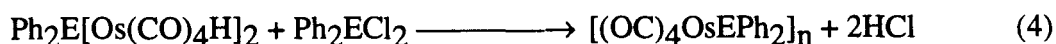
That the reaction for E = Sn, Pb proceeds more rapidly than for the reaction with E = Ge may be a reflection of the relative strengths and polarities of the E-Cl bonds. If this is correct, then **3** represents one of the intermediates in the formation of the clusters $[(OC)_4OsER_2]_n$ from our reactions of $[Os(CO)_4]^{2-}/[HOs(CO)_4]^-$ with R_2ECl_2, and may also explain why a significant amount of $[(OC)_4OsSnPh_2]_2$ is obtained even though $Os(CO)_4(SnPh_2Cl)_2$ exists mainly as the trans isomer.

In an attempt to utilize the knowledge gained about the influence of the geometry of the intermediate in determining the course of the reaction, $[Os(CO)_4]^{2-}$ was reacted with $Fe(CO)_4(SnMe_2Cl)_2$. It was hoped that the rapid *cis-trans* isomerization in the Fe compounds [7] would lead to a high yield of the tetracycle $OsFe(CO)_8(SnMe_2)_2$, **2(Sn)**, which would be entropically favoured. In the event, **2(Sn)** was obtained in fairly good yield, although the reaction was marred by the concurrent formation of **1(SnMe)** (Equation 5). The latter presumably resulted from the presence of free Me_2SnCl_2 in the $Fe(CO)_4(SnMe_2Cl)_2$, for which no efficient method to separate them could be found. Fortunately, **1(SnMe)** and **2(Sn)** are separable by chromatography on Florisil. An attempt at the synthesis of the germanium analogue of **2** was unsuccesful; we found that $Fe(CO)_4(GeMe_2Cl)_2$ could not be prepared free from a number of contaminants, including $[(OC)_4FeGeMe_2]_2$.

$$[Os(CO)_4]^{2-} + Fe(CO)_4(SnMe_2Cl)_2 \longrightarrow OsFe(CO)_8(SnMe_2)_2 \qquad (5)$$

$$\textbf{2(Sn)}$$
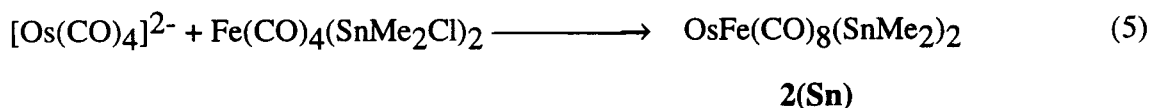
In contrast to the iron analogues of **1**, viz., $[(OC)_4FeER_2]_2$ (E = Ge, Sn, Pb), which have been observed to undergo homolytic cleavage of the Fe-E bonds to give base-stabilised compounds of formulae $(OC)_4Fe{\leftarrow}ER_2B$ (B = base) [8], the osmium-containing compounds **1** and **2** are much more resistant to such cleavage; no evidence for homolytic cleavage was observed in polar solvents like THF or pyridine, even on heating. This probably reflects the higher electron density on Os as compared to Fe, and hence reduced Lewis acidity on the E centre. An attempt was made to access such compounds by photolysing **1(SnMe)** in THF. A deep-red solution was obtained after a few hours, but both IR and $^{13}C\{^1H\}$ NMR evidence indicated that the major species present was still **1(SnMe)**. After 6 days of photolysis, however, the dark-red solution obtained showed signals at δ_C 184.05 and 153.53 in an approximately 1:1 ratio in the CO region, as well as a signal at δ_C -10.53 attributable to an $SnCH_3$ grouping, in the $^{13}C\{^1H\}$ NMR spectrum.

2.   Decarbonylation reactions : Complex and differing pathways

The main purpose for the preparation of the tetracycles **1** had originally been to try and decarbonylate them by some means to compounds of the type $Os_2(CO)_7(ER_2)_2$. In this section, the chemical results obtained from the photochemical, thermal, and chemical removal of COs in the tetracycles will be discussed.

It has been known for some time that the Fe analogues readily undergo decarbonylation on UV irradiation to compounds of $Fe_2(CO)_7(ER_2)_2$ formulation, which possess a bridging carbonyl (Fig. III.1) [9].
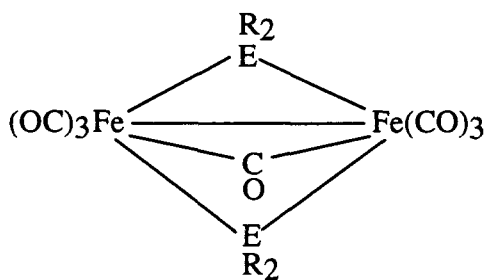
Fig. III.1.   Structure of $Fe_2(CO)_7(ER_2)_2$ (E = Si, Ge, Sn).

On UV irradiation of the tetracycle **1(GeMe)** in hexane, a number of products were observed to be present in the resultant red solution, although only three of these were isolated and identified, viz., $[(OC)_3OsGeMe_2]_3$, **5(Ge)**, $Os_3(CO)_{11}(GeMe_2)_2$, **8**, and $Os_4(CO)_{12}(GeMe_2)_4$, **9** (Equation 6).

The complexity of these compounds suggests that there is extensive rearrangement involved in their formation from **1(GeMe)**, and that the photochemistry of **1(GeMe)** probably involves both CO ejection and Os-Ge bond fission. Monitoring the photolysis in d_6-benzene by ^1H NMR spectroscopy over the course of about 29 h showed that numerous products were formed and further transformed during the photolysis (Fig. III.2). The initial photolysis product was formed in detectable quantities just after 5 mins into the

63

photolysis, but its resonance in the ^{1}H NMR spectrum quickly disappeared over about one hour. The experiment also indicated that one of the eventual products was **5(Ge)**.

$$[(OC)_4OsGeMe_2]_2 \xrightarrow{\text{hexane, } h\nu} [(OC)_3OsGeMe_2]_3 + Os_3(CO)_{11}(GeMe_2)_2 \quad (6)$$

1(GeMe)   **5(Ge)**   **8**

$$+ Os_4(CO)_{12}(GeMe_2)_4 + \text{other products}$$

9
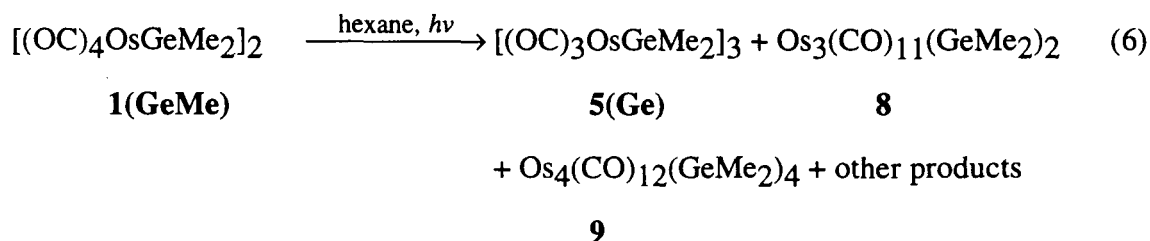
Both VT ^{1}H NMR and NOESY experiments indicated that in cluster **9**, two of the GeMe$_2$ groups were undergoing exchange; the ^{1}H NMR signals for the two exchanging GeMe$_2$ groups can be assigned with some degree of certainty (marked with an * in Fig. III.3), Although this observation is consistent with the $(OC)_4OsGeMe_2$ fragment acting as a germylene rotating about its bond to the Os_3Ge_3 core (Chapter II), the X-ray structural study does not support the presence of an Os=Ge bond in the $(OC)_4OsGeMe_2$ fragment (Chapter IV). Instead, the latter study indicates that the Os-Os bond connecting the $(OC)_4OsGeMe_2$ fragment to the Os_3Ge_3 core is rather long (3.069(1) Å) and hence probably weak, suggesting that the exchange may be effected via cleavage of this Os-Os bond followed by rotation about the intact connecting Os-Ge bond (Fig. III.3).
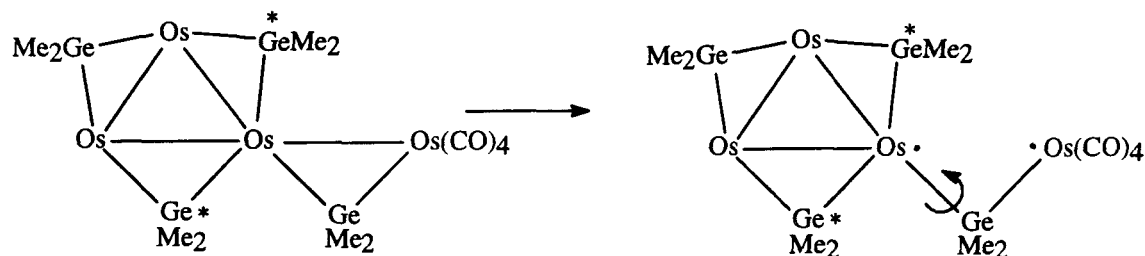
Fig. III.3.   Probable mechanism for the exchange of the GeMe$_2$ groups (marked *) in cluster **9**.
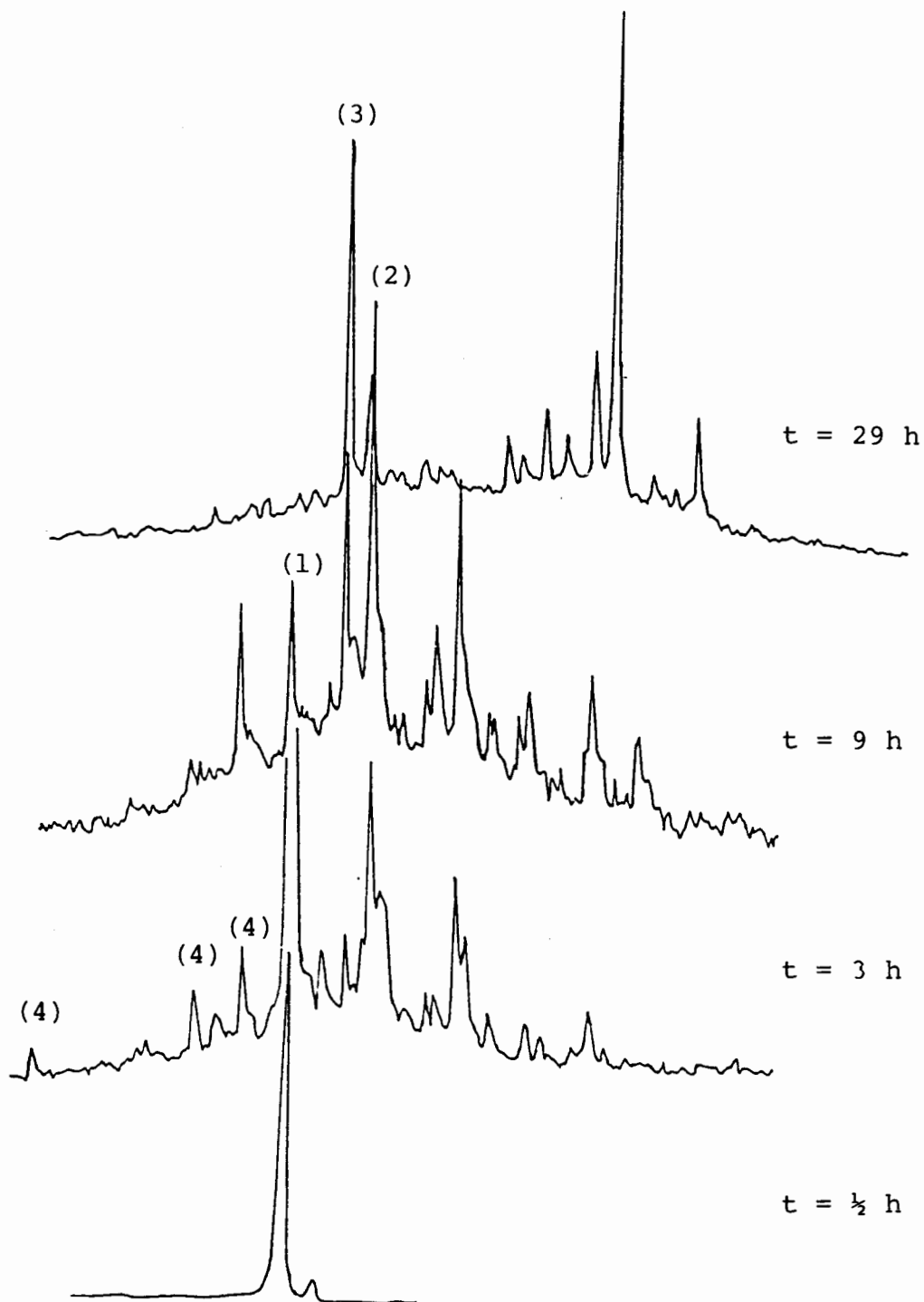
Fig. III.2. ^{1}H NMR monitoring of the photolysis of **1(GeMe)**. Assignments :

(1) = cluster **1(GeMe)**, (2) = cluster **8**, (3) = cluster **5(Ge)**, (4) = cluster **9**.

This mechanism involves cleavage of a bond (the exact nature of the bonding in the intermediate is of course not known, and need not be a diradical as represented in Fig. III.3), and is therefore probably energetically not very favourable; the observation that the exchange is slow even at 95 °C is consistent with this. Furthermore, if the $(OC)_4OsGeMe_2$ fragment were a germylene, then it may be expected, *a priori*, to be detachable if **9** were heated under a CO atmosphere. In fact, when **9** was heated for 14 h at 100 °C under 2 atmospheres of CO, no sign of reaction was observed.

The photolyses of both **1(SnMe)** and **1(PbMe)**, on the other hand, proceeded in quite different paths to that of **1(GeMe)**; both gave precipitation of a solid in hexane solution, and for **1(PbMe)**, it was almost quantitative after about 3 h. The product from **1(SnMe)** was $[Os_2(CO)_7(SnMe_2)_2]_2$, **6**, which was obtained in about 30% yield (Equation 7). The low yield was due to the precipitate preventing passage of UV light to the mother liquor; yields could be improved by further photolysis of the mother liquor, which contained almost exclusively **1(SnMe)**, so that after a few cycles of photolysis, a total yield of about 70% could be reached. The product from the photolysis of **1(PbMe)** has not been identified; it did not dissolve in any common solvent. It is, however, almost certainly not an analogue of **6**, and is probably a more condensed cluster.

$$[(OC)_4OsSnMe_2]_2 \xrightarrow{\text{hexane, } h\nu} [Os_2(CO)_7(SnMe_2)_2]_2 \qquad (7)$$
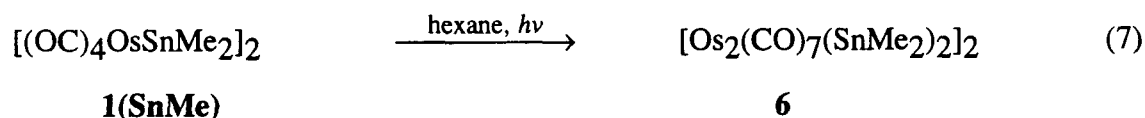
1(SnMe)   **6**

The differences in the photolysis results for the clusters **1(EMe)** is intriguing. For **1(SnMe)** and **1(PbMe)**, the main driving force is presumably the insolubility of the products in hexane. The cluster **6** can be envisaged to have resulted from an initial loss of a CO ligand from **1(SnMe)** to an "$Os_2(CO)_7(SnMe_2)_2$" intermediate which then undergoes rearrangement and dimerisation: The nature of this intermediate is open to speculation (but see later). In the case of **1(GeMe)**, such a simplistic view cannot even be contemplated, as

the products isolated cannot have resulted from simple loss of CO, rearrangement, or dimerisation. For example, the formation of cluster **8** must involve a net loss of a $GeMe_2$, or gain of an $Os(CO)_4$, moiety at some stage. As is evident from the ^{1}H NMR data (Fig. III.2), these clusters are almost certainly a result of further photochemical transformations of the initial product.

Pyrolyses of both **1(GeMe)** and **1(SnMe)** gave, as the major products, the corresponding raft-like Os_3E_3 clusters **5(Ge)** and **5(Sn)**, respectively (Equation 8). In both cases, minor products were also observed, though only in the Ge case were some of these identified. The cluster **1(GeMe)** is thermally less stable than the Sn analogue, as is evident from the fact that the pyrolysis of **1(GeMe)** proceeded fairly readily at 100 [o]C, while the pyrolysis of **1(SnMe)** was sluggish even at 130 [o]C. The reactions also suggest that the clusters **5(Ge)** and **5(Sn)** are thermodynamically quite stable, and act as the thermodynamic sink for OsGe and OsSn compounds; this is in agreement with earlier observations on the pyrolysis of $Os(CO)_4(GeMe_3)_2$ [10].

$$[(OC)_4OsEMe_2]_2 \xrightarrow{\text{hexane, heat}} [(OC)_3OsEMe_2]_3 \text{ (major product)} \qquad (8)$$

1(EMe) (E = Ge, Sn)   **5(EMe)**
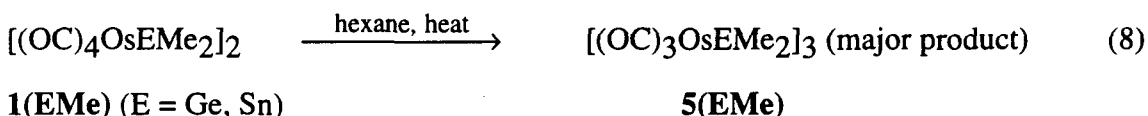
As mentioned in Chapter II, the chemical activation of **1(SnMe)** with Me_3NO was a very complicated reaction, as evident from monitoring of the reaction by infrared spectroscopy. The only isolated and identified product was the unusual cluster $[Os_2O(CO)_7(SnMe_2)_2]_2$, **7**, which contains a μ_3-O ligand bridging two Sn and an Os centres. The reaction was carried out in dry acetonitrile, with both freshly sublimed Me_3NO or its dihydrate; the results were the same in either case, indicating that the μ_3-O probably comes from Me_3NO. Thus cluster **7** can be considered as the result of both decarbonylation and attack at the Sn atom by Me_3NO. With hindsight, the attack at Sn should not have been unexpected since Sn is known to be oxophilic and the Sn-O bond is

fairly strong [11]. The possibility of attack at either the Sn centre or at a carbonyl ligand by Me$_3$NO accounts for the very complicated set of changes observed during the course of the reaction. This cluster provides a good example of the Sn centre modifying the behaviour at a neighbouring Os centre; a formally two-electron oxygen donation to Os is not common. The poor yield, however, limits further exploration of the chemistry of **7**.

Cluster **7** may also be viewed as a derivative of **6** in which two O atoms have been inserted (Fig. III.4). Attempts were made at introducing O atoms into **6** by using Me$_3$NO and N$_2$O, but these were unsuccessful.

6   **7**
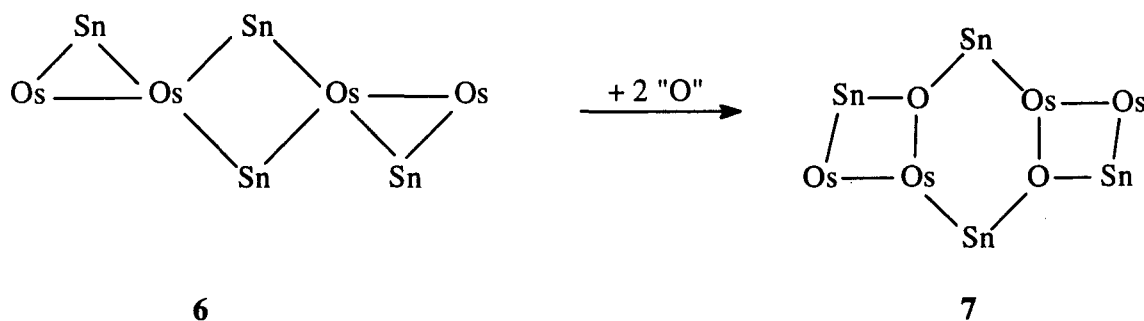
Fig. III.4.   Hypothetical formation of **7** from **6** (Me's and CO's omitted).

In spite of the obvious complexity and diversity shown in the decarbonylation reactions, there appears to be some structural similarity among the various products isolated. In the case of the decarbonylation products of **1(SnMe)**, it is possible to "decompose" the products structurally as shown in Scheme III.1. The most evident link is the presence of a fragment, Os$_2$(CO)$_7$(SnMe$_2$)$_2$, which may be related to the intermediate in the decarbonylations. One problem that stands in the way of equating this fragment with the intermediate itself is the stereochemistry of the stannylene moiety; for **6** and **7**, it is on the "wrong" side with respect to the equatorial carbonyl (shown in Scheme III.1), from what would be expected if it were derived from loss of a CO from **1(SnMe)** (as drawn for
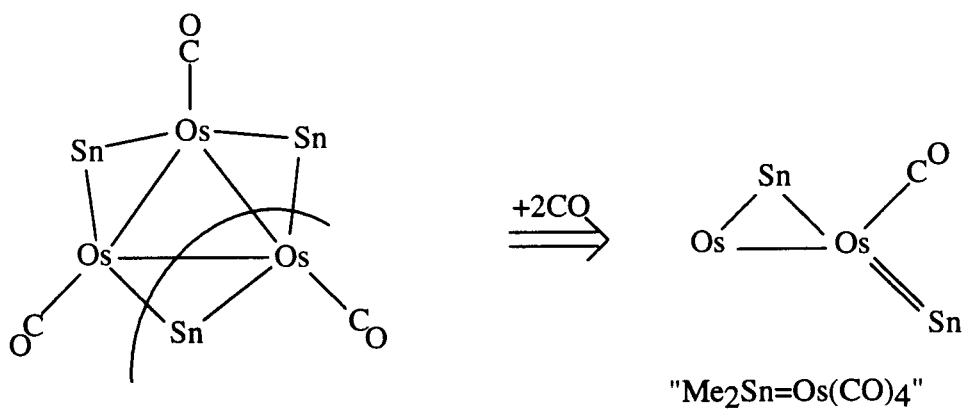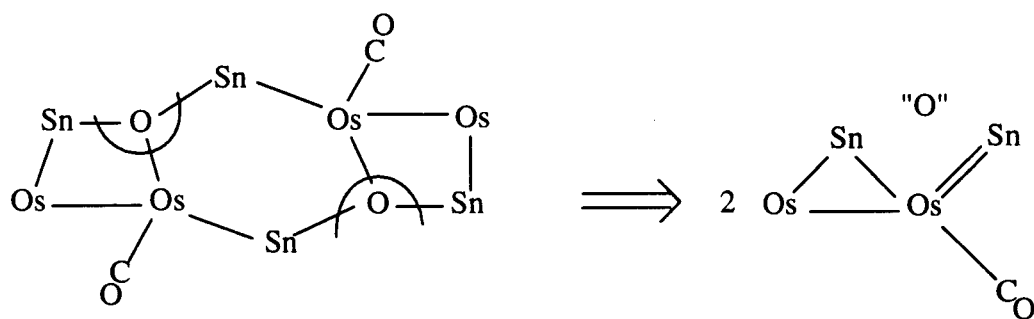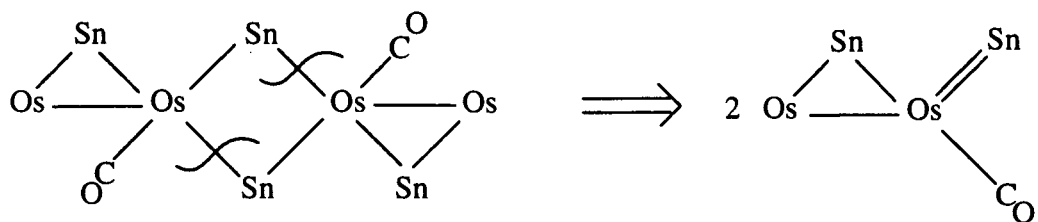
Scheme III.1. Structural "decomposition" of clusters **6**, **7** and **5(Sn)**.

(Only relevant ligands shown).

the case of **5(Sn)**). It is therefore necessary that this stannylene intermediate is able to isomerise to the correct stereochemistry; such an isomerisation may conceivably be achieved via cleavage of the Os-Os bond, just like the exchange process in cluster **9**.

Some of the decarbonylation products of **1(GeMe)** may then conceivably have been formed as depicted in Scheme III.2. (A similar scheme involving **1(SnMe)** is given later, in Scheme III.3.) The proposal for the formation of **9**, in particular, is attractive in that it involves an "intermediate" that is the analogue of **6**. The observation mentioned earlier, that **6** does not undergo replacement of its $(OC)_4OsGeMe_2$ unit with CO, also rules out the possibility that **9** is derived from **5(Ge)** by a germylene substitution with CO.
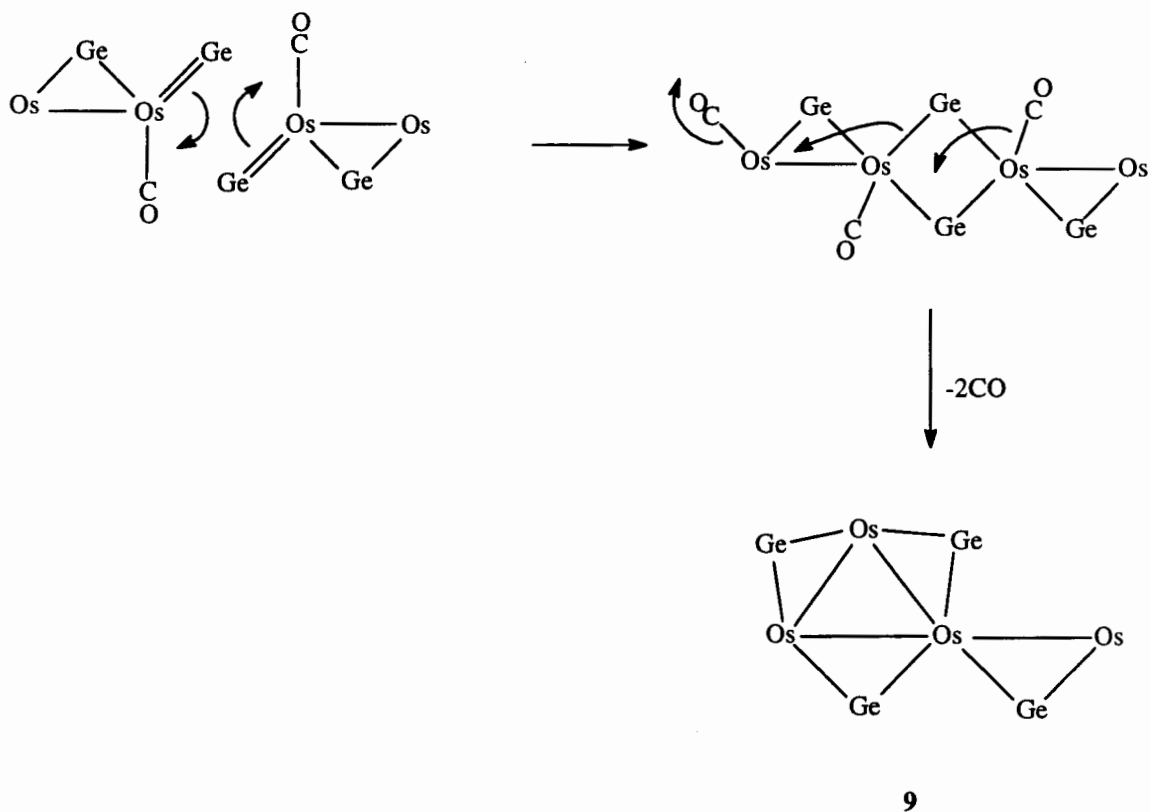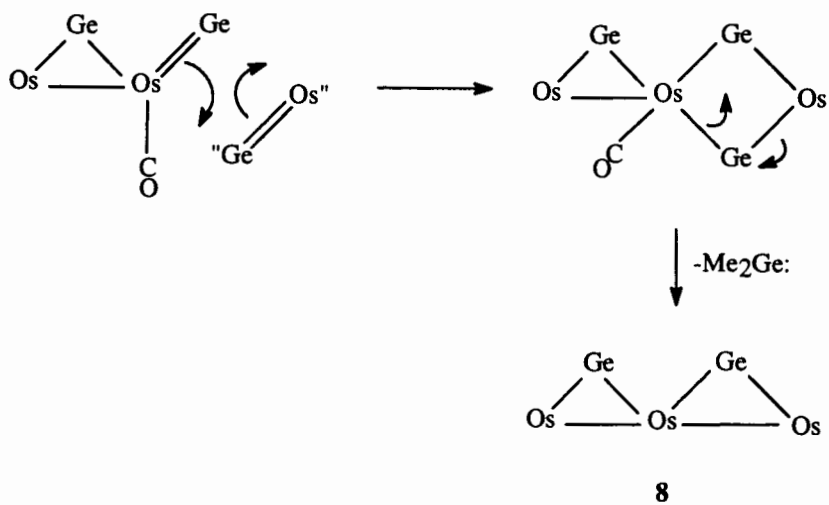
Scheme III.2. Proposed pathways for the formation of clusters **8** and **9**.

(Only relevant ligands shown).

71

3. Reactions with two-electron donors : Substitution chemistry

The robustness of the cluster **1(SnMe)** is demonstrated by the fact that heating a hexane solution at 120 $^{\circ}$C for 13 h or at 160 $^{\circ}$C for 4 h led to only a slight darkening in colour but with no spectroscopically-detectable product formation; product formation was only apparent on prolonged heating. Heating a toluene solution of **1(SnMe)** under 26 psi of ^{13}CO at 80 $^{\circ}$C did not show any incorporation of ^{13}CO even after a week. In contrast to the facile subsitution observed in the Fe system (Fig. III.6 and ref. [12]), **1(SnMe)** failed to react with excess PMe$_3$ even after 28½ hrs at 100 $^{\circ}$C.

Under photochemical conditions, however, **1(SnMe)** is more reactive. As has already been mentioned, it gives a red solution on photolysis in THF, although the product(s) has not been identified. It also reacts photolytically with the olefins C$_2$H$_4$ and CH$_2$=CHCOOMe to give the corresponding mono-substituted derivatives Os$_2$(CO)$_7$(SnMe$_2$)$_2$(olefin), **11**. In these olefin derivatives, the olefin ligand occupies an equatorial position on the metal core, in a similar manner to that observed in the mononuclear analogues Os(CO)$_4$(olefin) [13]. The methylacrylate derivative **11a** is unstable in solution, decomposing slowly at room temperature to form **6** and releasing methylacrylate. This thermal instability may be a general feature for such olefinic derivatives, and would explain why the C$_2$H$_4$ analogue was badly disordered in the solid state, appearing to contain both **1(SnMe)** and the disubstituted derivative, and also why we were not successful in obtaining analogous derivatives for a number of similar ligands such as methylmethacrylate, CF$_2$=CH$_2$, and diphenylacetylene.

Cluster **6** is a rather insoluble yellow solid. Its solubility is low in hot dichloromethane, chloroform and toluene, but it goes rapidly into solution in pyridine to form an orange solution with carbonyl stretches in the infrared (dichloromethane solution) at 2082w, 2001s,br and 1868vw cm^{-1}. A ^{13}C{^{1}H} NMR spectrum of this solution failed to yield any useful information. In an attempt at isolating the product, removal of solvent followed by trituration in hexane yielded a yellow powder [ν(CO) in nujol at 2075.5w,

1993.5s and 1942sh cm^{-1}], but we have not been able to establish its identity. Cluster **6** also reacts in dichloromethane at 60 ^{o}C with methylacrylate to give **11a**, and with P(OMe)$_3$ and PMe$_3$ to give the corresponding phosphorus-ligand substituted derivatives Os$_2$(CO)$_7$(SnMe$_2$)$_2$L (L = P(OMe)$_3$, **12a**; PMe$_3$, **12b**). The phosphorus ligands occupy an equatorial site, as was established by an X-ray structural study for **12b**. This parallels the situation in osmium clusters, in which the sterically more demanding ligands like phosphines are found to occupy equatorial sites, while sterically less demanding ligands, like nitriles, isonitriles and pyridine, occupy the presumably electronically more favourable axial sites [14]. It is, however, in contrast to that reported by Bigorgne and Kahn for [(OC)$_4$FeSnBu$_2$]$_2$, in which the monosubstituted phosphine derivative was, on the basis of the v(CO) pattern, assumed to have the phosphine ligand in an axial site while the disubstituted derivative has both phosphines in equatorial sites on different Fe centres and in a mutually *trans* orientation (Fig. III.5) [12].

The similarity between the patterns of the v(CO) in the infrared spectra of Fe$_2$(CO)$_7$(SnBu$_2$)$_2$(PEt$_3$) and **12b**, however, strongly suggests that both clusters have the same structure (Fig. III.6).
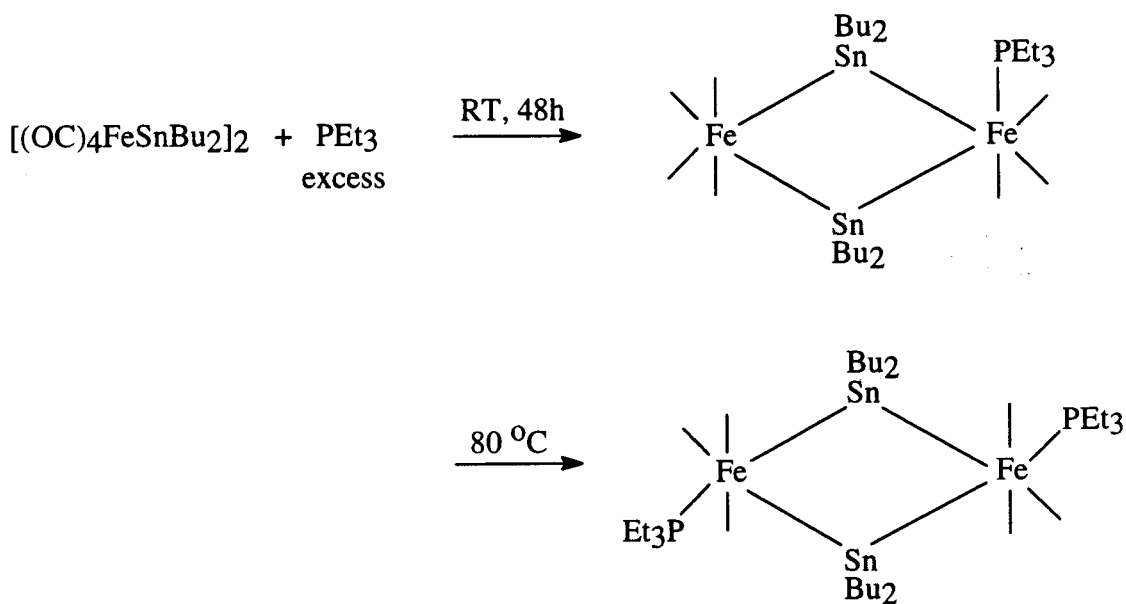
Fig. III.5.   Reactions of [(OC)$_4$FeSnBu$_2$]$_2$ with PEt$_3$ (from ref. [12]).

73
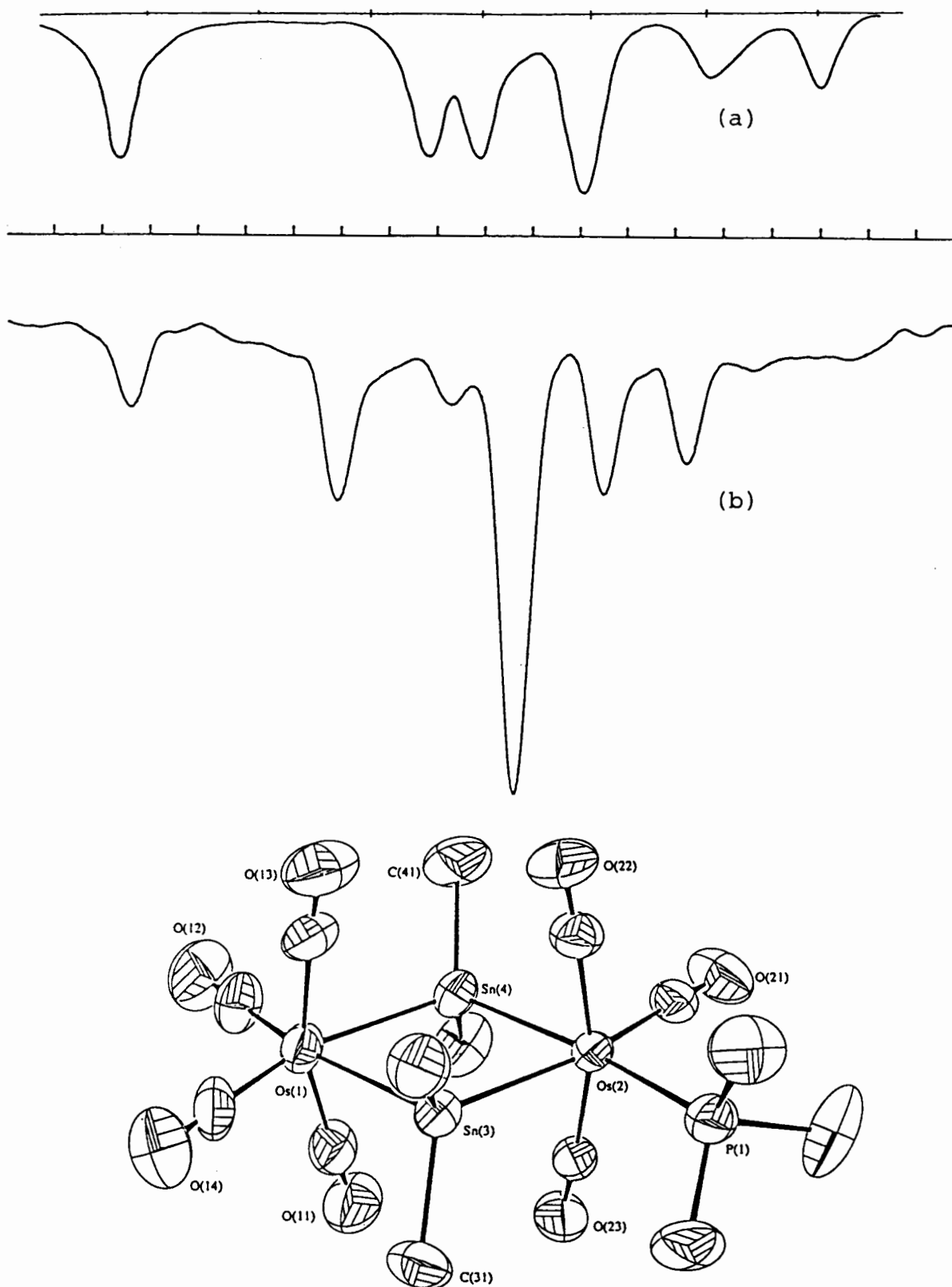
Fig. III.6. The v(CO) for (a) $Fe_2(CO)_7(SnBu_2)_2(PEt_3)$ (from ref. [12]) and,

(b) **12b**, and the X-ray structure of **12b**.

The ease with which **6** reacts with both phosphorus donor ligands and methylacrylate to form **12** and **11b** respectively, which are formally substituted derivatives of **1(SnMe)**, suggests that **6** may be regarded as an activated form of **1(SnMe)**. It also indicates the weakness of the Os-Os bonds in **6**. This point is further borne out by the fact that on heating a dichloromethane suspension of **6** under a CO atmosphere it was converted to **1(SnMe)**, as detected spectroscopically. Pyrolysis of **6** gave rise to similar products to that from the pyrolysis of **1(SnMe)**, suggesting that a common intermediate may be involved in both pyrolyses. These observations are also consistent with the proposal outlined in Scheme III.1 above, so that a simple scheme linking the formation and reactions of **1(SnMe)** and **6** would be that given in Scheme III.3. The availability of a high-yield route to **6** further recommends its utility as a convenient starting material to otherwise difficult to access, mono-substituted derivatives of **1(SnMe)** under mild conditions.

The ^{1}H NMR spectra of the three PMe$_3$-substituted derivatives of the hexametallic cluster [(OC)$_3$OsGeMe$_2$]$_3$, **5(Ge)**, viz., clusters **13**, **14** and **15**, are consistent with the phosphines occupying equatorial positions (Fig. III.7). This further underscores the site preference of phosphorus ligands observed in osmium cluster chemistry.
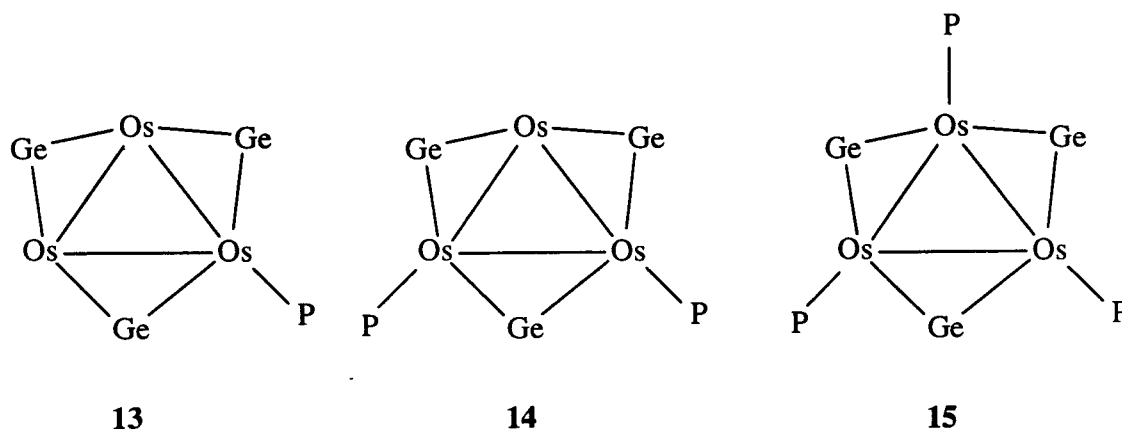
Fig. III.7. Structures of clusters **13**, **14** and **15** (Me's and CO's omitted).
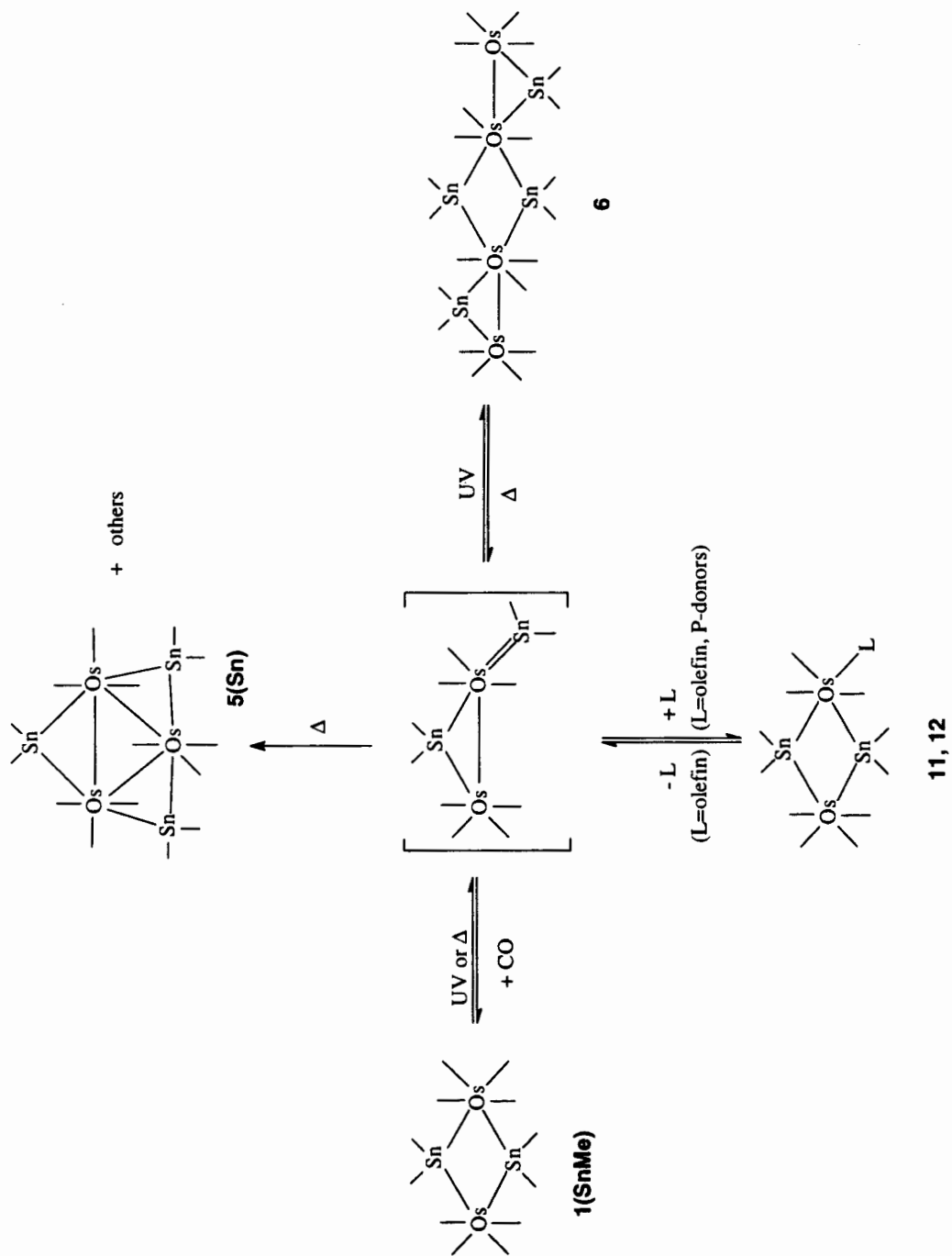
Scheme III.3. Proposed scheme for the formation and reaction of clusters **1(SnMe)**, **5(Sn)**, **6**, **11** and **12**.

76

That the substitution of **5(Ge)** by PMe$_3$ proceeded cleanly at 100 °C indicates the quite considerable robustness of **5(Ge)**, a point already noted earlier by Knox and Stone [10b] when they found that **5(Ge)** did not react with PPh$_3$ even on refluxing for several days in hexane. That clusters **5** may be obtained as major products from the pyrolysis or photolysis of **1(EMe)** and **6**, as well as from mononuclear species [10b], points to their thermodynamic stability, and particularly to the stability of the Os$_3$E$_3$ metal core. In this respect, the Os$_3$E$_3$ core is more like the triangular Os$_3$ unit than the isolobal raft-like Os$_6$ unit; the latter easily folds up by loss of COs [15]. This is probably the result of the considerable strength of the E-CH$_3$ bond (E = Ge, Sn), so that loss of methyl groups to form a more condensed cluster containing, for example, an edge-bridged trigonal bypyramidal metal core (Fig. III.8), is energetically unfavourable. It is envisaged, however, that the corresponding lead or phenyl compounds may undergo the necessary cleavage more readily. The chemistry of the Os$_3$E$_3$ clusters, therefore, certainly merits further investigation along these lines.
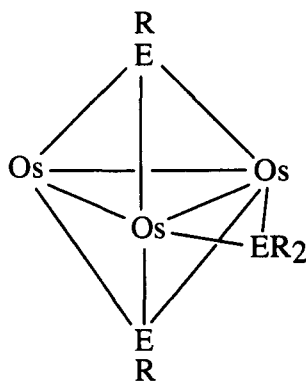
Fig. III.8.   A possible condensed cluster product by loss of R groups from
$[(OC)_3OsER_2]_3$ clusters (CO's omitted) .

4. References

[1]   L'Eplattenier, F.; Pélichet, M. C. *Helv. Chim. Acta*, **1970**, *53*, 1091.

[2]   George, R. D.; Knox, S. A. R.; Stone, F. G. A. *J. Chem. Soc., Dalton Trans.*, **1973**, 972.

[3]   (a) Carter, W. J.; Kelland, J. W.; Okrasinski, S. J.; Warner, K. ER.; Norton, J. R. *Inorg. Chem.*, **1982**, *21*, 3955. (b) Bhattacharya, N. K.; Coffy, T. J.; Quintana, W.; Salupo, T. A.; Bricker, J. C.; Shay, T. B.; Payne, M.; Shore, S. G. *Organometallics*, **1990**, *9*, 2368.

[4]   Collman, J.P.; Murphy, D.W.; Fleischer, E. B.; Swift, D. *Inorg. Chem.*, **1974**, *13*,1.

[5]   L'Eplattenier, F. *Inorg. Chem.*, **1969**, *8*, 965.

[6]   Cotton, J. D.; Knox, S. A. R.; Stone, F. G. A. *J. Chem. Soc. A*, **1968**, 2758.

[7]   Pomeroy, R. K.; Vancea, L.; Calhoun H. P.; Graham, W. A. G. *Inorg. Chem.* **1977**, *16*, 1508.

[8]   Marks, T. J.; Newman, A. R. *J. Am. Chem. Soc.*, **1973**, *95*, 769.

[9]   (a) Bonny, A.; MacKay, K. M. *J. Chem. Soc., Dalton Trans.*, **1978**, 722. (b) Kummer, D.; Furrer, J. *Z. Naturforsch., B*, **1971**, *26*, 162. (c) Marks, T. J.; Grynkewich, G. W. *J. Organomet. Chem.*, **1975**, *91*, C9. (d) Marks, T. J.; Grynkewich, G. W. *Inorg. Chem.*, **1976**, *15*, 1307. (e) Corriu, R. J. P.; Moreau, J. J. E. *J. Chem. Soc., Chem. Commun.*, **1980**, 278.

[10]   (a) Stone, F. G. A.; Howard, J.; Knox, S. A. R.; Woodward, P. *J. Chem. Soc. D,* **1970**, 1477. (b) Knox, S. A. R.; Stone, F. G. A. *J. Chem. Soc. A*, **1971**, 2874.

[11]   Harrison, P. G. In *Chemistry of Tin*; Harrison, P. G., Ed.; Blackie: Glasgow, 1989; Chapter 2.

[12]   Bigorgne, M.; Kahn, O. *J. Organomet. Chem.*, **1967**, *10*, 137.

[13]   Burke, M. R.; Takats, J.; Grevels, F-W.; Reuvers, J. G. A. *J. Am. Chem. Soc.*, **1983**, *105*, 4092.

[14]   (a) Deeming, A. J. *Adv. Organomet. Chem.*, **1986**, *26*, 1. (b) Pomeroy, R. K. *J. Organomet. Chem.*, **1990**, *383*, 387.

[15]   Nicholls, J. N.; Vargas, M. D. *Adv. Inorg. Chem. Radiochem.*, **1986**, *30*, 123.

Chapter IV   Discussion of X-ray structures : A whole gamut of clusters.

1.   Tri- and Tetrametallic clusters

(a)   Ph$_2$Ge[Os(CO)$_4$H]$_2$ and "(OC)$_3$HOs(SnBu^t$_2$)$_2$O"

The cluster "(OC)$_3$HOs(SnBu^t$_2$)$_2$O" may be viewed as a mononuclear Os compound with a chelating Bu^t$_2$SnOSnBu^t$_2$ ligand, but it is more interesting to view it as consisting of a metal chain isolobal to that in Ph$_2$Ge[Os(CO)$_4$H]$_2$, **3**, closed into a ring by an O atom. For this reason, these two clusters are discussed together.

Cluster **3** is the only example of an OsEOs chain that has been structurally characterised (Fig. IV.1); the only other known OsEOs chain is the cationic Cl$_2$Sn[OsCp$_2$]$_2$$^{2+}$, which was characterised spectroscopically [1]. A closely-related set of chain clusters are the compounds RM(SnCl$_2$)Os$_3$(CO)$_{12}$Cl (RM = Cp(OC)$_3$W, Cp(OC)$_3$Mo, CpFe, (OC)$_5$Re) [2]. Similar Fe analogues have, however, been known for some time, including for example, Cl$_2$E[Fe(CO)$_2$Cp]$_2$ (E = Ge, Sn) and Me$_2$E[Fe(CO)$_2$Cp]$_2$ (E = Ge, Sn, Pb) [3].

Although there is no crystallographically imposed symmetry, the molecule of **3** does possess an approximate C$_2$ axis passing through the Ge atom and the midpoint of the Os⋯Os vector. The hydrides are *cis* to the Ge atom, and point towards each other; the GeOsC planes (where C is the carbonyl *trans* to the hydride) are at a dihedral angle of 148.6^o, so that the hydrides are not in the same plane as the metal chain. That the hydrides are located on the inside bend of the metal chain may be attributed to the smaller steric bulk of the hydrides as compared to the other ligands. This reduced steric bulk of the hydrides may also have allowed the bending in of the CO's towards the hydrides, and the smaller OsGeOs angle of 114.41(6)^o as compared to the 128(1)^o in Cl$_2$Ge[Fe(CO)$_2$Cp]$_2$ [3c]. The larger than tetrahedral OsGeOs angle is also in accord with the trend found in tin-transition metal compounds [4].
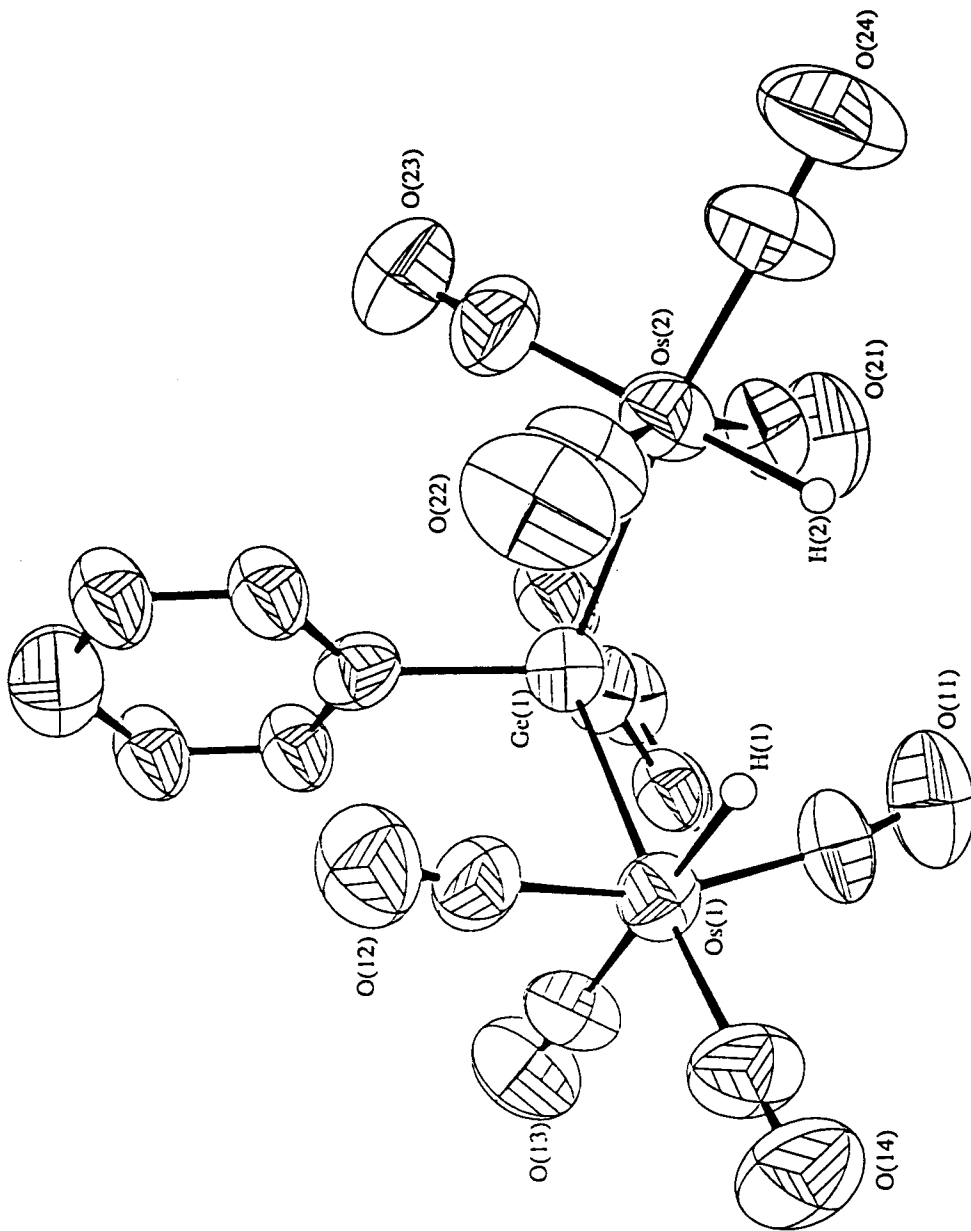
Fig. IV.1. ORTEP plot of Ph$_2$Ge[Os(CO)$_4$H]$_2$, **3**. Os(1)-Ge(1) = 2.599(2) Å, Os(2)-Ge(1) = 2.614(2) Å, Os(1)-Ge(1)-Os(2) = 114.41(6)°, C((11)-Os(1)-C(13) = 99.1(6)°, C(12)-Os(1)-C(13) = 96.6(7)°, C(13)-Os(1)-C(14) = 96.3(6)°, C(21)-Os(2)-C(23) = 95.4(7)°, C(22)-Os(2)-C(23) = 98.7(8)°, C(23)-Os(2)-C(24) = 98.2(8)°.

The Os-Ge bond lengths in **3** (2.599(2) and 2.614(2) Å) are longer than that in any of the clusters in this study (ranges from 2.475(2) Å to 2.593(1) Å for the other OsGe clusters). The difference in the two Os-Ge bond lengths is statistically significant, though it is probably of no chemical significance; there is no obvious chemical reason for it other than that of the "nebulous" crystal packing forces.

The cluster "$(OC)_3HOs(SnBu^t_2)_2O$" has not been fully-characterised. The EAN rule requires that there is very likely a second H atom in the cluster, possibly on the μ_2-O unit, i.e., that it is actually a μ_2-OH group. There is infrared spectroscopic evidence for the Os-H, but unfortunately, by the time we realized from the X-ray structural study that there should be a second H atom, we did not have any material remaining to obtain spectroscopic, i.e., IR or ^{1}H NMR, evidence for it. However, should the conjecture prove correct, then the bonding in the cluster may be described as shown in Fig. IV.3, which is reminiscent of that in the anionic compound $[(Ph_3Sn)_2(OC)_3W\{(SnPh_2)_2O^iPr\}]^-$ [5].

The molecule of "$(OC)_3HOs(SnBu^t_2)_2O$" has a pseudo mirror plane through the O, Sn and axial carbonyls, and is structurally similar to $(Ph_3P)_2(OC)(H)Ir\{(SiMe_2)_2O\}$ [6], which also has a OsSn$_2$O ring that is not quite planar; the dihedral angle between the SnOsSn and SnOSn planes of the molecule in this study is 5.9°, so that the O atom is a little out of the metal plane, towards the same side as the metal hydride. As in $Ph_2Ge[Os(CO)_4H]_2$, the two Os-Sn bonds (2.660(2), 2.680(2) Å) are crystallographically different, though probably not chemically so.
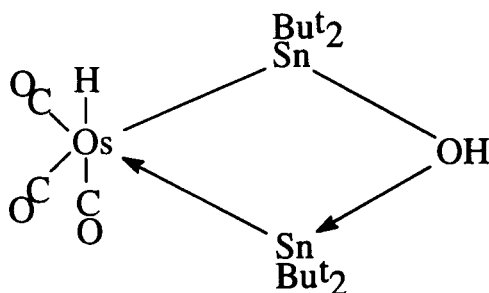
Fig. IV.3.   Bonding description for "$(OC)_3HOs(SnBu^t_2)_2(\mu\text{-OH})$".
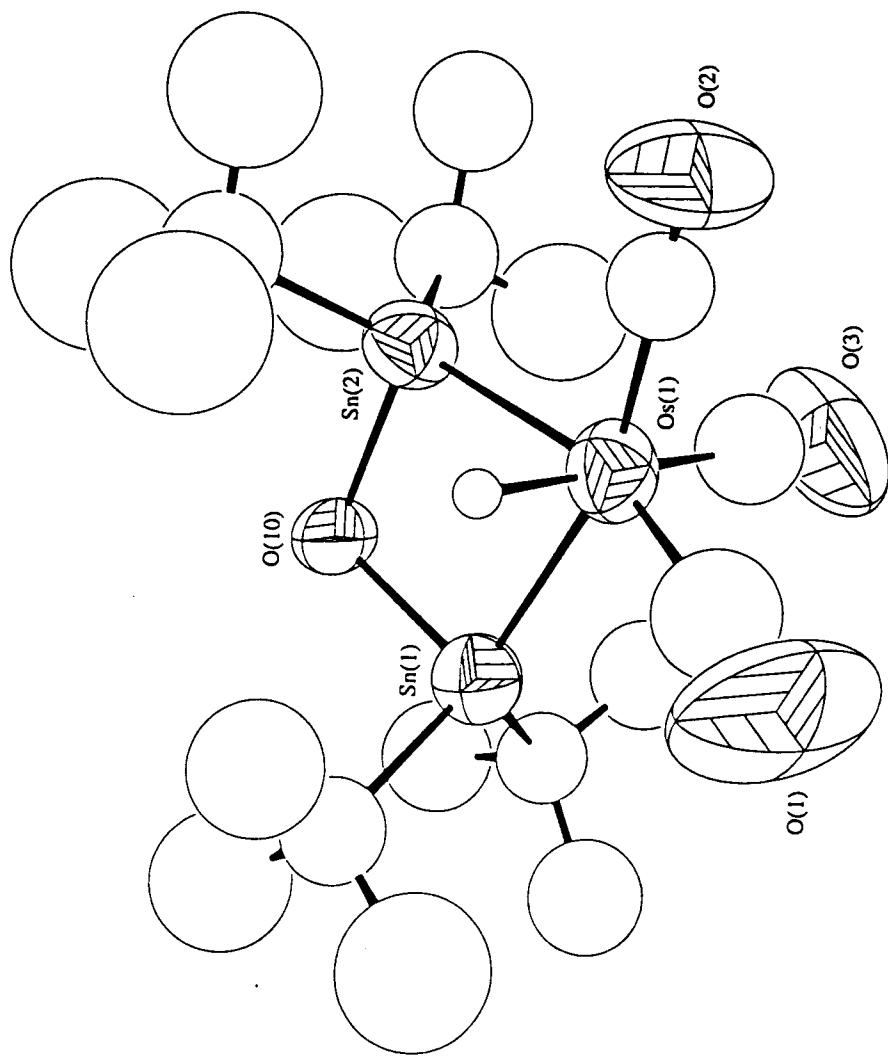
Fig. IV.2.   ORTEP plot of "(OC)$_3$HOs(SnBu$^t_2$)$_2$O". Os(1)-Sn(1) = 2.680(2) Å, Os(1)-Sn(2) = 2.660(2) Å, Sn(1)-O(10) = 2.13(1) Å, Sn(2)-O(10) = 2.13(1) Å, Sn(1)-Os(1)-Sn(2) = 76.61(5)°, Os(1)-Sn(1)-O(10) = 90.4(3)°, Os(1)-Sn(2)-O(10) = 91.0(3)°.

(b) $[(OC)_4OsEMe_2]_2$ (E = Ge, Sn, Pb) and $[(OC)_4OsSnBu^t_2]_2$
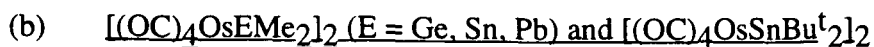
Crystals of the clusters $[(OC)_4OsEMe_2]_2$ (E = Ge, Sn, Pb), **1(EMe)**, and $[(OC)_4OsSnBu^t_2]_2$, **1(SnBu^t)**, all showed fairly rapid changes in the intensities of the intensity standards during X-ray data collection. In addition, **1(GeMe)** and **1(SnMe)** showed disorder of the Os_2E_2 rings. Despite fairly extensive investigation, we have not been able to obtain much insight into the nature of the intensity changes and the disorder. The intensity changes appear to be X-ray induced, as they were found to follow the exposure time to X-ray, and probably correspond to structural changes in the clusters. Two sets of data each were collected for **1(GeMe)** and **1(PbMe)** in an attempt to ascertain whether the disorder was X-ray induced; the second sets were collected after 22 h of exposure to UV, and directly after completion of data collection for the first set, for **1(GeMe)** and **1(PbMe)**, respectively. The refined structural solutions from either the initial datasets or the second datasets contained no significant differences, suggesting that the disorder was not induced by UV, and probably not by X-ray either.

In the structures of all four clusters a molecule sits on a crystallographic inversion centre; the Os_2E_2 rings are thus constrained by symmetry to be planar. An ORTEP plot of one of the two crystallographically distinct molecules of **1(PbMe)** is shown in Fig. IV.4. A common atomic numbering scheme and selected bond parameters for the four clusters are given in Table IV.1, together with those of two known iron analogues, viz., $[(OC)_4FeSnMe_2]_2$ (**FeSnMe**) [7] and $[(OC)_4FeSnCp_2]_2$ (**FeSnCp**) [8].

Other than the obvious increase in E-M bond lengths as we move from Ge to Pb, or from Fe to Os, there is also the same trend exhibited in the M(1)$\cdots$M(1') and E(1)$\cdots$E(1') distances. The differences in the Os-E bond lengths match, somewhat surprisingly, very closely the differences in the covalent radii of the Group 14 elements (covalent radii of Ge, Sn and Pb are 1.22, 1.41 and 1.47 Å respectively [9]). The E(1)-M(1)-E(1') and M(1)-E(1)-M(1') angles are also correlated with the changing covalent radii from Ge to Pb, and
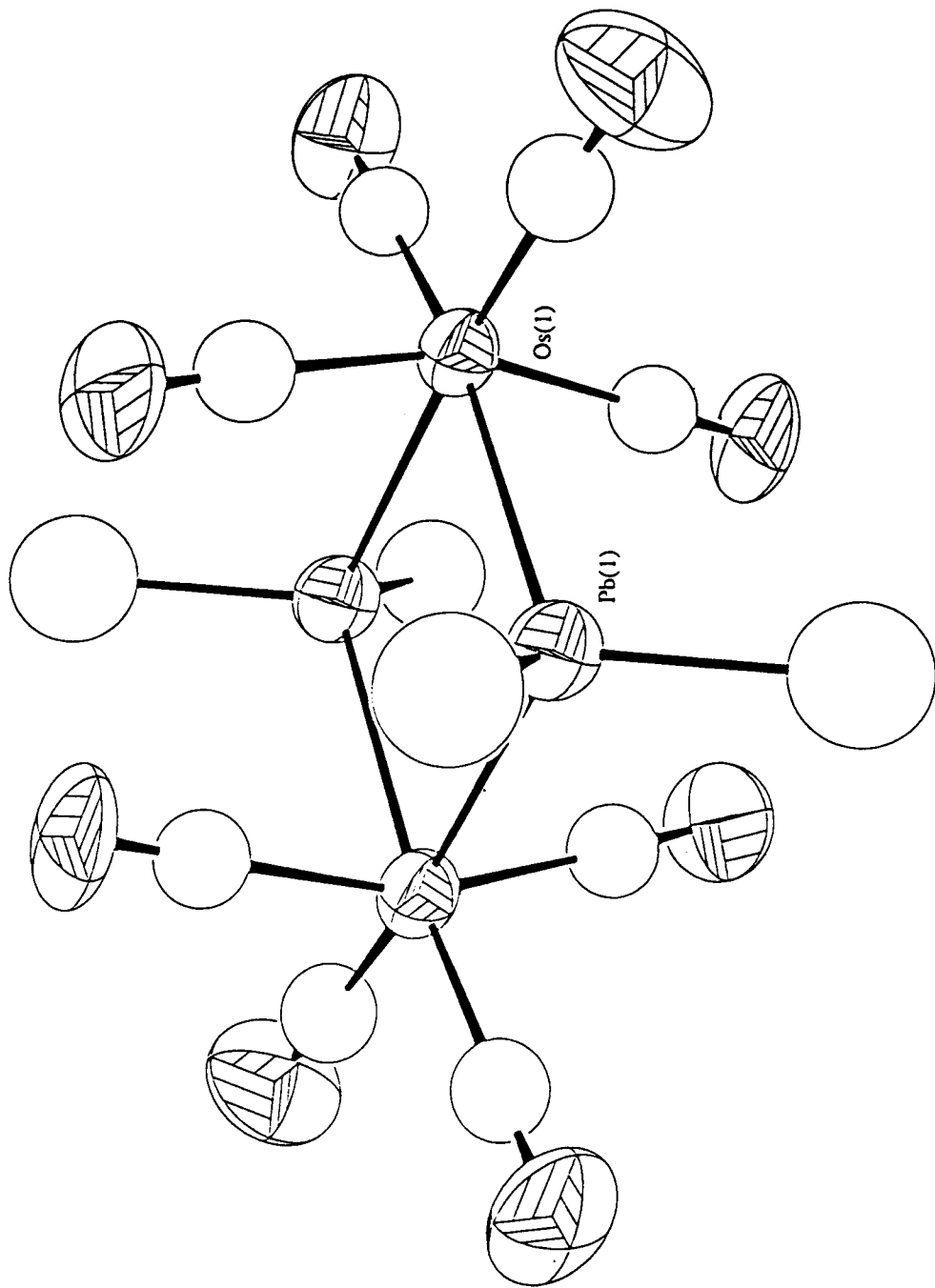
Fig. IV.4. ORTEP plot of one of the two crystallographically distinct molecules of [(OC)$_4$OsPbMe$_2$]$_2$, 1(PbMe).

85

Table IV.1. Atomic numbering scheme and selected bond parameters for 1(EMe) (E = Ge, Sn, Pb), 1(SnBu^t), FeSnMe and FeSnCp
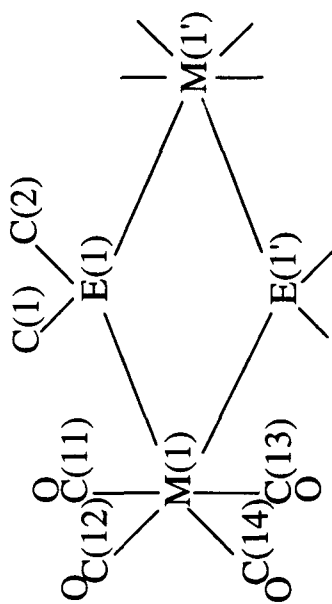
	1(GeMe)	1(SnMe)	1(PbMe)	1(SnBu^t)	FeSnMe[1]	FeSnCp
M(1)-E(1)	2.588(1) 2.593(1)	2.75781(8) 2.76755(9)	2.831(2), 2.832(1) 2.843(1), 2.832(1)	2.810(1) 2.815(1)	2.647(8)	2.670(1) 2.651(1)
M(1)...M(1')	4.105(1)	4.374(1)	4.436(2), 4.423(2)	4.414(1)	4.131(19)	4.136[2]
E(1)...E(1')	3.161(2)	3.376(1)	3.539(2), 3.540(2)	3.487(2)	3.312(8)	3.347[2]
E(1)-C	1.96(1)	2.14(1) 2.15(1)	2.32(2), 2.26(3) 2.18(2), 2.16(3)	2.3133(8) 2.15(6)	2.30(7) 2.257(5)	2.220(5)
E(1)-M(1)-E(1')	75.20(4)	75.32(3)	77.16(3), 77.35(3)	76.61(3)	77.4(3)	77.96(2)
M(1)-E(1)-M(1')	104.80(4)	104.68(3)	102.83(3), 102.65(3)	103.39(3)	102.6(3)	102.04(3)
C(1)-E(1)-C(2)	106.3(5)	106.5(5)	101(1), 109(1)	104.80(3)	109(2)	101.0(2)

[1] bond parameters are those of the second, undisordered molecule in the original literature.

[2] derived from published atomic coordinates.

from Fe to Os; the former angle increases with the increasing covalent radius in E and decreases with an increase in the covalent radius of M, while the latter angle shows the reverse trend. The significantly larger E(1)-M(1)-E(1') angle and smaller M(1)-E(1)-M(1') angle for **1(PbMe)** as compared to that for **1(SnMe)** and **1(GeMe)** is interesting, as the greater electronegativity of Pb(IV) compared to either Sn(IV) or Ge(IV) (2.33, 1.96 and 2.01, respectively, on the Pauling scale) [10] would have been expected to decrease the s character at the Os and increase the s character at the Pb atom [11].

The C(1)-E(1)-C(2) angles do not show any discernible trend. This is probably a reflection of (a) the influence of subtle but important packing forces, especially for atoms lying in the periphery of the molecule, and (b) the uncertainty in the positions of light atoms in a heavy-atom structure, an uncertainty not adequately reflected in the estimated standard deviations (σ) obtained from least-squares refinements. The first factor is readily seen in the two crystallographically distinct molecules of **1(PbMe)**, which show a difference of 0.12 Å between their mean Pb-C bond lengths. Furthermore, even the Os-Pb bond lengths show differences of as much as 19σ in the same molecule.

The second factor may be demonstrated by a consideration of the Os-C and C-O bond lengths for the carbonyls (Table IV.2). The ranges of C-O and Os-C bond lengths are 0.09 Å and 0.14 Å respectively, compared with the smaller range of 0.08 Å for the Os⋯O distances; the Os⋯O distances are essentially the same as the sums of the Os-C and C-O bond lengths. Inspection of individual Os-C and C-O bond lengths also suggest that the variations in these can be accounted for by errors in the C atom positions. Thus in heavy-atom structures, caution should be exercised in the interpretation of C-O bond parameters, as the positions of the C atoms may not be determined precisely enough or their precision adequately reflected in their e.s.d.s. From the E-C bond lengths and C-E-C bond angles (Table IV.3), the same can probably be said about the C atom positions of the methyl groups, so that the observation is probably quite general for light atoms in heavy-atom structures.

Table IV.2.　Os-C, C-O, Os···O and E-C bond lengths (Å) for **1(EMe)** (E = Ge, Sn, Pb) and **1(SnBuᵗ)**.

	1(GeMe)	**1(SnMe)**	**1(PbMe)**	**1(SnBuᵗ)**
Os-C(11)	1.96(1)	1.93(1)	1.99(2), 1.90(2)	1.95(2)
Os-C(12)	2.02(2)	1.92(1)	2.02(2), 1.94(2)	1.89(1)
Os-C(13)	1.94(1)	1.93(1)	1.93(3), 1.88(2)	1.94(2)
Os-C(14)	1.90(1)	1.93(1)	1.94(2), 1.90(2)	1.94(3)
C(11)-O(11)	1.12(1)	1.15(1)	1.10(2), 1.17(2)	1.12(2)
C(12)-O(12)	1.09(2)	1.16(1)	1.08(2), 1.10(2)	1.17(2)
C(13)-O(13)	1.13(1)	1.13(1)	1.14(3), 1.18(2)	1.13(2)
C(14)-O(14)	1.13(2)	1.15(1)	1.12(2), 1.16(2)	1.17(3)
Os···O(11)	3.073(8)	3.077(8)	3.091(14), 3.069(16)	3.069(11)
Os···O(12)	3.113(9)	3.073(9)	3.094(13), 3.042(16)	3.066(13)
Os···O(13)	3.072(7)	3.062(8)	3.065(19), 3.057(16)	3.071(13)
Os···O(14)	3.031(10)	3.085(9)	3.059(15), 3.059(15)	3.099(16)
E-C	1.96(1)	2.14(1)	2.18(2), 2.16(3)	2.3133(8)
	1.96(1)	2.15(1)	2.32(2), 2.26(3)	2.3057(9)

Given the above possibility of an error in the position of C atoms in carbonyl ligands, there is a case for considering steric and electronic effects on M-CO bond lengths in terms of M···O displacements instead. Since the effect on C-O bond lengths is usually small, any changes in M···O displacements can be attributed to changes in the M-C bond length; such a procedure has the advantage of being less susceptible to errors in the C atom position within the M···O vector. Using such a procedure, it can be seen that there is no obvious trends detectable in terms of differences between the axial and equatorial positions, or with variation in E, for the carbonyl ligands.

One trend in the carbonyl ligands that is readily observed, however, is the bending inwards of the axial carbonyls towards the Os_2E_2 ring centre (Table IV.3). This has also been observed in **FeSnMe**, in which it was concluded, from an examination of the non-bonded contacts, that the phenomenon is mainly the result of intermolecular rather than

intramolecular forces [7]. Furthermore, it has been argued that this "umbrella effect", which is quite common in tin-transition metal compounds, is most likely a consequence of packing or efficiency of space-filling rather than an unusual electronic effect [4]. Fig. IV.5 shows the views along the Os_2E_2 ring planes for **1(GeMe)** and **1(PbMe)**, and it can be seen that the bending in of the carbonyls in these clusters may be attributed to intermolecular steric interactions.

Table IV.3. CEC and $Os\cdots OsC_{ax}$ angles (^{O}) for **1(EMe)** (E = Ge, Sn, Pb) and **1(SnBu^t)**.

	1(GeMe)	**1(SnMe)**	**1(PbMe)**	**1(SnBu^t)**
C-E-C	106.3(5)	106.5(5)	108.7(10), 100.6(10)	104.80(3)
$Os\cdots Os$-C(11)	83.7(4)	82.0(4)	82.6(7), 81.0(7)	84.0(5)
$Os\cdots Os$-C(13)	81.6(4)	80.9(3)	79.5(6), 80.8(7)	87.5(5)

Given the prevalence of this effect, however, it is quite possible that there is also an electronic component. The strong σ donating but weak π accepting ability of the ER_2 fragments would increase electron density on the Os centre through σ donation without the concomitant withdrawal of electron density from it through π back-donation. One possible mechanism by which this imbalance may be redressed could be via the tilting-in of the axial CO's so that the M d to axial CO π^* back-bonding is enhanced (Fig.IV.6).
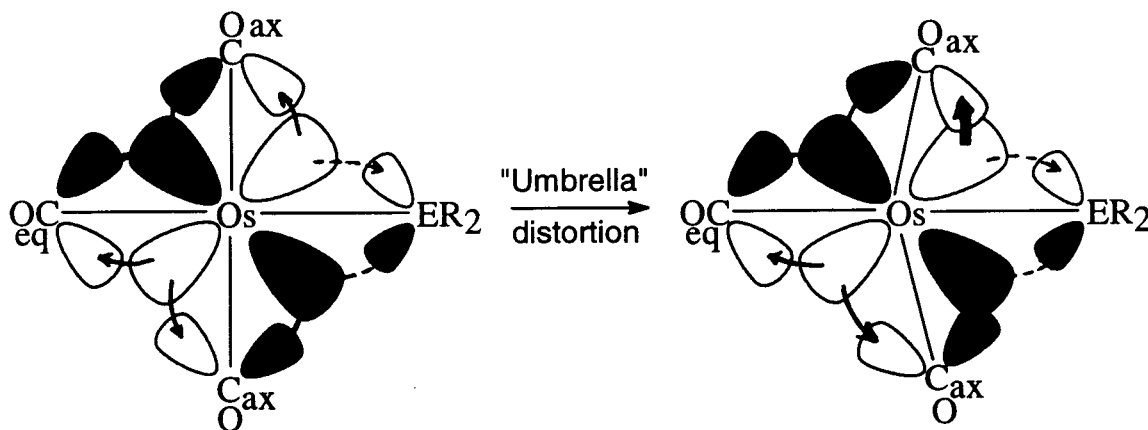
Fig. IV.6.   A qualitative MO diagram demonstrating how Md-COπ^* back-bonding may be enhanced by the "umbrella" effect to compensate for the poor π interaction with the ER_2 fragment.
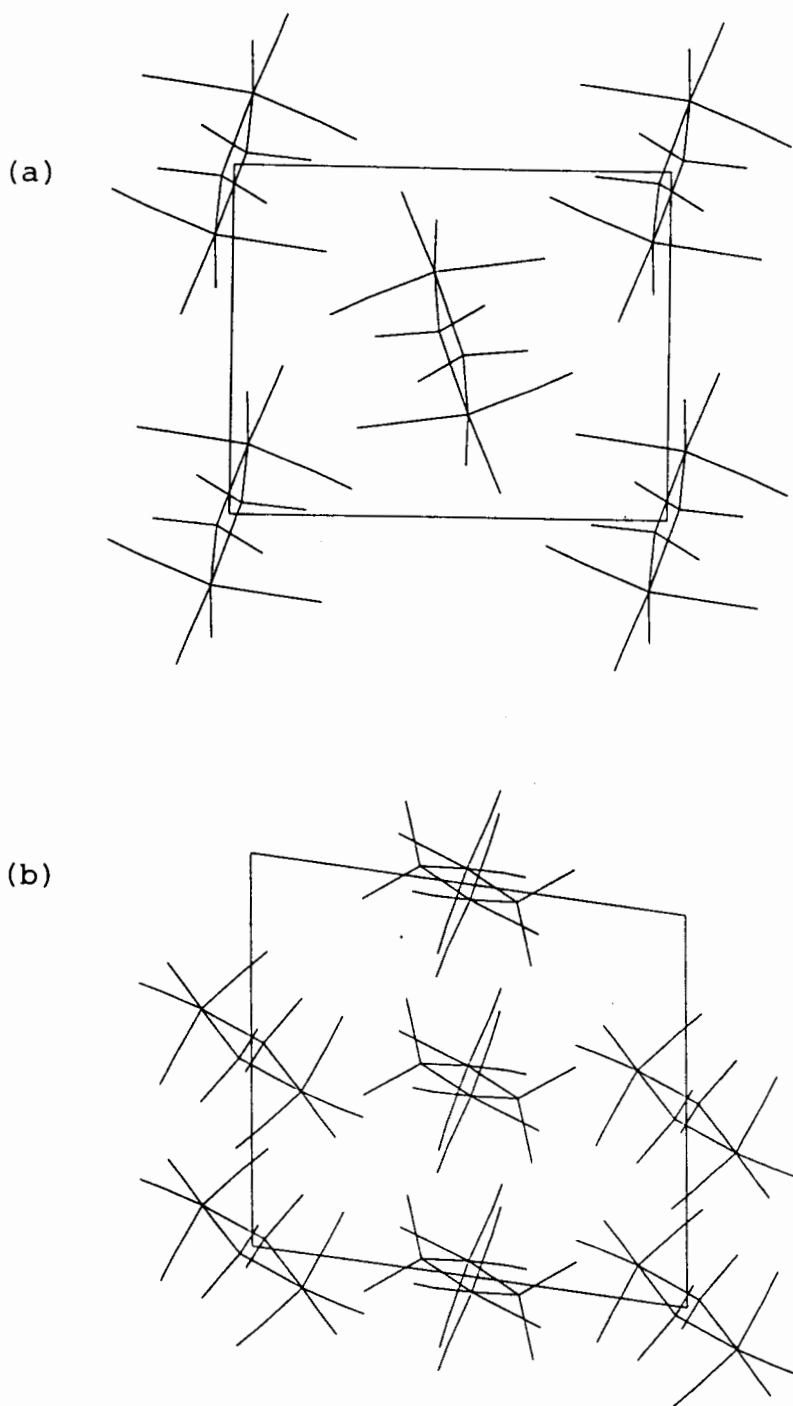
Fig. IV.5. View of the packing: (a) in the yz plane, along the x-axis, for **1(GeMe)** and,
(b) in the xz plane, along the y axis, for **1(PbMe)**.

90

(c)   <u>Os$_2$(CO)$_7$(SnMe$_2$)$_2$L (L = PMe$_3$, C$_2$H$_4$)</u>
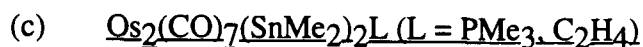
In both the ethene and phosphine derivatives, Os$_2$(CO)$_7$(SnMe$_2$)$_2$(C$_2$H$_4$), **11b**, and Os$_2$(CO)$_7$(SnMe$_2$)$_2$(PMe$_3$), **12b**, the Os$_2$Sn$_2$ metal cores are almost planar; the dihedral angles between the SnOsSn planes are 0.011^o and 0.313^o for **11b** and **12b**, respectively. Both the ethene and phosphine ligands occupy equatorial positions. Furthermore, as in the parent cluster **1(SnMe)**, the "umbrella effect" is quite apparent.

The Os-Sn bond lengths in **12b** (Fig. IV.7) are all significantly different from each other. In particular, those to Os(2) which has the phosphine attached, are shorter than those to Os(1) (mean of 2.744 Å and 2.789 Å, respectively); they should also be compared to the mean of 2.763 Å in **1(SnMe)**. One interpretation for the shorter Os-Sn bonds involving Os(2) is that the poorer π-acceptor property of PMe$_3$ as compared to CO leads to stronger π(d-d) back-bonding from Os to Sn and hence a stronger and shorter Os-Sn bond.

The X-ray molecular structure for **11b** was found to be badly disordered, and has been interpreted as consisting of a disordered Os$_2$(CO)$_7$(SnMe$_2$)$_2$(C$_2$H$_4$) molecule at one of the crystallographic inversion centres, and a disordered [(OC)$_3$(C$_2$H$_4$)OsSnMe$_2$]$_2$ molecule at the other crystallographically distinct inversion centre; an ORTEP plot of one molecule of the latter is given in Fig. IV.8. As a consequence of the disorder, the bond parameters are "averaged", so that for instance the Os-Sn bond lengths in **11b** are probably the mean for an unsubstituted and substituted Os (Table IV.4). In spite of this, it is apparent that the Os-Sn bond lengths are shorter than those for **1(SnMe)**, so that the situation is similar to that for Os(2) in **12b**.
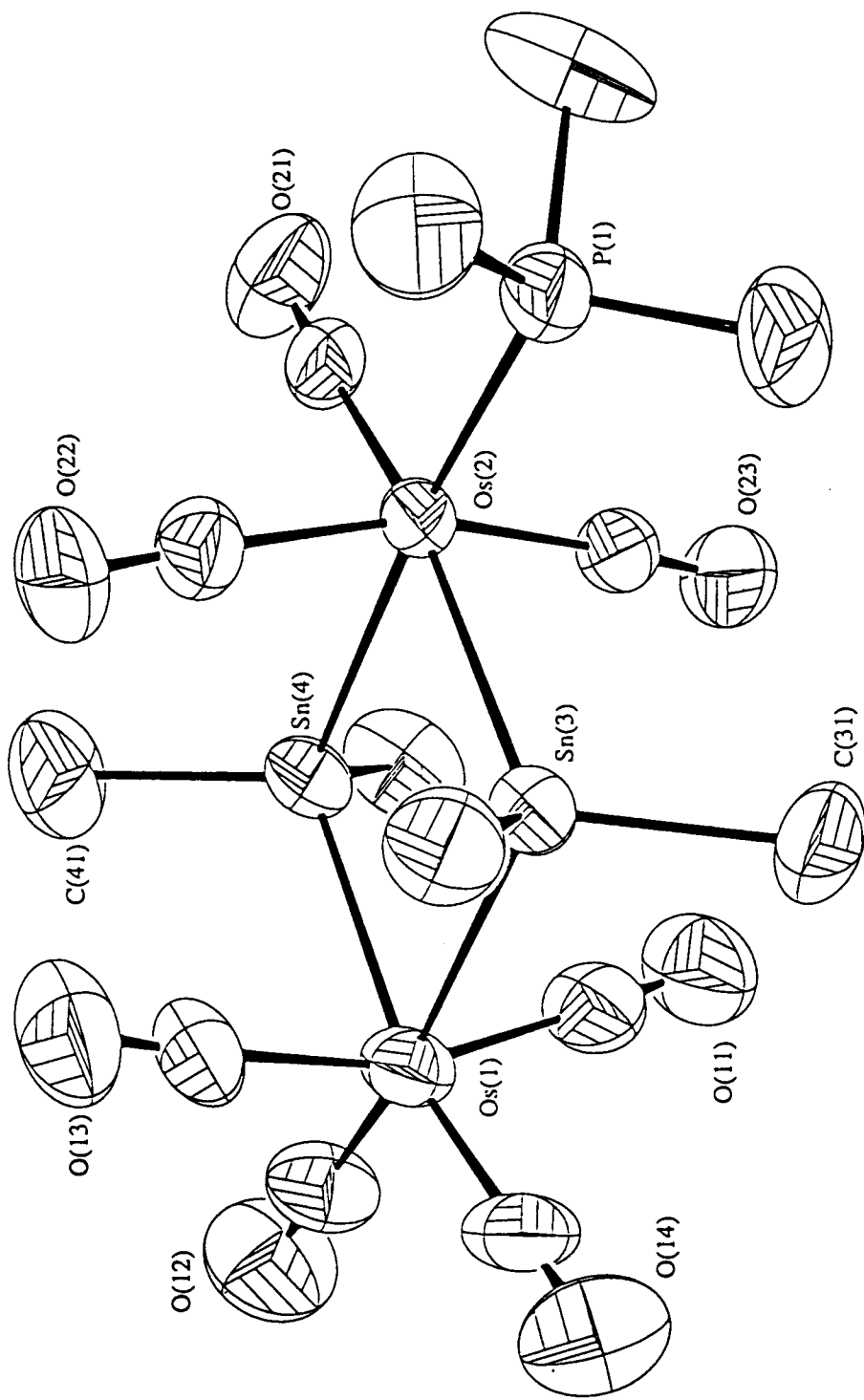
Fig. IV.7. ORTEP plot of $Os_2(CO)_7(SnMe_2)_2(PMe_3)$, **12b**. $Os(1)-Sn(3) = 2.7905(7)$ Å, $Os(1)-Sn(4) = 2.7867(7)$ Å, $Os(2)-Sn(3)$ = 2.7454(7) Å, $Os(2)-Sn(4) = 2.7317(6)$ Å, $Os(2)-P(1) = 2.363(2)$ Å, $Os(1)-Sn(3)-Os(2) = 104.10(2)°$, $Os(1)-Sn(4)-Os(2) = 104.57(2)°$, $Sn(3)-Os(1)-Sn(4) = 74.86(2)°$, $Sn(3)-Os(2)-Sn(4) = 76.47(2)°$.
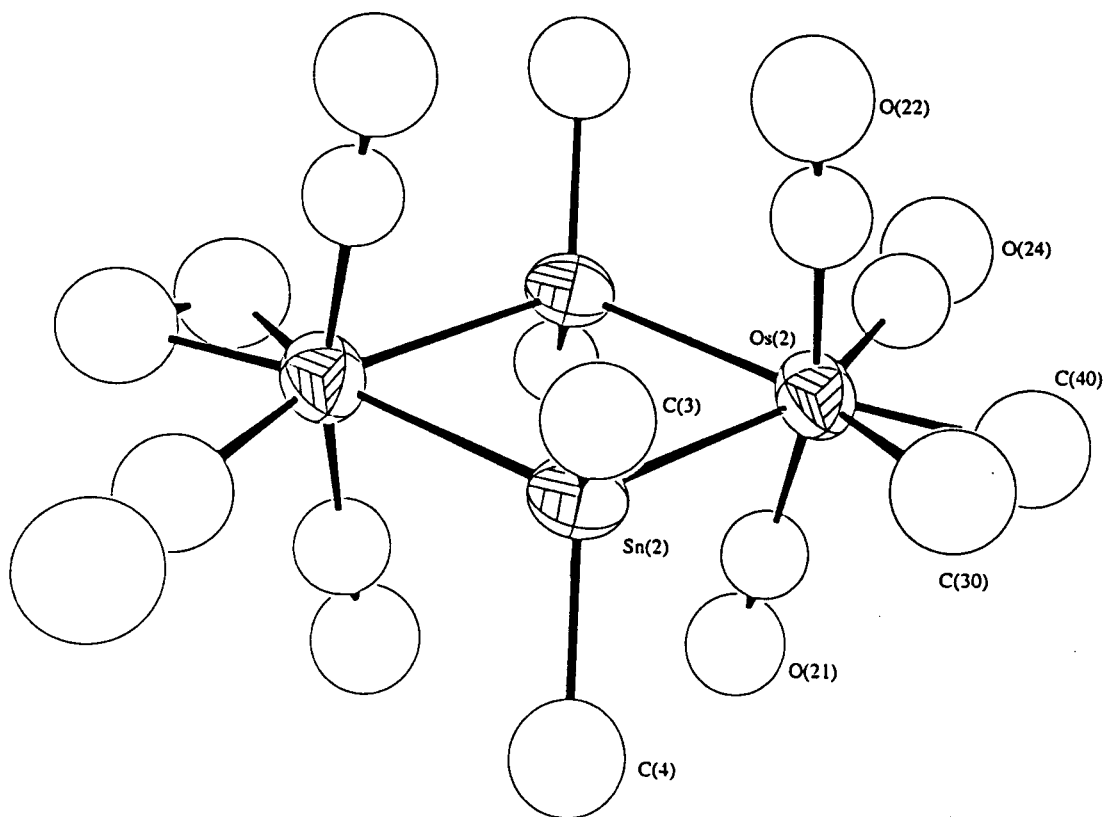
Fig. IV.8.   ORTEP plot of $[(OC)_3(C_2H_4)OsSnMe_2]_2$.

Table IV.4. Selected bond parameters for $Os_2(CO)_7(SnMe_2)_2(C_2H_4)$ and

$[(OC)_3(C_2H_4)OsSnMe_2]_2$.

	$Os_2(CO)_7(SnMe_2)_2(C_2H_4)$	$[(OC)_3(C_2H_4)OsSnMe_2]_2$
Os-Sn	2.741(1) Å, 2.753(1) Å	2.747(1) Å, 2.752(1) Å
Os-Sn-Os	105.88(3)°	107.02(4)°
Sn-Os-Sn	74.12(3)°	72.98(4)°

93

2.   Penta- and Hexametallic clusters

(a) $Os_2(CO)_6(GeMe_2)_3$ and $Os_3(CO)_{11}(GeMe_2)_2$

The gross structures of the metal cores in the clusters $Os_2(CO)_6(GeMe_2)_3$, **10**, and $Os_3(CO)_{11}(GeMe_2)_2$, **8**, (Fig. IV.9) can, with some stretching of the imagination, be regarded as similar to the homometallic clusters $Os_5(CO)_{16}$ [12] and $Os_5(CO)_{19}$ [13], which adopt trigonal bipyramidal and "bowtie" configurations respectively.

For the cluster **10**, however, the similarity breaks down even upon the most cursory examination; there are no Ge-Ge bonds corresponding to the equatorial edges of the bipyramid. In this respect, its more open structure can be better described as cage-like. Cluster **10** is in fact isostructural to its Fe analogue [14], and is isolobal to both $Fe_2(CO)_9$ and $Fe_2(CO)_6(\mu\text{-}CO)(GeMe_2)_2$ [15]. This is in itself interesting, as $Os_2(CO)_9$ is believed to have only one bridging carbonyl [16].

The crystal of **10** was found be twinned, in an approximately 4:1 ratio, in which the twin component may be obtained by a $\pi/3$ rotation about the three-fold axis on which the Os atoms sit. As can be seen from Table IV.5, the differences in bond parameters between **10** and its Fe analogue may be ascribed to the larger covalent radius of Os as compared to that of Fe, though many of the differences in bond lengths are larger than the difference of 0.08 Å between the covalent radii of Os and Fe. The Os-Os distance of 2.944(1) Å is indicative of a bond and is required if cluster **10** is to satisfy the EAN rule.

Table IV.5. Selected bond parameters and difference in bond lengths

(Δ = d(Os-X) - d(Fe-X)) for $M_2(CO)_6(GeMe_2)_3$ (M = Fe, Os)

	M-M (Å)	M-Ge (Å)	M-C (Å)	M-Ge-M (°)	Ge-M-C (°)
M = Fe	2.74(1)	2.398(5)	1.77(2)	69.8(2)	86.1(7)
M = Os	2.944(1)	2.545(1)	1.943(8)	70.68(4)	85.1(3)
Δ (Å)	0.20	0.147	0.17		
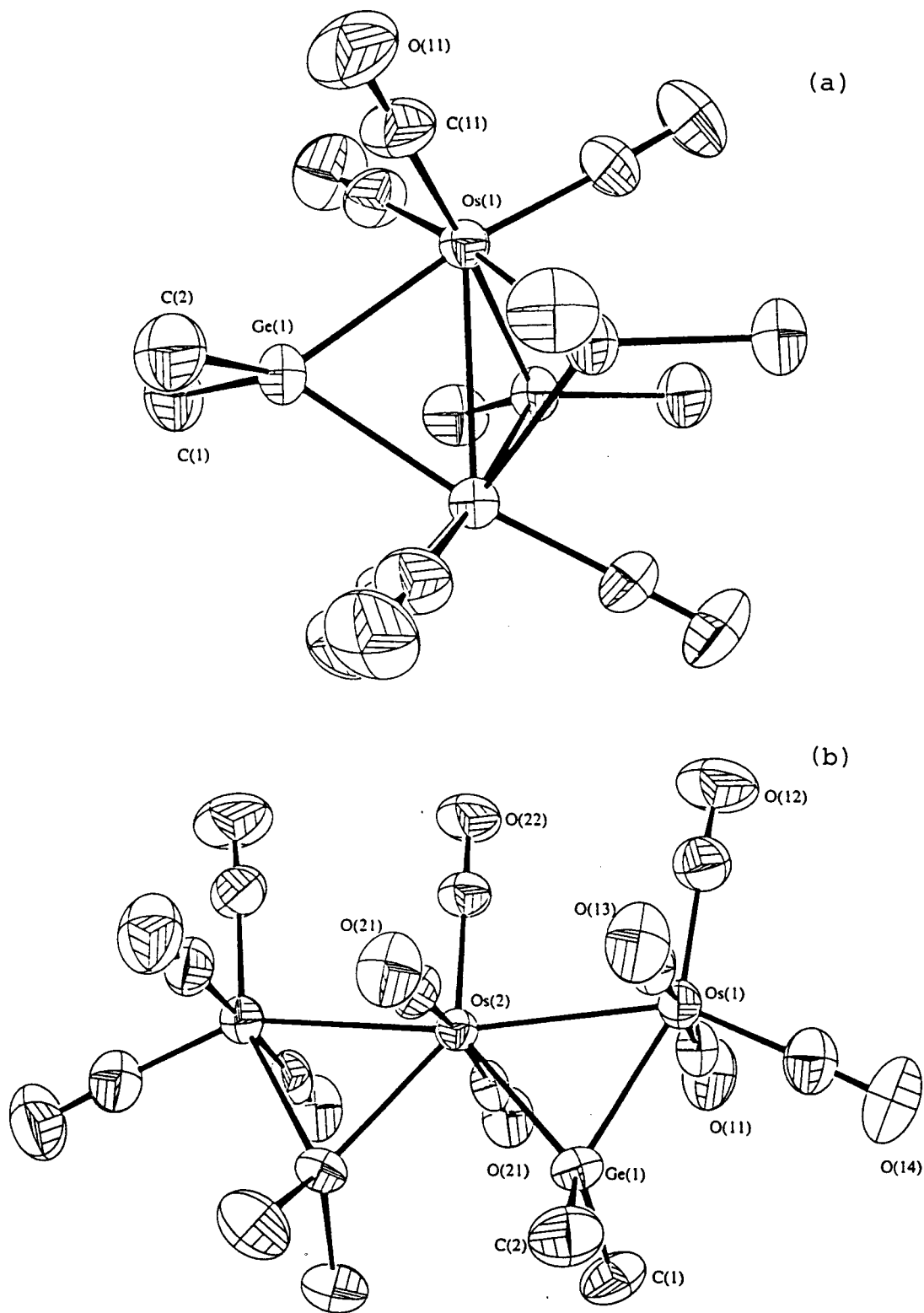
Fig.IV.9. ORTEP plots for (a) $Os_2(CO)_6(GeMe_2)_3$, **10**, and (b) $Os_3(CO)_{11}(GeMe_2)_2$, **8**.

The cluster **8** has a crystallographic C_2 axis through the central Os atom and its equatorial CO ligand. Unlike the poor analogy between cluster **10** and $Os_5(CO)_{16}$, cluster **8** is isolobal to $Os_5(CO)_{19}$ [13]. The gross features of the latter two clusters are very similar, though there are inherent differences due to the different sizes of the Os and Ge atoms (Table IV.6). Both clusters are in the shape of a "bowtie", and their two metal triangles are twisted with respect to each other; the dihedral angle between the two OsOsM planes are 21.2° and 5.6° for M = Os and Ge, respectively.

Table IV.6. Selected bond parameters for $Os_3(CO)_{11}(GeMe_2)_2$ and $Os_5(CO)_{19}$ [13].
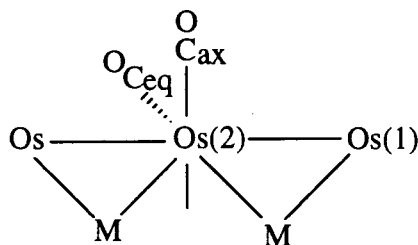
	M = Os	M = Ge
Os(1)-Os(2) (Å)	2.918(2), 2.913(2)	2.981(1)
Os(1)-M (Å)	2.853(2), 2.848(2)	2.5223(7)
Os(2)-M (Å)	2.940(2), 2.950(2)	2.5199(7)
Os(2)-C_{ax} (Å)	1.895(23), 1.911(21)	1.931(7)
Os(2)-C_{eq} (Å)	1.889(24)	1.95(1)
M-Os(2)-M (°)	95.2(1)	82.23(1)
Os(1)-Os(2)-M (°)	58.2(1)	53.79(2)

One of the very noticeable differences between the two clusters is the long Os-Os bond length in **8** compared to the analogous bonds in $Os_5(CO)_{19}$. This lengthening may be attributed to ring strain at the Ge atoms and steric repulsion between the two non-bonded

Ge atoms (the Ge···Ge distance is 3.314(1) Å). It is interesting to note, however, that in $Os_5(CO)_{19}$, the M···M steric repulsion appeared to have caused more pronounced lengthening of the Os(2)-M bond rather than the Os(1)-Os(2) bond. We believe that this is an indication of the 'softness' of an Os-Os bond as compared to an Os-Ge bond [17], i.e., an Os-Os bond is more easily distorted without great detriment to its bond strength.

(b)   [(OC)$_3$OsEMe$_2$]$_3$ (E = Ge, Sn)

The hexametallic clusters [(OC)$_3$OsEMe$_2$]$_3$ (E = Ge, Sn), **5(E)**, are isolobal to the clusters $M_3(CO)_{10}[Si\{CH(SiMe_3)_2\}_2]_2$ (M = Ru, Os) [18], $Os_5(CO)_{18}$ [19] and $Os_6(CO)_{21}$ [20] (Fig. IV.10); all have a planar, raft-like arrangement of metal atoms (including the bridging carbonyl in the case of the pentametallic clusters). An ORTEP plot for **5(Sn)** is shown in Fig. IV.11.
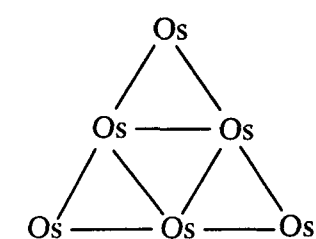
$Os_6(CO)_{21}$
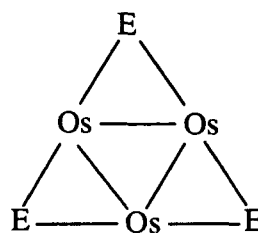
[(OC)$_3$OsEMe$_2$]$_3$

5(E) (E = Ge,Sn)
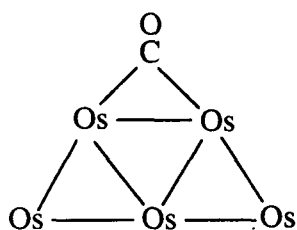
$Os_5(CO)_{18}$
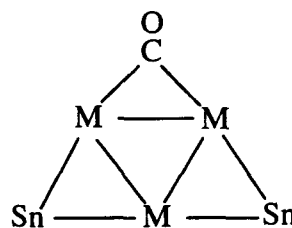
$M_3(CO)_{10}[Sn\{CH(SiMe_3)_2\}_2]_2$

(M = Ru, Os)

Fig. IV.10. Some isolobal raft-like penta- and hexametallic clusters (ligands, except bridging CO, omitted).
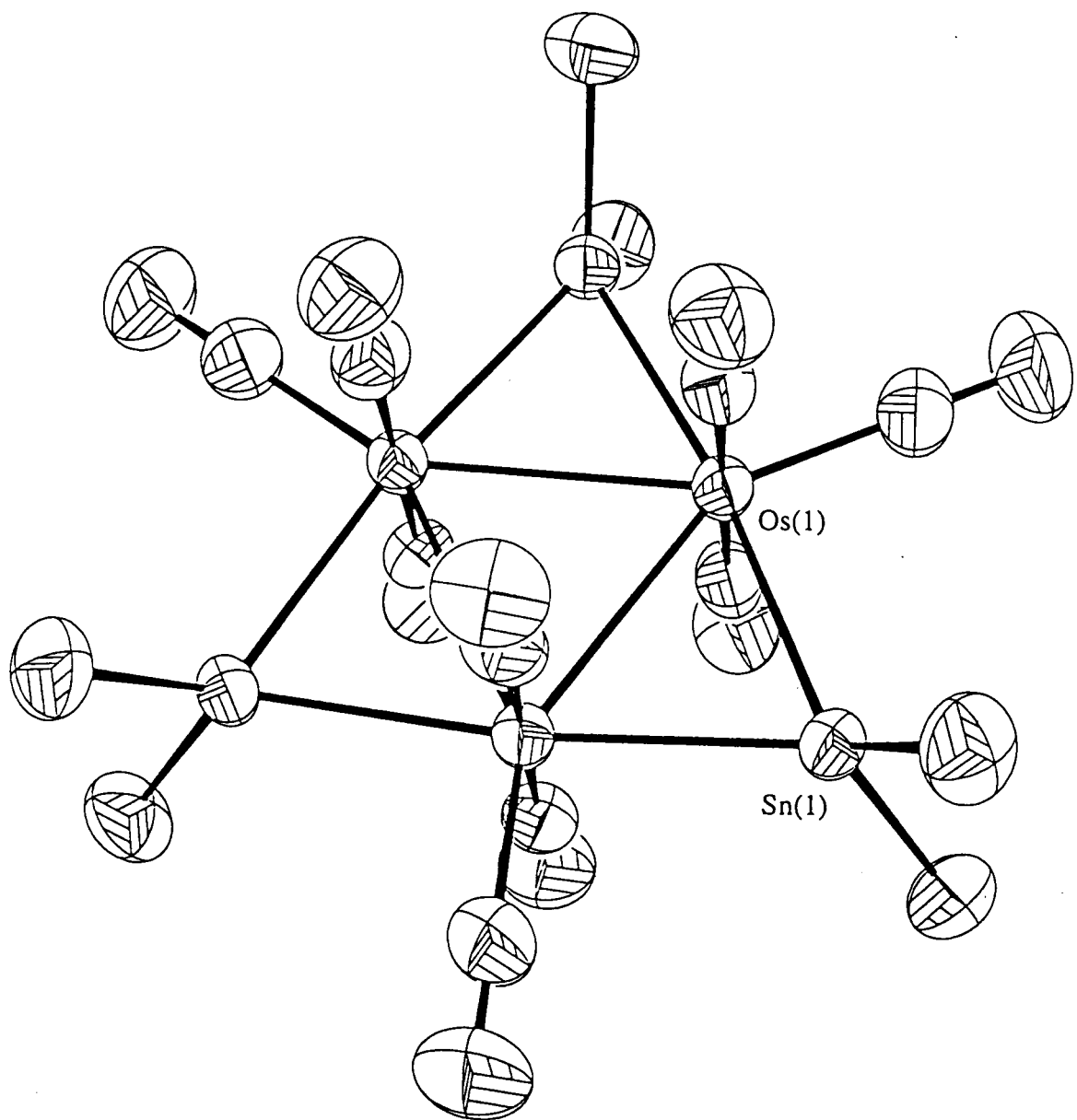
Fig. IV.11.   ORTEP plot for [(OC)$_3$OsSnMe$_2$]$_3$, **5(Sn)**.

As has already been noted earlier, the Os-Os bonds in the clusters **5(E)** tend to be longer than those in homometallic clusters (*cf*. 2.847-2.892 Å in Os$_5$(CO)$_{18}$ [19]), while the Os-E bonds are short; the Os-E bond lengths in **5(E)** are among the shortest found in this study.

The clusters **5(E)** are isostructural to that of the Ru analogue of **5(Ge)**, viz., [(OC)$_3$RuGeMe$_2$]$_3$ [21]. The molecules are constrained by their crystallographic site symmetry ($\bar{6}$) to be planar. The Os atoms are 7-coordinate, with approximate pentagonal bipyramidal coordination geometry. Once again, the differences in bond parameters (Table IV.7) among the clusters can be interpreted mainly on the basis of the differences in covalent radii of Ge and Sn, and of Ru and Os. Thus the M-M and M-E bond lengths increase from M = Ru and E = Ge to M = Os and E = Sn, while the M-E-M angle decreases along the same direction.

Table IV.7. Selected bond parameters for **5(E)** (E = Ge, Sn) and [(OC)$_3$RuGeMe$_2$]$_3$ [21].
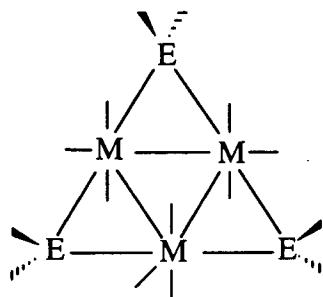
	5(Sn)	**5(Ge)**	[(OC)$_3$RuGeMe$_2$]$_3$
M-M	2.974(1)	2.920(1)	2.926(9)
M-E	2.6670(8), 2.6733(7)	2.514(1), 2.525(1)	2.482(11), 2.500(12)
M-C (*ax, eq*)	1.94(1), 1.88(1)	1.937(9), 1.90(1)	1.90(7), 2.02(13)
C-O (*ax, eq*)	1.12(1), 1.14(1)	1.15(1), 1.14(1)	1.12(6), 0.94(11)
E-C	2.141(7)	1.960(7)	2.02(7)
M-E-M	67.69(2)	70.82(4)	71.9(3)
C-E-C	106.4(5)	106.4(5)	96(4)

3. Higher nuclearity clusters

(a) [Os_2(CO)_7(SnMe_2)_2]_2 and [Os_2(CO)_7O(SnMe_2)_2]_2
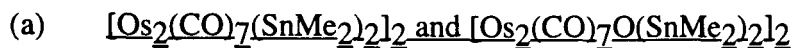
The structures of the clusters $[Os_2(CO)_7(SnMe_2)_2]_2$, **6**, and $[Os_2(CO)_7O(SnMe_2)_2]_2$, **7**, are closely related (Fig. IV.12); as mentioned previously, the latter structure can be regarded as derived from the former by insertion of an O atom between the Os(2)-Sn(1) and Os(2)-Sn(2') bonds. The metal atom core of **6** consists of two triangular Os_2Sn units each sharing an Os atom of the central rhomboidal Os_2Sn_2 unit. The molecule is centrosymmetric and almost planar; the dihedral angle between the triangular and rhomboidal metal units is 3.5°. The central framework of **7**, on the other hand, consists of a central 6-membered $Os_2Sn_2O_2$ ring which is joined through its Os-O edges to 4-membered Os_2SnO rings. The molecule has a C_2 axis running through the centre of the $Os_2Sn_2O_2$ ring. While the 4-membered rings are planar (the dihedral angle between Os(2)O(1)Sn(1) and Os(2)Os(1)Sn(1) is 1.5°), the central ring has a boat conformation, with the Os(2)Sn(2)O(1') plane at an angle of 46.2° to the O(1)Os(2)O(1')Os(2') plane.

The Os-Os bond lengths in both clusters (Table IV.8) are substantially longer than that in $Os_3(CO)_{12}$ (average of 2.877 Å); that in **6** (3.0414(5) Å) is especially so, and it is reflected in the reactivity of this cluster. The Os-Sn bond lengths in the triangular units of **6** (mean of 2.703 Å) are substantially shorter than those in the central rhomboid (mean of 2.770 Å); these lengths are comparable to those in $[(OC)_3OsSnMe_2]_3$ (mean of 2.670 Å) and $[(OC)_4OsSnMe_2]_2$ (mean of 2.763 Å), respectively. In contrast, the Os(1)-Sn(1) bond length in **7**, although part of 4-membered rings, is closer to that for a triangular Os_2Sn unit. The steric effect resulting from the proximity of the $SnMe_2$ groups in **6** is, however, evident in the elongation of the Os(2)-Sn(1) and Os(2)-Sn(2') bonds (2.7273(8) and 2.7802(6) Å, respectively) relative to the Os(1)-Sn(1) and Os(2)-Sn(2) bonds, respectively.

Table IV.8. Selected bond parameters for $[Os_2(CO)_7(SnMe_2)_2]_2$, **6**, and $[Os_2(CO)_7O(SnMe_2)_2]_2$, **7**.

	6	7
Os(1)-Os(2)	3.0414(5)	2.9706(8)
Os(1)-Sn(1)	2.6782(8)	2.673(1)
Os(2)-Sn(1)	2.7273(8)	-
Os(2)-Sn(2)	2.7603(7), 2.7802(6)	2.666(1)
Os(1)-Sn(1)-Os(2)/O(1)	68.47(2)	96.4(2)
Os(2)-Sn(2)-Os(2')/O(1')	109.28(2)	112.0(2)

Two noteworthy aspects of the structures of **6** and **7** are the coordination of the central Os atoms in **6** and the μ_3-O atoms in **7**. The central Os(1) in cluster **6** has pentagonal bipyramidal coordination, just as in the clusters **5(E)**. The μ_3-O atoms in **7** are almost trigonal planar in their bonding to the Os and Sn atoms; the O(1) atom is 0.13 Å above the Os(2)Sn(1)Sn(2') plane, indicating that the O atoms are essentially sp^2 hybridised. This is in contrast to the pyramidal O atoms in the cluster $[OsO(CO)_3]_4$ [22].
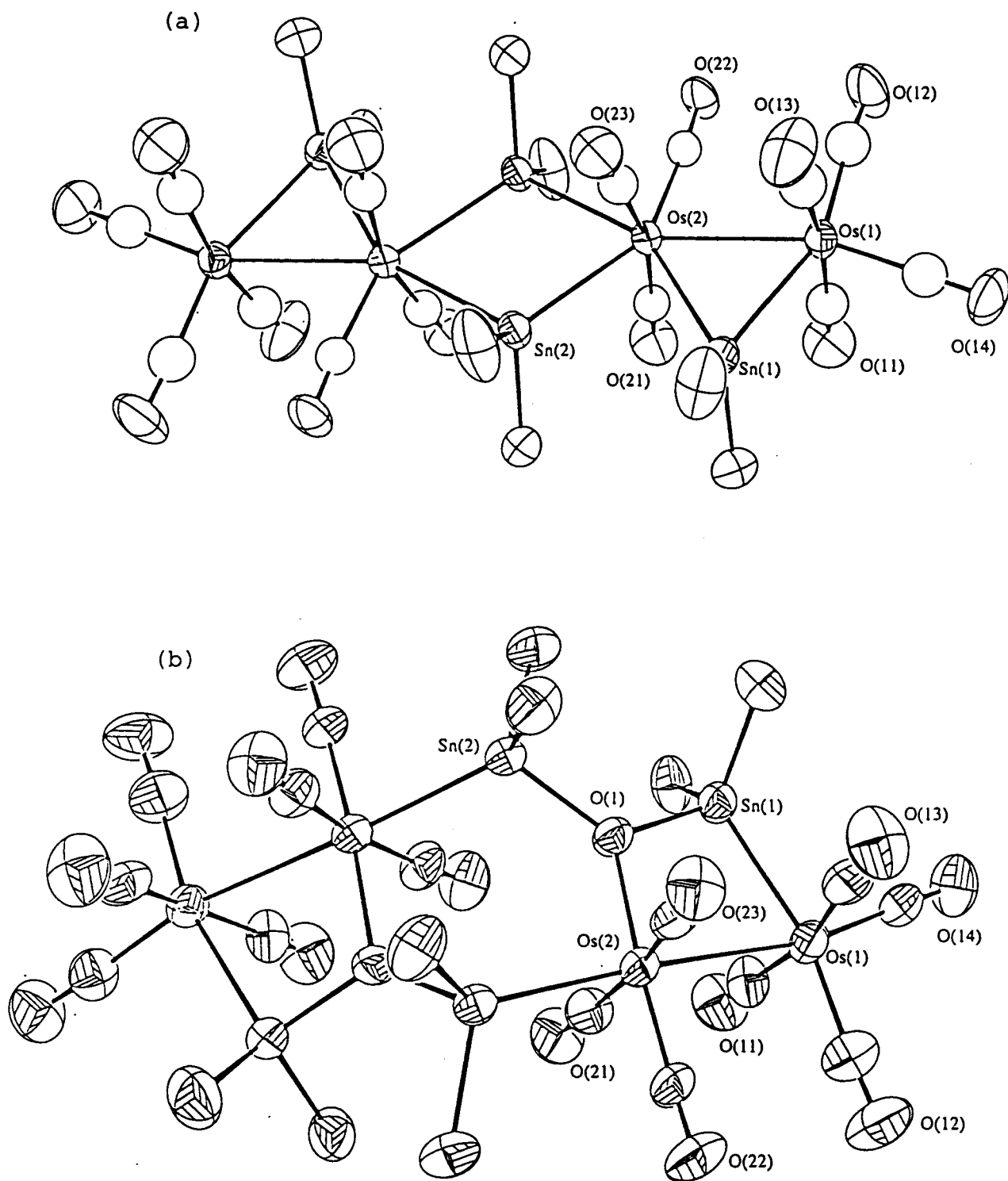
Fig. IV.12. ORTEP plots for (a) [Os$_2$(CO)$_7$(SnMe$_2$)$_2$]$_2$, **6**, and

(b) [Os$_2$(CO)$_7$O(SnMe$_2$)$_2$]$_2$, **7**.

(b)   <u>$Os_4(CO)_{12}(GeMe_2)_4$</u>

Although the cluster $Os_4(CO)_{12}(GeMe_2)_4$, **9**, (Fig. IV.13) may be regarded as a derivative of **5(Ge)** in which an equatorial carbonyl has been replaced by a germylene ($Me_2Ge=Os(CO)_4$) fragment, the long Os(1)-Ge(1) bond length suggests that the $Me_2GeOs(CO)_4$ fragment does not, however, possess Os=Ge character; this Os-Ge bond length of 2.556(2) Å is not exceptionally short in comparison with the other seven Os-Ge bond lengths (which ranges from 2.475(2) Å to 2.584(2) Å) in the same molecule. Furthermore, the long Os(1)-Os(2) bond (3.069(2) Å) suggests that the fluxionality of the $Me_2GeOs(CO)_4$ fragment observed by NMR spectroscopy may be accounted for by cleavage of this Os(1)-Os(2) bond followed by rotation about the Os(2)-Ge(1) bond, as described in Chapter III.

The metal skeleton of molecule **9** is essentially planar; the dihedral angle between the central Os(2)-Os(3)-Os(4) and the Os(1)-Os(2)-Ge(1) planes is 3.3°, while the largest displacement of any atom from the best plane in the Os_3Ge_3 core is 0.06 Å. The proximity of the methyl groups on Ge(1) and Ge(2) does not appear to have lengthened the Os(2)-Ge(1) and Os(2)-Ge(2) bonds. One final note is that while Os(3) and Os(4) are 7-coordinate, pentagonal bipyramidal, Os(2) is formally 8-coordinate, with hexagonal bipyramidal coordination geometry, an extremely rare geometry [23]; the hexagonal Os(1)Ge(1)Ge(2)Os(3)Os(4)Ge(4) plane is very close to planar, with displacements of the atoms off the best-fit plane ranging from 0.022 Å to 0.096 Å, and the C-Os(2)-C bond angle is 176.8(9)°. Although the Os-Os bond lengths involving Os(2) do show lengthening consistent with the expected steric crowding about Os(2), there is little evidence for it in the Os-Ge bond lengths. This is again probably a manifestation of the "softness" of an Os-Os bond compared to an Os-Ge bond.
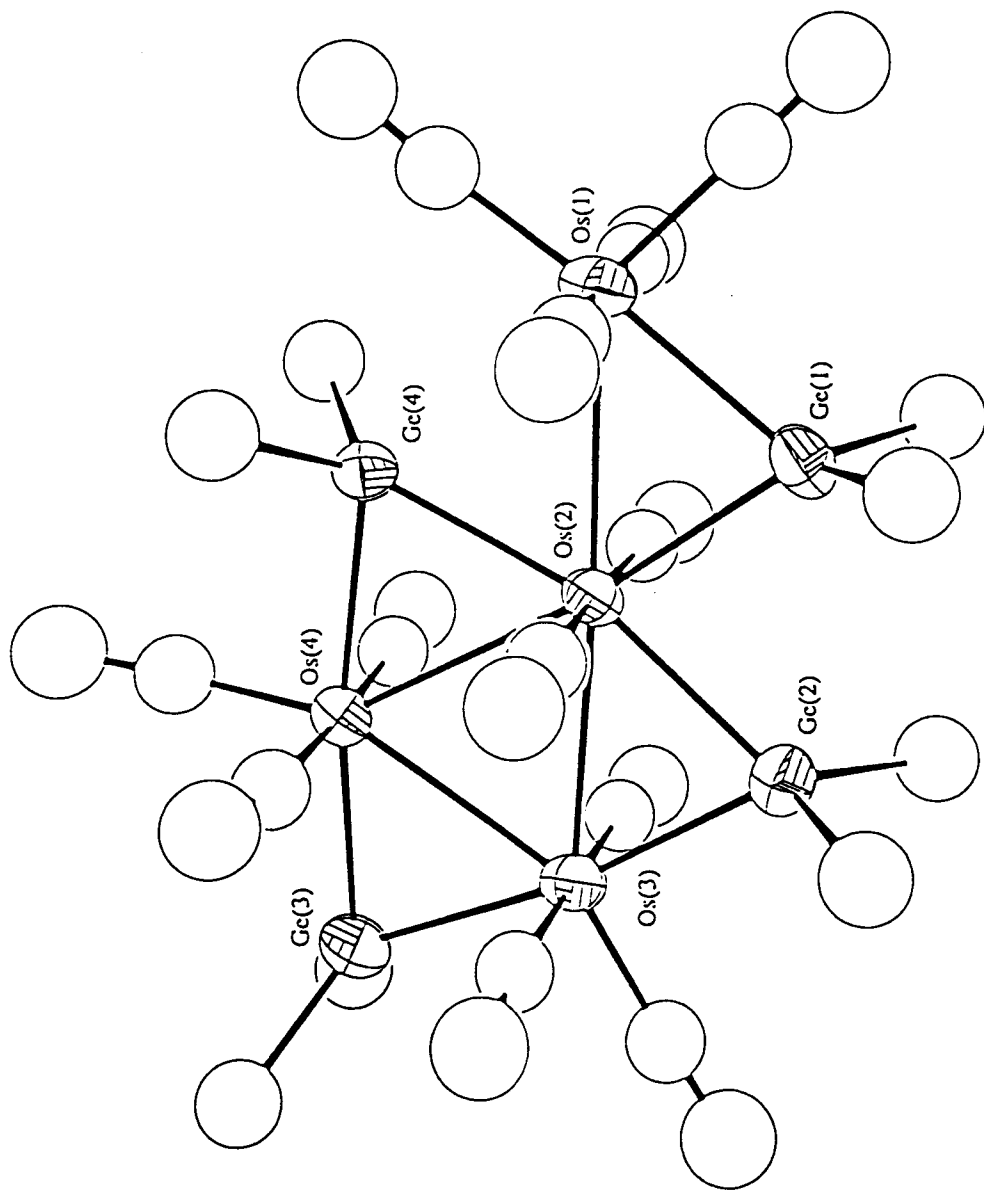
Fig. IV.13. ORTEP plot for $Os_4(CO)_{12}(GeMe_2)_4$, 9. $Os(1)-Os(2) = 3.069(1)$ Å, $Os(2)-Os(3) = 2.967(1)$ Å, $Os(2)-Os(4) = 2.974(1)$ Å, $Os(3)-Os(4) = 2.860(1)$ Å, $Os(1)-Ge(1) = 2.556(2)$ Å, $Os(2)-Ge(1) = 2.481(2)$ Å, $Os(2)-Ge(2) = 2.535(2)$ Å, $Os(2)-Ge(4) = 2.569(2)$ Å, $Os(3)-Ge(2) = 2.475(2)$ Å, $Os(3)-Ge(3) = 2.492(2)$ Å, $Os(4)-Ge(3) = 2.492(2)$ Å, $Os(4)-Ge(4) = 2.584(2)$ Å.

4.   Conclusions on crystallographic studies

The Os-E bond lengths for all the clusters studied here span the following ranges :
Os-Ge = 2.475(2) - 2.614(2) Å, Os-Sn = 2.660(2) - 2.815(1) Å, Os-Pb = 2.831(2) -
2.843(1) Å. Of these, the Os-Pb bond lengths are from the only OsPb cluster that has been
structurally characterised. The Os-Sn bond length range is well within that observed for
other OsSn clusters described in Chapter 1, while the range for the Os-Ge bond lengths
observed here is much longer than that for $Os_2(CO)_8(Cl)(GeCl_3)$ (there are three
independent molecules in the X-ray structure of this compound, with Os-Ge bond lengths
ranging from 2.931(1) Å to 2.916(2) Å) [24]. This difference in the Os-Ge bond lengths
can be attributed to the different electronegativities of the substituents on Ge, *viz.*, Me vs.
Cl. A similar trend is observed in transition metal-tin chemistry, and it has been attributed
to the increased Lewis π-acidity on the Sn centre in the presence of the more
electronegative halogen ligands [4].

It is also interesting to note that the Os-E bond lengths associated with the Os_2E_2
rings are longer than those in most of the other structural motifs, including the triangular
Os_2E ring; the latter ring may, *a priori*, be expected to exhibit more ring strain. This is all
the more remarkable considering that the OsEOs angles in the Os_2E_2 rings are typically at
104 ± 2°, which is very close to tetrahedral. The reason for this lengthening is thus not
clear, but it does serve to emphasize the fact that the heavy group 14 elements can tolerate
quite large deviations from ideal tetrahedral geometry. This point is also demonstrated in
the wide range of OsEOs angles observed : from $67.69(2)^o$ to $114.41(6)^o$.

The shorter Os-E bond lengths in triangular Os_2E units as compared to that in
Os_2E_2 rings may also be associated with greater thermodynamic stability in the former; a
point consistent with the observation that clusters with 4-membered Os_2E_2 rings collapse
to form clusters with Os_2E rings. The relative stabilities of these two structural motifs is
reminiscent of that in $Os_3(CO)_{12}$ and $Os_4(CO)_{16}$ [25], and is persuasive suggestion that
the triangular Os_2E units are indeed behaving in true cluster-type, centrally-directed

bonding. A recent report suggests that NMR spectroscopy may prove to be of value as a probe for such a bonding type [26].

With the exception of cluster **10**, the clusters in this study have planar metal skeletons. It is therefore clear that the ER_2 fragment must be considered as isolobal to an $Os(CO)_4$ unit which provides two orbitals and two electrons for cluster bonding. There is no case in which the ER_2 fragment acts like the unique, 4-connected $Os(CO)_4$ fragment in the $Os_5(CO)_{15}(L)$ (L = 2-electron donor ligand) clusters, in which it provides three orbitals and four electrons for cluster bonding. The closest example from the literature is the 3-connected $SnCl_2$ fragment in the cluster $Os_3(CO)_{11}(\mu\text{-}CH_2)(SnCl_2)$ [27], in which the bonding may also be described in terms of a Lewis acid behaviour for the $SnCl_2$ (Fig. IV.14). This suggests that electron-withdrawing groups are needed on the E centre to lower the d orbitals sufficiently in energy for use in cluster bonding. The implication of this restriction in the isolobal relationship is that for electron-counting purpose, the ER_2 fragments observed in the clusters here may be regarded as bridging ligands. The long Os-Os bond lengths observed here are also consistent with this view, as bridging ligands tend to lengthen Os-Os bonds, while higher nuclearity clusters tend to have shorter Os-Os bonds [28].
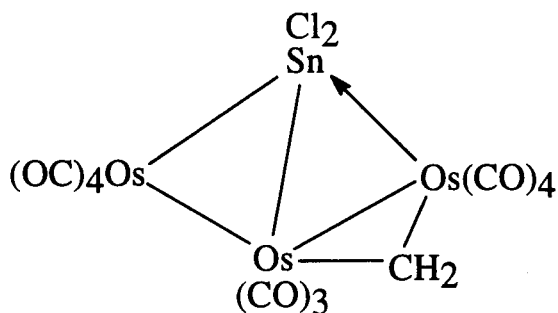
Fig. IV.14.   Bonding description for $Os_3(CO)_{11}(\mu\text{-}CH_2)(SnCl_2)$.

Conical $Os(CO)_3$ fragments, or $Os(CO)_4$ fragments contributing four electrons for cluster bonding, are essential in more condensed clusters: the group 14 fragment isolobal to these is a bare E or an ER^+. It is apparent from the chemistry observed in this study that the methyl group does not cleave easily from an Sn or Ge centre, though the point is arguable for the case of a Pb centre. This makes the formation of E or ER^+ fragments unlikely here. Both factors thus place severe restrictions on the structural motif that can be used by OsSn and OsGe clusters, but as the study also shows, there is a large number of possibilities even within that boundary.

5. References

[1] Watanabe, M.; Sano, H. *Bull. Chem. Soc. Jpn.*, **1990**, *63*, 1455.

[2] (a) Firfiray, D. B.; Irving, A.; Moss, J. R. *J. Chem. Soc., Chem. Commun.*, **1968**, 159. (b) Gubin, S. P.; Chentsova, O. M.; Burmakina, G. M.; Ioganson, A. A. *Izv. Akad. Nauk SSSR, Ser. Khim.*, **1981**, *12*, 2790.

[3] (a) O'Connor, J. E.; Corey, E. R. *Inorg. Chem.*, **1967**, *6*, 968. (b) Bonati, F.; Wilkinson, G. *J. Chem. Soc.*, **1964**, 179. (c) Bush, M. A.; Woodward, P. *J. Chem. Soc., Chem. Commun.*, **1967**, 166. (d) Biryukov, B. P.; Struchkov, Yu. T.; Anisimov, K. N.; Kolobova, N. E.; Skripkin, V. V. *J. Chem. Soc., Chem. Commun.*, **1968**, 159; *Zh. Strukt. Khim.*, **1967**, *8*, 556; ibid **1968**, *9*, 922.

[4] (a) Ho, B. Y. K.; Zuckerman, J. J. *J. Organomet. Chem.*, **1973**, *49*, 1. (b) Zubieta, J. A.; Zuckerman, J. J. *Prog. Inorg. Chem.*, **1978**, *24*, 251.

[5] Rochfort, G. L.; Ellis, J. E. *J. Organomet. Chem.*, **1983**, *250*, 277.

[6] Greene, J.; Curtis, M. D. *J. Amer. Chem. Soc.*, **1977**, *99*, 5176.

[7] Gilmore, C. J.; Woodward, P. *J. Chem. Soc., Dalton Trans.*, **1972**, 1387.

[8] Harrison, P. G.; King, T. J.; Richards, J. A. *J. Chem. Soc., Dalton Trans.*, **1975**, 2097.

[9]   Cotton, F. A.; Wilkinson, G. *Advanced Inorganic Chemistry*, 5th ed.; J. Wiley: New York, 1988; p 266.

[10]   Huheey, J. E.; Keiter, E. A.; Keiter, R. L. *Inorganic Chemistry : Principles of Structure and Reactivity*, 4th ed.; HarperCollins: New York, 1993; pp 187-190.

[11]   Bent, H. A. *Chem. Rev.*, **1961**, *61*, 275.

[12]   Eady, C. R.; Johnson, B. F. G.; Lewis, J.; Reichert, B. E.; Sheldrick, G. M. *J. Chem. Soc., Chem. Commun.*, **1976**, 271.

[13]   Farrar, D. H.; Johnson, B. F. G.; Lewis, J.; Raithby, P. R.; Rosales, M. J. *J. Chem. Soc., Dalton Trans.*, **1982**, 2051.

[14]   Brooks, E. H.; Elder, M.; Graham, W. A. G.; Hall, D. *J. Amer. Chem. Soc.*, **1968**, *90*, 3587.

[15]   Elder, M. *Inorg. Chem.*, **1969**, *8*, 2703.

[16]   Moss, J. R.; Graham, W. A. G. *J. Chem. Soc., Dalton Trans.*, **1977**, 95.

[17]   Mingos, D. M. P.; Wales, D. J. *Introduction to Cluster Chemistry*; Prentice-Hall: New Jersey, 1990.

[18]   Cardin, C. J.; Cardin, D. J.; Lawless, G. A.; Power, J. M.; Power, M. B. *J. Organomet. Chem.*, **1987**, *325*, 203.

[19]   Wang, W.; Einstein, F. W. B.; Pomeroy, R. K. *J. Chem. Soc., Chem. Commun.*, **1992**, 1737.

[20]   Goudsmit, R. J.; Johnson, B. F. G.; Raithby, P. R.; Whitmire, K. H. *J. Chem. Soc., Chem. Commun.*, **1982**, 640.

[21]   Howard, J.; Woodward, P. *J. Chem. Soc. A*, **1971**, 3648.

[22]   Bright, D. *J. Chem. Soc. D*, **1970**, 1169.

[23]   Keppert, D. L. *Prog. Inorg. Chem.*, **1978**, *24*, 179.

[24]   Einstein, F. W. B.; Pomeroy, R. K.; Rushman, P.; Willis, A. C. *J. Chem. Soc., Chem. Commun.*, **1983**, 854.

[25]   Pomeroy, R. K. *J. Organomet. Chem.*, **1990**, *383*, 387.

[26]   Wrackmeyer, B.; Distler, B.; Herberhold, M. *Z. Naturforsch.*, **1992**, *47b*, 1749.

[27]   Viswanathan, N.; Morrison, E. D.; Geoffroy, G. L.; Geib, S. J.; Rheingold, A. L. *Inorg. Chem.*, **1986**, *25*, 3100.

[28]   See for example (a) Mingos, D. M. P.; May, A. S. In *The Chemistry of Metal Cluster Complexes*; Shriver, D. F.; Kaesz, H. D.; Adams, R. D., Eds.; VCH: New York, 1990; Chapter 2. (b) Nicholls, J. N.; Vargas, M. D. *Adv. Inorg. Chem. Radiochem.*, **1986**, *30*, 123. (c) Churchill, M. R.; DeBoer, B. G.; Rotella, F. J. *Inorg. Chem.*, **1976**, *15*, 1843. (d) Bau, R.; Teller, R. G.; Kirtley, S. W.; Koetzle, T. F. *Acc. Chem. Res.*, **1979**, *12*, 176.

Epilogue

The major findings in this work are as follows :

1.   The reaction of $[Os(CO)_4]^{2-}$ and R_2ECl_2 (E = Ge, Sn, Pb; R = Me, Ph) appear to proceed via the intermediacy of $Os(CO)_4(ER_2Cl)_2$ compounds, which are known to exist in *cis* and *trans* isomeric forms. The interconversion of these isomers is presumed slow under the conditions used so that further reaction of the *cis* isomer gives the corresponding tetracycle $[(OC)_4OsER_2]_2$, while higher oligomers result from reaction of the *trans* isomer. This reaction may thus be amenable to steric, and also electronic, control over the ring size of the eventual product.

2.   The reactivities observed for the osmium-group 14 clusters demonstrate resoundingly that on going from Ge to Sn and then to Pb, the chemistry can change dramatically. This is most clearly borne out by the decarbonylation reactions. The factors influencing the changes in reactivity are far from clear, and further studies are therefore needed.

3.   The X-ray crystal structures of all the clusters containing the tetracyclic Os_2E_2 unit show a leaning of the axial carbonyl ligands towards the centre of the rings. This structural feature probably has an electronic component to it, vis á vis, the leaning of the carbonyls towards the group 14 atoms to compensate for the poor π-accepting abilities of the latter.

4.   This study shows that a variety of new structural types of osmium-group 14 clusters is still possible even within the apparent structural limitations imposed by the ER_2 units. Furthermore, the structural motifs accessible to OsE clusters are quite different from those of homometallic osmium clusters. This points to the potential for still further new structural types.

5.   The isolation of clusters with the triangular Os_2E unit, with acute OsEOs angles and short OsE bonds, and the thermal stability of these clusters, suggest that the group 14 atom in this unit is participating in a cluster-type, 3-centre bond.

Chapter V   Experimental

1.   General experimental procedures

Manipulations were generally carried out by using standard Schlenk techniques under a nitrogen atmosphere [1]. Manipulation of some volatile group 14 compounds were done on a high-vacuum system equipped with a fractionating train and a mercury diffusion pump. Photolyses were carried out with a medium pressure, 200 W, water-cooled, Hanovia UV lamp.

Starting materials were either purchased and used as received, or prepared using literature methods (or with minor variations) as cited. Compounds enriched in ^{13}CO were prepared from ^{13}CO-enriched $Os_3(CO)_{12}$, which was in turn prepared according to the literature method [2]. The extent of enrichment was determined by a comparison of the isotopic distribution of the parent mass spectrometric ion with values calculated using a program written by the author in GWBASIC. This comparison was made as follows : (1) the most abundant isotopic peak in the parent ion was identified and assigned a rank of 1. (2) ranks were then assigned accordingly for the isotopic peaks ±4 amu from the rank 1 peak. (3) a minimisation function was then calculated from the ranks of the experimental spectrum (R_{expt}) and the calculated spectrum (R_{calc}) using the expression :

$$\sum (\frac{R_{expt} - R_{calc}}{R_{expt}})^2$$

Solvents were dried over drying agents as follows : dichloromethane and acetonitrile (CaH_2), hexane and toluene (potassium), THF (K/benzophenone), diethyl ether (Na/benzophenone), diglyme ($LiAlH_4$), and methanol (Mg/I_2). They were then distilled under nitrogen and kept under nitrogen prior to use.

Infrared spectra were recorded with a Perkin Elmer 983 spectrometer; the internal calibration was checked periodically against the known absorption frequencies of gaseous CO. NMR spectra were recorded on either a Bruker WM400 by Ms. M. Tracey, or an SY-

100 spectrometer, with operating frequencies of 100.13 or 400.13 MHz (latter indicated as 400 MHz in experimental details) for ^1H, 100.6 MHz for ^{13}C, 162.0 MHz for ^{31}P and 149.16 MHz for ^{119}Sn. $^{31}P\{^1H\}$ chemical shifts were referenced with respect to an external 85% H_3PO_4 standard, and $^{119}Sn\{^1H\}$ chemical shifts with respect to an external neat Me_4Sn standard. Electron-impact (70 eV) mass spectra were recorded by Mr. G. Owen of the department on a Hewlett Packard 5985 GC-MS; mass spectral simulations were carried out with a program written by the author in GWBASIC. Elemental microanalyses were carried out by Mr. M. K. Yang of the Microanalytical Laboratory at Simon Fraser University. Melting points were determined with open capillaries on a Mel-temp apparatus.

2.   Preparation of $Os(CO)_4(SnR_2Cl)_2$ (R = Me, Bu^t, Ph)

(a)   Preparation of $Os(CO)_4(SnMe_2Cl)_2$

To $Na_2Os(CO)_4$ (prepared from 470 mg, 0.518 mmol, of $Os_3(CO)_{12}$ [3]) and Me_2SnCl_2 (626 mg, 2.85 mmol) was added THF (40.0 mL), prechilled at ca. -50 °C, via a cannula. The suspension was stirred at ca. -30 °C for 3 h and then allowed to warm to RT overnight. Solvent and volatiles were then removed on the vacuum line, and the residue extracted with hexane (2x20 and 12x10 mL). The extract was filtered through Celite, and then evaporated to dryness on the vacuum line. The remaining solid was recrystallised from warm hexane (30 mL) to afford pale yellow crystalline *cis*-$Os(CO)_4(SnMe_2Cl)_2$. Yield = 254 mg (24%).

IR (hexane) v(CO) : 2113.5w, 2060.5w, 2034s cm^{-1}

^1H NMR ($CDCl_3$) :   1.04s ($^3J_{SnH}$ = 47.9, 50.1 Hz, cis isomer, ~90 %)

1.08s ($^3J_{SnH}$ = 45.2, 47.1 Hz, trans isomer, ~10 %)

MS : 670 (Calculated for M^+, 672)

Elemental analysis : (Found) 14.67 %C, 1.89 %H ; (Calculated for $C_8H_{12}Cl_2O_4OsSn_2$)

14.33 %C, 1.80 %H

The solid remaining after the extraction above was further extracted with dichloromethane (4x20 mL). The extract was filtered through Celite, and the solvent removed on the vacuum line. The remaining solid was recrystallised from hot dichloromethane (20 mL) to afford yellow crystalline $trans$-$Os(CO)_4(SnMe_2Cl)_2$. Yield = 284 mg (27%).

IR (CH_2Cl_2) $v(CO)$: $2038vs$ cm^{-1}

^1H NMR $(CDCl_3)$: $1.04s$ $(^3J_{SnH} = 47.9, 50.1$ Hz, cis $isomer$, ~ 10 %)

$1.08s$ $(^3J_{SnH} = 45.2, 47.1$ Hz, $trans$ $isomer$, ~ 90 %)

(b)   Preparation of $Os(CO)_4(SnBu^t_2Cl)_2$

To $Na_2Os(CO)_4$ (prepared from 307 mg, 0.339 mmol, of $Os_3(CO)_{12}$) was added THF (40.0 mL). The suspension was cooled to ca. -15 ^oC, and then a solution of $Bu^t_2SnCl_2$ (610 mg, 2.01 mmol) in THF (10.0 mL), prechilled at ca. -15 ^oC, was transferred in via a cannula. The reaction mixture was stirred at -15 ^oC for ca. 1 h, and then allowed to warm to RT overnight.

Solvent and volatiles were then removed on the vacuum line, and the residue extracted with hexane (3x10, 2x5 mL), followed by extraction with dichloromethane (20 and 2x10 mL). The IR spectrum of both extracts showed mainly $v(CO)$ due to $trans$-$Os(CO)_4(SnBu^t_2Cl)_2$. The dichloromethane extract was filtered through Celite and then concentrated to ca. 10 mL whereupon precipitation commenced. The precipitate was redissolved by warming, and the solution then stored at -25 ^oC to yield very pale-green crystals. Further concentration of the supernatant solution gave a second crop of colourless product. Total yield = 332 mg (38%).

IR (CH_2Cl_2) $v(CO)$: $2114.5vw, 2065.5w, 2027.5vs$ cm^{-1}

$Elemental$ $analysis$: $(Found)$ 28.69 %C, 4.33 %H ;

$(Calculated$ for $C_{20}H_{36}Cl_2O_4OsSn_2)$ 28.63 %C, 4.33 %H

(c)   Preparation of Os(CO)$_4$(SnPh$_2$Cl)$_2$

To Na$_2$Os(CO)$_4$ (prepared from 320 mg, 0.353 μmol, of Os$_3$(CO)$_{12}$) and Ph$_2$SnCl$_2$ (723 mg, 2.10 mmol) was added THF (20.0 mL) via vacuum transfer, and the reaction mixture stirred at ca. -46 °C for 2.5 h and then allowed to warm to RT overnight.

An IR spectrum of the reaction mixture indicated only *trans*-Os(CO)$_4$(SnPh$_2$Cl)$_2$ to be present. Solvent and volatiles were then removed on the vacuum line, and the residue extracted with dichloromethane, followed by filtration through Celite. The filtrate was concentrated to ca. 10 mL and layered with hexane (20 mL) to afford a cream ppt. Yield = 390 mg (40%). A colourless crystalline sample was obtained by recrystallisation from hot methanol (30 mL). M.p. = 143 °C.

IR (CH$_2$Cl$_2$) ν(CO) : 2047s cm^{-1}

MS : 918 (Calculated for M$^+$, 920)

Elemental analysis :   (Found) 36.65 %C, 2.15 %H ;

(Calculated for C$_{28}$H$_{20}$Cl$_2$O$_4$OsSn$_2$) 36.60 %C, 2.19 %H

3. Preparation of [(OC)₄OsEMe₂]₂ (E = Ge, Sn, Pb)

(a) Preparation of [(OC)₄OsGeMe₂]₂

To Na$_2$Os(CO)$_4$ (prepared from 250 mg, 0.276 mmol, of Os$_3$(CO)$_{12}$) chilled in a -40 °C bath, was added THF (40.0 mL), followed by Me$_2$GeCl$_2$ in hexane solution (150 mg, 0.867 mmol). The reaction mixture was stirred under a slight vacuum in darkness, and allowed to warm to room temperature overnight. Solvent and volatiles were removed from the lemon-yellow suspension, and the cream residue extracted with hexane (3x15 and 4x10 mL), followed by filtration through a short silica column. Concentration and cooling of the yellow filtrate to -25 °C gave 156 mg (45 %) of yellow, crystalline [(OC)₄GeMe₂]₂, **1(GeMe)**.

IR (hexane) v(CO) : 2077m, 2019.5vs, 2007s cm⁻¹

¹H NMR (CDCl₃) : 1.247s

MS : 782 (Calculated for [M-CO]⁺, 782)

Elemental analysis : (Found) 17.93 %C, 1.44 %H ;

(Calculated for C₁₂H₁₂Ge₂O₈Os₂) 17.80 %C, 1.49 %H

(b) Preparation of [(OC)₄OsSnMe₂]₂

The compound [(OC)₄OsSnMe₂]₂, **1(SnMe)**, was prepared according to the literature method [3], from the reaction of Na$_2$Os(CO)$_4$ with Me$_2$SnCl$_2$.

IR (hexane) v(CO) : 2068.5m, 2010s, 2007ms,sh cm⁻¹

¹H NMR (CDCl₃) : 1.01s (²J$_{SnH}$ = 42.9, 44.9 Hz)

¹¹⁹Sn{¹H} NMR (CDCl₃) : -605.9s

MS : 902 (Calculated for M⁺, 902)

Elemental analysis : (Found) 16.14 %C, 1.33 %H ;

(Calculated for C₁₂H₁₂O₈Os₂Sn₂) 15.98 %C, 1.34 %H

(c)   Preparation of [(OC)$_4$OsPbMe$_2$]$_2$

(i)   From pyrolysis of Os(CO)$_4$(PbMe$_3$)$_2$

The compound Os(CO)$_4$(PbMe$_3$)$_2$ was prepared according to the literature method [3a], from the reaction of Na$_2$Os(CO)$_4$ (prepared from 81mg, 0.089 mmol, of Os$_3$(CO)$_{12}$) with Me$_3$PbCl (153 mg, 532 µmol) in THF (10.0 mL). After removal of the THF on the vacuum line, the residue was suspended in degassed hexane (10.0 mL). The IR of the supernatant solution at this stage showed the presence of Os(CO)$_4$(PbMe$_3$)$_2$ only (v(CO) : 2081m, 2022m, 2009s,sh, 2005vs cm^{-1}).

The reaction mixture was stirred over 19 days under exclusion of light. Initial stirring at RT showed emergence of product in the IR spectrum after one day. The temperature was subsequently raised stepwise; the highest temperature used was 80 $^{\circ}$C. Monitoring of the reaction showed that despite daily degassing, as well as a complete removal of solvent and volatiles followed by replacement with fresh hexane, the relative amounts of product to starting material did not appear to change after one week, at which point the temperature was 50 $^{\circ}$C. The reddish-orange suspension was filtered through Celite. Removal of solvent gave a red oil, which was column chromatographed on silica, with hexane as eluant, to give an overlapping yellow band of Os(CO)$_4$(PbMe$_3$)$_2$ and an orange band of the product. These were recrystallised from hexane to give orange crystals of [(OC)$_4$OsPbMe$_2$]$_2$, **1(PbMe)**, in very low yield.

IR (hexane) v(CO) : 2060m, 2005s cm^{-1}

^{1}H NMR (CDCl$_3$) : 1.90s ($^2J_{PbH}$ = 44.9 Hz)

Elemental analysis : (Found) 13.44 %C, 1.05 %H ;

(Calculated for C$_{12}$H$_{12}$O$_8$Os$_2$Pb$_2$) 13.36 %C, 1.12 %H

(ii)   From $Na_2Os(CO)_4$ and Me_2PbCl_2

To $Na_2Os(CO)_4$ (prepared from 231 mg, 0.255 mmol, of $Os_3(CO)_{12}$) and Me_2PbCl_2 (235 mg, 0.961 mmol) was added THF (40.0 mL) at -78 °C via cannula. The reaction mixture was stirred under nitrogen in the dark at -46 °C. After about 2 hours, it was allowed to warm to room temperature overnight. Solvent and volatiles were removed on the vacuum line from the dark red suspension, and the residue extracted with hexane (5x20 and 2x10 mL) followed by filtration through Celite. Concentration of the hexane extract followed by storage at -25 °C gave 72 mg (17 %) of dark red blocks of $[(OC)_4OsPbMe_2]_2$, **1(PbMe)**.

4. Reactions of Os(CO)₄²⁻ with Ph₂ECl₂ (E = Ge, Sn, Pb)

(a) With Ph₂GeCl₂

To Na₂Os(CO)₄ (prepared from 312 mg, 0.344 mmol, of Os₃(CO)₁₂) was added THF (40.0 mL, prechilled to -50 °C) and Ph₂GeCl₂ (306 mg, 1.03 mmol). The mixture was stirred under exclusion of light in a -45 °C bath and then allowed to warm to room temperature overnight. The solvent was removed *in vacuo* and the residue extracted with hexane (2x20 and 3x10 mL). The hexane extract was filtered through silica, concentrated and then left at -25 °C to afford pale yellow crystals of Ph₂Ge[Os(CO)₄H]₂, **3**.

IR (hexane) ν(CO) : 2128w, 2113.5m, 2063m, 2041.5s, 2037sh, 2024m, 1965.5w,br cm⁻¹

¹H NMR (CD₂Cl₂) : 7.55m, 7.23m (Ph); -8.12s (OsH)

Elemental analysis : (Found) 29.03 %C, 1.50 %H ; (Calculated) 28.83 %C, 1.45 %H

The residue remaining after the hexane extraction described above was extracted with dichloromethane (3x20 and 10 mL). The dichloromethane extract was filtered through silica, concentrated and chromatographed on silica (14 cm x 36 mm diameter, 1/1, dichloromethane/hexane eluant) to give 95 mg (17 %)of [(OC)₄OsGePh₂]₂, **1(GePh)**, as a cream powder.

IR (CH₂Cl₂) ν(CO) : 2088m, 2032s, 2014m cm⁻¹

Elemental analysis : (Found) 36.56 %C, 1.88 %H ;

(Calculated for C₃₂H₂₀Ge₂O₈Os₂) 36.33 %C, 1.91 %H

(b) With Ph₂SnCl₂

To Na₂Os(CO)₄ (prepared from 178 mg, 0.194 mmol, of ¹³CO-enriched Os₃(CO)₁₂, ca. 70%) in a -50 °C bath was added Ph₂SnCl₂ (210 mg, 0.610 mmol), followed by THF (30.0 mL, prechilled to -78 °C) via cannula. The reaction mixture was stirred under exclusion of light and then allowed to warm to room temperature overnight. The solvent was then removed in vacuo and the residue first extracted with hexane (15 and 2x10 mL). Concentration and cooling of the hexane extract gave a small amount of **1(SnPh)**.

The residue remaining after the hexane extraction above was further extracted with dichloromethane (20 and 2x10 and 5 mL). The dichloromethane extract was filtered through silica, concentrated to ca. 15 mL, layered with 10.0 mL of hexane, then placed in a -25 °C freezer. Pale yellow needles of $[(OC)_4OsSnPh_2]_6$, **4** were obtained (yield = 5 mg). A $^{13}C\{^1H\}$ NMR spectrum of the supernatant solution (126 mg of dry residue) showed that it consisted of 26% and 47% by weight of **4** and **1(SnPh)** respectively. Colourless needles of compound **1(SnPh)** was obtained on further concentration and cooling of the supernatant solution. Better separation of the two identified products was achieved by chromatography on a size-exclusion column (Biobeads SX-8, 90 cm x 14 mm diameter) with dichloromethane as eluant; the lightly coloured **4** eluted just ahead of the colourless **1(SnPh)**. The IR and elemental analyses below were on samples not labelled with ^{13}CO.

$[(OC)_4OsSnPh_2]_2$:

IR (CH_2Cl_2) ν(CO) : 2079.5m, 2019.5s cm^{-1}

^1H NMR (CD_2Cl_2, 400 MHz) : 7.3m

$^{13}C\{^1H\}$ NMR (CD_2Cl_2) : 182.06 ($^2J_{SnC}$ = 39.6 Hz, CO, ax); 173.52 ($^2J_{SnC}$ = 123.6 Hz, CO, eq); 136.74 (2C, Ph) ; 128.78 (1C, Ph) ; 128.60 (2C, Ph)

Elemental analysis :   (Found) 33.17 %C, 1.76 %H ;

(Calculated for $C_{32}H_{20}O_8Os_2Sn_2$) 33.41 %C, 1.75 %H

$[(OC)_4OsSnPh_2]_6$:

IR (CH_2Cl_2) ν(CO) : 2105.5w, 2030.5vs, 2013.5s, 2002m,sh cm^{-1}

^1H NMR (CD_2Cl_2) : 7.47m ; 7.30m

$^{13}C\{^1H\}$ NMR (CD_2Cl_2) : 185.38 ($^2J_{SnC}$ = 30.2 Hz; CO); 136.42 (2C, Ph); 128.62 (2C, Ph); 128.48 (1C, Ph)

Elemental analysis :   (Found) 33.56 %C, 1.77 %H ;

(Calculated for $C_{96}H_{60}O_{24}Os_6Sn_6$) 33.41 %C, 1.75 %H

Crystal data : Monoclinic C2/c, a=35.061(8) Å, b=10.160(5) Å, c=34.216(16) Å, β =117.96(3)^o, V=10766(8) Å^3, Z=4, μ(MoKα)=8.49mm^{-1}, R=0.265, wR=0.311 on 994 observed reflections (I>2σ , 2.0<θ<13.0) for only Os and Sn atoms, with fixed isotropic temperature factors (19 parameters) and unit weights [4].

(c)   <u>With Ph$_2$PbCl$_2$</u>

To Na$_2$Os(CO)$_4$ (prepared from 312 mg, 0.344 mmol, of Os$_3$(CO)$_{12}$) was added Ph$_2$PbCl$_2$ (360 mg, 0.830 mmol) and THF (50.0 mL, prechilled to -78 ^{o}C) and . The mixture was stirred under exclusion of light at -78 ^{o}C and allowed to warm to room temperature overnight. The IR spectrum of the reaction mixture showed bands at 2097.5vw, 2069.5m and 2017vs, br cm^{-1}. The solvent was then removed *in vacuo* from the blood-red reaction mixture and the residue extracted with dichloromethane. An attempt to filter through silica failed due to clogging by a fine, red-brown precipitate. The extract was finally filtered through a cotton wool plug, concentrated to ca. 20 mL, layered with hexane (20 mL), and stored at -25 ^{o}C. A small amount (ca. 10 mg) of orange crystals of [(OC)$_4$OsPbPh$_2$]$_2$, **1(PbPh)**, was obtained.

[(OC)$_4$OsPbPh$_2$]$_2$: IR (CH$_2$Cl$_2$) ν(CO) : 2071.5s, 2017s,br cm^{-1}

^{13}C{^{1}H} NMR (CD$_2$Cl$_2$) :   185.17 (CO, ax); 172.03 (CO, eq); 136.95 (2C, Ph, ortho); 131.13 (Ph, ipso); 128.38 (2C, Ph, meta); 128.10 (1C, Ph, para)

Elemental analysis :   (Found) 28.73 %C, 1.49 %H ;

(Calculated for C$_{32}$H$_{20}$O$_8$Os$_2$Pb$_2$) 28.96 %C, 1.52 %H

5. Reactions of $Os(CO)_4^{2-}$ with $Bu^t_2SnCl_2$ and $Fe(CO)_4(SnMe_2Cl)_2$

(a) With $Bu^t_2SnCl_2$

To $Na_2Os(CO)_4$ (prepared from 745 mg, 0.822 mmol, of $Os_3(CO)_{12}$) and THF (25.0 mL) at -50 °C, was added $Bu^t_2SnCl_2$ (782 mg, 2.57 mmol) dissolved in ca. 3 mL THF. A golden yellow colour developed immediately. Stirring was continued for ca. 30 min, and then allowed to warm to room temperature overnight.

An IR spectrum of the supernatant solution at this point showed the presence of at least two products. The reaction mixture was refluxed for 4 h whereupon the colour darkened to brown. The reaction was cooled to RT, volatiles removed under vacuum, and the residue extracted, first with hexane (5x10 and 4x5 mL), then with dichloromethane (2x10 mL). The extracts were separately filtered through silica and concentrated, before storage at -25 °C.

The hexane extract gave some insoluble brown powder, which were decanted, and the supernatant solution subjected to chromatographic separation on silica (9 cm x 36 mm diameter). Elution with hexane gave a pale greenish-yellow band which on concentrating and cooling gave pale yellow crystals of $[(OC)_4OsSnBu^t_2]_2$, **1(SnBu^t)**, (43 mg, 3%).

IR (hexane) $\nu(CO)$: 2067.5m, 2013w, 2005.5s, 2001.5ms cm^{-1}

^1H NMR (CDCl$_3$) : 1.372 ($^3J_{SnH}$ = 71.8, 75.0 Hz; $^1J_{CH}$ = 124.8 Hz)

$^{119}Sn\{^1H\}$ NMR (CDCl$_3$) : -476.17

Elemental analysis : (Found) 26.93 %C, 3.38 %H ;

(Calculated for $C_{24}H_{36}O_8Os_2Sn_2$) 26.93 %C, 3.39 %H

The dichloromethane extract gave some yellow crystals which were identified by IR spectroscopy to be $Os_3(CO)_{12}$. Further concentration and cooling yielded some almost colourless plates, tentatively assigned the formula "$(OC)_3HOs(SnBu^t_2)_2(\mu\text{-}OH)$", which showed infrared absorptions at 2051.5s, 2006m, 1979.5s cm^{-1} ($\nu(CO)$), and 1925.5w,br cm^{-1} ($\nu(OsH)$).

(b)   With Fe(CO)$_4$(SnMe$_2$Cl)$_2$

(i)   Preparation of Fe(CO)$_4$(SnMe$_2$Cl)$_2$

To a suspension of Fe(CO)$_4$Na$_2$.1.5dioxane (1.101 g, 3.18 mmol) in THF (20.0 mL) at -78 ^{o}C was added Me$_2$SnCl$_2$ (1.398 g, 6.36 mmol), and the mixture stirred for 15 min. Solvent and volatiles were then removed at room temperature on a vacuum line, and the residue extracted with hexane (3x20 mL). The extract was filtered through Celite and then concentrated until precipitation commenced. The hexane suspension was then kept at -25 ^{o}C for 3 days to afford the product as a white, very air-sensitive powder, which was decanted and washed with cold hexane (2x2 mL). The supernatant solution and washings were concentrated to give a second crop of products. Total yield = 636 mg (37%).

IR (hexane) v(CO) : 2084.5m, 2034.5m, 2014m, 2001.5s cm^{-1}

^{1}H NMR (CDCl$_3$) : 1.12s ($^2J_{SnH}$ = 50.5 Hz)

Elemental analysis :   (Found) 19.06 %C, 1.58 %H ;

(Calculated for C$_8$H$_{12}$Cl$_2$FeO$_4$Sn$_2$) 18.78 %C, 1.58 %H

(ii)   Reaction of Na$_2$Os(CO)$_4$ with Fe(CO)$_4$(SnMe$_2$Cl)$_2$

To Na$_2$Os(CO)$_4$ (prepared from 323 mg, 0.356 mmol, of Os$_3$(CO)$_{12}$) and Fe(CO)$_4$(SnMe$_2$Cl)$_2$ (597 mg, 1.11 mmol) was added cold THF (ca. -60 ^{o}C, 40.0 mL). The reaction mixture was stirred and allowed to warm to RT overnight under exclusion of light. The solvent was removed *in vacuo*, and the residue extracted with hexane (4x20 mL). The extract was filtered through silica to give a yellow filtrate. The volume of this filtrate was reduced to ca. 20 mL on the vacuum line and stored at -25 ^{o}C . Yellow-green crystalline blocks of the product [OsFe(CO)$_8$(SnMe$_2$)$_2$], **2**, were obtained in 484 mg (59%) yield. This crude product was found by IR spectroscopy to contain **1(SnMe)**, which could be separated by careful column chromatography on Florisil, with hexane as eluant.

IR (hexane) v(CO) : 2091w, 2048s, 2028w, 2013vs, 1991.5m, 1981.5w, 1958m cm^{-1}

MS : 768 (Calculated for M$^+$, 770). Elemental analysis : (Found) 13.44 %C, 1.05 %H ;

(Calculated for C$_{12}$H$_{12}$FeO$_8$OsSn$_2$) 13.36 %C, 1.12 %H

6. Decarbonylation reactions

(a) Pyrolysis of [(OC)$_4$OsSnMe$_2$]$_2$

A solution of **1(SnMe)** (55 mg, 0.061 mmol) in hexane (10.0 mL) was degassed (three freeze-pump-thaw cycles) in a Carius tube and then heated at 170 °C for 3 d. The initial pale yellow solution turned to a golden yellow during the course of the reaction, together with the formation of a brown precipitate. The solvent was removed on the vacuum line, and the residue extracted with hexane (3x2 mL) and toluene (5 and 3 mL). Column chromatography on silica of both fractions gave the same 3 yellow bands :

Band 1 gave yellow [(OC)$_3$OsSnMe$_2$]$_3$, **5(Sn)**, (11 mg, 22%). Recrystallisation from hot toluene gave either long needles which contained 0.5 molecule of toluene, or hexagonal prisms which did not contain solvent molecules:

IR (hexane) ν(CO) : 2043m, 2009.5s, 1978m cm^{-1}

^{1}H NMR (CDCl$_3$) : 0.99s ($^2J_{SnH}$ = 43.0, 44.4 Hz)

Elemental analysis : (Obtained, long needles) 17.11 %C, 1.63 %H ; (Calculated for Os$_3$Sn$_3$C$_{15}$H$_{18}$O$_9$.1/2C$_7$H$_8$) 16.90 %C, 1.69 %H ; presence of toluene confirmed by ^{1}H NMR spectroscopy.

Band 2 gave red crystals (1 mg) :

IR (hexane) ν(CO) : 2079.5w, 2048.5s, 2042.5m, 2015vs, 1982.5s cm^{-1}

^{1}H NMR (CDCl$_3$) : no signals

Band 3 gave a yellow solid (2 mg) :

IR (hexane)ν(CO) : 2086.5w, 2051.5s, 2044ms, 2020vs, 2013ms, 1984mw, 1981mw cm^{-1}

(b) Photolysis of [(OC)$_4$OsSnMe$_2$]$_2$

A solution of **1(SnMe)** (220 mg, 0.244 mmol) in hexane (8.0 mL) was degassed (two freeze-pump-thaw cycles) in a Carius tube and then subjected to UV photolysis for 14 h. The initial pale yellow solution turned to a golden yellow in the course of the photolysis, and a yellow powder was precipitated. An IR spectrum of the supernatant

solution showed mainly unchanged starting material, with additional very weak bands at 2085, 1969 and 1953 cm^{-1}. The yellow precipitate of $[Os_2(CO)_7(SnMe_2)_2]_2$, **6**, was washed with hexane (1 mL). Yield = 65 mg (30%).

IR (CH$_2$Cl$_2$) ν(CO) : 2089.5m, 2019s, 1994.5m,sh, 1964.5w cm^{-1}

(nujol) : 2084ms, 2031m, 2005s, 1989ms, 1979.5ms, 1968w, 1957ms cm^{-1}

Elemental analysis : (Found) 15.30 %C, 1.41 %H ;

(Calculated for C$_{22}$H$_{24}$O$_{14}$Os$_4$Sn$_4$) 15.12 %C, 1.38 %H

(c)   Reaction of Me$_3$NO with [(OC)$_4$OsSnMe$_2$]$_2$

To a solution of $[(OC)_4OsSnMe_2]_2$ (184 mg, 0.204 mmol) in dichloromethane (15.0 ml) at -5 $^\circ$C was added dropwise, over ca. 30 min, a solution of freshly sublimed Me$_3$NO (31mg, 0.413 mmol) in acetonitrile (15.0 ml). The solution rapidly turned yellow. The reaction was then stirred a further hour, and the resultant deep-yellow solution then flash-filtered through a short column of silica (ca. 2.5 cm length) sandwiched between layers of Celite. The column was washed through with dichloromethane (2x5 mL). Solvent and volatiles were removed under vacuum, and the residue extracted with hexane (4x5 mL). The hexane extract was filtered through Celite, concentrated, and then cooled to give a pale yellow powdery precipitate, which was identified by its IR spectrum as starting material, and some orange crystals. The latter were separated by hand and recrystallised from warm toluene. The recrystallised yellow crystals of the product, $[Os_2(CO)_7O(SnMe_2)_2]_2$.toluene, **7**, was again separated by hand from the almost colourless blocks of the starting material.

IR (hexane) ν(CO) : 2088w, 2044.5m, 2021s, 2012vs, 2002s, 1968.5w cm^{-1}

^{1}H NMR (CDCl$_3$) : 0.701s; 0.584s

Elemental analysis :   (Found) 18.48 %C, 1.67 %H ;

(Calculated for Os$_4$Sn$_4$C$_{22}$H$_{24}$O$_{16}$.C$_7$H$_8$) 18.61 %C, 1.72 %H (Presence of toluene confirmed by X-ray crystallography.)

(d)   <u>Photolysis of [(OC)$_4$OsGeMe$_2$]$_2$</u>

A solution of **1(GeMe)** (147 mg, 0.182 mmol) in hexane (40.0 mL) was degassed (three freeze-pump-thaw cycles) in a quartz Carius tube and then photolysed for 16.5 h. The initial pale yellow solution turned orange. The solution was transferred via cannula to a Schlenk vessel, the solvent removed on the vacuum line, and the residue redissolved in hexane for column chromatography on silica. Elution with hexane gave 2 major coloured bands.

The first band was bright yellow. Concentration and cooling to 0 °C gave orange crystals of [(OC)$_3$OsGeMe$_2$]$_3$, **5(Ge)**, (11 mg yield) and pale yellow crystals of Os$_3$(CO)$_{11}$(GeMe$_2$)$_2$, **8**, (2 mg yield), which were separated by hand. The second band was rechromatographed to give a major orange band, which yielded orange-red crystals of Os$_4$(CO)$_{12}$(GeMe$_2$)$_4$, **9**, (6 mg yield).

The photolysis was also carried out on a d_6-benzene solution in an NMR tube and monitored by ^{1}H NMR spectroscopy. The major products after ca. 15 h were **5(Ge)** and **8**. Further photolysis led to a decrease in the relative amounts of **8** and the formation of another (unidentified) species.

[(OC)$_3$OsGeMe$_2$]$_3$:

IR (hexane) ν(CO) : 2052m, 2014s, 1984.5m cm^{-1}

^{1}H NMR (C$_6$D$_6$) :   1.178 ppm

^{13}C{^{1}H} NMR (toluene) : 17.565 (Me); 181.20 (2C, CO, ax); 186.25 (1C, CO, eq)

Elemental analysis :   (Found) 16.19 %C, 1.58 %H ;

                        (Calculated for C$_{15}$H$_{30}$Ge$_3$O$_9$Os$_3$) 15.93 %C, 1.60 %H

Os$_3$(CO)$_{11}$(GeMe$_2$)$_2$:

IR (hexane) ν(CO) : 2112.5w, 2088.5m, 2028s, 2014w, 2002mw, 1997mw, 1985w cm^{-1}

^{1}H NMR (C$_6$D$_6$) :   1.125 ppm

Elemental analysis :   (Found) 16.62 %C, 1.03 %H ;

                        (Calculated for C$_{15}$H$_{12}$Ge$_2$O$_{11}$Os$_3$) 16.62 %C, 1.12 %H

Os$_4$(CO)$_{12}$(GeMe$_2$)$_4$:

IR (hexane) ν(CO) :   2107.5w, 2078mw, 2046m, 2036s, 2016.5m, 2002s, 1983.5mw,

1972m cm^{-1}

^{1}H NMR (d$_8$-toluene, 400 MHz) :   1.160 s; 1.238s; 1.257s; 1.843s

^{13}C{^{1}H} NMR (d$_8$-toluene) : 9.516, 16.539, 17.756, 26.096 (Me);

170.35, 182.74, 184.92, 185.03 (2C, CO, ax);

178.77, 180.31, 187.44, 191.39 (1C, CO, eq)

Elemental analysis :   (Found) 16.16 %C, 1.62 %H ;

(Calculated for C$_{20}$H$_{24}$Ge$_4$O$_{12}$Os$_4$) 15.93 %C, 1.60 %H

(e)   <u>Pyrolysis of [(OC)$_4$OsGeMe$_2$]$_2$</u>

A sample of **1(GeMe)** (163 mg, 0.201 mmol) was placed in a quartz Carius tube with hexane (10.0 mL), and the solution degassed by three freeze-pump-thaw cycles. The solution was then heated at 100 °C under exclusion of light for 4 d to give a red solution. The reaction mixture was cooled to room temperature, then stored at -25 °C, whereupon orange-yellow crystals of **5(Ge)** (113 mg, 50%) and bright yellow crystals of Os$_2$(CO)$_6$(GeMe$_2$)$_3$, **10**, (< 1 mg) precipitated; ν(CO) 2024.5s, 1986.5m cm^{-1} (lit. [5] 2021s, 1990s,br). The supernatant solution was concentrated and chromatographed on silica (30 cm x 15 mm diameter) with hexane as eluant to give a light yellow band of **5(Ge)** in 5 mg yield, followed by a bright yellow band which on recrystallisation from hexane gave 7 mg of **8**, and finally a red band which gave 6 mg of **9**.

(f)   <u>Photolysis of [(OC)$_4$OsPbMe$_2$]$_2$</u>

A solution of **1(PbMe)** (70 mg, 0.065 mmol) in hexane (20.0 mL) was placed in a quartz Schlenk vessel. The solution was degassed by three freeze-pump-thaw cycles and then photolysed for 3.25 h. The initial red-orange solution gave a brown precipitate and a

colourless supernatant solution. An IR spectrum of the supernatant solution showed no carbonyl stretches.

The brown powder showed carbonyl stretching bands in its IR spectrum (nujol mull) at 2093w, 2014s and 1936m cm^{-1}; elemental analyses gave 11.28% C and 1.21% H. The powder was insoluble in all common solvents. Heating to 66 $^\circ$C with excess PMe$_3$ in dichloromethane/hexane did not give any observable reaction.

7. Reactions of [Os$_2$(CO)$_7$(SnMe$_2$)$_2$]$_2$

(a) Pyrolysis of [Os$_2$(CO)$_7$(SnMe$_2$)$_2$]$_2$

A Carius tube was charged with [Os$_2$(CO)$_7$(SnMe$_2$)$_2$]$_2$ (12 mg, 6.9 µmol) and hexane (5.0 mL). The suspension was degassed by three freeze-pump-thaw cycles, and then heated at 100 °C for 1 d, at 120 °C for 6 d, degassed again and finally heated at 150 °C for a week. The final reaction mixture consisted of a yellow supernatant solution with a brown solid. An IR spectrum of the supernatant solution showed that it consisted mainly of the same compounds that were present in bands 1 and 2 of reaction 6(a). Column chromatography of the supernatant solution gave ca. 1 mg of **5(Sn)**, and < 1 mg of band 2.

(b) With methylacrylate

A Carius tube with [Os$_2$(CO)$_7$(SnMe$_2$)$_2$]$_2$ (18 mg, 0.010 mmol), methyl acrylate (5 drops) and dichloromethane (5.0 mL) was heated at 60 °C for 30 min. The solvent and volatiles were removed on the vacuum line, and the residual orange gum was extracted with hexane (4x5 mL). The extracts were filtered through Celite, combined, and then evaporated to dryness on the vacuum line. The residue so obtained was redissolved in the minimum volume of hexane and chromatographed on silica in a Pasteur pipette. Elution with dichloromethane/hexane (1/1, v/v) gave a colourless band which yielded Os$_2$(CO)$_7$(SnMe$_2$)$_2$[H$_2$C=CHCO$_2$Me], **11a**, as a cream solid. A dichloromethane solution of the product was thermally unstable; heating a sample of **11a** in dichloromethane gave 5 mg of **6** (28% yield with respect to the initial amount of **1(SnMe)** used), identified by its IR spectrum (nujol mull), and methyl acrylate (by smell).

IR (hexane) ν(CO) : 2085w, 2061m, 2004vs, 1981.5mw cm^{-1}; ν(COOMe) 1726w cm^{-1}

^{1}H NMR (CDCl$_3$) : 0.96s, 1.05s, 1.06s, 1.08s (SnMe$_2$); 2.43dd ($^2J_{HH}$ = 1.47 Hz, $^3J_{HH}$ = 8.07 Hz, CH$_2$); 2.75dd ($^2J_{HH}$ = 1.47 Hz, $^3J_{HH}$ = 10.63 Hz, CH$_2$); 3.45dd ($^3J_{HH}$ = 8.07, 10.63 Hz, CHCOO); 3.73s (COOMe)

Elemental analysis : (Found) 19.17 %C, 1.99 %H ;

(Calculated for C$_{15}$H$_{18}$O$_9$Os$_2$Sn$_2$) 18.77 %C, 1.89 %H

(c)   With P(OMe)$_3$

A Carius tube was charged with [Os$_2$(CO)$_7$(SnMe$_2$)$_2$]$_2$ (84 mg, 0.048 mmol), P(OMe)$_3$ (3 drops) and dichloromethane (3.0 mL). The suspension was degassed (two freeze-pump-thaw cycles), and then heated at 60 °C for about 5 min, whereupon an orange solution was obtained. The solvent and volatiles were removed on the vacuum line, and the residual brown oil dissolved in the minimum volume of dichloromethane and filtered through silica to give a yellow solution. This gave a yellow product (11 mg, 11%) which on chromatographic separation (silica in a Pasteur pipette, 1/1 dichloromethane/hexane as eluant) and recrystallisation from hexane gave colourless blocks of Os$_2$(CO)$_7$(SnMe$_2$)$_2$[P(OMe)$_3$], **12a**.

IR (hexane) v(CO) : 2076w, 2035mw, 2009w, 1996vs, 1980.5m, 1963.5w cm^{-1}

^{1}H NMR (CDCl$_3$) : 3.579d ($^3J_{PH}$ = 12.46 Hz, P(OMe)$_3$); 0.970d ($^4J_{PH}$ = 0.91 Hz, J_{SnH} ~ 42, 44 Hz, SnMe$_2$); 0.881s (J_{SnH} = 42.1, 44.2 Hz, SnMe$_2$)

^{31}P{^{1}H} NMR (CDCl$_3$) : 112.03s

Elemental analysis : (Found) 17.01 %C, 2.14 %H ;

(Calculated for C$_{14}$H$_{21}$O$_{10}$Os$_2$PSn$_2$) 16.85 %C, 2.12 %H

(d)   With PMe₃

A sample of [Os$_2$(CO)$_7$(SnMe$_2$)$_2$]$_2$ (22 mg, 0.013 mmol) was placed in a Carius tube with PMe$_3$ (5 drops) and dichloromethane (5.0 mL), and the suspension degassed (three freeze-pump-thaw cycles) and then stirred overnight at RT to give a yellow solution. Removal of the solvent and volatiles on the vacuum line gave an orange-yellow oil, which was which was redissolved in the minimum volume of dichloromethane, adsorbed on silica, and then chromatographed on silica (4 cm x 36 mm diameter). Elution with dichloromethane/hexane (1/1) gave 7 mg (29%) yield of the product Os$_2$(CO)$_7$(SnMe$_2$)$_2$(PMe$_3$), **12b**, which appeared to be unstable in dichloromethane solution, but which can be recrystallised from hexane to give colourless blocks.

IR (hexane) ν(CO) : 2074w, 2030.5m, 2007w, 1993vs, 1975m, 1957.5mw cm⁻¹

MS : 950 (Calculated for M⁺, 950)

Elemental analysis :   (Found) 17.92 %C, 2.18 %H ;

(Calculated for C$_{14}$H$_{21}$O$_7$Os$_2$PSn$_2$) 17.70 %C, 2.23 %H

8. Substitution reactions

(a) Reaction of [(OC)$_4$OsSnMe$_2$]$_2$ with methyl acrylate (H$_2$C=CHCO$_2$Me)

A sample of [(OC)$_4$OsSnMe$_2$]$_2$ (53 mg, 0.059 mmol) was placed in a Carius tube with H$_2$C=CHCO$_2$Me (51 mg, 0.59 mmol) and hexane (5.0 mL), and the reaction mixture degassed by three freeze-pump-thaw cycles. After 2 h of photolysis, a yellow powder with an orange supernatant solution was obtained. The IR spectrum of the powder show that it was [Os$_2$(CO)$_7$(SnMe$_2$)$_2$]$_2$, but that of the supernatant solution showed the formation of products. The mixture was again degassed (two freeze-pump-thaw cycles) and then heated at 60 °C for 30 min. The IR spectrum of this showed no observable change, so the solvent and volatiles were removed under vacuum, a drop of methyl acrylate was added, with dichloromethane (5 mL), and the reaction mixture degassed and then heated again. The solids dissolved completely in < 15 min, and the reaction allowed to cool to RT after 1 h. Solvent and volatiles were removed on the vacuum line, and the residue redissolved in the minimum volume of dichloromethane and chromatographed twice (silica, 1/1 hexane/dichloromethane eluant) to give pale yellow **11a** (18 mg, 32 %).

(b) Reaction of [(OC)$_4$OsSnMe$_2$]$_2$ with ethene (C$_2$H$_4$)

A sample of [(OC)$_4$OsSnMe$_2$]$_2$ (67 mg, 0.074 mmol) was placed in a Carius tube with hexane (5.0 mL). Ethene gas was bubbled in for ca. 5 min, and then the Carius tube was sealed. After 3 h of photolysis, a yellow suspension was obtained. IR spectroscopy showed that the powder was [Os$_2$(CO)$_7$(SnMe$_2$)$_2$]$_2$, and the supernatant solution contained mainly starting material, with some products. Ethene gas was again bubbled in (ca. 3 min), and the reaction mixture photolysed for a further 16 h. The supernatant solution was decanted and the solids washed with hexane (2x2 mL). The washings and supernatant solution were combined, and solvent and volatiles were then removed on the vacuum line. Chromatographic separation of the residue on silica (hexane as eluant) gave

an orange-yellow band, from which a few diffraction-quality crystals of **11b** were obtained, in low yield, from dichloromethane/hexane.

IR (hexane) $\nu(CO)$: 2081w, 2069mw, 2050m, 2040m, 2010s, 2000.5vs, 1980.5vs, 1969.5m cm^{-1}

(c)   Reaction of [(OC)$_3$OsGeMe$_2$]$_3$ with PMe$_3$

A sample of **5(Ge)** (113 mg, 0.100 mmol) was placed in a Carius tube with PMe$_3$ (0.386 mmol) in hexane (10.0 mL). The reaction mixture was degassed (three freeze-pump-thaw cycles) and then heated at 100 °C for 6 d. On cooling to RT, a light yellow crystalline solid was precipitated. This gave 39 mg (33 %) of Os$_3$(CO)$_7$(GeMe$_2$)$_3$(PMe$_3$)$_2$, **13**, after recrystallisation from a dichloromethane/hexane mixture. The supernatant solution was chromatographed on silica to give the following four yellow bands:

Band 1 (hexane eluant) gave unreacted **5(Ge)**. Yield = 5 mg.

Band 2 (5/95, dichloromethane/hexane eluant) gave Os$_3$(CO)$_8$(GeMe$_2$)$_3$(PMe$_3$), **13**. Yield = 9 mg (8 %).

IR (hexane) $\nu(CO)$: 2080.5w, 2044.5s, 2037w, 2013.5m, 2000.5vs, 1993m, 1981m, 1973.5s, 1932m cm^{-1}

^{1}H NMR (CDCl$_3$) : 1.981d ($^2J_{PH}$ = 9.7 Hz, 9H, P$\underline{Me}_3$); 1.207s (6H, Ge$\underline{Me}_2$); 1.137s(12H, Ge$\underline{Me}_2$)

Elemental analysis : (Found) 17.42 %C, 2.25 %H ;

(Calculated for C$_{17}$H$_{27}$Ge$_3$O$_8$Os$_3$P) 17.32 %C, 2.31 %H

Band 3 (1/9, dichloromethane/hexane eluant) gave Os$_3$(CO)$_7$(GeMe$_2$)$_3$(PMe$_3$)$_2$, **14**. Yield = 8 mg (7 %).

IR (hexane) $\nu(CO)$: 2109.5vw, 2064.5w, 2016mw, 1997w, 1984.5vs, 1966.5m, 1936ms cm^{-1}

^1H NMR (CDCl$_3$) : 1.948d ($^2J_{PH}$ = 9.5 Hz, 18H, P$\underline{Me}_3$); 1.075s (12H, Ge$\underline{Me}_2$); 0.996s(6H, Ge$\underline{Me}_2$)

Elemental analysis : (Found) 18.89 %C, 2.93 %H ;

(Calculated for C$_{19}$H$_{36}$Ge$_3$O$_7$Os$_3$P$_2$) 18.60 %C, 2.96 %H

<u>Band 4</u> (3/7, dichloromethane/hexane eluant) gave Os$_3$(CO)$_6$(GeMe$_2$)$_3$(PMe$_3$)$_3$, **15**. Yield = 45 mg (35 %).

IR (hexane) ν(CO) : 1991m, 1954.5vs cm^{-1}

^1H NMR (CDCl$_3$) : 1.924d ($^2J_{PH}$ = 9.4 Hz, 24H, P$\underline{Me}_3$); 0.943s(18H, Ge$\underline{Me}_2$)

Elemental analysis : (Found) 19.99 %C, 3.61 %H ;

(Calculated for C$_{21}$H$_{45}$Ge$_3$O$_6$Os$_3$P$_3$) 19.78 %C, 3.56 %H

9. Reference

[1]   Shriver, D. F.; Drzedzon, M. A. *The Manipulation of Air-Sensitive Compounds*, 2nd ed.; Wiley: New York, 1986.

[2]   See for example Einstein, F. W. B.; Johnston, V. J.; Ma A. K.; Pomeroy, R. K. *Organometallics*, **1990**, *9*, 52.

[3]   (a) George, R. D.; Knox, S. A. R.; Stone, F. G. A. *J. Chem. Soc., Dalton Trans.*, **1973**, 972. (b) Collman, J. P.; Murphy, D. W.; Fleischer, E. B.; Swift, D. *Inorg. Chem.*, **1974**, *13*, 1.

[4]   A complete X-ray structural study was subsequently carried out on a pale yellow plate (0.08 x 0.16 x 0.01 mm) by Dr. Chuck Campana of Siemens Industrial Automation, Inc., using a Siemens SMART system. Crystal data for that study are: $C_{96}H_{60}O_{24}Os_6Sn_6$, *Monoclinic C2/c, a=35.0385(5) Å, b=10.1038(2) Å, c=34.2232(5) Å, β =118.278(1)^o, V=10669.86 Å^3, F(000)=6336, Z=4, $\mu(MoK\alpha)$=8.55mm^{-1}, 7448 independent reflections, R=0.139,wR=0.258 on 5362 observed reflections (I>2σ) for all atoms isotropic, T=173K.*

[5]   Knox, S. A. R.; Stone, F. G. A. *J. Chem. Soc. A*, **1971**, 2874.

Chapter VI Crystallographic studies

1.   General procedures

The following general procedures for crystal handling through to data collection and structure refinement were employed in all crystal structure studies in this thesis, unless stated otherwise.

Crystals were mounted on glass fibres in air. Intensity data were collected at 20 °C on an Enraf Nonius diffractometer with Kappa geometry design. Graphite-monochromated Mo Kα radiation, with the X-ray generator at 46 kV, was employed. Bisecting geometry was generally used. Background measurements for each scan were made by extending the scan width by 25% on each side of the peak. The unique set of data was collected; a hemisphere for triclinic (±h, +k, ±l), and a quadrant for monoclinic (±h, +k, +l). The reflections were generally measured in 2 or 3 shells; $2.0 \leq \theta \leq 15.0$, $15.0 \leq \theta \leq 22.5$, and $22.5 \leq \theta \leq 25.0$. The final unit cell was determined from a least-squares fit for 25 well-centered high-angle ($\theta \geq 15°$) reflections chosen to be as widely scattered in reciprocal space as possible. Crystal orientation was checked by monitoring 3 orientation standards after every 200 to 300 reflections. Two intensity standards were measured at intervals of 60 min of X-ray exposure time.

Raw data were corrected for Lorentz and polarization effects; absorption corrections were made with either a Gaussian numerical integration method [1] and checked against azimuthal scans at $10°$ intervals in ψ on 3 reflections ($\chi \geq 80°$), or the empirical method of North et al [2]. The intensity data were also scaled against the intensity standards to account for any temporal variations. Reflections were considered observed if $I_0 > 2.5\sigma(I_0)$.

Initial structural solution generally consisted of locating the heavy-atom positions by direct methods or from Patterson maps, followed by location of the light atoms by subsequent difference maps. H atoms were generally not located and were placed in calculated positions with a C-H bond distance of 0.96 Å and an isotropic temperature

factor 1.10 times that of the carbon atom to which they were attached. Their coordinate shifts were linked to that of the carbon atom that they were bonded to, while their temperature factor shifts were equivalenced. Unit weights were used in all initial solutions and structural refinements, but final stages of refinement were with counterweights together with an appropriate instrumental factor. Complex scattering factors for neutral atoms [3] were used in the calculation of structure factors.

The NRCVAX [4] Crystal Structure System suite of programs was used in data reduction, structural solution and initial refinement. The program suite CRYSTALS [5] was employed in the latter stages, including placement of the H atoms. All computations were carried out either on a MicroVAX-II computer or on an Intel 486DX2-based microcomputer operating at 66 MHz clock speed.

The following parameter definitions were used :

$R = \Sigma||F_o| - |F_c||/\Sigma|F_o|$

$wR = \sqrt{[\Sigma w(|F_o| - |F_c|)^2/\Sigma w|F_o|^2]}, w = 1/(\sigma^2(F_o) + k|F_o|^2)$

$G.O.F. = \sqrt{[\Sigma w(|F_o|-|F_c|)^2)/(\text{degrees of freedom})]}$

$F_c^* = K|F_c|(1 + 2r^*|F_c|^2\delta)^{-1/4} ; \delta = (e^2/mc^2V)^2(\lambda^3/\sin2\theta)(p_2/p_1)\overline{T}$ [6]

Thermal ellipsoids in all ORTEP [7] plots show 50% probability; H atoms are plotted as circles corresponding to an arbitrarily small isotropic thermal parameter.

2. X-ray structural studies of tri- and tetrametallic clusters

(a) <u>Details of X-ray Structural Study for Ph$_2$Ge[Os(CO)$_4$H]$_2$, 3, and</u>
     <u>"(OC)$_3$HOs(SnBu$^t_2$)$_2$O"</u>

(i) Ph$_2$Ge[Os(CO)$_4$H]$_2$, **3**

A pale yellow rectangular prismatic crystal, grown from hexane, was used for intensity measurements. The two intensity standards showed steady decreases in intensities over time (long-term instabilities of about 32% and 18%). A Gaussian absorption correction was employed.

There was one molecule in the asymmetric unit. The final model had all non-H atoms anisotropic. The phenyl carbons were regularised, with a C-C bond length of 1.39 Å; a model in which the phenyl carbons were refined freely showed little deviation from the idealised geometry. The phenyl rings were refined as rigid groups pivoted about dummy atoms placed at the centroids. Equivalent phenyl C atoms were given the same temperature factors and their shifts made equivalent, giving four different sets of U$_{ij}$'s per phenyl ring. The metal hydrides were also placed in calculated positions, at 1.66 Å from the Os atoms and trans to a CO. An extinction parameter was also included in the refinement.

The largest residual peak in the final difference map was 1.6(2) eÅ^{-3}, located 0.93 Å from Os(2).

(ii) "(OC)$_3$HOs(SnBu$^t_2$)$_2$O"

A colourless rectangular plate, grown from hexane, was cut to 0.2-0.3 mm in size. Reflections were measured at ψ positions corresponding to minimum absorption. The two intensity standards showed rapid decay over the period of data collection (~50% drop in intensities). A redetermination of the unit cell at the end of the data collection showed a change of about 1% in the cell volume. An absorption correction based on Gaussian integration was applied.

A vacant site on the Os atom *cis* to the Sn atoms was assumed to be occupied by a hydride ligand, which was placed 1.66 Å from the Os and *trans* to a CO. The final model had the Os, Sn and O atoms anisotropic. An extinction parameter was also refined. The largest residual in the final difference map was 1.5(2) e$Å^{-3}$, located in a "capping" position above the OsSn$_2$ metal core at 1.98 Å from the osmium atom.

Table VI(A) : Crystal data for $Ph_2Ge[Os(CO)_4H]_2$, **3**, and "$(OC)_3HOs(SnBu^t_2)_2O$".

	3	"$(OC)_3HOs(SnBu^t_2)_2O$"
Formula	$C_{20}H_{12}GeO_8Os_2$	$C_{19}H_{37}O_4OsSn_2$
FW	833.30	757.08
F(000)	1519.43	1455.70
Crystal System	Monoclinic	Monoclinic
Space Group	$C\,2/c$	$P\,2_1/c$
a, Å	33.775(6)	10.9367(15)
b, Å	9.5143(11)	17.468(3)
c, Å	14.937(3)	14.913(2)
β, deg	105.433(14)	106.161(13)
V, Å³	4642.3(14)	2736.3(8)
2θ range of unit cell	30.0-34.0	30.0-34.0
Z	8	4
D_{calc}, g cm⁻³	2.385	1.838
μ(Mo, Kα), cm⁻¹	122.43	64.74
Crystal dimensions, mm	0.16 x 0.18 x 0.22	0.11 x 0.27 x 0.31
Transmission coefficient	0.1321-0.2593	0.2296-0.4983
Scan range (2θ), deg	3.6-45.0	4.0-45.0
Scan width (ω), deg	0.54+0.35tanθ	0.48+0.35tanθ
Scan rate (ω), deg min⁻¹	0.442-3.296	0.393-3.296
No. of unique reflections	2995	3548
No. of observed reflections	2339	2522
No. of parameters	215	142
R	0.045	0.070
wR	0.055	0.087
Instrument instability factor (k)	0.0001	0.0001
Extinction parameter (r*)	0.16(3)	0.52(9)
Largest (shift/e.s.d.) in final ls cycle	0.11	0.10
Minimum electron density in final difference map, e Å⁻³	-1.0(2)	-1.4(2)
G.O.F.	3.0	4.5

Table VI.1(a) : Fractional Atomic Coordinates and Isotropic or Equivalent Isotropic Temperature Factors (Å) for **3**.

Atom	x/a	y/b	z/c	U(iso)
Os(1)	0.58045(2)	0.04318(6)	0.16885(4)	0.0628
Os(2)	0.58275(2)	0.43598(7)	0.32288(5)	0.0736
Ge(1)	0.62468(4)	0.2281(1)	0.27946(9)	0.0584
O(11)	0.5489(4)	-0.014(2)	0.3394(8)	0.1090
O(12)	0.5988(4)	0.222(1)	0.0145(7)	0.0949
O(13)	0.6571(4)	-0.151(1)	0.2056(8)	0.0949
O(14)	0.5205(4)	-0.156(1)	0.0363(8)	0.1068
O(21)	0.6015(4)	0.306(2)	0.5175(9)	0.1202
O(22)	0.5519(4)	0.467(1)	0.1112(9)	0.1122
O(23)	0.6611(4)	0.625(1)	0.3640(9)	0.1137
O(24)	0.5226(4)	0.654(1)	0.362(1)	0.1213
C(11)	0.5606(4)	-0.006(2)	0.276(1)	0.0781
C(12)	0.5933(5)	0.151(1)	0.071(1)	0.0709
C(13)	0.6294(4)	-0.083(2)	0.193(1)	0.0708
C(14)	0.5424(5)	-0.085(2)	0.084(1)	0.0851
C(21)	0.5956(5)	0.353(2)	0.447(1)	0.0825
C(22)	0.5642(5)	0.460(2)	0.190(1)	0.0896
C(23)	0.6325(5)	0.557(2)	0.348(1)	0.0856
C(24)	0.5451(5)	0.572(2)	0.349(1)	0.0946
C(101)	0.6585	0.1391	0.3950	0.0584
C(102)	0.6864	0.2277	0.4548	0.0626
C(103)	0.7129	0.1756	0.5372	0.0657
C(104)	0.7115	0.035	0.5600	0.0775
C(105)	0.6836	-0.0536	0.5003	0.0657
C(106)	0.6571	-0.0015	0.4178	0.0626
C(201)	0.6684	0.2987	0.2250	0.0601
C(202)	0.6625	0.4199	0.1696	0.0627
C(203)	0.6941	0.4666	0.1309	0.0679
C(204)	0.7317	0.392	0.1477	0.0936
C(205)	0.7376	0.271	0.2032	0.0679
C(206)	0.7060	0.2242	0.2418	0.0627
H(1)	0.5397	0.1479	0.1492	0.19(6)
H(2)	0.5412	0.3351	0.3027	0.19(6)

Table VI.1(b) : Anisotropic Temperature Factors (Å) for **3**.

Atom	U(11)	U(22)	U(33)	U(23)	U(13)	U(12)
Os(1)	0.0529(4)	0.0717(4)	0.0626(4)	-0.0014(3)	0.0101(3)	-0.0009(3)
Os(2)	0.0665(4)	0.0776(5)	0.0795(5)	-0.0093(3)	0.0180(3)	0.0087(3)
Ge(1)	0.0546(8)	0.0642(9)	0.0565(9)	0.0049(7)	0.0135(7)	0.0008(7)
O(11)	0.101(8)	0.17(1)	0.096(8)	0.028(9)	0.048(7)	-0.006(9)
O(12)	0.112(9)	0.105(9)	0.082(8)	0.019(5)	0.036(7)	0.008(7)
O(13)	0.094(8)	0.113(9)	0.096(8)	0.008(7)	0.022(7)	0.043(6)
O(14)	0.101(9)	0.12(1)	0.110(9)	-0.033(7)	0.000(7)	-0.030(7)
O(21)	0.14(1)	0.17(1)	0.095(7)	0.020(8)	0.054(9)	-0.004(9)
O(22)	0.13(1)	0.14(1)	0.083(4)	0.009(8)	0.002(8)	0.044(9)
O(23)	0.118(9)	0.101(9)	0.14(1)	0.002(8)	0.033(9)	-0.035(6)
O(24)	0.095(9)	0.13(1)	0.21(1)	-0.07(1)	0.03(1)	0.031(7)
C(11)	0.054(8)	0.12(1)	0.09(1)	0.02(1)	0.030(8)	0.013(9)
C(12)	0.075(9)	0.07(1)	0.069(9)	-0.008(6)	0.020(8)	-0.019(8)
C(13)	0.065(9)	0.09(1)	0.07(1)	-0.020(8)	0.012(8)	0.012(6)
C(14)	0.08(1)	0.09(1)	0.09(1)	-0.024(8)	0.001(9)	-0.004(8)
C(21)	0.07(1)	0.11(1)	0.080(8)	-0.002(8)	0.027(9)	0.01(1)
C(22)	0.08(1)	0.12(1)	0.080(3)	-0.01(1)	0.00(1)	0.02(1)
C(23)	0.08(1)	0.07(1)	0.11(1)	0.02(1)	0.03(1)	0.000(6)
C(24)	0.09(1)	0.11(1)	0.11(1)	-0.04(1)	0.02(1)	0.026(9)
C(101)	0.056(8)	0.075(9)	0.048(8)	0.012(7)	0.007(7)	-0.008(7)
C(102)	0.069(3)	0.069(3)	0.069(3)	0.019(3)	0.032(3)	0.019(3)
C(103)	0.075(3)	0.075(3)	0.075(3)	0.025(3)	0.038(3)	0.025(3)
C(104)	0.07(1)	0.11(1)	0.053(9)	0.009(9)	0.005(8)	0.002(9)
C(105)	0.075(3)	0.075(3)	0.075(3)	0.025(3)	0.038(3)	0.025(3)
C(106)	0.069(3)	0.069(3)	0.069(3)	0.019(3)	0.032(3)	0.019(3)
C(201)	0.076(9)	0.048(7)	0.057(8)	0.006(7)	0.011(7)	0.000(7)
C(202)	0.069(3)	0.069(3)	0.069(3)	0.019(3)	0.032(3)	0.019(3)
C(203)	0.079(3)	0.079(3)	0.079(3)	0.029(3)	0.043(3)	0.029(3)
C(204)	0.10(1)	0.12(1)	0.08(1)	-0.01(1)	0.02(1)	-0.03(1)
C(205)	0.079(3)	0.079(3)	0.079(3)	0.029(3)	0.043(3)	0.029(3)
C(206)	0.069(3)	0.069(3)	0.069(3)	0.019(3)	0.032(3)	0.019(3)

Table VI.2(a) :   Fractional Atomic Coordinates and Isotropic or Equivalent Isotropic Temperature Factors (Å) for "$(OC)_3HOs(SnBu^t_2)_2O$".

Atom	x/a	y/b	z/c	U(iso)
Os(1)	0.79281(9)	0.60041(5)	0.13001(6)	0.0867
Sn(1)	0.6133(1)	0.62507(7)	0.2177(1)	0.0781
Sn(2)	0.9074(1)	0.69269(8)	0.2701(1)	0.0833
O(1)	0.639(3)	0.462(2)	0.029(2)	0.2213
O(2)	1.048(2)	0.565(1)	0.089(1)	0.1359
O(3)	0.701(2)	0.720(2)	-0.019(1)	0.1771
O(10)	0.745(1)	0.6903(7)	0.3225(8)	0.0768
C(1)	0.700(3)	0.510(2)	0.064(2)	0.14(1)
C(2)	0.956(2)	0.576(1)	0.104(2)	0.095(6)
C(3)	0.738(2)	0.675(1)	0.038(2)	0.120(8)
C(11)	0.456(2)	0.707(1)	0.175(1)	0.093(6)
C(12)	0.569(2)	0.536(1)	0.304(2)	0.104(7)
C(13)	0.329(2)	0.668(1)	0.141(2)	0.15(1)
C(14)	0.447(2)	0.758(1)	0.256(2)	0.15(1)
C(15)	0.478(2)	0.760(1)	0.102(2)	0.139(9)
C(16)	0.682(2)	0.485(2)	0.344(2)	0.15(1)
C(17)	0.460(3)	0.486(2)	0.247(2)	0.21(2)
C(18)	0.525(3)	0.564(2)	0.383(2)	0.19(1)
C(21)	1.055(3)	0.643(2)	0.388(2)	0.134(9)
C(22)	0.931(2)	0.814(1)	0.256(2)	0.124(8)
C(23)	1.184(3)	0.654(2)	0.372(2)	0.21(1)
C(24)	1.057(4)	0.684(2)	0.476(3)	0.28(2)
C(25)	1.035(4)	0.562(2)	0.398(3)	0.27(2)
C(26)	1.058(2)	0.836(2)	0.239(2)	0.16(1)
C(27)	0.832(3)	0.846(2)	0.173(2)	0.23(2)
C(28)	0.926(4)	0.854(2)	0.338(3)	0.30(2)

Table VI.2(b) : Anisotropic Temperature Factors (Å) for "$(OC)_3HOs(SnBu^t_2)_2O$".

Atom	U(11)	U(22)	U(33)	U(23)	U(13)	U(12)
Os(1)	0.0932(7)	0.0961(7)	0.0760(7)	-0.0104(5)	0.0256(5)	0.0055(5)
Sn(1)	0.082(1)	0.0708(8)	0.082(1)	0.0045(7)	0.0223(8)	0.0023(7)
Sn(2)	0.087(1)	0.0830(9)	0.089(1)	-0.0098(8)	0.0354(9)	-0.0076(7)
O(1)	0.24(3)	0.28(3)	0.38(4)	-0.21(3)	0.13(3)	-0.14(3)
O(2)	0.10(1)	0.16(2)	0.22(2)	-0.02(1)	0.08(1)	0.02(1)
O(3)	0.20(2)	0.29(3)	0.16(2)	0.10(2)	0.09(2)	0.10(2)
O(10)	0.072(8)	0.12(1)	0.070(8)	-0.036(7)	0.029(7)	-0.027(7)

(b)   Details of X-ray Structural Studies for [(OC)$_4$OsEMe$_2$]$_2$ (E=Ge, Sn, Pb), 1(EMe),
        and [(OC)$_4$OsSnBu$^t_2$]$_2$, 1(SnBu^t)

    (i)   [(OC)$_4$OsGeMe$_2$]$_2$, 1(GeMe)

A colourless rectangular block, cut from a larger crystal that was grown from toluene, was used for intensity measurements. A full shell of data was also collected for 14.0≤θ≤16.0, to check for possible doubling of *a* and *c* axes; no evidence suggesting doubling of either axes was found.

Two intensity standards were monitored over the period of data collection; one showed a steady decrease over time (long-term instability of ca. 1%), while the other showed a rapid *increase* with time (long-term instability of 8%). Closer inspection of the latter intensity standard revealed that the increase in intensity was a function of X-ray exposure time. The crystal was thus photolysed under UV for about 22 h, and a complete set of data recollected with the same parameters but with an additional intensity standard. This second dataset showed a steady decrease in intensities for all 3 intensity standards (long-term instabilities of 3.2%, 3.0% and 1.8% respectively). Analysis of peak profiles suggested that the reflections were sharper in the second dataset; the peak-width for five reflections that were examined were in the 0.2-0.3^o range, as opposed to 0.5-0.6^o in the initial set.

The refined model for the two datasets, however, did not show any significant differences. It was therefore concluded that the anomalous intensity changes were associated with a crumbling decomposition together with some degree of annealing. The results reported here are from the second dataset. The absorption correction used was based on the Gaussian integration method.

There was half a molecule in the asymmetric unit. The final model had the Os, Ge and O atoms anisotropic. Two large residual peaks were found in the difference map, which were interpreted as disordered Os and Ge atoms; these were located such that the Ge and Os atom positions were interchanged, with the plane of the disordered molecule

tilted with respect to the main molecule. The disorder was thus modelled with partial-occupancy Os and Ge atoms having isotropic temperature factors; the occupancy of the disordered molecule was linked to that of the main molecule such that their occupancies summed to unity. The disorder was about 4.7%. An extinction parameter was also included in the refinement.

The largest residual peak in the final difference map was 1.52(16) eÅ^{-3}, located 1.26 Å from Ge(1).

(ii)   [(OC)$_4$OsSnMe$_2$]$_2$, **1(SnMe)**

A colourless rectangular block, grown from hexane, was used for intensity measurements. The two intensity standards showed steady decay with time (20-30%). The absorption correction used was based on the Gaussian integration method.

As with **1(GeMe)**, there was half a molecule in the asymmetric unit. The final model had the Os, Sn and O atoms anisotropic. A similar disorder to that found in **1(GeMe)** was also found, and was modelled with a complete, partial-occupancy molecule, as follows: The Os and Sn atoms were given anisotropic temperature factors, which were linked to those of the main Sn and Os atoms, respectively. The O atoms were given one common isotropic temperature factor, the C atoms' isotropic temperature factors were linked to those of their counterparts in the main molecule. The Os(CO)$_4$ and SnMe$_2$ fragments were refined as rigid groups by linking their coordinate shifts. Finally, the occupancy for the whole molecule was such that it summed to unity with that of the main molecule; the disorder was about 11%. An extinction parameter was also included in the refinement.

The largest residual peak in the final difference map was 0.63(12) eÅ^{-3}, located 1.03 Å from Os(1).

(iii)   [(OC)$_4$OsPbMe$_2$]$_2$, **1(PbMe)**

An orange, irregular block, grown from hexane, was used for intensity measurements. The three intensity standards showed intensity increases of about 45% (long-term instabilities of 10.4%, 10.0% and 4.7%). There were signs that the intensity

changes were reaching a steady-state at the end of the data collection, so a second full dataset was also collected with the same parameters. This second dataset showed constant intensities in the standards for about half the data, followed by slow decreases, culminating in about a 15% drop by the end of the dataset. Long-term instabilities for this dataset was 3.5%, 3.6% and 2.6% for the intensity standards. A check on the cell parameters at this stage showed that there had been no significant change in the unit cell from the initial one. It was therefore assumed that a similar phenomenon as that observed for the Ge analogue was also present here. The final models obtained from the two datasets did not show any significant difference; the data reported here is from the second dataset. The absorption correction used was based on the Gaussian integration method.

There were two crystallographically non-equivalent half-molecules in the asymmetric unit. The final model had the Os, Pb and O atoms anisotropic. An extinction parameter was also included in the refinement. The largest residual peak in the final difference map was 1.5(2) eÅ^{-3}, located 1.16 Å from Os(1).

(iv) $[(OC)_4OsSn^tBu_2]_2$, **1(SnBu^t)**

A colourless rectangular plate, grown from hexane, was used for intensity measurements. Reflections were measured at ψ positions corresponding to minimum absorption. The three intensity standards showed rapid but steady decay (long-term instabilities of 17.7%, 14.9% and 17.7%). A second search for reflections and indexing was carried out after data collection was completed, and showed a slight but (statistically) significantly different cell. Close examination of a few strong reflections showed streaking or broadening along the θ direction but did not show evidence of double maxima. It was thus concluded that the crystal was degrading, presumably photochemically, to a non-crystalline product, and that the slight difference in cell parameters was due to the broadening of the reflections. The absorption correction used was based on the Gaussian integration method.

The initial solution was obtained by working in the space group $P\,1$ using direct methods, and then transferring half of the molecule in the asymmetric unit back into the space group $P\,\bar{1}$. The final model had the Os, Sn and O atoms anisotropic. At this stage, the largest residual peak in the difference map was 1.15(18) eÅ^{-3}, located 1.29 Å from H(52), which suggested that there was significant disorder of the Bu^t groups. The disorder was modelled with two alternative sites for each of the CH$_3$ groups. All the methyl carbons were given a common temperature factor, and the C-CH$_3$ distances and CH$_3$-C-CH$_3$ angles were restrained to their mean values.

The largest residual in the final difference map was 1.0(3) eÅ^{-3}, located 0.80 Å from the osmium atom.

Table VI(B) : Crystal data for $[(OC)_4OsEMe_2]_2$ (E=Ge, Sn, Pb), 1(EMe), and $[(OC)_4OsSn^tBu_2]_2$, 1(SnBu^t).

	1(GeMe)	1(SnMe)	1(PbMe)	1(SnBu^t)
Formula	$C_{12}H_{12}Ge_2O_8Os_2$	$C_{12}H_{12}O_8Os_2Sn_2$	$C_{12}H_{12}O_8Os_2Pb_2$	$C_{24}H_{36}O_8Os_2Sn_2$
FW	809.80	902.00	1079.0	1070.32
F(000)	727.68	799.76	1855.14	495.87
Crystal System	Monoclinic	Monoclinic	Monoclinic	Triclinic
Space Group	$P2_1/n$	$P2_1/n$	$P2_1/a$	$P\bar{1}$
a, Å	9.0673(6)	9.1465(13)	13.4404(13)	9.016(1)
b, Å	11.8070(9)	11.9544(16)	10.7494(14)	9.370(1)
c, Å	9.5914(9)	9.8120(10)	14.8967(18)	11.334(1)
α, deg	-	-	-	103.56(1)
β, deg	97.182(7)	95.592(10)	98.204(9)	100.30(1)
γ, deg	-	-	-	115.03(1)
V, Å^3	1018.78(14)	1067.8(2)	2130.2(4)	800.2(2)
2θ range of unit cell	30.0-40.2	30.0-37.0	30.0-37.8	30.0-45.0
Z	2	2	4	1
D$_{calc}$, g cm^{-3}	2.640	2.806	3.365	2.221
μ(Mo, Kα), cm^{-1}	153.62	142.29	278.24	95.10
Crystal dimensions, mm	0.18 x 0.21 x 0.30	0.09 x 0.06 x 0.09	0.13 x 0.21 x 0.21	0.08 x 0.14 x 0.18
Transmission coefficient	0.0488-0.1204	0.3242-0.4615	0.0370-0.0768	0.2329-0.5171
Scan range (2θ), deg	3.6-45.0	4.0-45.0	2.8-45.0	2.0-50.0
Scan width (ω), deg	0.70+0.35tanθ	0.90+0.35tanθ	0.45+0.35tanθ	0.90+0.35tanθ
Scan rate (ω), deg min^{-1}	0.573-3.30	0.659-3.30	0.392-5.49	0.736-4.120

147

Table VI(B) continued.

	1(GeMe)	1(SnMe)	1(PbMe)	1(SnBu^t)
No. of unique reflections	1323	1386	2762	2800
No. of observed reflections	1148	1034	1983	2026
No. of parameters	90	89	159	111
R	0.031	0.024	0.035	0.046
wR	0.041	0.026	0.043	0.050
Instrument instability factor (k)	0.00005	0.00009	0.000008	0.00005
Extinction parameter (r*)	0.230(17)	0.179(14)	0.096(7)	-
Largest (shift/e.s.d.) in final ls cycle	0.01	0.02	0.01	0.30
Minimum electron density in final difference map, e Å^{-3}	-0.94(16)	-0.43(12)	-1.0(2)	-1.2(3)
G.O.F.	2.9	1.3	2.7	2.8

148

Table VI.3(a) : Fractional Atomic Coordinates and Isotropic or Equivalent Isotropic Temperature Factors (Å) for **1(GeMe)**.

Atom	x/a	y/b	z/c	U(iso)	Occ
Os(1)	0.58347(5)	0.04066(3)	0.20264(4)	0.0514	0.953(2)
Ge(1)	0.6624(1)	-0.02798(9)	-0.0334(1)	0.0510	0.953(2)
O(11)	0.608(1)	0.2780(7)	0.0761(9)	0.0883	1.0000
O(12)	0.908(1)	0.0376(8)	0.353(2)	0.1034	1.0000
O(13)	0.531(1)	-0.2133(6)	0.2463(9)	0.0828	1.0000
O(14)	0.402(1)	0.1178(9)	0.430(1)	0.1155	1.0000
C(11)	0.596(1)	0.194(1)	0.126(1)	0.071(3)	1.0000
C(12)	0.794(2)	0.038(1)	0.300(2)	0.090(4)	1.0000
C(13)	0.548(1)	-0.120(1)	0.230(1)	0.063(3)	1.0000
C(14)	0.468(2)	0.090(1)	0.343(2)	0.093(4)	1.0000
C(1)	0.799(2)	0.076(1)	-0.111(2)	0.105(5)	1.0000
C(2)	0.763(1)	-0.1755(9)	-0.016(1)	0.076(3)	1.0000
Os(10)	0.368(1)	-0.0018(8)	0.162(1)	0.058(4)	0.047(2)
Ge(10)	0.613(3)	0.081(2)	0.087(3)	0.061(7)	0.047(2)

Table VI.3(b) : Anisotropic Temperature Factors (Å) for **1(GeMe)**.

Atom	U(11)	U(22)	U(33)	U(23)	U(13)	U(12)
Os(1)	0.0684(4)	0.0429(3)	0.0458(4)	-0.0024(2)	-0.0021(2)	0.0016(2)
Ge(1)	0.0448(6)	0.0510(7)	0.0600(8)	0.0028(6)	0.0114(6)	0.0012(5)
O(11)	0.131(8)	0.054(5)	0.104(7)	0.015(5)	-0.010(6)	-0.015(5)
O(12)	0.110(8)	0.101(8)	0.18(1)	0.017(7)	-0.097(8)	-0.009(5)
O(13)	0.126(7)	0.050(5)	0.095(7)	0.009(4)	0.026(6)	-0.002(4)
O(14)	0.22(1)	0.119(8)	0.088(7)	0.007(6)	0.067(8)	0.056(8)

Table VI.4(a) : Fractional Atomic Coordinates and Isotropic or Equivalent Isotropic Temperature Factors (Å) for **1(SnMe)**.

Atom	x/a	y/b	z/c	U(iso)	Occ
Os(1)	0.58782(5)	0.54045(3)	0.20953(4)	0.0516	0.8921(7)
Sn(1)	0.32878(8)	0.53075(6)	0.03883(7)	0.0517	0.8921(7)
O(11)	0.615(1)	0.7739(6)	0.0824(9)	0.0879	0.8921(7)
O(12)	0.401(1)	0.6141(9)	0.4375(9)	0.1060	0.8921(7)
O(13)	0.536(1)	0.2895(6)	0.2451(8)	0.0851	0.8921(7)
O(14)	0.903(1)	0.5388(7)	0.355(1)	0.1029	0.8921(7)
C(11)	0.603(1)	0.687(1)	0.131(1)	0.067(3)	0.8921(7)
C(12)	0.475(1)	0.589(1)	0.353(1)	0.074(3)	0.8921(7)
C(13)	0.554(1)	0.382(1)	0.232(1)	0.060(3)	0.8921(7)
C(14)	0.785(1)	0.538(1)	0.301(1)	0.072(3)	0.8921(7)
C(1)	0.228(1)	0.6938(9)	0.027(1)	0.084(4)	0.8921(7)
C(2)	0.176(1)	0.421(1)	0.123(1)	0.103(4)	0.8921(7)
Os(10)	0.3516(4)	0.4955(3)	0.1616(4)	0.0517	0.1079(7)
Sn(10)	0.6139(7)	0.5871(5)	0.0961(6)	0.0516	0.1079(7)
O(111)	0.5433(4)	0.2946(3)	0.2578(4)	0.08(2)	0.1079(7)
O(112)	0.4019(4)	0.6261(3)	0.4326(4)	0.08(2)	0.1079(7)
O(113)	0.2122(4)	0.6907(3)	-0.0062(4)	0.08(2)	0.1079(7)
O(114)	0.0597(4)	0.3737(3)	0.1849(4)	0.08(2)	0.1079(7)
C(111)	0.4722(4)	0.3687(3)	0.2219(4)	0.067(3)	0.1079(7)
C(112)	0.3829(4)	0.5774(3)	0.3355(4)	0.074(3)	0.1079(7)
C(113)	0.2678(4)	0.6229(3)	0.0556(4)	0.060(3)	0.1079(7)
C(114)	0.1712(4)	0.4189(3)	0.1720(4)	0.072(3)	0.1079(7)
C(101)	0.7912(7)	0.5368(5)	0.2412(6)	0.084(4)	0.1079(7)
C(102)	0.6036(7)	0.7692(5)	0.1050(6)	0.103(4)	0.1079(7)

Table VI.4(b) : Anisotropic Temperature Factors (Å) for **1(SnMe)**.

Atom	U(11)	U(22)	U(33)	U(23)	U(13)	U(12)
Os(1)	0.0682(3)	0.0468(3)	0.0430(3)	-0.0039(2)	-0.0015(2)	0.0014(2)
Sn(1)	0.0515(4)	0.0537(5)	0.0509(4)	-0.0002(4)	0.0090(3)	0.0002(4)
O(11)	0.124(7)	0.052(4)	0.113(8)	0.014(4)	-0.003(6)	-0.017(5)
O(12)	0.20(1)	0.117(8)	0.076(6)	-0.009(6)	0.056(6)	0.048(8)
O(13)	0.134(8)	0.059(2)	0.083(6)	0.016(4)	0.013(6)	0.001(5)
O(14)	0.110(5)	0.083(6)	0.150(9)	0.001(6)	-0.059(6)	-0.000(6)
Os(10)	0.0515(4)	0.0537(5)	0.0509(4)	-0.0002(4)	0.0090(3)	0.0002(4)
Sn(10)	0.0682(3)	0.0468(3)	0.0430(3)	-0.0039(2)	-0.0015(2)	0.0014(2)

Table VI.5(a) : Fractional Atomic Coordinates and Isotropic or Equivalent Isotropic Temperature Factors (Å) for **1(PbMe)**.

Atom	x/a	y/b	z/c	U(iso)
Os(1)	0.53872(6)	0.29965(8)	0.49653(5)	0.0517
Os(2)	0.91252(5)	0.51813(8)	0.11428(5)	0.0518
Pb(1)	0.52810(6)	0.51838(8)	0.38827(5)	0.0583
Pb(2)	0.97650(6)	0.65833(8)	-0.02800(5)	0.0568
O(11)	0.748(1)	0.402(2)	0.575(1)	0.0935
O(12)	0.3104(9)	0.290(2)	0.428(1)	0.0771
O(13)	0.538(2)	0.084(2)	0.631(1)	0.1168
O(14)	0.603(1)	0.153(2)	0.339(1)	0.0881
O(21)	0.744(1)	0.445(2)	-0.038(1)	0.0931
O(22)	0.807(1)	0.735(2)	0.192(1)	0.0883
O(23)	1.121(1)	0.590(2)	0.210(1)	0.0949
O(24)	0.869(1)	0.328(2)	0.257(1)	0.0880
C(11)	0.674(2)	0.361(2)	0.550(1)	0.065(6)
C(12)	0.390(2)	0.293(2)	0.450(1)	0.060(5)
C(13)	0.541(2)	0.166(2)	0.583(2)	0.074(6)
C(14)	0.580(1)	0.207(2)	0.396(2)	0.063(6)
C(21)	0.806(2)	0.472(2)	0.022(2)	0.071(6)
C(22)	0.846(2)	0.659(2)	0.162(2)	0.070(6)
C(23)	1.041(2)	0.557(2)	0.175(1)	0.066(6)
C(24)	0.883(1)	0.402(2)	0.203(1)	0.064(6)
C(1)	0.688(2)	0.568(3)	0.356(2)	0.13(1)
C(2)	0.425(2)	0.490(3)	0.256(2)	0.11(1)
C(3)	0.849(2)	0.735(3)	-0.117(2)	0.106(9)
C(4)	1.058(2)	0.826(3)	0.014(2)	0.114(9)

Table VI.5(b) : Anisotropic Temperature Factors (Å) for **1(PbMe)**.

Atom	U(11)	U(22)	U(33)	U(23)	U(13)	U(12)
Os(1)	0.0484(4)	0.0569(6)	0.0521(5)	-0.0024(4)	0.0120(4)	0.0012(4)
Os(2)	0.0481(4)	0.0619(6)	0.0491(5)	0.0021(4)	0.0127(4)	0.0014(4)
Pb(1)	0.0720(6)	0.0623(6)	0.0531(5)	-0.0004(4)	0.0265(4)	0.0009(4)
Pb(2)	0.0601(5)	0.0588(6)	0.0573(5)	0.0080(4)	0.0173(4)	0.0077(4)
O(11)	0.050(9)	0.12(2)	0.16(2)	-0.04(1)	-0.02(1)	-0.012(9)
O(12)	0.034(7)	0.14(2)	0.10(1)	-0.03(1)	-0.006(8)	-0.014(8)
O(13)	0.19(2)	0.10(2)	0.10(1)	0.03(1)	0.04(1)	-0.02(1)
O(14)	0.10(1)	0.14(2)	0.07(1)	-0.04(1)	0.03(1)	0.00(1)
O(21)	0.08(1)	0.11(1)	0.10(1)	-0.01(1)	-0.00(1)	-0.01(1)
O(22)	0.09(1)	0.09(1)	0.10(1)	-0.01(1)	0.04(1)	0.01(1)
O(23)	0.07(1)	0.13(2)	0.11(1)	0.03(1)	0.02(1)	-0.03(1)
O(24)	0.10(1)	0.11(1)	0.07(1)	0.02(1)	0.005(9)	-0.02(1)

Table VI.6(a) : Fractional Atomic Coordinates and Isotropic or Equivalent Isotropic Temperature Factors (Å) for **1(SnBu^t)**.

Atom	x/a	y/b	z/c	U(iso)	Occ
Os(1)	0.24425(6)	0.66222(6)	0.97340(6)	0.0714	1.0000
Sn(1)	-0.0984(1)	0.4139(1)	0.83470(8)	0.0639	1.0000
O(11)	0.318(2)	0.369(2)	0.960(2)	0.1451	1.0000
O(12)	0.595(2)	0.918(2)	1.174(2)	0.1680	1.0000
O(13)	0.130(2)	0.930(2)	0.990(2)	0.1804	1.0000
O(14)	0.333(3)	0.685(3)	0.724(2)	0.2416	1.0000
C(11)	0.287(2)	0.473(2)	0.966(2)	0.106(5)	1.0000
C(12)	0.464(2)	0.821(2)	1.094(2)	0.124(6)	1.0000
C(13)	0.166(2)	0.827(2)	0.979(2)	0.120(5)	1.0000
C(14)	0.310(3)	0.683(3)	0.822(2)	0.164(8)	1.0000
C(1)	-0.2429	0.5053	0.7079	0.1230	1.0000
C(2)	-0.1153	0.1809	0.6945	0.1296	1.0000
C(3)	-0.407(3)	0.373(3)	0.628(3)	0.130(4)	0.57(1)
C(4)	-0.268(4)	0.643(3)	0.805(3)	0.130(4)	0.57(1)
C(5)	-0.118(3)	0.606(4)	0.641(3)	0.130(4)	0.57(1)
C(30)	-0.445(4)	0.389(5)	0.698(4)	0.130(4)	0.43(1)
C(40)	-0.183(5)	0.678(4)	0.745(4)	0.130(4)	0.43(1)
C(50)	-0.233(5)	0.430(5)	0.572(3)	0.130(4)	0.43(1)
C(6)	-0.293(3)	0.058(4)	0.618(3)	0.130(4)	0.57(2)
C(7)	-0.048(4)	0.094(4)	0.784(3)	0.130(4)	0.57(2)
C(8)	0.009(4)	0.232(4)	0.618(3)	0.130(4)	0.57(2)
C(60)	-0.300(4)	0.028(4)	0.677(4)	0.130(4)	0.43(2)
C(70)	0.023(4)	0.147(5)	0.722(4)	0.130(4)	0.43(2)
C(80)	-0.132(5)	0.218(5)	0.566(3)	0.130(4)	0.43(2)

Table VI.6(b) : Anisotropic Temperature Factors (Å) for **1(SnBu^t)**.

Atom	U(11)	U(22)	U(33)	U(23)	U(13)	U(12)
Os(1)	0.0718(4)	0.0553(3)	0.1150(5)	0.0398(3)	0.0425(3)	0.0311(3)
Sn(1)	0.0804(6)	0.0675(5)	0.0564(5)	0.0176(4)	0.0113(4)	0.0464(5)
O(11)	0.12(1)	0.11(1)	0.39(3)	0.00(1)	-0.00(1)	0.086(9)
O(12)	0.088(8)	0.093(9)	0.38(3)	-0.00(1)	-0.01(1)	0.013(7)
O(13)	0.27(2)	0.12(1)	0.35(3)	0.03(1)	-0.04(2)	0.14(1)
O(14)	0.45(3)	0.27(2)	0.26(2)	0.15(2)	0.26(2)	0.14(2)

(c)   <u>Details of X-ray Structural Studies for Os$_2$(CO)$_7$(SnMe$_2$)$_2$L (L = C$_2$H$_4$, 11b;</u>
       <u>PMe$_3$, 12b)</u>

(i)   Os$_2$(CO)$_7$(SnMe$_2$)$_2$(C$_2$H$_4$), **11b**

A yellow, irregularly cut crystal, grown from hexane, was used for intensity measurements. The two intensity standards showed random variations in scale of ±1%. The absorption correction used was based on the empirical ψ-scan method, together with a θ-dependent correction for a sphere of 130 μm diameter.

Peaks found in the equatorial planes of both the crystallographically distinct half-molecules were interpreted as disorder between C$_2$H$_4$ and CO positions. Refinement of the occupancies of the equatorial CO and ethene ligands suggested that there was a 50% occupancy of ethene at only one equatorial CO position for one half-molecule (A), and 50% occupancy of ethene at each of the two equatorial CO positions in the second half-molecule (B). The data was thus interpreted as indicating the presence of a mono-substituted product (molecule A) and a disubstituted product (molecule B), and the occupancies fixed as such. There was also indication of a disorder similar to that in **1(SnMe)** in the metal framework of molecule B. This was modelled with isotropic Os and Sn atoms only, and the occupancy of the disorder converged at 2%.

The final model had the Os and Sn atoms of the main molecules anisotropic. The ethene H atoms were placed in calculated positions in the same manner as the methyl H atoms assuming sp^3 hybridisation at the ethene C's. The equatorial CO's were given common temperature factors which were linked to those of the only ordered equatorial CO of molecule A. Restraints were placed on the C=C bond lengths (1.34(1) Å), C-O$_{eq}$ bond lengths (1.11(2)Å), Os-C$_{eq}$ bond lengths (1.97(2) Å) and Os-C-O$_{eq}$ bond angles (177(2)°).

The largest residual in the final difference map was 1.09(17) eÅ^{-3}, located 0.94 Å from Os(2). The rather large shift/e.s.d.s in the final cycle were all associated with the

disordered parts of the molecules, and showed oscillations; the largest shift/e.s.d. for the ordered parts was 0.07.

(ii) $Os_2(CO)_7(SnMe_2)_2(PMe_3)$, **12b**

A colourless block, grown from hexane, was cut to about 0.2 mm in size. A full shell for the indices ±h, -k, ±l was also collected for $10.0 \leq \theta \leq 12.0$. The two intensity standards showed random fluctuations corresponding to a ±2% variation in scale. An empirical absorption correction was employed, together with a θ-dependent correction for a sphere of 160 μm diameter.

The final model had all non-H atoms anisotropic. An extinction parameter was also refined. The largest residual in the final difference map was 1.02(15) $eÅ^{-3}$, located 0.54 Å from H(13). This may indicate some disorder of the methyl groups on the phosphine, but no attempt was made to model it.

Table VI(C) :   Crystal data for $Os_2(CO)_7(SnMe_2)_2L$ (L = C_2H_4, **11b**; PMe_3, **12b**).

	11b	**12b**
Formula	$C_{13.5}H_{18}O_{6.5}Os_2Sn_2$	$C_{14}H_{21}O_7Os_2PSn_2$
FW	902.07	950.1
F(000)	805.76	855.76
Crystal System	Triclinic	Triclinic
Space Group	$P\bar{1}$	$P\bar{1}$
a, Å	9.2933(11)	8.7244(9)
b, Å	9.7181(13)	10.9318(6)
c, Å	12.2508(15)	13.2560(13)
α, deg	89.21(1)	87.815(6)
β, deg	87.61(1)	83.655(8)
γ, deg	86.13(1)	82.343(6)
V, Å^3	1102.8(2)	1244.97(19)
2θ range of unit cell	30.0-45.0	30.0-42.0
Z	2	2
D_{calc}, g cm^{-3}	2.716	2.534
μ(Mo, Kα), cm^{-1}	137.71	122.68
Crystal dimensions, mm	0.13 x 0.14 x 0.18	0.16 x 0.20 x 0.22
Transmission coefficient	0.1641-0.2897	0.1757-0.2607
Scan range (2θ), deg	2.0-50.0	4.0-50.0
Scan width (ω), deg	$0.95+0.35\tan\theta$	$0.84+0.35\tan\theta$
Scan rate (ω), deg min^{-1}	0.916-3.296	0.785-3.296
No. of unique reflections	2376	4364
No. of observed reflections	2770	3497
No. of parameters	140	203
R	0.037	0.030
wR	0.043	0.037
Instrument instability factor (k)	0.00003	0.00007
Extinction parameter (r*)	-	0.283(13)
Largest (shift/e.s.d.) in final ls cycle	1.6*	0.00
Minimum electron density in final difference map, e Å^{-3}	-0.96(17)	-1.05(15)
G.O.F.	2.7	2.1

*see text

Table VI.7(a) : Fractional Atomic Coordinates and Isotropic or Equivalent Isotropic Temperature Factors (Å) for **11b**.

Atom	x/a	y/b	z/c	U(iso)	Occ
Os(1)	0.09356(6)	0.79445(6)	0.45498(4)	0.0589	1.0000
Os(2)	0.64344(6)	0.67231(7)	1.00180(4)	0.0645	0.9829
Sn(1)	0.16307(9)	1.0472(1)	0.52537(7)	0.0593	1.0000
Sn(2)	0.3949(1)	0.5887(1)	0.91711(7)	0.0591	0.9829
O(11)	0.115(1)	0.929(1)	0.2305(9)	0.100(3)	1.0000
O(13)	0.036(1)	0.748(1)	0.6980(9)	0.098(3)	1.0000
O(21)	0.443(1)	0.759(1)	1.1966(9)	0.101(3)	1.0000
O(23)	0.792(1)	0.520(1)	0.801(1)	0.116(4)	1.0000
O(12)	-0.083(2)	0.569(2)	0.384(1)	0.137(4)	1.0000
O(14)	0.410(3)	0.659(3)	0.449(2)	0.137(4)	0.5000
O(22)	0.544(3)	0.944(3)	0.860(2)	0.137(4)	0.5000
O(24)	0.924(3)	0.643(3)	1.146(2)	0.137(4)	0.5000
C(1)	0.311(2)	1.146(2)	0.416(1)	0.106(6)	1.0000
C(2)	0.268(2)	1.034(2)	0.675(1)	0.095(5)	1.0000
C(3)	0.209(2)	0.726(2)	0.958(1)	0.100(5)	1.0000
C(4)	0.411(2)	0.593(2)	0.740(1)	0.076(4)	1.0000
C(11)	0.116(2)	0.872(2)	0.317(1)	0.078(4)	1.0000
C(13)	0.057(1)	0.760(1)	0.607(1)	0.068(4)	1.0000
C(21)	0.520(2)	0.728(2)	1.124(1)	0.071(4)	1.0000
C(23)	0.739(2)	0.579(2)	0.876(1)	0.089(5)	1.0000
C(12)	-0.013(2)	0.654(2)	0.410(1)	0.094(4)	1.0000
C(14)	0.304(3)	0.705(4)	0.455(2)	0.094(4)	0.5000
C(22)	0.601(5)	0.877(4)	0.914(4)	0.094(4)	0.5000
C(24)	0.829(3)	0.644(4)	1.096(3)	0.094(4)	0.5000
C(10)	0.264(3)	0.649(3)	0.444(3)	0.106(5)	0.5000
C(20)	0.316(2)	0.772(3)	0.460(3)	0.106(5)	0.5000
C(30)	0.587(4)	0.833(3)	0.905(3)	0.106(5)	0.5000
C(40)	0.706(3)	0.859(2)	0.955(3)	0.106(5)	0.5000
C(50)	0.812(3)	0.788(3)	1.027(3)	0.106(5)	0.5000
C(60)	0.821(3)	0.674(4)	1.090(3)	0.106(5)	0.5000
Os(20)	0.420(3)	0.710(3)	0.955(2)	0.043(6)	0.0171
Sn(20)	0.668(4)	0.550(5)	0.976(3)	0.033(9)	0.0171

Table VI.7(b) : Anisotropic Temperature Factors (Å) for **11b**.

Atom	U(11)	U(22)	U(33)	U(23)	U(13)	U(12)
Os(1)	0.0696(4)	0.0576(4)	0.0519(3)	-0.0064(3)	-0.0055(2)	0.0026(3)
Os(2)	0.0644(4)	0.0729(5)	0.0621(3)	-0.0082(3)	0.0094(3)	-0.0159(3)
Sn(1)	0.0516(5)	0.0696(7)	0.0607(5)	-0.0072(5)	-0.0036(4)	-0.0101(5)
Sn(2)	0.0562(6)	0.0701(7)	0.0528(5)	0.0019(5)	-0.0024(4)	0.0067(5)

Table VI.8(a) : Fractional Atomic Coordinates and Isotropic or Equivalent Isotropic

Temperature Factors (Å) for **12b**.

Atom	x/a	y/b	z/c	U(iso)
Os(1)	0.03179(4)	0.38492(3)	0.17964(3)	0.0549
Os(2)	0.35649(3)	0.08989(3)	0.29814(2)	0.0401
Sn(3)	0.11562(6)	0.12951(5)	0.17898(4)	0.0471
Sn(4)	0.27752(7)	0.34022(5)	0.29933(5)	0.0508
P(1)	0.3914(3)	-0.1266(2)	0.2809(2)	0.0522
O(11)	0.3049(9)	0.3755(8)	0.0129(6)	0.0987
O(12)	-0.018(1)	0.6658(8)	0.2041(8)	0.1196
O(13)	-0.1580(9)	0.3247(8)	0.3805(6)	0.0951
O(14)	-0.208(1)	0.3363(8)	0.0398(6)	0.1034
O(21)	0.5458(7)	0.1386(6)	0.0958(5)	0.0707
O(22)	0.0965(8)	0.0983(7)	0.4758(5)	0.0779
O(23)	0.6167(9)	0.0990(8)	0.4328(5)	0.0853
C(11)	0.199(1)	0.3817(9)	0.0744(7)	0.0706
C(12)	0.004(1)	0.5588(9)	0.1955(8)	0.0760
C(13)	-0.091(1)	0.3500(9)	0.3052(7)	0.0620
C(14)	-0.119(1)	0.3580(9)	0.0912(8)	0.0662
C(21)	0.4815(8)	0.1198(8)	0.1720(6)	0.0471
C(22)	0.194(1)	0.0906(8)	0.4112(6)	0.0554
C(23)	0.517(1)	0.0950(8)	0.3839(6)	0.0543
C(1)	0.384(1)	-0.182(1)	0.1561(8)	0.098(4)
C(2)	0.252(1)	-0.2101(9)	0.3598(7)	0.077(3)
C(3)	0.577(1)	-0.202(1)	0.314(1)	0.113(4)
C(31)	0.171(1)	0.0806(9)	0.0226(7)	0.074(3)
C(32)	-0.084(1)	0.0334(9)	0.2316(7)	0.066(2)
C(41)	0.471(1)	0.439(1)	0.2359(8)	0.096(3)
C(42)	0.213(1)	0.410(1)	0.4500(8)	0.099(4)

Table VI.8(b) : Anisotropic Temperature Factors (Å) for **12b**.

Atom	U(11)	U(22)	U(33)	U(23)	U(13)	U(12)
Os(1)	0.0519(2)	0.0505(2)	0.0645(2)	0.0048(2)	-0.0067(2)	0.0079(2)
Os(2)	0.0429(2)	0.0375(2)	0.0392(2)	-0.0010(1)	-0.0029(1)	-0.0006(1)
Sn(3)	0.0447(3)	0.0492(3)	0.0477(3)	-0.0043(2)	-0.0072(2)	-0.0008(3)
Sn(4)	0.0515(3)	0.0393(3)	0.0646(4)	-0.0067(3)	-0.0062(3)	0.0005(3)
P(1)	0.071(2)	0.041(1)	0.048(1)	-0.0011(9)	-0.003(1)	-0.001(1)
O(11)	0.094(6)	0.116(7)	0.094(6)	0.022(5)	0.020(5)	0.007(5)
O(12)	0.147(8)	0.071(6)	0.160(9)	-0.001(6)	-0.012(7)	0.003(6)
O(13)	0.098(6)	0.114(7)	0.084(5)	-0.008(5)	0.029(5)	-0.006(5)
O(14)	0.105(6)	0.108(7)	0.120(7)	0.024(5)	-0.045(5)	-0.018(5)
O(21)	0.067(4)	0.101(5)	0.055(4)	0.015(4)	0.013(3)	0.006(4)
O(22)	0.075(5)	0.111(6)	0.068(4)	-0.002(4)	0.030(4)	-0.004(4)
O(23)	0.087(5)	0.136(7)	0.062(4)	0.007(4)	-0.025(4)	-0.028(5)
C(11)	0.087(7)	0.066(6)	0.068(6)	0.022(5)	0.004(6)	-0.005(6)
C(12)	0.098(8)	0.046(6)	0.099(8)	-0.003(5)	-0.017(6)	0.009(6)
C(13)	0.056(5)	0.062(6)	0.069(6)	-0.007(5)	0.005(5)	0.004(5)
C(14)	0.057(6)	0.069(7)	0.087(7)	0.011(5)	-0.021(5)	0.014(5)
C(21)	0.033(4)	0.065(5)	0.048(5)	0.002(4)	-0.001(3)	0.001(4)
C(22)	0.064(6)	0.056(5)	0.047(5)	-0.000(4)	-0.002(4)	-0.008(4)
C(23)	0.053(5)	0.073(6)	0.041(4)	-0.002(4)	-0.007(4)	0.005(5)

3. X-ray structural studies of penta- and hexametallic clusters

(d) <u>Details of X-ray Structural Studies for $Os_3(CO)_{11}(GeMe_2)_2$, **8**, and $Os_2(CO)_6(GeMe_2)_3$, **10**</u>

(i) $Os_3(CO)_{11}(GeMe_2)_2$, **8**

A colourless plate, grown from hexane, was used for intensity measurements. The two intensity standards showed random variations in scale of ±3%. A Gaussian absorption correction was applied. The initial solution was obtained by direct methods in the space group $C\,\bar{1}$. The molecule sits on a two-fold axis. The final model had all non-H atoms anisotropic. An extinction parameter was also refined. The largest residual in the final difference map was $0.53(14)$ eÅ^{-3}, located 1.03 Å from Os(2).

(ii) $Os_2(CO)_6(GeMe_2)_3$, **10**

A yellow, hexagonal needle, grown from hexane, was cut to about 0.3 mm in length. The unique set of data (1/6th of a sphere) for the Laue class $\bar{3}$ was collected [8]. The two intensity standards showed random fluctuations corresponding to a ±2% variation in scale. An empirical absorption correction was employed, together with a θ-dependent correction for a sphere of 190 μm diameter.

After obtaining an isotropic model for the heavy atom positions, the difference map showed peaks that suggested alternative sites for the Ge atoms, with low occupancy. This was successfully modelled as due to 21% of twinning; the twin operator was a two-fold rotation about the (x + y) direction. An error analysis at this stage, with Os, Ge and O atoms anisotropic, suggested presence of extinction, but our present version of the software did not permit us to refine extinction on twinned structures. Removal of the 15 strongest reflections (based on observed Fo's) led to a dramatic improvement in R from ca. 5% to 2.5%. The final model had all non-H atoms anisotropic. The largest residual in the final difference map was $0.77(16)$ eÅ^{-3}, located 2.19 Å from H(12).

Table VI(D) : Crystal data for $Os_3(CO)_{11}(GeMe_2)_2$, **8**, and $Os_2(CO)_6(GeMe_2)_3$, **10**.

	8	**10**
Formula	$C_{15}H_{12}Ge_2O_{11}Os_3$	$C_{12}H_{18}Ge_3O_6Os_2$
FW	1084.03	856.44
F(000)	1927.16	771.64
Crystal System	Monoclinic	Hexagonal
Space Group	$C\,2/c$	$P\,6_3/m$
a, Å	19.5964(15)	9.8931(19)
b, Å	9.3322(10)	-
c, Å	13.2785(8)	12.1864(14)
β, deg	90.949(6)	-
V, Å^3	2428.0(4)	1032.9
2θ range of unit cell	30.0-40.0	37.8-43.8
Z	4	2
D_{calc}, g cm^{-3}	2.966	2.754
μ(Mo, Kα), cm^{-1}	181.26	165.52
Crystal dimensions, mm	0.07 x 0.12 x 0.15	0.19 x 0.20 x 0.25
Transmission coefficient	0.1599-0.2973	0.1003-0.1339
Scan range (2θ), deg	2.0-50.0	4.0-50.0
Scan width (ω), deg	0.75+0.35tanθ	1.40+0.70tanθ
Scan rate (ω), deg min^{-1}	0.614-3.296	0.35
No. of unique reflections	2121	648
No. of observed reflections	1778	605(590)*
No. of parameters	144	44
R	0.020	0.025
wR	0.025	0.033
Instrument instability factor (k)	0.00007	0.0001
Extinction parameter (r*)	0.269(12)	-
Largest (shift/e.s.d.) in final ls cycle	0.00	0.00
Minimum electron density in final difference map, e Å^{-3}	-0.69(14)	-0.72(16)
G.O.F.	1.4	2.4

*see text.

Table VI.9(a) : Fractional Atomic Coordinates and Isotropic or Equivalent Isotropic
Temperature Factors (Å) for **8**.

Atom	x/a	y/b	z/c	U(iso)
Os(1)	0.14286(1)	0.11717(3)	0.67859(2)	0.0393
Os(2)	0.0000	0.14402(3)	0.7500	0.0323
Ge(1)	0.08126(3)	0.34745(7)	0.71741(4)	0.0385
O(11)	0.1938(3)	0.1144(7)	0.8994(4)	0.0733
O(12)	0.1636(4)	-0.2095(6)	0.6557(5)	0.0855
O(13)	0.0896(3)	0.1535(6)	0.4604(4)	0.0616
O(14)	0.2731(3)	0.2636(8)	0.6173(4)	0.0807
O(21)	0.0506(3)	0.1764(6)	0.9688(3)	0.0556
O(22)	0.0000	-0.1866(8)	0.7500	0.0635
C(1)	0.1184(4)	0.4640(8)	0.8274(5)	0.0625
C(2)	0.0662(4)	0.4790(8)	0.6052(5)	0.0614
C(11)	0.1734(3)	0.1136(7)	0.8181(6)	0.0490
C(12)	0.1545(4)	-0.0904(8)	0.6640(6)	0.0593
C(13)	0.1084(3)	0.1390(7)	0.5411(6)	0.0467
C(14)	0.2240(4)	0.2053(9)	0.6405(5)	0.0560
C(21)	0.0316(3)	0.1619(7)	0.8880(5)	0.0416
C(22)	0.0000	-0.064(1)	0.7500	0.0462

Table VI.9(b) : Anisotropic Temperature Factors (Å) for **8**.

Atom	U(11)	U(22)	U(33)	U(23)	U(13)	U(12)
Os(1)	0.0339(2)	0.0434(2)	0.0417(2)	-0.0009(1)	0.0029(1)	-0.0005(1)
Os(2)	0.0324(2)	0.0320(2)	0.0323(2)	0.0000	0.0007(1)	0.0000
Ge(1)	0.0463(4)	0.0339(4)	0.0372(4)	-0.0006(3)	0.0006(3)	-0.0056(3)
O(11)	0.059(4)	0.114(6)	0.062(4)	0.012(3)	-0.011(3)	-0.002(3)
O(12)	0.121(5)	0.048(4)	0.115(5)	-0.010(3)	-0.015(4)	0.016(4)
O(13)	0.059(3)	0.103(4)	0.039(3)	-0.004(3)	0.000(2)	-0.006(3)
O(14)	0.056(4)	0.118(6)	0.091(4)	0.019(4)	0.002(3)	-0.026(4)
O(21)	0.058(3)	0.088(4)	0.034(3)	-0.001(3)	-0.004(2)	0.004(3)
O(22)	0.082(6)	0.034(4)	0.092(6)	0.0000	0.008(4)	0.0000
C(1)	0.080(6)	0.061(5)	0.062(5)	-0.016(4)	-0.004(4)	-0.024(4)
C(2)	0.082(6)	0.049(4)	0.061(4)	0.010(4)	0.003(4)	-0.006(4)
C(11)	0.036(4)	0.062(5)	0.053(4)	0.004(3)	0.002(3)	0.003(3)
C(12)	0.059(5)	0.055(5)	0.067(5)	-0.002(4)	-0.009(4)	0.005(4)
C(13)	0.036(4)	0.056(4)	0.058(5)	-0.009(3)	0.014(3)	-0.007(3)
C(14)	0.048(4)	0.077(5)	0.048(4)	0.004(4)	0.001(3)	-0.002(4)
C(21)	0.034(3)	0.051(4)	0.045(4)	0.005(3)	0.002(3)	0.011(3)
C(22)	0.053(6)	0.038(5)	0.049(5)	0.0000	-0.003(4)	0.0000

Table VI.10(a) : Fractional Atomic Coordinates and Isotropic or Equivalent Isotropic Temperature Factors (Å) for **10**.

Atom	x/a	y/b	z/c	U(iso)
Os(1)	0.3333	0.6667	0.12921(4)	0.0334
Ge(1)	0.1092(1)	0.6343(1)	0.2500	0.0370
O(11)	0.2934(8)	0.9169(9)	0.0086(6)	0.0706
C(11)	0.306(1)	0.825(1)	0.0537(6)	0.0521
C(1)	0.046(2)	0.793(2)	0.250000(7)	0.0544
C(2)	-0.087(1)	0.437(2)	0.250000(7)	0.0565

Table VI.10(b) : Anisotropic Temperature Factors (Å) for **10**.

Atom	U(11)	U(22)	U(33)	U(23)	U(13)	U(12)
Os(1)	0.0334(2)	0.0334(2)	0.0333(3)	0.0000	0.0000	0.0167(1)
Ge(1)	0.0303(6)	0.0364(6)	0.0474(7)	0.0000	0.0000	0.0174(5)
O(11)	0.099(6)	0.072(5)	0.079(4)	0.031(3)	-0.002(4)	0.050(4)
C(11)	0.069(6)	0.057(5)	0.048(5)	0.011(4)	-0.004(5)	0.038(5)
C(1)	0.065(8)	0.067(8)	0.069(8)	0.0000	0.0000	0.051(7)
C(2)	0.038(5)	0.054(6)	0.067(7)	0.0000	0.0000	0.005(3)

(e)   <u>Details of X-ray Structural Studies for [(OC)$_3$OsEMe$_2$]$_3$ (E=Ge,Sn), **5(E)**</u>

Yellow-orange hexagonal prisms, grown from hot toluene (E = Sn) or hexane (E = Ge), were used for intensity measurements. The unique sets of data (1/16th of a sphere) for a hexagonal *P* cell in the Laue class *6/m* were collected. The intensity standards showed random variations in scale of ±1%. Gaussian absorption corrections were applied.

The molecules sit on $\bar{6}$ sites. All non-H atoms are anisotropic in the final models. Extinction parameters were also refined. The largest residuals in the final difference map were 0.60(11) eÅ^{-3}, located 0.13 Å from the Sn atom, for E = Sn, and 0.52(14) eÅ^{-3}, located 1.11 Å from C(11), for E = Ge.

Table VI(E) : Crystal data for $[(OC)_3OsEMe_2]_3$ (E = Ge, Sn), 5(E)

	5(Sn)	5(Ge)
Formula	$C_{15}H_{18}O_9Os_3Sn_3$	$C_{15}H_{18}Ge_3O_9Os_3$
FW	1268.96	1130.67
F(000)	1102.53	1007.54
Crystal System	Hexagonal	Hexagonal
Space Group	$P\,6_3/m$	$P\,6_3/m$
a, Å	11.007(2)	10.937(4)
c, Å	12.818(2)	12.213(2)
V, Å^3	1345.0(4)	1265.0(4)
2θ range of unit cell	29.8-39.1	30.0-40.0
Z	2	2
D_{calc}, g cm^{-3}	3.134	2.968
μ(Mo, Kα), cm^{-1}	169.27	185.36
Crystal dimensions, mm	0.09 x 0.12 x 0.13	0.10 x 0.12 x 0.12
Transmission coefficient	0.196-0.333	0.2372-0.3064
Scan range (2θ), deg	2.0-50.0	3.0-45.0
Scan width (ω), deg	0.85+0.35tanθ	0.60+0.35tanθ
Scan rate (ω), deg min^{-1}	0.785-3.296	0.491-2.747
No. of unique reflections	818	584
No. of observed reflections	635	483
No. of parameters	54	54
R	0.022	0.018
wR	0.023	0.021
Instrument instability factor (k)	0.00005	0.00006
Extinction parameter (r*)	0.415(15)	0.091(9)
Largest (shift/e.s.d.) in final ls cycle	0.01	0.00
Minimum electron density in final difference map, e Å^{-3}	-0.49(11)	-0.44(14)
G.O.F.	1.5	1.3

Table VI.11(a) : Fractional Atomic Coordinates and Isotropic or Equivalent Isotropic Temperature Factors (Å) for **5(Sn)**.

Atom	x/a	y/b	z/c	U(iso)
Os(1)	0.54047(4)	0.38156(4)	0.2500	0.0385
Sn(1)	0.75249(6)	0.64566(7)	0.2500	0.0420
O(11)	0.3212(9)	0.4699(9)	0.2500	0.0915
O(12)	0.5365(5)	0.3841(5)	0.0110(5)	0.0738
C(1)	0.7879(8)	0.7757(8)	0.1162(7)	0.0682
C(11)	0.404(1)	0.437(1)	0.2500	0.0665
C(12)	0.5396(7)	0.3819(7)	0.0985(8)	0.0533

Table VI.11(b) : Anisotropic Temperature Factors (Å) for **5(Sn)**.

Atom	U(11)	U(22)	U(33)	U(23)	U(13)	U(12)
Os(1)	0.0320(2)	0.0318(2)	0.0557(3)	0.0000	0.0000	0.0158(2)
Sn(1)	0.0394(4)	0.0313(4)	0.0604(5)	0.0000	0.0000	0.0176(3)
O(11)	0.080(6)	0.099(7)	0.151(9)	0.0000	0.0000	0.064(6)
O(12)	0.085(4)	0.093(4)	0.058(4)	-0.001(4)	-0.007(4)	0.051(4)
C(1)	0.075(5)	0.057(5)	0.087(6)	0.026(5)	0.015(5)	0.033(5)
C(11)	0.061(7)	0.056(7)	0.10(1)	0.0000	0.0000	0.034(6)
C(12)	0.051(4)	0.053(5)	0.066(6)	-0.004(4)	-0.003(4)	0.031(4)

Table VI.12(a) : Fractional Atomic Coordinates and Isotropic or Equivalent Isotropic Temperature Factors (Å) for **5(Ge)**.

Atom	x/a	y/b	z/c	U(iso)
Os(1)	0.15990(4)	0.54522(4)	0.2500	0.0340
Ge(1)	0.1240(1)	0.7550(1)	0.2500	0.0397
O(11)	0.1518(5)	0.5361(5)	-0.0026(5)	0.0605
O(12)	-0.1519(8)	0.3223(9)	0.2500	0.0821
C(1)	0.0407(8)	0.7930(8)	0.1215(7)	0.0568
C(11)	0.1584(6)	0.5426(6)	0.0914(8)	0.0408
C(12)	-0.035(1)	0.405(1)	0.2500	0.0629

Table VI.12(b) : Anisotropic Temperature Factors (Å) for **5(Ge)**.

Atom	U(11)	U(22)	U(33)	U(23)	U(13)	U(12)
Os(1)	0.0304(3)	0.0314(3)	0.0403(3)	0.0000	0.0000	0.0148(2)
Ge(1)	0.0356(6)	0.0387(6)	0.0507(9)	0.0000	0.0000	0.0213(5)
O(11)	0.064(4)	0.080(4)	0.042(4)	-0.012(3)	-0.014(3)	0.030(3)
O(12)	0.039(5)	0.081(7)	0.13(1)	0.0000	0.0000	-0.004(5)
C(1)	0.055(5)	0.065(5)	0.074(7)	0.008(5)	-0.016(5)	0.036(4)
C(11)	0.030(4)	0.036(4)	0.059(6)	-0.001(4)	-0.003(4)	0.015(3)
C(12)	0.066(9)	0.056(7)	0.06(1)	0.0000	0.0000	0.024(7)

4. X-ray structural studies of higher nuclearity clusters

(f) Details of X-ray Structural Studies for [Os$_2$(CO)$_7$(SnMe$_2$)$_2$]$_2$, 6 and [Os$_2$(CO)$_7$O(SnMe$_2$)$_2$]$_2$ .C$_7$H$_8$, 7

(i) [Os$_2$(CO)$_7$(SnMe$_2$)$_2$]$_2$, 6

A yellow, rectangular prism, obtained by cooling a hot chloroform solution to room temperature, was used in the data collection. The two intensity standards showed random variations of ±2 % over the period of data collection. A Gaussian absorption correction was applied.

The final least-squares refinement included coordinates for all non-H atoms, anisotropic thermal parameters for Os, Sn, O and the methyl C atoms, and isotropic thermal parameters for the carbonyl C atoms. An extinction parameter was also refined. The final difference map showed highest residual peaks of 1.3(2) and 1.0(2) e Å^{-3}, located at a distance of 1.06 Å from Os(2) and 1.11 Å from Os(1), respectively.

(ii) [(Me$_2$Sn)$_2$Os$_2$(CO)$_7$O]$_2$ .C$_7$H$_8$, 7

Diffraction-quality crystals were obtained from a toluene solution at low temperature, as yellow plates. A thin, yellow plate-like crystal was used in this study. Data collection was initially carried out in bisecting geometry; data for $\theta > 15°$ were collected with the azimuth position corresponding to minimum absorption. Both the intensity standards showed a steady 30% decrease in intensities over the entire period of the data collection. A Gaussian absorption correction was applied.

A toluene molecule was also found in the unit cell of the crystal, which was disordered about the crystallographic two-fold axis, with the methyl group located off it; the presence of the toluene was confirmed by ^{1}H NMR spectroscopy. The toluene molecule was modelled with isotropic carbon and hydrogen atoms, with the phenyl ring carbons regularised to a hexagon of side 1.39 Å; the C and H atoms were given a common temperature factor for each atom type. The molecules were refined as rigid groups,

pivoted at the ring centres by dummy atoms. Two different full molecules were used, giving a total of 4 orientations by the two-fold rotation symmetry axis; the occupancies for the two molecules were constrained to 0.5.

The final least-squares refinement for the cluster molecule included coordinates and anisotropic thermal parameters for all non-H atoms. An extinction parameter was also refined. The largest residual peak in the final difference map was 2.4(3) e Å^{-3}, located 1.12 Å from Os(2).

Table VI(F) :   Crystal Data for $[Os_2(CO)_7(SnMe_2)_2]_2$, **6**, and
$[Os_2(CO)_7O(SnMe_2)_2]_2 \cdot C_7H_8$, **7**.

	6	**7**
Formula	$C_{22}H_{24}O_{14}Os_4Sn_4$	$C_{29}H_{32}O_{16}Os_4Sn_4$
FW	1748.0	1872.1
F(000)	1543.53	1675.51
Crystal system	Monoclinic	Monoclinic
Space group	$P\,2_1/n$	$P\,2/a$
a, Å	9.668(2)	13.895(2)
b, Å	17.825(2)	12.550(2)
c, Å	11.203(1)	14.053(2)
β, deg	105.05(1)	113.56(1)
V, Å^3	1864.4(4)	2246.3(6)
2θ range of unit-cell	32-40	40-50
Z	2	2
D_{calc}, g cm^{-3}	3.114	2.768
μ(Mo, Kα), cm^{-1}	162.89	135.32
Crystal dimensions, mm	0.138x0.083x0.066	0.227x0.159x0.053
Transmission coefficient	0.357-0.545	0.156-0.706
Scan range (2θ), deg	4-48	4-50
Scan width (ω), deg	$0.80 + 0.35\tan\theta$	$0.85 + 0.35\tan\theta$
Scan rate (ω), deg	0.75-3.3	0.96-1.3
No. of unique reflections	2914	3942
No. of observed reflections	2338	3078
No. of parameters	169	200
R	0.022	0.040
wR_w	0.024	0.042
Instrument instability factor (k)	0.00005	0.00007
Extinction parameter (r*)	0.072(12)	0.083(19)
Largest (shift/e.s.d.) in final ls cycle	0.11	0.07
Minimum electron density in final difference map, e Å^{-3}	-0.6(2)	-1.3(3)
G.O.F.	1.3	2.2

Table VI.13(a) : Fractional Atomic Coordinates and Isotropic or Equivalent Isotropic
Temperature Factors (Å) for **6**.

Atom	x/a	y/b	z/c	U(iso)
Os(1)	1.02359(4)	0.32479(2)	0.38549(3)	0.0389
Os(2)	0.99253(3)	0.42968(2)	0.16599(3)	0.0308
Sn(1)	1.23932(6)	0.35853(3)	0.28569(5)	0.0395
Sn(2)	1.16434(6)	0.47662(3)	0.01839(5)	0.0376
O(11)	1.1447(8)	0.4602(4)	0.5498(6)	0.0765
O(12)	0.7180(8)	0.3271(5)	0.4195(8)	0.0767
O(13)	0.9633(9)	0.1938(4)	0.1989(6)	0.0816
O(14)	1.1632(8)	0.2194(4)	0.5961(6)	0.0724
O(21)	1.1137(8)	0.5708(3)	0.3139(6)	0.0674
O(22)	0.6940(6)	0.4398(3)	0.2121(6)	0.0502
O(23)	0.9319(7)	0.3019(4)	-0.0233(6)	0.0622
C(1)	1.412(1)	0.4234(6)	0.3966(8)	0.0679
C(2)	1.331(1)	0.2726(6)	0.1972(9)	0.0685
C(3)	1.348(1)	0.5426(6)	0.1136(8)	0.0650
C(4)	1.242(1)	0.3884(5)	-0.080(1)	0.0627
C(11)	1.096(1)	0.4098(5)	0.4903(9)	0.056(2)
C(12)	0.829(1)	0.3291(5)	0.4030(9)	0.061(3)
C(13)	0.982(1)	0.2419(5)	0.2686(9)	0.060(3)
C(14)	1.111(1)	0.2579(5)	0.5159(9)	0.059(2)
C(21)	1.0679(9)	0.5177(5)	0.2599(8)	0.044(2)
C(22)	0.8071(9)	0.4334(4)	0.1991(7)	0.041(2)
C(23)	0.9517(9)	0.3485(4)	0.0488(8)	0.045(2)

Table VI.13(b) : Anisotropic Temperature Factors (Å) for **6**.

Atom	U(11)	U(22)	U(33)	U(23)	U(13)	U(12)
Os(1)	0.0418(2)	0.0430(2)	0.0368(2)	0.0090(2)	0.0135(2)	0.0052(2)
Os(2)	0.0338(2)	0.0302(2)	0.0303(2)	0.0015(1)	0.0109(1)	0.0014(1)
Sn(1)	0.0379(3)	0.0498(3)	0.0361(3)	0.0021(3)	0.0127(3)	0.0089(3)
Sn(2)	0.0352(3)	0.0429(3)	0.0426(3)	0.0119(3)	0.0155(3)	0.0064(3)
O(11)	0.095(6)	0.077(5)	0.072(5)	-0.025(4)	0.026(4)	-0.010(4)
O(12)	0.051(4)	0.144(7)	0.132(7)	0.080(6)	0.048(5)	0.026(5)
O(13)	0.146(8)	0.058(4)	0.062(5)	-0.011(4)	-0.003(5)	-0.008(5)
O(14)	0.073(5)	0.104(6)	0.074(5)	0.045(4)	0.012(4)	0.033(4)
O(21)	0.100(6)	0.055(4)	0.072(5)	-0.025(4)	0.027(4)	-0.025(4)
O(22)	0.039(4)	0.070(4)	0.073(4)	0.023(3)	0.031(3)	0.016(3)
O(23)	0.085(5)	0.067(4)	0.055(4)	-0.025(3)	0.023(4)	-0.018(4)
C(1)	0.049(6)	0.103(8)	0.059(7)	0.008(6)	0.002(5)	-0.010(6)
C(2)	0.106(9)	0.099(8)	0.067(7)	0.012(6)	0.044(7)	0.062(7)
C(3)	0.051(6)	0.100(8)	0.061(7)	0.030(6)	0.002(5)	-0.013(6)
C(4)	0.112(9)	0.067(7)	0.094(8)	0.025(6)	0.076(8)	0.043(7)

Table VI.14(a) : Fractional Atomic Coordinates and Isotropic or Equivalent Isotropic

Temperature Factors (Å) for **7**.

Atom	x/a	y/b	z/c	U(iso)
Os(1)	0.40715(4)	0.18024(4)	0.24854(4)	0.0459
Os(2)	0.38972(4)	0.26702(4)	0.43765(4)	0.0390
Sn(1)	0.20311(6)	0.20582(7)	0.20598(7)	0.0443
Sn(2)	0.38846(6)	0.34108(7)	0.61493(7)	0.0414
O(1)	0.2225(5)	0.2667(6)	0.3466(6)	0.0416
O(11)	0.3799(9)	-0.0383(8)	0.3306(9)	0.0798
O(12)	0.6489(8)	0.1747(9)	0.349(1)	0.0824
O(13)	0.3917(9)	0.4142(8)	0.1747(9)	0.0784
O(14)	0.3768(9)	0.0946(9)	0.0363(9)	0.0762
O(21)	0.3709(8)	0.0486(7)	0.5286(8)	0.0697
O(22)	0.6241(7)	0.2597(8)	0.5455(9)	0.0709
O(23)	0.4010(7)	0.5042(7)	0.3820(8)	0.0632
C(11)	0.390(1)	0.042(1)	0.303(1)	0.0561
C(12)	0.560(1)	0.178(1)	0.316(1)	0.0724
C(13)	0.397(1)	0.329(1)	0.205(1)	0.0594
C(14)	0.386(1)	0.125(1)	0.115(1)	0.0574
C(21)	0.378(1)	0.128(1)	0.491(1)	0.0517
C(22)	0.5364(9)	0.261(1)	0.507(1)	0.0482
C(23)	0.3959(9)	0.415(1)	0.401(1)	0.0478
C(1)	0.105(1)	0.070(1)	0.191(1)	0.0658
C(2)	0.126(1)	0.328(1)	0.100(1)	0.0739
C(3)	0.5298(9)	0.299(1)	0.745(1)	0.0632
C(4)	0.361(1)	0.508(1)	0.638(1)	0.0607

Table VI.14(a) continued.

Atom	x/a	y/b	z/c	U(iso)	Occ
C(51)	0.750(4)	0.370(2)	0.000(4)	0.068(6)	0.26(1)
C(52)	0.717(3)	0.279(2)	0.057(3)	0.068(6)	0.26(1)
C(53)	0.750(4)	0.179(2)	0.000(4)	0.068(6)	0.26(1)
C(54)	0.797(4)	0.170(2)	-0.033(4)	0.068(6)	0.26(1)
C(55)	0.825(3)	0.262(3)	-0.071(3)	0.068(6)	0.26(1)
C(56)	0.800(4)	0.362(2)	-0.046(4)	0.068(6)	0.26(1)
C(57)	0.658(4)	0.288(4)	0.126(4)	0.111(6)	0.26(1)
C(61)	0.776(4)	0.386(2)	-0.035(4)	0.068(6)	0.24(1)
C(62)	0.730(4)	0.335(2)	0.025(3)	0.068(6)	0.24(1)
C(63)	0.719(3)	0.225(2)	0.019(3)	0.068(6)	0.24(1)
C(64)	0.753(3)	0.166(2)	-0.045(3)	0.068(6)	0.24(1)
C(65)	0.799(3)	0.217(3)	-0.104(3)	0.068(6)	0.24(1)
C(66)	0.810(3)	0.327(3)	-0.099(3)	0.068(6)	0.24(1)
C(67)	0.669(4)	0.169(4)	0.084(4)	0.111(6)	0.24(1)

Table VI.14(b) :   Anisotropic Temperature Factors (Å) for **7**.

Atom	U(11)	U(22)	U(33)	U(23)	U(13)	U(12)
Os(1)	0.0423(3)	0.0526(3)	0.0506(4)	-0.0030(3)	0.0242(3)	0.0013(2)
Os(2)	0.0314(3)	0.0465(3)	0.0416(3)	-0.0003(3)	0.0154(2)	-0.0003(2)
Sn(1)	0.0400(5)	0.0518(5)	0.0437(6)	-0.0015(4)	0.0181(4)	-0.0030(4)
Sn(2)	0.0321(4)	0.0534(5)	0.0410(6)	-0.0018(4)	0.0137(4)	-0.0037(4)
O(1)	0.032(4)	0.055(5)	0.041(5)	-0.006(4)	0.013(4)	0.001(4)
O(11)	0.118(9)	0.050(6)	0.09(1)	0.018(6)	0.044(8)	0.006(6)
O(12)	0.048(6)	0.111(9)	0.11(1)	-0.030(8)	0.022(7)	0.002(6)
O(13)	0.125(9)	0.048(6)	0.10(1)	0.009(6)	0.055(8)	-0.010(6)
O(14)	0.110(9)	0.087(8)	0.076(9)	-0.027(7)	0.056(8)	0.001(7)
O(21)	0.097(8)	0.054(6)	0.088(9)	0.029(6)	0.045(7)	0.006(6)
O(22)	0.036(6)	0.095(8)	0.103(9)	0.002(7)	0.024(6)	-0.000(5)
O(23)	0.090(7)	0.038(5)	0.083(8)	0.007(6)	0.043(6)	-0.002(5)
C(11)	0.08(1)	0.043(8)	0.06(1)	0.001(8)	0.039(9)	0.004(8)
C(12)	0.06(1)	0.08(1)	0.09(1)	0.00(1)	0.03(1)	0.009(8)
C(13)	0.036(7)	0.08(1)	0.07(1)	0.00(1)	0.019(8)	-0.008(8)
C(14)	0.053(8)	0.07(1)	0.07(1)	0.004(9)	0.030(8)	0.017(7)
C(21)	0.055(8)	0.050(8)	0.07(1)	0.023(8)	0.027(8)	-0.001(7)
C(22)	0.034(7)	0.063(9)	0.056(9)	-0.002(7)	0.020(7)	-0.003(6)
C(23)	0.036(7)	0.054(8)	0.06(1)	0.005(7)	0.019(7)	0.009(6)
C(1)	0.0862	0.0721	0.0597	-0.0165	0.0383	-0.0231
C(2)	0.0765	0.1035	0.0545	0.0210	0.0246	0.0141
C(3)	0.0365	0.0883	0.0700	0.0009	0.0124	-0.0011
C(4)	0.0662	0.0497	0.0887	-0.0129	0.0440	-0.0039

(g)   Details of X-ray Structural Study for $Os_4(CO)_{12}(GeMe_2)_4$, **9**

A red plate, grown from hexane, was used for intensity measurements. The two intensity standards showed random variations corresponding to a change in scale of ±2%. An empirical absorption correction was employed, together with a θ-dependent correction for a sphere of 150 μm diameter.

The Os and Ge atoms were given anisotropic thermal parameters in the final model, while a common isotropic temperature factor each was given to all the axial and equatorial O atoms; the carbonyl C atoms were treated likewise. All the methyl C atoms were also given a common isotropic temperature factor. The largest residual peak in the final difference map was 2.5(5) $eÅ^{-3}$, located 1.22 Å from Os(4), while the largest negative peak was also located near the same Os atom (0.97 Å).

A 'robust-resistant' weighting scheme was used in the final refinement :

$$w = w'[1 - (\Delta/6\Delta_{est})^2]^2 \quad ; \quad \Delta < 6\Delta_{est}$$

$$0 \quad\quad\quad\quad\quad ; \quad \Delta \geq 6\Delta_{est}$$

where Δ_{est} is the $|F_o|$-$|F_c|$ estimated from a least-squares procedure which minimises $\Sigma\Delta^4$ over all reflections to give the coefficients a_i of the truncated Chebyshev series

$$1/w' = a_0 t_0'(x) + a_1 t_1'(x) + ... + a_{n-1}t_{n-1}'(x); \text{ where } x = F_c/F_c^{max}.$$

In this structure, n = 3 was used.

Table VI(G) : Crystal data for $Os_4(CO)_{12}(GeMe_2)_4$, **9**.

Formula	$C_{20}H_{24}Ge_4O_{12}Os_4$
FW	1507.56
F(000)	2686.76
Crystal System	Monoclinic
Space Group	*P 2_1/c*
a, Å	10.9761(14)
b, Å	16.317(9)
c, Å	19.377(5)
β, deg	91.473(15)
V, Å^3	3469(1)
2θ range of unit cell	30.0-38.0
Z	4
D_{calc}, g cm^{-3}	2.886
μ(Mo, Kα), cm^{-1}	180.26
Crystal dimensions, mm	0.12 x 0.19 x 0.19
Transmission coefficient	0.0494-0.1630
Scan range (2θ), deg	3.6-45.0
Scan width (ω), deg	$0.90+0.35\tan\theta$
Scan rate (ω), deg min^{-1}	0.405-3.296
No. of unique reflections	4491
No. of observed reflections	3441
No. of parameters	163
R	0.064
wR	0.074
Largest (shift/e.s.d.) in final ls cycle	0.05
Minimum electron density in final difference map, e Å^{-3}	-4.0(5)
G.O.F.	1.1

Table VI.15(a) : Fractional Atomic Coordinates and Isotropic or Equivalent Isotropic
Temperature Factors (Å) for **9**.

Atom	x/a	y/b	z/c	U(iso)
Os(1)	1.00789(7)	-0.01800(5)	0.22674(4)	0.0482
Os(2)	0.76712(6)	0.07603(4)	0.23861(3)	0.0362
Os(3)	0.53655(6)	0.16707(5)	0.25818(4)	0.0403
Os(4)	0.66329(6)	0.10279(5)	0.37708(4)	0.0415
Ge(1)	0.8801(2)	0.0514(2)	0.1313(1)	0.0527
Ge(2)	0.6270(2)	0.1356(1)	0.1455(1)	0.0475
Ge(3)	0.4728(2)	0.1855(2)	0.3818(1)	0.0516
Ge(4)	0.8607(2)	0.0227(1)	0.3529(1)	0.0417
O(11)	1.136(2)	0.144(1)	0.2565(9)	0.082(2)
O(13)	0.855(2)	-0.172(1)	0.1955(9)	0.082(2)
O(21)	0.902(2)	0.240(1)	0.2483(9)	0.082(2)
O(23)	0.620(2)	-0.082(1)	0.2197(9)	0.082(2)
O(31)	0.667(2)	0.333(1)	0.2717(9)	0.082(2)
O(33)	0.372(2)	0.017(1)	0.2479(9)	0.082(2)
O(41)	0.815(2)	0.255(1)	0.4019(9)	0.082(2)
O(43)	0.521(2)	-0.059(1)	0.3700(9)	0.082(2)
O(12)	1.149(2)	-0.102(1)	0.344(1)	0.093(3)
O(14)	1.184(2)	-0.054(1)	0.109(1)	0.093(3)
O(32)	0.332(2)	0.257(1)	0.185(1)	0.093(3)
O(42)	0.705(2)	0.063(1)	0.527(1)	0.093(3)
C(11)	1.090(2)	0.083(1)	0.243(1)	0.058(2)
C(13)	0.912(2)	-0.113(1)	0.207(1)	0.058(2)
C(21)	0.853(2)	0.176(1)	0.246(1)	0.058(2)
C(23)	0.675(2)	-0.023(1)	0.227(1)	0.058(2)
C(31)	0.623(2)	0.270(1)	0.268(1)	0.058(2)
C(33)	0.441(2)	0.072(1)	0.253(1)	0.058(2)
C(41)	0.755(2)	0.199(1)	0.390(1)	0.058(2)
C(43)	0.571(2)	0.006(1)	0.370(1)	0.058(2)
C(12)	1.0944	-0.0667	0.3034	0.066(3)
C(14)	1.1154	-0.0457	0.1505	0.066(3)
C(32)	0.4102	0.2247	0.2153	0.066(3)
C(42)	0.6929	0.0848	0.4684	0.066(3)

Table VI.15(a) continued.

Atom	x/a	y/b	z/c	U(iso)
C(1)	0.961(2)	0.141(2)	0.083(1)	0.074(2)
C(2)	0.818(2)	-0.025(2)	0.060(1)	0.074(2)
C(3)	0.676(2)	0.229(2)	0.088(1)	0.074(2)
C(4)	0.530(2)	0.064(2)	0.084(1)	0.074(2)
C(5)	0.467(2)	0.293(2)	0.421(1)	0.074(2)
C(6)	0.322(2)	0.143(2)	0.417(1)	0.074(2)
C(7)	0.992(2)	0.074(2)	0.408(1)	0.074(2)
C(8)	0.843(2)	-0.090(2)	0.390(1)	0.074(2)

Table VI.15(b) : Anisotropic Temperature Factors (Å) for **9**.

Atom	U(11)	U(22)	U(33)	U(23)	U(13)	U(12)
Os(1)	0.0384(5)	0.0529(5)	0.0591(5)	-0.0026(4)	0.0087(4)	0.0074(4)
Os(2)	0.0313(4)	0.0416(5)	0.0376(4)	-0.0008(3)	0.0057(3)	-0.0006(3)
Os(3)	0.0317(4)	0.0436(5)	0.0473(5)	0.0009(3)	0.0020(3)	0.0005(3)
Os(4)	0.0369(4)	0.0493(5)	0.0406(4)	0.0019(3)	0.0067(3)	0.0029(3)
Ge(1)	0.057(1)	0.068(1)	0.045(1)	0.004(1)	0.018(1)	0.010(1)
Ge(2)	0.050(1)	0.054(1)	0.040(1)	0.0011(9)	-0.0022(9)	0.002(1)
Ge(3)	0.043(1)	0.064(1)	0.056(1)	-0.002(1)	0.013(1)	0.011(1)
Ge(4)	0.033(1)	0.050(1)	0.044(1)	0.0010(9)	-0.0014(8)	-0.0016(8)

5. References

[1] Busing, W. R.; Levy, H. A. *Acta Crystallogr.*, **1957**, *10*, 180.

[2] North, A. C. T.; Phillips, D. C.; Matthews, F. S. *Acta Crystallogr., Sect. A,* **1968**, *24*, 351.

[3] *International Tables for X-ray Crystallography*; Kynoch: Birmingham, England (present distributor: Kluwer Academic, Dordrecht, Netherlands), 1974; Vol. IV, p 99.

[4] Gabe, E. J.; Le Page, Y.; Charland, J-P.; Lee, F. L.; White, P. S. *J. Appl. Cryst.,* **1989**, *22*, 384.

[5] Watkin, D. J.; Carruthers, J. R.; Betteridge, P. W. *CRYSTALS*; Chemical Crystallography Laboratory, University of Oxford, Oxford, England, 1984.

[6] Larson, A. L. In *Crystallographic Computing*; Ahmed, F. R., Ed.; Munksgaard: Copenhagen, **1970**; Chapter G5.

[7] Johnson, C. K. *ORTEP: A Fortran Thermal Ellipsoid Plot Program for Crystal Structure Illustrations*, Oak Ridge National Laboratory Rept. ORNL-3794, **1965**.

[8] Data collected using the program DIFRAC.

Appendix   Other X-ray Structural Studies.

In the spirit of the reasons stated in the foreward, I have included in this appendix structural determinations which were carried out during the same period of time as the rest of the thesis. Some of these were clusters which resulted from experiments that did not yield the products sought; these are given in section 1. Others were the result of collaborative work with coworkers in our laboratory; these are given in sections 2 and 3. Only details of the structural studies are provided.

1.   **X-ray structural studies of three homometallic clusters : $Os_5(\mu\text{-}H)_2(CO)_{16}$ and $Os_n(\mu\text{-}H)_3(CO)_{2n+4}Cl$ (n = 4,5)**

(a) $\underline{Os_5(\mu\text{-}H)_2(CO)_{16}}$

A brown, irregular crystal, grown from hot toluene, was used for intensity measurements. The unique set of data (one quadrant) for a monoclinic P cell was collected, with indices ±h, +k, +l. The two intensity standards showed random variations corresponding to a change in scale of ±2%. An empirical absorption correction was employed, together with a θ-dependent correction for a sphere of 150 μm diameter.

The molecule sits on a crystallographic mirror plane. The H atom was placed in a position calculated from the HYDEX program[*], but was not refined; it was in a bridging position astride the Os(2)-Os(3) edge. The Os and O atoms were given anisotropic temperature factors in the final model. An extinction parameter was also refined. A 'robust-resistant' weighting scheme similar to that for **9** described above was used. The largest residual peak in the final difference map was 4.7(6) eÅ^{-3}, located 0.99 Å from Os(1).

---

[*] Orpen, A. G. *J. Chem. Soc., Dalton Trans.*, **1980**, 2509.

(b)   <u>Os$_4$(μ-H)$_3$(CO)$_{12}$Cl</u>

A yellow, hexagonal block, grown from hexane, was used for intensity measurements. The two intensity standards showed random variations corresponding to a change in scale of ±1%. An empirical absorption correction was employed, together with a θ-dependent correction for a sphere of 220 μm diameter.

The H atoms were placed in positions calculated from the HYDEX program*, but were not refined; they were in bridging positions across the Os(1)-Os(4), Os(2)-Os(3) and Os(2)-Os(4) edges. The Os, Cl and O atoms were given anisotropic temperature factors in the final model. An extinction parameter was also refined. The largest residual peak in the final difference map was 2.4(3) eÅ^{-3}, located 1.08 Å from Os(2).

(c)   <u>Os$_5$(μ-H)$_3$(CO)$_{14}$Cl</u>

A red plate, with a broken-off edge, and grown from hexane, was used for intensity measurements. The data was collected in two shells, viz., 1.8≤θ≤15.0 and 15.0≤θ≤22.5; the inner-shell data were measured at ψ positions corresponding to minimum absorption. The two intensity standards showed random variations corresponding to a change in scale of ±1%. A Gaussian absorption correction was applied.

The H atoms were placed in positions calculated from the HYDEX program*, but were not refined; they bridged the Os(2)-Os(3), Os(3)-Os(4) and Os(3)-Os(5) edges. The Os, Cl and O atoms were given anisotropic temperature factors in the final model. The largest residual peak in the final difference map was 2.7(5) eÅ^{-3}, located 1.06 Å from Os(2).
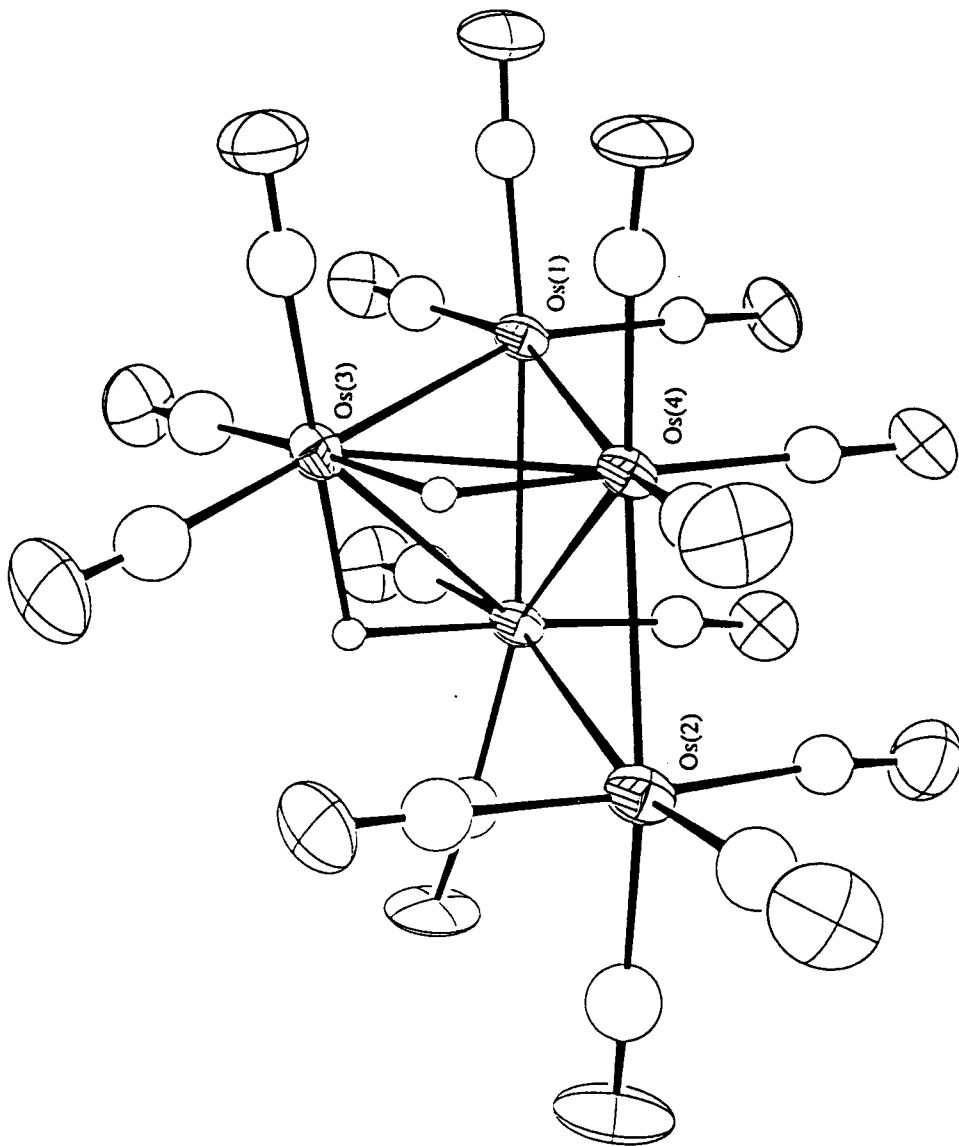
Fig. A.1.   ORTEP plot of $Os_5(\mu\text{-}H)_2(CO)_{16}$.

182
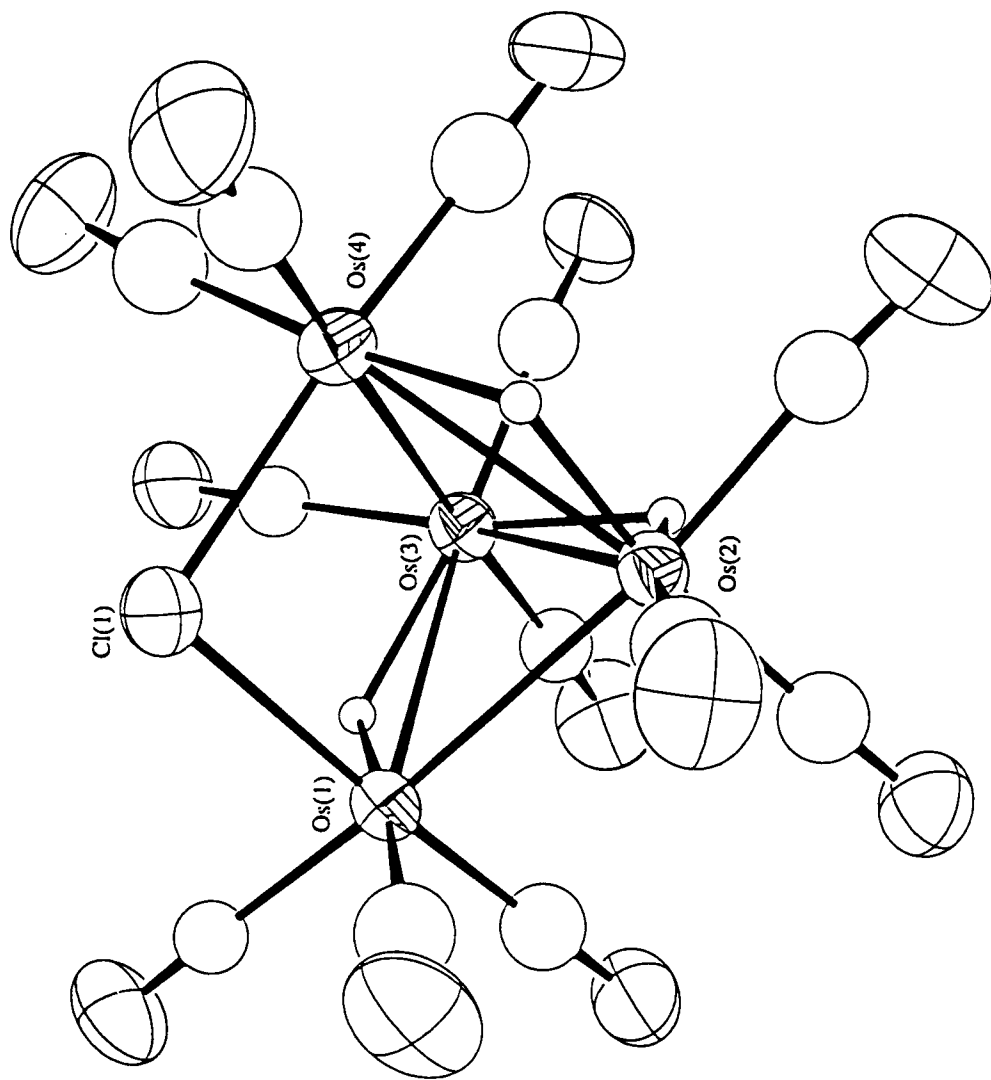
Fig. A.2.   ORTEP plot of $Os_4(\mu\text{-}H)_3(CO)_{12}Cl$.

183
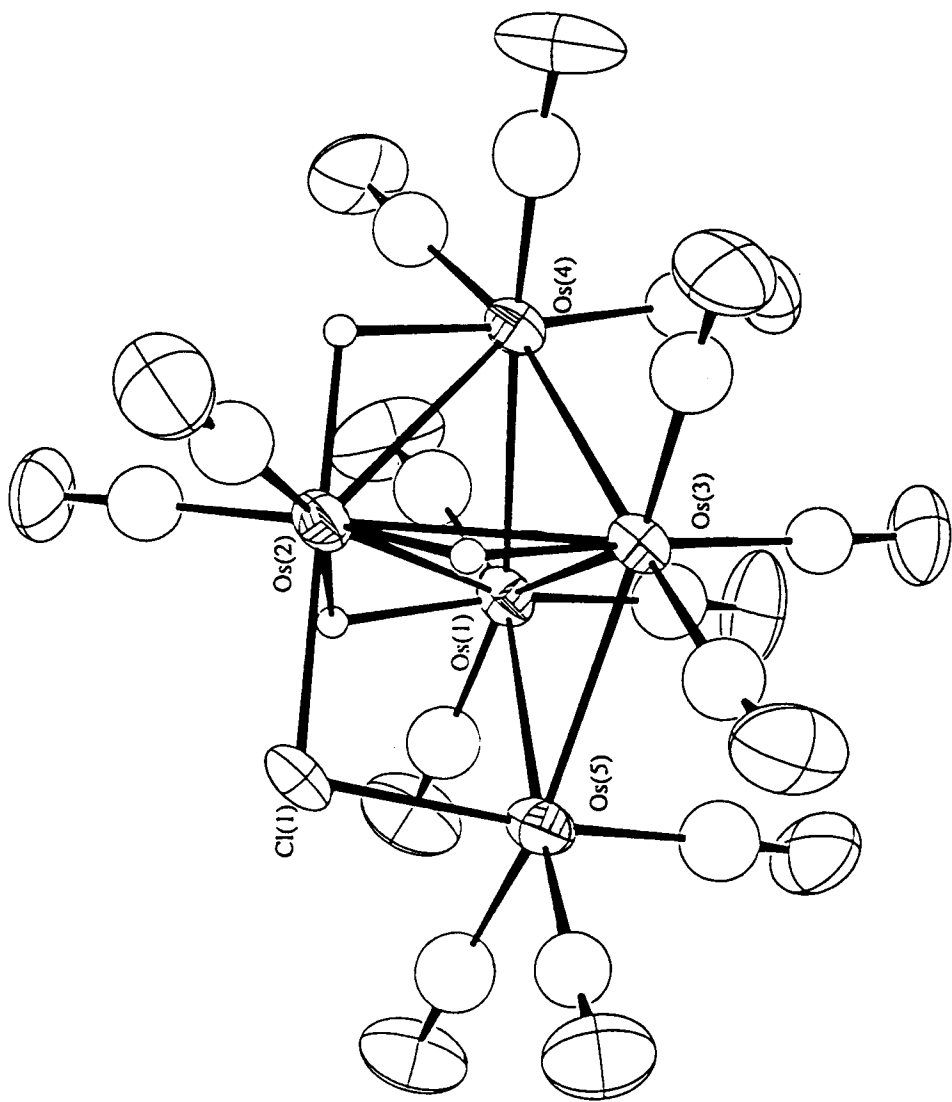
Fig. A.3.   ORTEP plot of $Os_5(\mu\text{-}H)_3(CO)_{14}Cl$.

Table A(I) : Crystal data for $Os_5(\mu\text{-H})_2(CO)_{16}$, $Os_4(\mu\text{-H})_3(CO)_{12}Cl$ and $Os_5(\mu\text{-H})_3(CO)_{14}Cl$.

	$Os_5(\mu\text{-H})_2(CO)_{16}$	$Os_4(\mu\text{-H})_3(CO)_{12}Cl$	$Os_5(\mu\text{-H})_3(CO)_{14}Cl$
Formula	$C_{16}H_2O_{16}Os_5$	$C_{12}H_3O_{12}Os_4$	$C_{14}H_3O_{14}Os_5$
FW	1401.18	1135.40	1381.62
F(000)	2422.94	1967.16	1191.47
Crystal System	Orthorhombic	Monoclinic	Triclinic
Space Group	$P\ mnb$	$P\ 2_1/n$	$P\ \bar{1}$
a, Å	10.5672(20)	9.5247(8)	8.8621(15)
b, Å	15.9577(12)	16.7749(18)	9.3825(15)
c, Å	14.5196(12)	12.9718(19)	15.9148(23)
α, deg	-	-	80.815(13)
β, deg	-	97.574(9)	85.332(13)
γ, deg	-	-	62.828(13)
V, Å³	2448.4(5)	2054.5(4)	1162.1(4)
2θ range of unit cell	30.0-44.0	31.0-40.0	30.0-36.3
Z	4	4	2
D_{calc}, g cm^{-3}	3.801	3.671	3.948
μ(Mo, Kα), cm^{-1}	259.59	248.76	274.50
Crystal dimensions, mm	0.14 x 0.18 x 0.27	0.24 x 0.33 x 0.42	0.08 x 0.16 x 0.19
Transmission coefficient	0.0472-0.0884	0.0139-0.0487	0.0273-0.1687
Scan range (2θ), deg	3.6-50.0	3.6-46.0	3.6-45.0

185

Table A(I) continued.

	$Os_5(\mu\text{-}H)_2(CO)_{16}$	$Os_4(\mu\text{-}H)_3(CO)_{12}Cl$	$Os_5(\mu\text{-}H)_3(CO)_{14}Cl$
Scan width (ω), deg	$0.70+0.35\tan\theta$	$0.80+0.35\tan\theta$	$0.70+0.35\tan\theta$
Scan rate (ω), deg min^{-1}	0.573-2.747	0.655-3.296	0.573-3.296
No. of unique reflections	2279	2842	3012
No. of observed reflections	1782	2453	2536
No. of parameters	143	203	237
R	0.051	0.038	0.055
wR	0.058	0.050	0.069
Instrument instability factor (k)	-	0.00005	0.0002
Extinction parameter (r*)	0.06(3)	0.052(10)	-
Largest (shift/e.s.d.) in final ls cycle	0.00	0.00	0.04
Minimum electron density in final difference map, e Å^{-3}	-4.4(6)	-2.4(3)	-3.5(5)
G.O.F.	1.2	3.2	3.2

Table A1(a) : Fractional Atomic Coordinates and Isotropic or Equivalent Isotropic Temperature Factors (Å) for $Os_5(\mu\text{-}H)_2(CO)_{16}$.

Atom	x/a	y/b	z/c	U(iso)
Os(1)	0.2500	0.60168(6)	-0.08461(7)	0.0316
Os(2)	0.11701(6)	0.75077(3)	-0.02260(4)	0.0232
Os(3)	0.2500	0.76754(6)	0.15535(6)	0.0271
Os(4)	0.2500	0.89823(5)	0.02873(6)	0.0251
O(11)	0.2500	0.676(1)	-0.279(1)	0.0505
O(12)	0.044(2)	0.477(1)	-0.141(1)	0.0616
O(13)	0.2500	0.531(1)	0.114(1)	0.0412
O(21)	0.081(1)	0.8188(8)	-0.2144(9)	0.0470
O(22)	-0.097(1)	0.8636(9)	0.045(1)	0.0438
O(23)	-0.094(1)	0.6221(9)	-0.034(1)	0.0453
O(31)	0.2500	0.625(1)	0.296(2)	0.0582
O(32)	0.458(1)	0.864(1)	0.254(1)	0.0516
O(41)	0.2500	0.984(1)	-0.158(1)	0.0415
O(42)	0.448(1)	1.0123(8)	0.112(1)	0.0470
C(11)	0.2500	0.654(1)	-0.211(2)	0.033(5)
C(12)	0.120(2)	0.522(1)	-0.121(1)	0.049(5)
C(13)	0.2500	0.555(1)	0.042(2)	0.031(5)
C(21)	0.098(2)	0.795(1)	-0.145(1)	0.027(3)
C(22)	-0.012(2)	0.826(1)	0.021(1)	0.038(4)
C(23)	-0.010(2)	0.668(1)	-0.033(1)	0.036(4)
C(31)	0.2500	0.673(2)	0.243(2)	0.045(6)
C(32)	0.380(2)	0.827(1)	0.218(1)	0.041(4)
C(41)	0.2500	0.954(1)	-0.087(1)	0.021(4)
C(42)	0.375(2)	0.968(1)	0.082(1)	0.036(4)

Table A2(a) : Fractional Atomic Coordinates and Isotropic or Equivalent Isotropic Temperature Factors (Å) for $Os_4(\mu\text{-}H)_3(CO)_{12}Cl$.

Atom	x/a	y/b	z/c	U(iso)
Os(1)	0.71691(7)	0.84954(4)	0.06846(5)	0.0361
Os(2)	1.00660(7)	0.80307(4)	0.10918(5)	0.0349
Os(3)	0.86445(8)	0.65701(4)	0.00956(5)	0.0398
Os(4)	0.80075(7)	0.70887(4)	0.20724(5)	0.0357
Cl(1)	0.6771(5)	0.7483(3)	-0.0706(4)	0.0496
O(11)	0.404(1)	0.8842(9)	0.039(1)	0.0655
O(12)	0.769(2)	0.9621(9)	0.253(1)	0.0670
O(13)	0.789(2)	0.9702(9)	-0.096(1)	0.0736
O(21)	1.090(2)	0.9357(8)	0.262(1)	0.0663
O(22)	1.087(2)	0.900(1)	-0.069(1)	0.0778
O(23)	1.299(2)	0.729(1)	0.167(1)	0.0844
O(31)	0.657(2)	0.5150(9)	0.009(1)	0.0767
O(32)	1.106(2)	0.5587(8)	0.110(1)	0.0732
O(33)	0.946(2)	0.621(1)	-0.204(1)	0.0786
O(41)	0.975(2)	0.5741(8)	0.315(1)	0.0584
O(42)	0.536(1)	0.6077(8)	0.186(1)	0.0627
O(43)	0.761(2)	0.791(1)	0.412(1)	0.0757
C(11)	0.516(2)	0.870(1)	0.050(1)	0.038(4)
C(12)	0.747(2)	0.919(1)	0.184(2)	0.055(5)
C(13)	0.765(2)	0.928(1)	-0.037(2)	0.058(5)
C(21)	1.058(2)	0.885(1)	0.206(2)	0.054(5)
C(22)	1.056(2)	0.864(1)	-0.003(2)	0.050(5)
C(23)	1.191(2)	0.754(1)	0.144(1)	0.051(5)
C(31)	0.731(2)	0.570(1)	0.010(2)	0.059(5)
C(32)	1.012(2)	0.595(1)	0.076(2)	0.061(5)
C(33)	0.914(2)	0.634(1)	-0.123(2)	0.055(5)
C(41)	0.907(2)	0.621(1)	0.275(2)	0.054(5)
C(42)	0.631(2)	0.645(1)	0.192(1)	0.041(4)
C(43)	0.777(2)	0.759(1)	0.336(1)	0.047(5)

Table A3(a) : Fractional Atomic Coordinates and Isotropic or Equivalent Isotropic
Temperature Factors (Å) for $Os_5(\mu\text{-H})_3(CO)_{14}Cl$.

Atom	x/a	y/b	z/c	U(iso)
Os(1)	0.8084(1)	0.2786(1)	0.14057(7)	0.0393
Os(2)	0.9293(1)	0.3500(1)	0.28145(6)	0.0353
Os(3)	0.7667(1)	0.6619(1)	0.17241(6)	0.0342
Os(4)	0.5763(1)	0.4888(1)	0.25493(6)	0.0323
Os(5)	0.7083(1)	0.6299(1)	0.35458(6)	0.0358
Cl(1)	0.8173(8)	0.5178(8)	0.0526(4)	0.0395
O(11)	0.601(3)	0.274(3)	-0.001(1)	0.0706
O(12)	0.785(3)	0.009(3)	0.259(1)	0.0752
O(13)	1.131(3)	0.059(3)	0.051(2)	0.0632
O(21)	1.166(3)	0.414(3)	0.385(2)	0.0722
O(22)	0.933(3)	0.083(3)	0.418(2)	0.0729
O(23)	1.257(2)	0.106(3)	0.211(2)	0.0704
O(31)	0.520(3)	0.992(2)	0.085(1)	0.0723
O(32)	1.044(2)	0.765(2)	0.132(1)	0.0581
O(41)	0.349(3)	0.432(3)	0.144(1)	0.0701
O(42)	0.539(2)	0.251(2)	0.397(1)	0.0583
O(43)	0.247(2)	0.769(2)	0.301(1)	0.0629
O(51)	0.933(3)	0.738(3)	0.439(2)	0.0692
O(52)	0.690(3)	0.416(2)	0.516(1)	0.0584
O(53)	0.391(3)	0.930(2)	0.398(1)	0.0627
C(11)	0.675(3)	0.279(3)	0.048(2)	0.047(7)
C(12)	0.792(4)	0.108(4)	0.218(2)	0.064(8)
C(13)	1.019(4)	0.139(4)	0.085(2)	0.064(8)
C(21)	1.072(4)	0.394(4)	0.350(2)	0.068(8)
C(22)	0.923(4)	0.185(4)	0.369(2)	0.064(8)
C(23)	1.131(4)	0.197(4)	0.232(2)	0.060(8)
C(31)	0.615(4)	0.862(3)	0.119(2)	0.055(7)
C(32)	0.942(4)	0.725(3)	0.149(2)	0.054(7)
C(41)	0.441(4)	0.448(3)	0.180(2)	0.054(7)
C(42)	0.558(3)	0.334(3)	0.345(2)	0.041(6)
C(43)	0.373(4)	0.665(3)	0.288(2)	0.054(7)
C(51)	0.850(4)	0.701(3)	0.405(2)	0.059(8)
C(52)	0.696(3)	0.495(3)	0.457(2)	0.046(7)
C(53)	0.508(4)	0.824(4)	0.377(2)	0.067(8)

Table A1(b) : Anisotropic Temperature Factors (Å) for $Os_5(\mu\text{-H})_2(CO)_{16}$.

Atom	U(11)	U(22)	U(33)	U(23)	U(13)	U(12)
Os(1)	0.0262(5)	0.0271(5)	0.0443(6)	0.0013(4)	0.0000	0.0000
Os(2)	0.0150(3)	0.0241(4)	0.0349(4)	0.0022(2)	-0.0016(2)	-0.0009(2)
Os(3)	0.0217(5)	0.0311(5)	0.0302(5)	0.0053(4)	0.0000	0.0000
Os(4)	0.0200(5)	0.0219(5)	0.0362(5)	0.0016(4)	0.0000	0.0000
O(11)	0.10(2)	0.06(1)	0.023(9)	0.001(9)	0.0000	0.0000
O(12)	0.052(9)	0.062(9)	0.11(1)	-0.009(9)	-0.022(9)	-0.024(8)
O(13)	0.07(1)	0.04(1)	0.05(1)	0.029(9)	0.0000	0.0000
O(21)	0.057(9)	0.044(7)	0.047(7)	0.013(6)	-0.007(7)	0.001(6)
O(22)	0.025(7)	0.064(9)	0.074(9)	-0.022(8)	0.006(7)	0.015(6)
O(23)	0.036(8)	0.058(8)	0.09(1)	-0.023(8)	0.003(7)	-0.029(7)
O(31)	0.13(2)	0.04(1)	0.05(1)	0.03(1)	0.0000	0.0000
O(32)	0.050(8)	0.064(9)	0.064(8)	-0.008(7)	-0.025(8)	-0.015(7)
O(41)	0.06(1)	0.05(1)	0.04(1)	0.023(8)	0.0000	0.0000
O(42)	0.035(7)	0.043(7)	0.08(1)	-0.010(7)	-0.004(7)	-0.008(6)

Table A2(b) : Anisotropic Temperature Factors (Å) for $Os_4(\mu\text{-H})_3(CO)_{12}Cl$.

Atom	U(11)	U(22)	U(33)	U(23)	U(13)	U(12)
Os(1)	0.0309(4)	0.0375(4)	0.0404(4)	0.0003(3)	0.0025(3)	0.0029(3)
Os(2)	0.0279(4)	0.0399(4)	0.0381(4)	-0.0011(3)	0.0042(3)	-0.0007(3)
Os(3)	0.0400(4)	0.0395(4)	0.0406(4)	-0.0058(3)	0.0046(3)	0.0011(3)
Os(4)	0.0329(4)	0.0381(4)	0.0364(4)	0.0022(3)	0.0049(3)	0.0005(3)
Cl(1)	0.054(3)	0.053(3)	0.044(3)	-0.007(2)	-0.010(2)	0.006(2)
O(11)	0.044(9)	0.10(1)	0.070(9)	-0.004(9)	0.008(7)	0.019(8)
O(12)	0.06(1)	0.09(1)	0.07(1)	-0.039(9)	-0.006(8)	0.017(8)
O(13)	0.08(1)	0.09(1)	0.09(1)	0.05(1)	0.01(1)	0.001(9)
O(21)	0.07(1)	0.07(1)	0.060(9)	-0.014(8)	0.002(8)	-0.004(8)
O(22)	0.08(1)	0.09(1)	0.07(1)	0.006(9)	0.017(9)	-0.016(9)
O(23)	0.06(1)	0.10(1)	0.11(1)	0.00(1)	0.02(1)	0.02(1)
O(31)	0.10(1)	0.062(9)	0.10(1)	-0.013(9)	0.02(1)	-0.041(9)
O(32)	0.08(1)	0.07(1)	0.10(1)	-0.018(9)	0.00(1)	0.034(9)
O(33)	0.09(1)	0.11(1)	0.052(9)	-0.021(9)	0.009(9)	-0.00(1)
O(41)	0.07(1)	0.055(9)	0.08(1)	0.029(8)	-0.024(9)	0.016(8)
O(42)	0.039(8)	0.063(9)	0.10(1)	-0.005(8)	0.003(8)	-0.008(7)
O(43)	0.10(1)	0.13(1)	0.047(8)	-0.023(9)	0.026(9)	0.00(1)

Table A3(b) : Anisotropic Temperature Factors (Å) for $Os_5(\mu\text{-}H)_3(CO)_{14}Cl$.

Atom	U(11)	U(22)	U(33)	U(23)	U(13)	U(12)
Os(1)	0.0433(6)	0.0412(6)	0.0338(6)	-0.0120(5)	0.0070(5)	-0.0148(5)
Os(2)	0.0313(6)	0.0384(6)	0.0314(6)	-0.0027(4)	0.0018(4)	-0.0105(4)
Os(3)	0.0386(6)	0.0372(6)	0.0268(6)	-0.0026(4)	0.0049(4)	-0.0159(5)
Os(4)	0.0313(5)	0.0379(6)	0.0269(6)	-0.0058(4)	0.0044(4)	-0.0130(4)
Os(5)	0.0418(6)	0.0436(6)	0.0257(6)	-0.0082(5)	0.0041(4)	-0.0186(5)
Cl(1)	0.055(4)	0.057(4)	0.023(3)	-0.009(3)	0.014(3)	-0.027(3)
O(11)	0.08(1)	0.08(1)	0.07(2)	-0.02(1)	-0.02(1)	-0.03(1)
O(12)	0.15(2)	0.06(1)	0.07(2)	-0.00(1)	-0.00(2)	-0.06(1)
O(13)	0.05(1)	0.08(1)	0.09(2)	-0.05(1)	0.03(1)	0.00(1)
O(21)	0.04(1)	0.11(2)	0.17(3)	-0.06(2)	-0.03(2)	-0.03(1)
O(22)	0.11(2)	0.09(2)	0.09(2)	0.05(1)	-0.03(2)	-0.06(2)
O(23)	0.04(1)	0.09(2)	0.09(2)	-0.03(1)	0.01(1)	0.01(1)
O(31)	0.07(1)	0.05(1)	0.08(2)	0.01(1)	0.01(1)	-0.01(1)
O(32)	0.05(1)	0.08(1)	0.09(2)	-0.01(1)	0.01(1)	-0.05(1)
O(41)	0.05(1)	0.11(2)	0.08(2)	-0.04(1)	-0.01(1)	-0.03(1)
O(42)	0.06(1)	0.05(1)	0.08(2)	0.02(1)	0.01(1)	-0.03(1)
O(43)	0.04(1)	0.06(1)	0.09(2)	-0.03(1)	0.01(1)	-0.01(1)
O(51)	0.09(2)	0.11(2)	0.09(2)	-0.05(2)	-0.02(1)	-0.06(2)
O(52)	0.08(1)	0.09(1)	0.04(1)	-0.01(1)	0.01(1)	-0.05(1)
O(53)	0.08(1)	0.07(1)	0.06(1)	-0.04(1)	-0.01(1)	0.01(1)

2. X-ray structural studies of three mononuclear osmium carbonyls :

Cp*Os(CO)$_2$Cl, *fac* and *mer,cis*-Os(CO)$_3$(PMe$_3$)Cl$_2$

(a)   <u>Cp*Os(CO)$_2$Cl</u>

A colourless plate, obtained by slow cooling of a hexane solution, was used in the data collection. The data was collected in two shells, viz., $2.0 \le \theta \le 15.0$ and $15.0 \le \theta \le 22.5$; the outer shell was measured at ψ positions corresponding to minimum absorption. The two intensity standards showed random variations of ± 2 % over the period of data collection. A Gaussian absorption correction was applied.

The short C-O bond lengths and excessive thermal motion along bonds observed suggested that there was disorder of CO with Cl at all three CO/Cl sites. This disorder was modelled with isotropic C atoms and anisotropic O and Cl atoms; the C atoms were given a common isotropic temperature factor, while the same anisotropic temperature factor was given to the O and Cl atoms at each site. The occupancies of the Cl atoms were summed to unity. The final least-squares refinement also included anisotropic thermal parameters for Os, and the Cp* carbon atoms. An extinction parameter was also refined. The final difference map showed a largest residual peak of 0.6(1) eÅ^{-3}, at 0.93 Å from the Os atom.

(b)   <u>cis,mer-Os(CO)$_3$(PMe$_3$)Cl$_2$</u>

A colourless block, cut from a large needle provided by Mr. J. L. Male, was used for intensity measurements. The two intensity standards showed random variations corresponding to scale changes of $\pm 2\%$. A Gaussian correction was applied.

The H atoms were located directly from a difference map. The final model had all the non-H atoms anisotropic. The H atoms were given a common isotropic temperature factor, and their coordinates refined, with the C-H distances restrained to their mean. An extinction parameter was also refined. The largest residual peak in the final difference map was 0.44(9) eÅ^{-3}, located 1.10 Å from the Os atom.

(c) *fac*-Os(CO)₃(PMe₃)Cl₂

A colourless block, cut from a large needle provided by Mr. J. L. Male, was used for intensity measurements. The two intensity standards showed steady decay corresponding to scale changes of about 14%. An empirical absorption correction was employed, together with a θ-dependent correction for a sphere of 150 μm diameter.

There were two crystallographically distinct molecules in the asymmetric unit. The final model had all the non-H atoms anisotropic. An extinction parameter was also refined. The largest residual peak in the final difference map was 1.07(15) eÅ^{-3}, located 0.90 Å from Os(2).
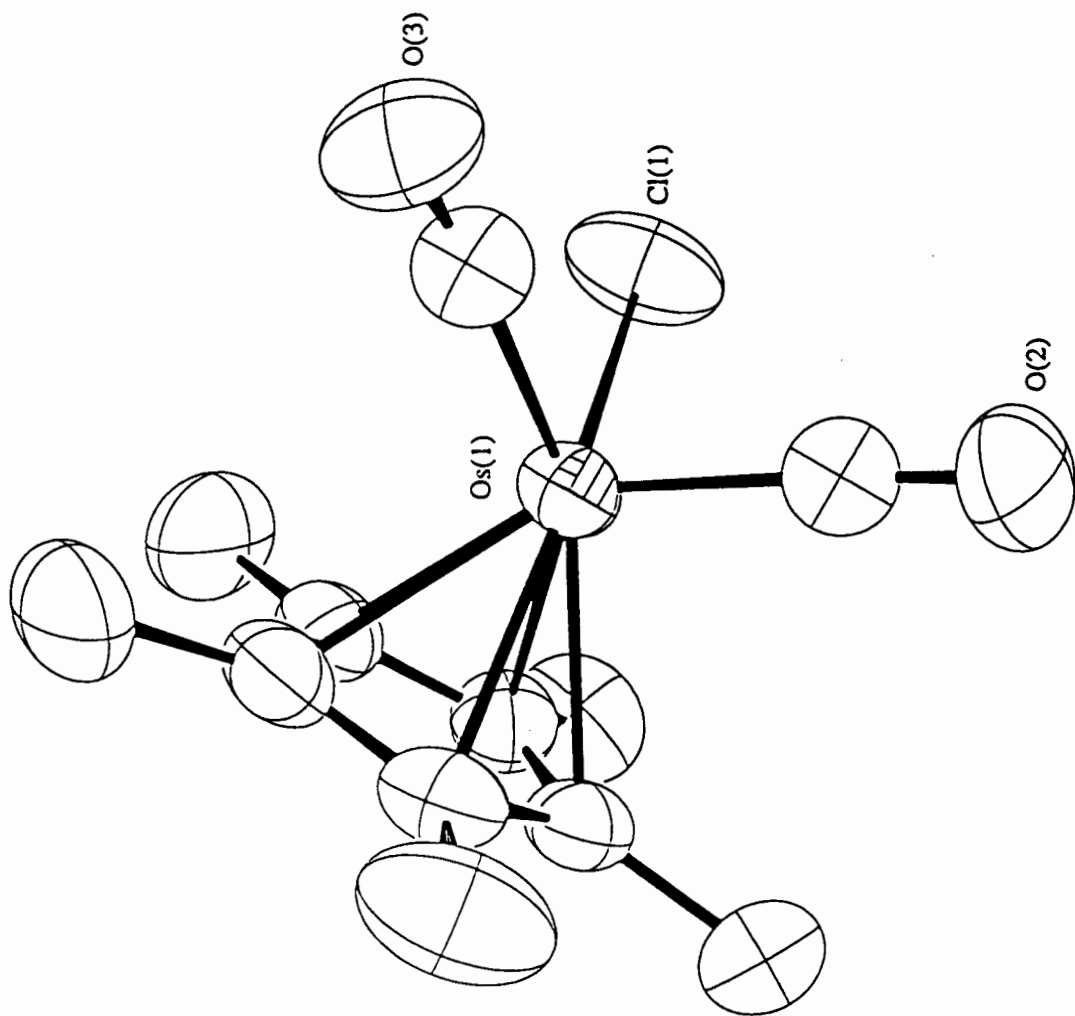
Fig. A.4.   ORTEP plot of Cp*Os(CO)₂Cl (disorder not shown).

194
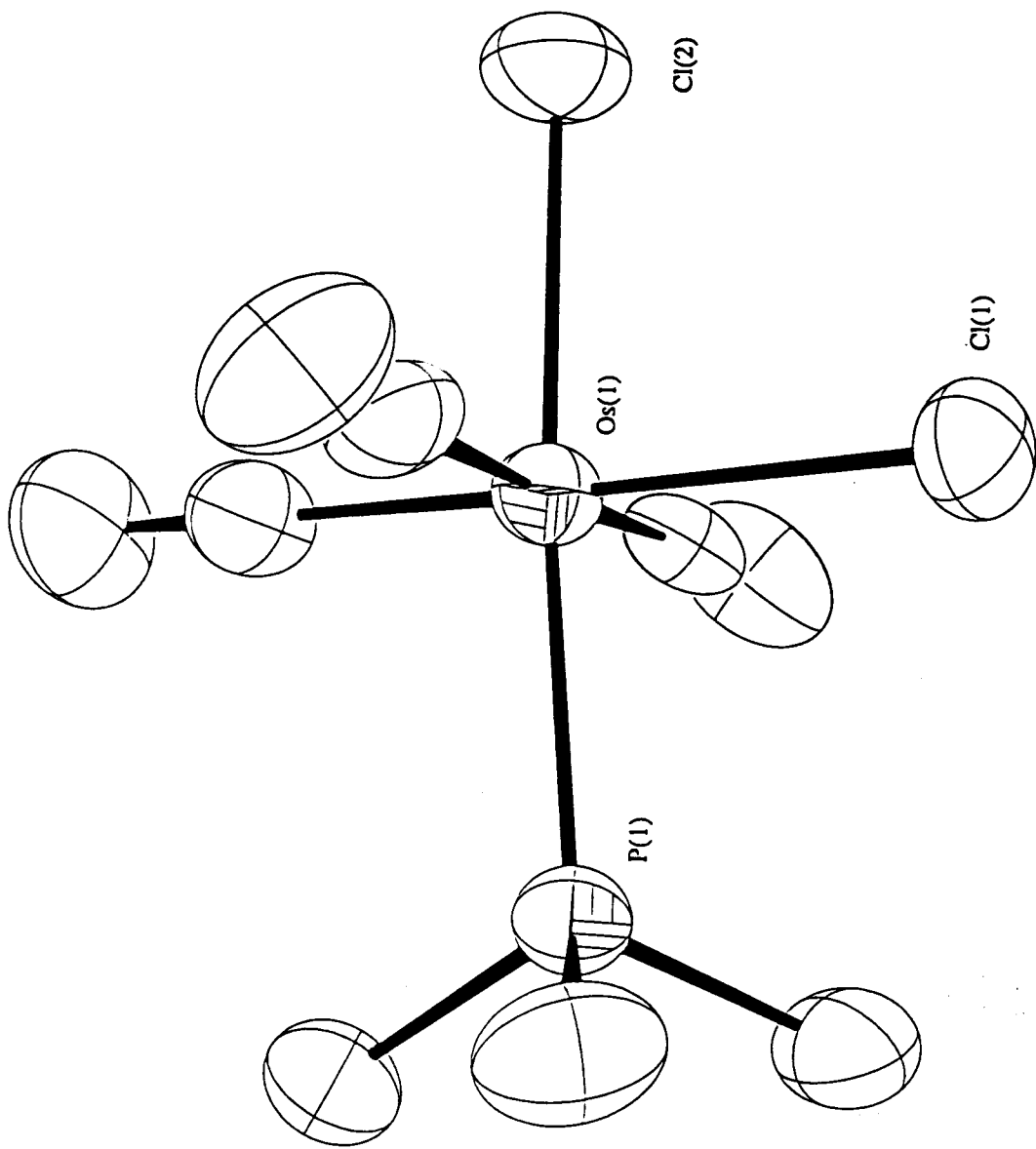
Fig. A.5. ORTEP plot of *cis,mer*-Os(CO)$_3$(PMe$_3$)Cl$_2$.

Cl(2)

Cl(1)

Os(1)

P(1)

195

Os(1)

Cl(12)

Cl(11)

P(1)
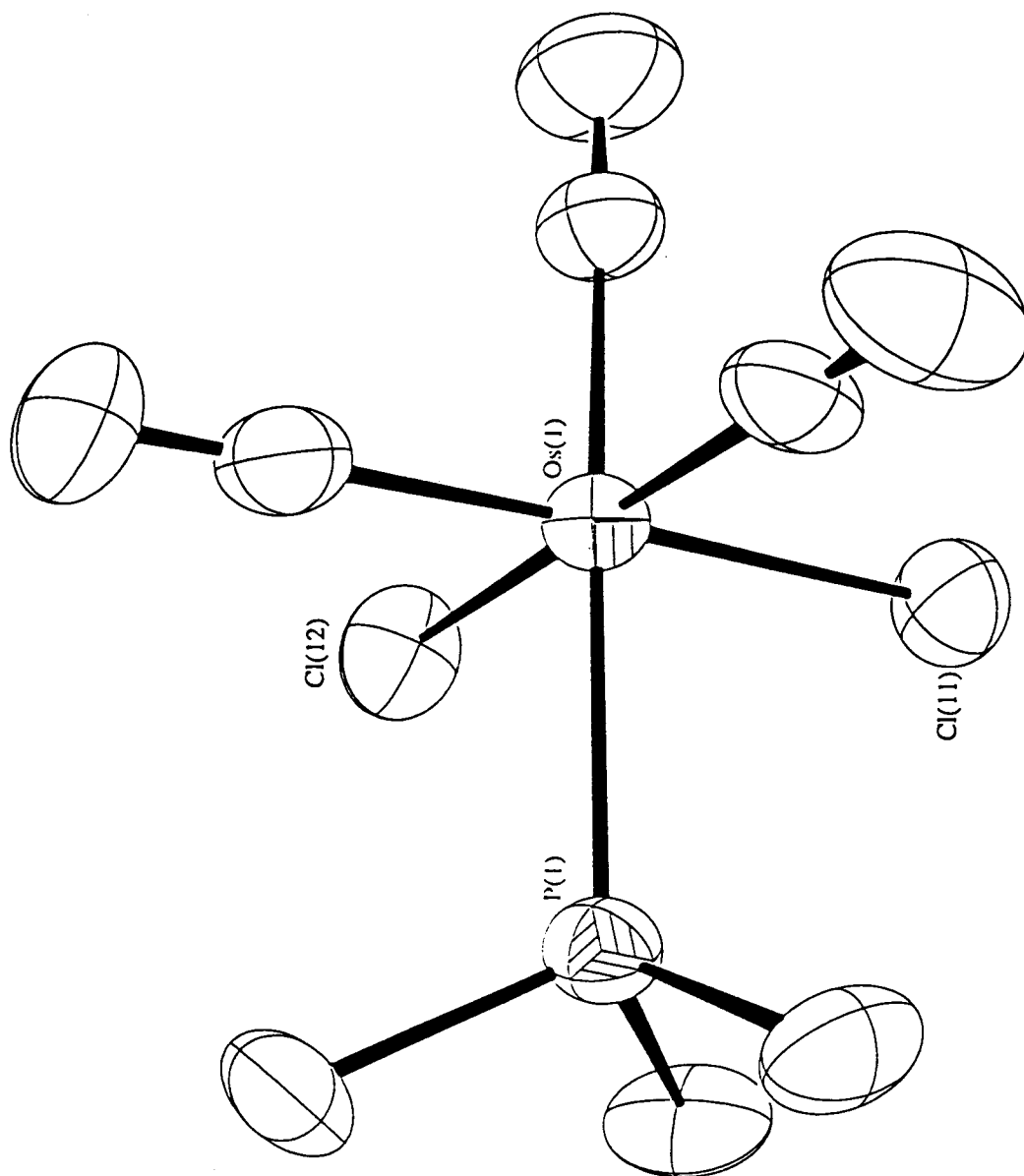
Fig. A.6.   ORTEP plot of molecule (1) of *fac*-Os(CO)$_3$(PMe$_3$)Cl$_2$.

196

Table A(II) :   Crystal data for Cp*Os(CO)$_2$Cl, cis,mer- and fac-Os(CO)$_3$(PMe$_3$)Cl$_2$

	Cp*Os(CO)$_2$Cl	cis,mer	fac
Formula	C$_{12}$H$_{15}$ClO$_2$Os	C$_6$H$_9$Cl$_2$O$_3$OsP	C$_6$H$_9$Cl$_2$O$_3$OsP
FW	416.9	421.22	421.22
F(000)	391.88	755.78	1553.56
Crystal System	Triclinic	Monoclinic	Monoclinic
Space Group	$P\bar{1}$	$P\,2_1/n$	$P\,2_1/n$
a, Å	6.8552(6)	6.4377(7)	6.4691(4)
b, Å	7.8627(6)	15.3782(13)	13.2890(11)
c, Å	13.0097(10)	12.3148(10)	27.2890(21)
α, deg	85.082(7)	-	-
β, deg	87.468(7)	100.744(8)	95.261(6)
γ, deg	73.529(7)	-	-
V, Å^3	669.82(10)	1197.8(2)	2389.7(3)
2θ range of unit cell	30.0-42.0	35.0-45.0	32.2-42.1
Z	2	4	8
D$_{calc}$, g cm^{-3}	2.067	2.336	2.342
μ(Mo, Kα), cm^{-1}	97.13	112.15	112.43
Crystal dimensions, mm	0.07 x 0.11 x 0.19	0.16 x 0.21 x 0.27	0.11 x 0.18 x 0.32
Transmission coefficient	0.3615-0.6030	0.1758-0.2708	0.0857-0.3760
Scan range (2θ), deg	4.0-45.0	3.6-47.0	3.6-50.0
Scan width (ω), deg	0.50+0.35tanθ	0.70+0.35tanθ	0.70+0.35tanθ

Table A(II) continued.

	Cp*Os(CO)$_2$Cl	cis,mer	fac
Scan rate (ω), deg min^{-1}	0.515-3.296	0.573-3.296	0.573-3.296
No. of unique reflections	1750	1759	4176
No. of observed reflections	1602	1583	3559
No. of parameters	151	147	206
R	0.022	0.016	0.024
wR	0.023	0.021	0.034
Instrument instability factor (k)	0.0001	0.00005	0.0002
Extinction parameter (r*)	0.46(3)	0.411(14)	0.56(3)
Largest (shift/e.s.d.) in final ls cycle	0.10	0.05	0.34
Minimum electron density in final difference map, e Å^{-3}	-0.6(1)	-0.51(9)	-0.81(15)
G.O.F.	1.4	1.6	1.6

Table A4(a) : Fractional Atomic Coordinates and Isotropic or Equivalent Isotropic

Temperature Factors for Cp*Os(CO)$_2$Cl

Atom	x/a	y/b	z/c	U(iso)	Occ
Os(1)	0.51456(3)	0.31735(2)	0.25335(1)	0.0456	1.0000
Cl(1)	0.2125(5)	0.5580(5)	0.2173(4)	0.0806	0.596(8)
Cl(2)	0.386(2)	0.192(2)	0.4057(7)	0.0859	0.305(7)
Cl(3)	0.433(5)	0.126(4)	0.148(2)	0.0759	0.099(8)
O(1)	0.135(2)	0.607(2)	0.203(2)	0.0806	0.404(8)
O(2)	0.331(2)	0.163(2)	0.4417(8)	0.0859	0.695(7)
O(3)	0.4039(9)	0.0736(8)	0.1171(5)	0.0759	0.901(8)
C(1)	0.264(3)	0.499(3)	0.236(2)	0.060(2)	0.404(8)
C(2)	0.394(2)	0.226(2)	0.3693(9)	0.060(2)	0.695(7)
C(3)	0.433(1)	0.164(1)	0.1665(7)	0.060(2)	0.901(8)
C(4)	0.7000(8)	0.5065(7)	0.2774(4)	0.0550	1.0000
C(5)	0.7756(7)	0.3546(7)	0.3429(4)	0.0512	1.0000
C(6)	0.8479(7)	0.2047(7)	0.2804(4)	0.0539	1.0000
C(7)	0.8200(8)	0.2762(8)	0.1753(5)	0.0584	1.0000
C(8)	0.7255(8)	0.4620(8)	0.1740(4)	0.0571	1.0000
C(41)	0.618(1)	0.6939(8)	0.3082(6)	0.0798	1.0000
C(51)	0.792(1)	0.343(1)	0.4586(4)	0.0767	1.0000
C(61)	0.956(1)	0.0180(9)	0.3184(7)	0.0838	1.0000
C(71)	0.889(1)	0.168(1)	0.0824(6)	0.0860	1.0000
C(81)	0.682(1)	0.593(1)	0.0811(5)	0.0892	1.0000

Table A5(a) : Fractional Atomic Coordinates and Isotropic or Equivalent Isotropic Temperature Factors (Å) for *cis,mer*-Os(CO)$_3$(PMe$_3$)Cl$_2$

Atom	x/a	y/b	z/c	U(iso)
Os(1)	0.14387(3)	0.17259(1)	0.18583(1)	0.0368
P(1)	0.2799(2)	0.04252(7)	0.26884(9)	0.0384
Cl(1)	-0.1847(2)	0.09506(8)	0.1222(1)	0.0504
Cl(2)	-0.0272(2)	0.30110(9)	0.0895(1)	0.0603
O(11)	0.2705(7)	0.1203(3)	-0.0350(3)	0.0652
O(12)	-0.0172(6)	0.2212(3)	0.3980(3)	0.0708
O(13)	0.5460(6)	0.2730(3)	0.2601(4)	0.0762
C(1)	0.5353(8)	0.0521(4)	0.3556(4)	0.0535
C(2)	0.117(1)	-0.0080(4)	0.3565(5)	0.0622
C(3)	0.313(1)	-0.0413(3)	0.1731(5)	0.0587
C(11)	0.2293(8)	0.1392(3)	0.0454(4)	0.0450
C(12)	0.0420(7)	0.2054(3)	0.3203(4)	0.0455
C(13)	0.3937(8)	0.2337(3)	0.2308(4)	0.0506
H(11)	0.572(9)	0.001(2)	0.398(4)	0.089(6)
H(12)	0.544(9)	0.091(3)	0.417(3)	0.089(6)
H(13)	0.636(7)	0.085(3)	0.325(5)	0.089(6)
H(21)	0.12(1)	0.031(3)	0.417(3)	0.089(6)
H(22)	-0.015(5)	-0.022(4)	0.309(4)	0.089(6)
H(23)	0.176(8)	-0.060(2)	0.394(4)	0.089(6)
H(31)	0.176(5)	-0.062(4)	0.138(5)	0.089(6)
H(32)	0.407(8)	-0.020(4)	0.127(4)	0.089(6)
H(33)	0.332(9)	-0.095(2)	0.215(4)	0.089(6)

Table A6(a) : Fractional Atomic Coordinates and Isotropic or Equivalent Isotropic
Temperature Factors (Å) for *fac*-Os(CO)$_3$(PMe$_3$)Cl$_2$

Atom	x/a	y/b	z/c	U(iso)
Os(1)	0.04489(3)	0.78481(2)	0.064959(8)	0.0354
Os(2)	0.52014(4)	0.19879(2)	0.153012(8)	0.0385
Cl(11)	-0.1520(3)	0.7108(1)	-0.00420(6)	0.0546
Cl(12)	-0.2354(2)	0.7478(1)	0.11426(6)	0.0573
Cl(21)	0.2137(3)	0.3034(1)	0.15110(7)	0.0609
Cl(22)	0.3895(3)	0.0974(1)	0.21593(6)	0.0617
P(1)	0.1708(2)	0.6181(1)	0.08345(5)	0.0377
P(2)	0.6700(3)	0.3021(1)	0.21777(6)	0.0463
O(11)	0.3030(8)	0.8700(4)	0.1515(2)	0.0613
O(12)	0.3871(8)	0.8297(4)	0.0014(2)	0.0678
O(13)	-0.190(1)	0.9827(4)	0.0409(2)	0.0809
O(21)	0.6703(9)	0.3373(4)	0.0780(2)	0.0686
O(22)	0.279(1)	0.0644(4)	0.0770(2)	0.0735
O(23)	0.8932(9)	0.0622(5)	0.1558(2)	0.0859
C(11)	0.205(1)	0.8388(5)	0.1190(2)	0.0469
C(12)	0.262(1)	0.8130(5)	0.0249(2)	0.0445
C(13)	-0.099(1)	0.9117(5)	0.0491(2)	0.0520
C(21)	0.615(1)	0.2849(5)	0.1058(2)	0.0487
C(22)	0.370(1)	0.1138(5)	0.1042(2)	0.0517
C(23)	0.754(1)	0.1140(5)	0.1553(3)	0.0571
C(1)	0.3645(9)	0.5761(5)	0.0458(2)	0.0499
C(2)	-0.0303(9)	0.5237(5)	0.0764(3)	0.0461
C(3)	0.286(1)	0.6014(5)	0.1448(2)	0.0523
C(4)	0.775(1)	0.4196(5)	0.1996(3)	0.0558
C(5)	0.878(1)	0.2409(7)	0.2543(2)	0.0616
C(6)	0.489(1)	0.3390(7)	0.2594(3)	0.0659

Table A4(b) : Anisotropic Temperature Factors (Å) for Cp*Os(CO)$_2$Cl

Atom	U(11)	U(22)	U(33)	U(23)	U(13)	U(12)
Os(1)	0.0392(2)	0.0462(2)	0.0543(2)	-0.00873(9)	0.00012(9)	-0.0128(1)
Cl(1)	0.048(2)	0.072(3)	0.147(3)	-0.006(2)	-0.019(2)	0.001(1)
Cl(2)	0.108(6)	0.151(6)	0.069(5)	-0.000(4)	0.011(4)	-0.088(4)
Cl(3)	0.096(4)	0.074(4)	0.085(4)	-0.025(2)	-0.016(3)	-0.033(3)
O(1)	0.048(2)	0.072(3)	0.147(3)	-0.006(2)	-0.019(2)	0.001(1)
O(2)	0.108(6)	0.151(6)	0.069(5)	-0.000(4)	0.011(4)	-0.088(4)
O(3)	0.096(4)	0.074(4)	0.085(4)	-0.025(2)	-0.016(3)	-0.033(3)
C(4)	0.058(3)	0.060(3)	0.061(3)	-0.012(3)	0.000(3)	-0.029(3)
C(5)	0.041(3)	0.062(3)	0.060(2)	-0.009(3)	-0.005(2)	-0.019(2)
C(6)	0.041(3)	0.054(3)	0.076(4)	-0.011(3)	-0.007(3)	-0.014(2)
C(7)	0.041(3)	0.084(4)	0.072(4)	-0.029(3)	0.009(3)	-0.023(3)
C(8)	0.049(3)	0.072(4)	0.064(3)	0.000(2)	0.002(3)	-0.031(3)
C(41)	0.093(5)	0.056(3)	0.116(6)	-0.018(4)	0.004(4)	-0.032(3)
C(51)	0.075(4)	0.104(5)	0.060(2)	-0.003(3)	-0.013(3)	-0.025(4)
C(61)	0.061(4)	0.059(3)	0.156(7)	0.001(4)	-0.020(4)	-0.006(3)
C(71)	0.064(4)	0.149(7)	0.100(5)	-0.070(5)	0.023(4)	-0.025(4)
C(81)	0.110(6)	0.119(6)	0.070(4)	0.023(3)	-0.006(4)	-0.056(5)

Table A5(b) : Anisotropic Temperature Factors (Å) for *cis,mer*-Os(CO)$_3$(PMe$_3$)Cl$_2$

Atom	U(11)	U(22)	U(33)	U(23)	U(13)	U(12)
Os(1)	0.0384(1)	0.0327(1)	0.0385(1)	-0.00129(7)	-0.00040(9)	-0.00076(7)
P(1)	0.0426(6)	0.0381(6)	0.0346(6)	0.0004(5)	0.0056(5)	0.0035(5)
Cl(1)	0.0465(7)	0.0575(7)	0.0491(7)	-0.0038(6)	0.0000(5)	-0.0120(6)
Cl(2)	0.0702(9)	0.0428(7)	0.0751(9)	0.0120(7)	-0.0071(7)	0.0046(6)
O(11)	0.101(3)	0.069(3)	0.045(2)	0.000(2)	0.026(2)	-0.009(2)
O(12)	0.075(3)	0.108(4)	0.059(3)	-0.027(2)	0.012(2)	0.028(2)
O(13)	0.062(3)	0.067(3)	0.115(4)	-0.014(2)	-0.005(2)	-0.018(2)
C(1)	0.050(3)	0.062(3)	0.048(3)	0.001(3)	-0.003(3)	0.007(3)
C(2)	0.066(4)	0.068(4)	0.072(4)	0.027(3)	0.026(3)	0.015(3)
C(3)	0.089(4)	0.042(3)	0.053(3)	-0.005(2)	0.005(3)	0.006(3)
C(11)	0.053(3)	0.034(2)	0.051(3)	0.009(2)	0.000(2)	-0.006(2)
C(12)	0.042(3)	0.048(3)	0.050(3)	-0.005(2)	-0.004(2)	0.014(2)
C(13)	0.051(3)	0.040(3)	0.061(3)	-0.003(2)	-0.003(3)	-0.003(2)

Table A6(b) : Anisotropic Temperature Factors (Å) for *fac*-$Os(CO)_3(PMe_3)Cl_2$

Atom	U(11)	U(22)	U(33)	U(23)	U(13)	U(12)
Os(1)	0.0362(1)	0.0316(1)	0.0388(1)	0.00170(8)	0.0033(1)	0.00057(9)
Os(2)	0.0415(2)	0.0363(1)	0.0378(1)	0.00146(9)	-0.0003(1)	-0.00319(9)
Cl(11)	0.0578(9)	0.061(1)	0.0482(9)	-0.0041(7)	-0.0108(7)	0.0059(8)
Cl(12)	0.0501(9)	0.071(1)	0.0601(9)	-0.0069(9)	0.0183(7)	-0.0083(8)
Cl(21)	0.054(1)	0.063(1)	0.071(1)	0.0059(8)	-0.0027(8)	0.0145(8)
Cl(22)	0.073(1)	0.061(1)	0.062(1)	0.0213(8)	0.0056(8)	-0.0100(9)
P(1)	0.0385(8)	0.0329(8)	0.0424(8)	0.0025(6)	-0.0010(6)	-0.0032(6)
P(2)	0.0462(9)	0.056(1)	0.0389(8)	-0.0065(7)	0.0001(7)	-0.0034(7)
O(11)	0.073(3)	0.063(3)	0.058(3)	-0.017(2)	-0.009(2)	-0.011(3)
O(12)	0.066(3)	0.073(3)	0.092(4)	0.028(3)	0.036(3)	0.011(3)
O(13)	0.100(4)	0.053(3)	0.110(5)	0.004(3)	-0.006(3)	0.023(3)
O(21)	0.101(4)	0.078(4)	0.050(3)	0.007(3)	0.007(3)	-0.036(3)
O(22)	0.112(4)	0.064(4)	0.072(3)	-0.006(3)	-0.020(3)	-0.034(3)
O(23)	0.074(4)	0.088(5)	0.115(5)	-0.020(4)	-0.011(3)	0.029(4)
C(11)	0.057(4)	0.035(3)	0.053(4)	0.002(3)	0.009(3)	0.002(3)
C(12)	0.054(4)	0.040(3)	0.051(3)	0.015(3)	0.012(3)	0.014(3)
C(13)	0.055(4)	0.041(4)	0.062(4)	0.001(3)	0.002(3)	0.005(3)
C(21)	0.070(4)	0.044(4)	0.041(3)	-0.005(3)	0.002(3)	-0.015(3)
C(22)	0.065(4)	0.045(4)	0.049(4)	0.002(3)	-0.006(3)	-0.011(3)
C(23)	0.056(4)	0.049(4)	0.068(4)	-0.005(3)	0.000(3)	0.006(3)
C(1)	0.0543	0.0386	0.0705	-0.0034	0.0202	0.0099
C(2)	0.0439	0.0338	0.0988	0.0050	-0.0117	-0.0217
C(3)	0.0837	0.0483	0.0433	0.0162	-0.0160	-0.0038
C(4)	0.0658	0.0397	0.0739	-0.0110	0.0017	-0.0132
C(5)	0.0615	0.0967	0.0462	0.0127	-0.0173	0.0059
C(6)	0.0732	0.0992	0.0554	-0.0307	0.0240	-0.0088

3. X-ray structural studies of some donor-acceptor compounds : (PMe$_3$)(OC)$_4$MRu(CO)$_3$(SiCl$_3$)$_2$ (M = Ru, Os)

(a)   (Me$_3$P)(OC)$_4$RuRu(CO)$_3$(SiCl$_3$)$_2$
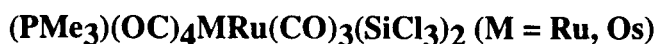
A yellow block, provided by Mr. J. L. Male, was mounted in a Lindemann capillary and used for intensity measurements. There was a steady decay in the intensities of the two intensity standards, corresponding to a scale change of about 20%. A Gaussian correction was employed.

The initial solution was obtained in the space group *P 1*. The solution was then transferred into the space group *P 2$_1$*. There were two crystallographically distinct moelcules in the asymmetric unit. The final model had the Ru, Si, P, Cl and O atoms anisotropic, while the C and H atoms were given isotropic temperature factors. An extinction parameter was also refined. In an attempt at confirming the handedness, the intensities of 11 Bijvoet pairs expected to show the largest differences in intensities ($F_o^+ - F_o^-$) were measured; the largest calculated difference ($F_c^+ - F_c^-$) was, however, only 9.8σ. Nine out of the 11 pairs agreed with the hand chosen. The largest residual peak in the final difference map was 0.56(8) eÅ^{-3}, located near the methyl groups.

(b)   (Me$_3$P)(OC)$_4$OsRu(CO)$_3$(SiCl$_3$)$_2$
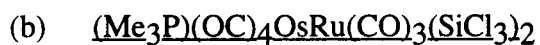
A colourless block, provided by Mr. J. L. Male, was mounted in a Lindemann capillary and used for intensity measurements. The data was collected in five shells, viz., 1.5≤θ≤10.0, 10.0≤θ≤12.0, 12.0≤θ≤17.0, 17.0≤θ≤22.5, and 22.5≤θ≤25.0; the second shell was for a complete sphere. There was a steady decay in the intensities of the two intensity standards, corresponding to a scale change of about 18%. An empirical absorption correction was employed, together with a θ-dependent correction for a sphere of 220 μm diameter.

The solution for the Ru analogue above was used, as the cell dimensions showed that the crystals were isomorphous. The calculated differences in the intensities of Bijvoet

pairs were much larger in this compound, so that the intensities of an additional 24 Bijvoet pairs were measured. In all, 92 Bijvoet pairs with $|F_o^+ - F_o^-| > 18\sigma$ were available, and an analysis showed that all agreed with the handedness chosen, which was the same as that for the Ru analogue above. The final model had the Os, Ru, Si, P, Cl and O atoms anisotropic, while the C and H atoms were given isotropic temperature factors. An extinction parameter was also refined. The largest residual peak in the final difference map was 1.03(12) eÅ^{-3}, located 0.29 Å from Os(3).
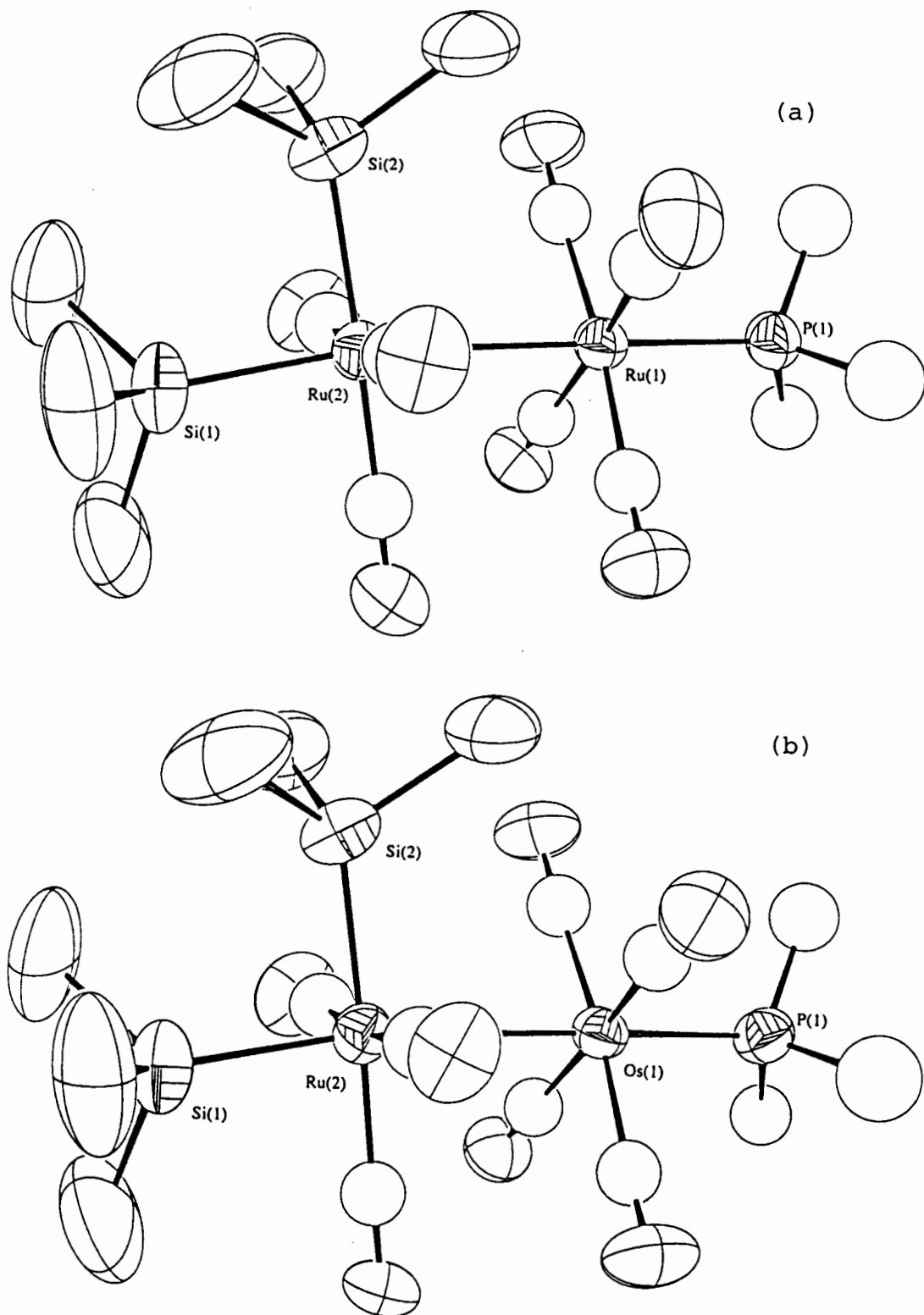
Fig. A.7. ORTEP plots of molecule (1) of (a) $(Me_3P)(OC)_4RuRu(CO)_3(SiCl_3)_2$ and
(b) $(Me_3P)(OC)_4OsRu(CO)_3(SiCl_3)_2$.

Table A(III) :   Crystal data for $(Me_3P)(OC)_4MRu(CO)_3(SiCl_3)_2$ (M = Ru, Os)

	M = Ru	M = Os
Formula	$C_{10}H_9Cl_6O_7PRu_2Si_2$	$C_{10}H_9Cl_6O_7OsPRuSi_2$
FW	743.18	832.30
F(000)	1431.90	1553.07
Crystal System	Monoclinic	Monoclinic
Space Group	$P\,2_1$	$P\,2_1$
a, Å	12.3965(13)	12.4036(14)
b, Å	15.8154(16)	15.7892(15)
c, Å	13.1860(15)	13.1866(13)
β, deg	100.624(9)	100.888(9)
V, Å^3	2540.9(9)	2534.6(5)
2θ range of unit cell	30.0-38.0	31.0-39.0
Z	2	2
D_{calc}, g cm^{-3}	1.94	2.18
μ(Mo, Kα), cm^{-1}	19.85	108.49
Crystal dimensions, mm	0.23 x 0.32 x 0.33	0.21 x 0.22 x 0.23
Transmission coefficient	0.5359-0.6713	0.3239-0.3658
Scan range (2θ), deg	4.0-50.0	4.0-50.0
Scan width (ω), deg	0.70+0.35tanθ	0.70+0.35tanθ
Scan rate (ω), deg min^{-1}	0.749-3.296	0.634-2.747
No. of unique reflections	4623	4870
No. of observed reflections	3636	4191
No. of parameters	408	408
R	0.034	0.032
wR	0.039	0.030
Instrument instability factor (k)	0.00008	0.00001
Extinction parameter (r*)	0.043(14)	0.129(9)
Largest (shift/e.s.d.) in final ls cycle	0.23	0.16
Minimum electron density in final difference map, e Å^{-3}	-0.41(8)	-1.20(12)
G.O.F.	2.1	2.3

Table A7(a) : Fractional Atomic Coordinates and Isotropic or Equivalent Isotropic Temperature Factors (Å) for $(Me_3P)(OC)_4RuRu(CO)_3(SiCl_3)_2$

Atom	x/a	y/b	z/c	U(iso)
Ru(1)	0.52122(6)	0.25207(9)	0.46913(5)	0.0476
Ru(2)	0.49466(6)	0.24594(9)	0.69023(6)	0.0502
P(1)	0.5310(2)	0.2558(2)	0.2914(2)	0.0571
Si(1)	0.4666(3)	0.2178(3)	0.8575(2)	0.0741
Si(2)	0.5158(3)	0.3952(2)	0.7292(3)	0.0678
Ru(3)	0.00046(7)	0.4941(1)	-0.02235(5)	0.0499
Ru(4)	-0.00561(6)	0.49848(9)	0.20210(6)	0.0489
P(2)	0.0158(2)	0.4927(3)	-0.1993(2)	0.0618
Si(3)	-0.0135(3)	0.5286(3)	0.3745(2)	0.0735
Si(4)	0.0375(3)	0.3524(2)	0.2443(2)	0.0646
Cl(11)	0.6024(3)	0.2120(4)	0.9710(2)	0.1176
Cl(12)	0.3649(4)	0.2953(4)	0.9214(3)	0.1245
Cl(13)	0.3911(5)	0.1032(4)	0.8722(4)	0.1488
Cl(21)	0.6042(3)	0.4689(2)	0.6423(3)	0.1000
Cl(22)	0.3720(3)	0.4645(2)	0.7129(3)	0.1038
Cl(23)	0.5958(4)	0.4299(3)	0.8743(3)	0.1192
Cl(31)	-0.1642(3)	0.5189(4)	0.4146(3)	0.1210
Cl(32)	0.0929(4)	0.4687(3)	0.4896(2)	0.1110
Cl(33)	0.0286(5)	0.6532(3)	0.4167(3)	0.1345
Cl(42)	0.1967(3)	0.3253(3)	0.3076(3)	0.1084
Cl(41)	0.0127(5)	0.2642(2)	0.1280(3)	0.1159
Cl(43)	-0.0474(4)	0.2969(3)	0.3476(4)	0.1199
O(11)	0.7466(7)	0.3400(6)	0.5296(7)	0.0982
O(12)	0.6614(7)	0.0921(5)	0.5086(7)	0.0879
O(13)	0.3051(6)	0.1513(5)	0.4336(6)	0.0758
O(14)	0.3909(7)	0.4200(5)	0.4565(7)	0.0893
O(21)	0.7447(5)	0.2411(7)	0.7537(6)	0.0882
O(22)	0.4690(8)	0.0553(6)	0.6487(7)	0.0986
O(23)	0.2476(6)	0.2787(6)	0.6306(6)	0.0946
O(31)	-0.1576(8)	0.3445(6)	-0.0556(8)	0.1098

Table A7(a) continued.

Atom	x/a	y/b	z/c	U(iso)
O(32)	-0.2041(7)	0.6066(6)	-0.0619(7)	0.0966
O(33)	0.1499(9)	0.6485(7)	0.0292(8)	0.1060
O(34)	0.2085(9)	0.389(1)	0.0446(8)	0.1125
O(41)	-0.2398(6)	0.4291(7)	0.1564(7)	0.1020
O(42)	-0.068(1)	0.6861(6)	0.1599(8)	0.0999
O(43)	0.2399(6)	0.5324(6)	0.2532(6)	0.0885
C(1)	0.6609(9)	0.2255(9)	0.2638(9)	0.098(4)
C(2)	0.4359(9)	0.1905(8)	0.2109(8)	0.081(3)
C(3)	0.509(1)	0.3562(9)	0.2299(9)	0.093(4)
C(4)	-0.098(1)	0.540(1)	-0.285(1)	0.117(5)
C(5)	0.037(1)	0.386(1)	-0.248(1)	0.157(7)
C(6)	0.130(1)	0.5538(9)	-0.227(1)	0.101(4)
C(11)	0.660(1)	0.3102(8)	0.5096(8)	0.070(3)
C(12)	0.6054(9)	0.1492(8)	0.4923(8)	0.062(3)
C(13)	0.3845(8)	0.1895(7)	0.4471(8)	0.058(3)
C(14)	0.4390(8)	0.3572(7)	0.4644(8)	0.064(3)
C(21)	0.6518(8)	0.2426(8)	0.7291(7)	0.062(2)
C(22)	0.4780(9)	0.1278(8)	0.6637(8)	0.064(3)
C(23)	0.3399(9)	0.2663(8)	0.6506(8)	0.071(3)
C(31)	-0.094(1)	0.3966(8)	-0.0405(9)	0.074(3)
C(32)	-0.1292(9)	0.5657(8)	-0.0438(9)	0.062(3)
C(33)	0.099(1)	0.5915(8)	0.0129(9)	0.067(3)
C(34)	0.133(1)	0.4251(9)	0.022(1)	0.090(4)
C(41)	-0.1547(9)	0.4571(7)	0.1724(8)	0.071(3)
C(42)	-0.0466(9)	0.620(1)	0.175(1)	0.082(3)
C(43)	0.1499(8)	0.5215(7)	0.2344(7)	0.059(3)

Table A7(b) : Anisotropic Temperature Factors (Å) for (Me$_3$P)(OC)$_4$RuRu(CO)$_3$(SiCl$_3$)$_2$

Atom	U(11)	U(22)	U(33)	U(23)	U(13)	U(12)
Ru(1)	0.0551(4)	0.0456(5)	0.0431(4)	-0.0002(4)	0.0090(3)	-0.0033(4)
Ru(2)	0.0545(4)	0.0530(6)	0.0445(4)	-0.0014(5)	0.0108(3)	0.0010(5)
P(1)	0.068(2)	0.059(2)	0.048(1)	-0.000(2)	0.013(1)	-0.005(2)
Si(1)	0.078(2)	0.115(3)	0.052(2)	0.000(2)	0.026(1)	-0.001(2)
Si(2)	0.071(2)	0.060(2)	0.078(2)	-0.018(2)	0.003(2)	0.006(2)
Ru(3)	0.0571(4)	0.0572(6)	0.0385(4)	0.0038(5)	0.0091(3)	0.0041(4)
Ru(4)	0.0580(5)	0.0522(5)	0.0393(4)	0.0008(5)	0.0107(3)	0.0030(5)
P(2)	0.076(2)	0.079(2)	0.041(1)	0.005(2)	0.013(1)	0.011(2)
Si(3)	0.103(2)	0.107(3)	0.042(1)	-0.009(2)	0.023(2)	0.014(2)
Si(4)	0.078(2)	0.058(2)	0.060(2)	0.013(1)	0.002(1)	-0.001(2)
Cl(11)	0.105(2)	0.298(7)	0.060(2)	0.043(3)	0.016(2)	0.036(3)
Cl(12)	0.142(3)	0.237(5)	0.092(2)	0.001(3)	0.057(2)	0.071(3)
Cl(13)	0.284(6)	0.182(4)	0.132(3)	0.002(3)	0.115(4)	-0.094(5)
Cl(21)	0.123(3)	0.068(2)	0.160(3)	-0.032(2)	0.050(2)	-0.035(2)
Cl(22)	0.107(2)	0.092(3)	0.141(3)	-0.000(2)	0.031(2)	0.039(2)
Cl(23)	0.197(4)	0.113(3)	0.104(2)	-0.050(2)	-0.047(3)	0.013(3)
Cl(31)	0.127(3)	0.237(5)	0.094(2)	-0.014(3)	0.062(2)	0.033(3)
Cl(32)	0.150(3)	0.194(4)	0.048(2)	0.003(2)	0.005(2)	0.042(3)
Cl(33)	0.271(6)	0.121(3)	0.102(3)	-0.059(3)	0.025(3)	-0.006(3)
Cl(42)	0.095(2)	0.114(3)	0.142(3)	0.030(2)	-0.007(2)	0.036(2)
Cl(41)	0.313(6)	0.054(2)	0.095(2)	-0.005(2)	-0.038(3)	0.012(3)
Cl(43)	0.142(3)	0.126(3)	0.157(3)	0.070(3)	0.041(3)	-0.024(3)
O(11)	0.078(5)	0.133(9)	0.103(7)	-0.012(6)	0.020(5)	-0.031(6)
O(12)	0.092(6)	0.068(6)	0.111(7)	0.000(5)	0.016(5)	0.015(5)
O(13)	0.066(5)	0.083(6)	0.081(5)	0.009(5)	0.002(4)	-0.014(4)
O(14)	0.111(7)	0.062(6)	0.110(7)	0.001(5)	0.004(6)	0.025(5)
O(21)	0.061(4)	0.130(8)	0.085(5)	-0.004(6)	-0.000(4)	0.011(5)
O(22)	0.136(8)	0.079(7)	0.102(7)	0.013(5)	0.041(6)	-0.012(6)
O(23)	0.061(5)	0.128(8)	0.116(7)	-0.034(6)	0.009(5)	0.001(5)
O(31)	0.130(8)	0.092(8)	0.117(8)	0.013(6)	-0.009(6)	-0.028(7)
O(32)	0.094(6)	0.107(7)	0.102(7)	0.018(6)	0.012(5)	0.036(6)
O(33)	0.151(9)	0.112(8)	0.105(7)	0.009(6)	-0.005(7)	-0.076(7)
O(34)	0.141(9)	0.28(2)	0.095(7)	0.022(9)	0.028(6)	0.16(1)
O(41)	0.062(5)	0.137(9)	0.134(8)	0.005(7)	0.021(5)	-0.020(5)
O(42)	0.21(1)	0.046(6)	0.127(8)	-0.008(5)	-0.011(8)	0.045(7)
O(43)	0.074(5)	0.112(7)	0.089(6)	0.011(5)	0.001(4)	-0.025(5)

Table A8(a) : Fractional Atomic Coordinates and Isotropic or Equivalent Isotropic Temperature Factors (Å) for (Me$_3$P)(OC)$_4$OsRu(CO)$_3$(SiCl$_3$)$_2$

Atom	x/a	y/b	z/c	U(iso)
Os(1)	0.52101(4)	0.25012(9)	0.46817(4)	0.0477
Os(3)	0.00121(5)	0.49041(9)	-0.02431(3)	0.0505
Ru(2)	0.49494(8)	0.2433(1)	0.6907(1)	0.0523
Ru(4)	-0.00571(8)	0.4954(1)	0.20058(8)	0.0490
P(1)	0.5312(3)	0.2530(3)	0.2925(3)	0.0611
P(2)	0.0164(3)	0.4891(4)	-0.2016(3)	0.0620
Si(1)	0.4678(3)	0.2146(3)	0.8580(4)	0.0801
Si(2)	0.5156(3)	0.3916(3)	0.7290(4)	0.0705
Si(3)	-0.0148(4)	0.5239(3)	0.3736(3)	0.0783
Si(4)	0.0358(3)	0.3488(3)	0.2433(3)	0.0661
Cl(11)	0.6015(4)	0.2113(5)	0.9709(3)	0.1260
Cl(12)	0.3670(5)	0.2937(4)	0.9212(4)	0.1290
Cl(13)	0.3916(7)	0.1016(5)	0.8732(5)	0.1686
Cl(21)	0.6026(4)	0.4672(3)	0.6400(4)	0.1050
Cl(22)	0.3731(3)	0.4614(3)	0.7117(4)	0.1068
Cl(23)	0.5978(5)	0.4274(3)	0.8722(4)	0.1241
Cl(31)	-0.1618(4)	0.5163(4)	0.4144(4)	0.1233
Cl(32)	0.0934(4)	0.4650(4)	0.4889(3)	0.1119
Cl(33)	0.0292(6)	0.6506(4)	0.4149(4)	0.1403
Cl(41)	0.1957(3)	0.3214(3)	0.3074(4)	0.1090
Cl(42)	0.0093(5)	0.2602(3)	0.1274(4)	0.1142
Cl(43)	-0.0475(4)	0.2945(3)	0.3474(4)	0.1217
O(11)	0.7452(8)	0.3359(7)	0.5277(9)	0.0985
O(12)	0.6635(8)	0.0899(7)	0.509(1)	0.0897
O(13)	0.3052(8)	0.1474(6)	0.4340(9)	0.0804
O(14)	0.3906(8)	0.4168(6)	0.4566(9)	0.0863
O(21)	0.7447(7)	0.2341(8)	0.7517(7)	0.0795
O(22)	0.4684(9)	0.0515(6)	0.6487(9)	0.0784
O(23)	0.2482(7)	0.2738(8)	0.6270(9)	0.1004
O(31)	-0.155(1)	0.3402(8)	-0.058(1)	0.1079
O(32)	-0.2049(9)	0.6015(7)	-0.062(1)	0.0917

211

Table A8(a) continued

Atom	x/a	y/b	z/c	U(iso)
O(33)	0.152(1)	0.6421(9)	0.027(1)	0.1073
O(34)	0.205(1)	0.377(1)	0.046(1)	0.1069
O(41)	-0.2434(8)	0.4274(8)	0.1521(9)	0.1006
O(42)	-0.073(1)	0.6836(8)	0.160(1)	0.1146
O(43)	0.2404(8)	0.5270(8)	0.2526(8)	0.1016
C(1)	0.661(1)	0.223(1)	0.266(1)	0.118(6)
C(2)	0.430(1)	0.1846(8)	0.212(1)	0.071(4)
C(3)	0.511(1)	0.355(1)	0.233(1)	0.087(5)
C(4)	-0.093(1)	0.533(1)	-0.286(1)	0.135(7)
C(5)	0.024(2)	0.384(2)	-0.257(2)	0.19(1)
C(6)	0.133(1)	0.546(1)	-0.231(1)	0.108(6)
C(11)	0.661(1)	0.3071(9)	0.511(1)	0.064(4)
C(12)	0.607(1)	0.147(1)	0.493(1)	0.061(4)
C(13)	0.387(1)	0.1866(9)	0.447(1)	0.061(4)
C(14)	0.437(1)	0.353(1)	0.461(1)	0.068(4)
C(21)	0.653(1)	0.239(1)	0.727(1)	0.067(4)
C(22)	0.478(1)	0.1234(9)	0.666(1)	0.060(4)
C(23)	0.342(1)	0.2643(9)	0.648(1)	0.070(4)
C(31)	-0.091(1)	0.391(1)	-0.041(1)	0.072(4)
C(32)	-0.129(1)	0.5620(9)	-0.046(1)	0.062(4)
C(33)	0.099(1)	0.585(1)	0.011(1)	0.061(4)
C(34)	0.133(1)	0.421(1)	0.019(1)	0.096(6)
C(41)	-0.155(1)	0.4543(9)	0.170(1)	0.073(4)
C(42)	-0.050(1)	0.615(1)	0.175(1)	0.089(5)
C(43)	0.147(1)	0.5169(9)	0.232(1)	0.066(4)

Table A8(b) : Anisotropic Temperature Factors (Å) for

$(Me_3P)(OC)_4OsRu(CO)_3(SiCl_3)_2$

Atom	U(11)	U(22)	U(33)	U(23)	U(13)	U(12)
Os(1)	0.0547(3)	0.0441(3)	0.0450(3)	0.0003(3)	0.0078(3)	-0.0045(3)
Os(3)	0.0556(3)	0.0564(4)	0.0411(3)	0.0025(4)	0.0084(2)	0.0045(3)
Ru(2)	0.0549(6)	0.0545(8)	0.0481(7)	-0.0023(8)	0.0102(6)	0.0018(7)
Ru(4)	0.0565(6)	0.0488(7)	0.0429(6)	-0.0002(8)	0.0095(5)	0.0038(7)
P(1)	0.067(2)	0.056(2)	0.061(2)	-0.006(3)	0.012(2)	0.001(3)
P(2)	0.077(3)	0.073(3)	0.043(2)	0.001(3)	0.010(2)	0.010(3)
Si(1)	0.079(3)	0.118(4)	0.065(3)	-0.001(3)	0.031(2)	-0.001(2)
Si(2)	0.077(3)	0.061(3)	0.078(3)	-0.016(2)	0.007(2)	0.008(2)
Si(3)	0.095(3)	0.108(4)	0.053(2)	-0.007(3)	0.024(2)	0.013(3)
Si(4)	0.083(3)	0.055(2)	0.065(3)	0.015(2)	-0.000(2)	0.000(2)
Cl(11)	0.110(3)	0.303(9)	0.070(3)	0.047(4)	0.015(2)	0.044(4)
Cl(12)	0.155(4)	0.260(6)	0.099(4)	0.006(4)	0.070(3)	0.087(4)
Cl(13)	0.341(9)	0.199(5)	0.140(5)	-0.001(5)	0.118(6)	-0.124(6)
Cl(21)	0.134(3)	0.072(3)	0.158(4)	-0.031(3)	0.052(3)	-0.035(3)
Cl(22)	0.114(3)	0.092(3)	0.141(4)	-0.002(3)	0.030(3)	0.039(3)
Cl(23)	0.204(5)	0.111(4)	0.106(3)	-0.043(3)	-0.044(3)	0.014(4)
Cl(31)	0.125(3)	0.250(7)	0.095(3)	-0.015(4)	0.061(3)	0.038(4)
Cl(32)	0.154(4)	0.190(5)	0.049(2)	0.003(3)	0.004(2)	0.039(4)
Cl(33)	0.277(7)	0.125(4)	0.103(4)	-0.054(3)	0.025(5)	-0.001(4)
Cl(41)	0.093(3)	0.109(4)	0.148(4)	0.028(3)	-0.002(3)	0.034(3)
Cl(42)	0.318(7)	0.049(3)	0.098(3)	-0.003(2)	-0.042(4)	0.008(4)
Cl(43)	0.135(4)	0.123(4)	0.168(5)	0.067(3)	0.046(4)	-0.020(3)
O(11)	0.082(7)	0.108(9)	0.12(1)	-0.019(8)	0.020(7)	-0.028(7)
O(12)	0.096(8)	0.059(7)	0.13(1)	0.002(7)	0.010(8)	0.020(6)
O(13)	0.070(6)	0.079(8)	0.098(9)	-0.001(7)	0.016(6)	-0.014(6)
O(14)	0.104(8)	0.058(7)	0.108(9)	-0.004(7)	-0.003(7)	0.017(6)
O(21)	0.060(5)	0.114(9)	0.074(7)	-0.007(7)	-0.007(6)	0.013(6)
O(22)	0.128(9)	0.043(6)	0.101(9)	0.008(6)	0.039(7)	-0.009(6)
O(23)	0.060(6)	0.13(1)	0.128(9)	-0.021(8)	0.014(6)	-0.001(6)
O(31)	0.13(1)	0.087(9)	0.12(1)	0.018(8)	-0.024(9)	-0.030(8)
O(32)	0.085(8)	0.11(1)	0.095(9)	0.011(9)	0.011(7)	0.039(8)
O(33)	0.14(1)	0.12(1)	0.084(9)	0.008(8)	-0.006(8)	-0.052(9)
O(34)	0.12(1)	0.24(2)	0.12(1)	0.00(1)	0.036(9)	0.13(1)
O(41)	0.059(6)	0.15(1)	0.12(1)	0.013(8)	0.020(7)	-0.008(6)
O(42)	0.22(2)	0.068(8)	0.11(1)	0.014(8)	-0.01(1)	0.033(9)
O(43)	0.076(7)	0.14(1)	0.098(9)	0.012(8)	-0.003(7)	-0.011(7)